B E R I C H T E
aus dem
I N S T I T U T F Ü R M E E R E S K U N D E
an der
Christian-Albrechts-Universität Kiel

Nr. 143

1 9 8 5

S E A R O V E R

DATA REPORT I

NORTH ATLANTIC SUMMER 1981

- N O A '81 -

by

Joachim Bauer, Jürgen Fischer, Harry Leach, John Woods

DOI 10.3289 / IFM_BER_143

ISSN 0341 - 8561

PREFACE

The NOA'81 SEA ROVER experiment was carried out during Cruise 76 of FS "Poseidon" between the Azores, Greenland and the British Isles during the summer of 1981.

The experiment was part of a long-term research programme designed to investigate structures in the seasonal boundary layer. The spectral range covers over three decades in the horizontal ranging from the gyre scale (order 1000 km) to the mesoscale (order 1 km) and it includes finestructure with vertical scales of more than one metre. Covering this broad spectral range was only possible with the development of the "Seasonal and Regional Ocean Variability Explorer" (SEA ROVER). A detailed description of various parts of the system can be found in Fischer et al. (1985), Leach (1984) and Horch (1984).

Although these technical reports represent the present status of the system most of the parts were already operational in 1981. A brief description of the system including the data processing will be given within this report.

There were two main scientific targets:

(1) large-scale variability of the boundary layer between the Azores (38° N) and 55° N,

(2) three-dimensional mesoscale structure of the polar front near the Gibbs Fracture Zone.

Although the scientific applications were different, the data sampling, processing and reduction of this large data set was identical for both parts of the experiment, the products are, however, presented separately according to the scientific objectives.

Within this report we describe the experiment and data processing, assess the experimental errors and present a selection of the possible products from various stages of the data processing. Many of the diagnostic techniques were developed to analyse the Batfish data set collected from RRS "Discovery" during GATE (Woods and Minnett, 1979; Leach, Minnett and Woods, 1985). This data report does not offer scientific interpretation of the data. It is possible to gain some insight in the variability encountered in the seasonal boundary layer from the selection of products derived from routine computer processing of the data set.

Page

1. INTRODUCTION

1.1 Aims of the experiment

The exploration of the thermohaline variability in the seasonal thermocline as a function of space and time in different hydrographic regions of the North Atlantic Ocean is a long-term aim of the research in the Regional Oceanography Department at IfM-Kiel. The "Seasonal and Regional Ocean Variability Explorer" (SEA ROVER) measurement system was developed to monitor these structures with the best possible resolution. The first use of this system was in the experiment called NOA '81 described in this report.

Scientifically the experiment was designed for two major problems:

(a) Long Sections

The regional climate of the ocean boundary layer as a link between the atmosphere and the interior of the ocean is not yet well understood. The reason for that is the failure of the too scarce coverage of hydrographic measurements, mainly based on station data, to resolve the regional, seasonal and interannual variations.

The SEA ROVER system is a tool to improve data collection. It measures profiles of temperature, conductivity and horizontal velocities at the sea surface and records navigation and meteorological data while the ship is moving at full speed. The speed and the high horizontal resolution of the SEA ROVER system enable the surveying of large areas much more synoptically and with better resolution than classical station measurements do. Real-time data processing on board helps to reduce the enormous amount of data.

It is planned to use the ready-processed data set to study the system atmosphere - mixed layer - thermocline, for calculations of heat and fresh water budget and for investigation of seasonal cycles of various parameters for example, mixed layer depth, potential vorticity.

(b) Frontal Structures

The mesoscale waveband in the spectrum of oceanic motion extends from the spectral peak of synoptic-scale motions (near the Rossby radius of deformation) to the spectral peak of microscale turbulence (at the Ozmidov scale). In the seasonal thermocline, the mesoscale waveband

ranges from about 30 km to 30 cm. This spectral band includes internal waves and the enstrophy cascade of isopycnic turbulence and finestructure in hydrographic profiles. Mesoscale jets and fronts are a key phenomenon in these latter processes.

The aim of this part of the experiment was to survey the three-dimensional structure of thermoclinicity, baroclinicity, velocity and potential vorticity to spatial and temporal resolutions and accuracies commensurate with the processes described by the computer models (Onken, Bleck and Woods, 1985).

Surveying mesoscale fronts with a rapidly moving ship seems to be the best strategy to minimize the difficulties of interpreting the structures caused by non-synoptic or poorly-resolving measurements.

The experiment should take place in a region where the relevant quantities show strong signals, that means in a region with the best signal-to-noise ratio. Therefore we decided to choose the North Atlantic Polar Front as a good test site for these studies.

1.2 Experimental design

For the experiment the full capabilities of the measurement system were used. The towed fish undulation in the form of a saw tooth wave should reach clearly the mixed layer and dive as deep as possible into the seasonal thermocline with a minimum wavelength to resolve the expected steep temperature gradients. The ship should move at full speed of about 5 m s^{-1} to improve synopticity and save time during measurements. The data should be recorded and processed continuously.

(a) Long Sections

For the investigation of the long sections the ship followed along standard tracks whose choice had both technical and scientific reasons. They are the links between the front survey area at the polar front, the supply base at the Azores and the home port. They pass through the location of the Ocean Weather Ships to provide a comparison of the data with the long-term measurements at the Ocean Weather Stations. Repeated measurements along the same standard tracks on return trips and in different seasons and years should allow investigations about persistence of features and seasonal and interannual variations.

(b) Frontal Survey

A general survey pattern was designed to localize the synoptic-scale structures, meanders and eddies of the North Atlantic Polar Front and to find a region with high thermoclinicity, which is defined as the horizontal temperature gradient on an isopycnic surface. Then, focussing in on that region, a high resolution survey, which should resolve the mesoscale structures and cut the front as many times as the available ship-time allows, should be made. In order to control the experiment, real-time graphs of the thermoclinicity signal should be used to predict the orientation of the front for the following section.

The towed fish undulation in form of a sawtooth wave should cover the upper 80 metres of the structures with a minimum wavelength to resolve the expected high thermoclinicity. The ship's speed was aimed to be about 5 m s^{-1} in order to minimize the effect of non-synopticity in the measurements.

1.3 Experimental site and oceanographic conditions

Our Long Sections range from the Azores to about 55° N from the anticyclonic Subtropical Gyre well into the cyclonic Subartic Gyre, where the Polar Front is the boundary between these gyres, and from the Azores to the English Channel.

Both sections should intersect the streamlines of the North Atlantic Gyre (Dietrich, 1969). The mass transport across the Azores - Greenland section is concentrated in the region of the Polar Front otherwise known as the North Atlantic Current, between 48° N and 51° N, whereas the Azores - English Channel section is expected to cross the various branches of the recirculation between the Azores and the European continent (Dietrich et al., 1980).

Both sections cross the zero line of the net annual water flux resulting from precipitation minus evaporation (Baumgartner and Reichel, 1975).

Along the Azores - English Channel section the net annual heat flux through the surface is nearly zero while the Azores - Greenland section intersects the axis of maximum heat loss (Budyko, 1974).

The Azores - Greenland section follows the track of the long hydrocast section measured during the International Geophysical Year (Dietrich, 1969).

A recent summary of the seasonal and regional variation along our sections can be found in the Isopycnic Atlas of the North Atlantic Ocean (Bauer and Woods, 1984) which was derived from the well-known Robinson-Bauer-Schroeder Atlas (1979). The general structure during July and August is a well-developed seasonal pycnocline with a shallow mixed layer.

Winter mixing reaches deeper than 150 m in the whole region we surveyed. That means that the water column in the depth range of the towed fish all lies within the seasonal pycnocline.

1.4 Sonderforschungsbereich 133 - "Warm Water Sphere of the Atlantic"

Our work including the investigation of large-scale structures in the seasonal thermocline as well as frontal structures can be seen in the context of the long running "Warm Water Sphere" cooperative research programme (Sonderforschungsbereich) funded by the Deutsche Forschungsgemeinschaft (German Research Council). The aim of this programme is to gain some insight into the dynamics and thermodynamics of the North Atlantic, the transports of heat and mass from the western basin across the Mid-Atlantic Ridge into the eastern basin, and the recirculation in the subtropics.

Although many groups participate in this programme the interactions with the following groups are especially relevant to our work:

Satellite images of sea surface temperature at the Polar Front will help us to identify regions of strong thermoclinicity and give some hint of the time scales of the observed structures (Hardtke and Meincke, 1984). Surface fluxes after Isemer and Hasse (1985) based on Bunker's data will help us to interpret the large-scale variation of the seasonal thermocline.

From long sections with deep CTD-stations along the Mid-Atlantic Ridge (Meincke and Sy, 1983) the maximum depth of winter mixing can be estimated by the "thermoclinicity elbow" method (Woods, 1985). Drifter trajectories (Krauss and Meincke, 1982; Krauss and Käse, 1984) will be used to identify the seasonal catchment area of the water being advected through our area.

1.5 Publications and Reports

Bauer, J. and J.D. Woods (1984) Isopycnic Atlas of the North Atlantic Ocean. IfM Kiel Berichte Nr. 132.

The North Atlantic part of the numerical atlas produced by M. Robinson, E. Schroeder and R. Bauer (1979) from NODC data was used to present the annual cycle of the hydrography on density surfaces. Monthly mean temperatures were combined with annual mean salinities to calculate pseudo-monthly mean densities.

The first part presented monthly mean maps of the distribution of pressure, temperature and salinity on various density surfaces.

Vertical sections in isopycnic coordinates were presented in part two. They follow the standard ship's tracks of the SFB-133 TP-B1: Azores - Greenland and Azores - English Channel.

Fischer, J., C. Meinke, P. J. Minnett, V. Rehberg and V. Strass (1985) A description of the Institut für Meereskunde Schleppfisch-System. Technischer Bericht Nr. 1, 2. Auflage.

This is a detailed technical description of the mechanics, electronics and software of the Schleppfisch-system. This report includes also an operating manual for the use of the Schleppfisch (towed fish) and the basic CTD data processing for quick-look data. Although this is a description of the present configuration of the system (1985), it is still relevant for the 1981 state.

Fischer, J., H. Leach and J.D. Woods (1985) Synoptic-scale structures in the seasonal thermocline at the North Atlantic Polar Front. (in preparation)

This is a description of synoptic-scale structures at the North Atlantic Polar Front measured with the SEA ROVER system. This paper draws attention to the similarities between hydrographic data in the seasonal thermocline and sea surface currents. Derived quantities such as relative vorticity and spacing between isopycnals show significant correlations.

Horch, A. (1984) Eine Beschreibung der NOVA-Software für Schleppfisch-experimente.
Technischer Bericht Nr. 5, 2. Auflage.

This is a technical report about the CTD-data processing and editing on the shipboard minicomputer "NOVA-4C". The second edition describes the state of the software in 1984, but includes the 1981 programs. (in German)

Leach, H. (1984) Eine Beschreibung des wissenschaftlichen Navigationssystems des FS "Poseidon".
Technischer Bericht Nr. 2, 2. Auflage.

This is a description of the scientific navigation system based on an HP-1000 minicomputer, which was used in 1981 on board FS "Poseidon". This system is the basic tool for measuring sea surface currents by using both absolute and relative navigation. The second edition describes the state of the system in 1984, but the main concept remains unchanged.

Leach, H. (1985) The analysis of currents measured from a moving ship in the region of the North Atlantic Polar Front.
(submitted)

Ship drift measurements were used to calculate sea surface currents independently from the hydrographic data. By using the relative vorticity, which was derived from the objectively analysed current field, it was possible to calculate the surface streamfunction. Synoptic-scale meanders were the dominant features in the streamfunction and some similarities with the thermohaline structures have been observed.

2. INSTRUMENTATION - The SEA ROVER

2.1 The towed undulating CTD-system as a concept

The investigation of processes in the upper ocean with strong variability in space and time, such as eddies and fronts, set a specification for the measurement system, which is not or not satisfactorily fulfilled by conventional profiling systems.

For studying such processes the measurement system should allow for synopticity combined with high resolution in the space and time scales. These scales cover a broad spectral range in both space and time. High accuracy and long-term stability of the calibration of the sensors is another important requirement.

Quasi-synoptic measurements can only be obtained from a moving ship, using freefall probes (XBT's, XSTD's) or towed, undulating systems.

In order to describe the kinematics and the dynamics of the ocean at least temperature and salinity as a function of depth have to be measured. These are the usual sensors of a normal CTD.

In contrast to any profiling from a stationary or slowly drifting ship, where a "true" vertical profile is obtained, a towed system will give the parameters as a function of the vertical and horizontal coordinates depending on the ship's speed and the descent/ascent rate of the system. This effect may distort the measured parameter field according to the inclination of the profile. High vertical speeds will minimize this distortion, but sometimes a correction will be necessary, which is only possible if the positioning of the system is very accurate.

The quintessence of all these requirements led to a system, which is derived from the Bedford Institute "Batfish" (Dessureault, 1976) and the IOS (Wormley) "Sea Soar" (Collins et al., 1983). It should carry a high resolution CTD with fast response sensors to reduce the time lag effects caused by the high penetration speed of the fish. Accurate navigation with the possibility of calculating positions relative to a moving body of water will complete the system, especially if the experiment requires quasi-"Lagrangian" coordinates (Woods and Minnett, 1979).

The SEA ROVER system was used for the first time during the experiment NOA'81. According to the requirements described above, the system has three main tasks:

1) Continuous CTD data sampling with a towed system.

2) Collection of navigation data during the experiment in absolute and relative coordinates.

3) Real-time data processing.

2.2 The IfM towed fish system

One key part of the system developed at the Institut für Meereskunde Kiel (IfM) is a towed depth-controlled underwater vehicle, which is a further development of the "Sea Soar" designed at the Institute of Oceanographic Sciences (IOS) in Wormley, England, which is itself a development of the original Hermes/Guildline "Batfish" (Dessureault, 1976).

The main components of this system are the vehicle with its hydraulics and underwater electronics, a CTD-probe and the control unit on board the ship. For illustration of the various tasks of the system see figure 2.2.1.

The nose, tail-plane and wings of the towed fish are made from fibre-glass-reinforced polyester resin, whereas the fuselage is constructed from stainless steel. The latter holds the wing axle and the fittings for the electronics pressure vessels and the hydraulics unit. The wings are mounted on a horizontal axle so that their angle relative to the fuselage can be varied to cause the fish to climb or dive.

In order to reduce rolling of the fish, a stabilizing fin is freely hinged at the tail (Dessureault, 1976) (see figure 2.2.3).

The fish contains two pressure vessels, one for the control electronic and the other being the CTD underwater unit. The hydraulics are contained in a cylindrical oil bath which is pressure-equalized with the surroundings. The control electronics are based on those developed at the Forschungsanstalt für Wasserschall- und Geophysik der Bundeswehr, Kiel (FWG). This unit performs four tasks:

(1) monitoring the parameters which describe the condition of the fish, i.e. depth, wing angle, roll and pitch angles;

(2) transmitting these data to the control unit on board the towing ship;

(3) receiving and decoding the command signal from the control unit;

(4) generating the analogue signal to control the Moog-servo-valve which determines the wing movement.

A separate strain-gauge pressure cell is used to monitor the depth of the fish, in order to enable the fish to be controlled independently without recourse to the pressure signal from the CTD. This modularization of the system, making the fish independent of the payload, proved useful in practice particularly during the development phase.

A very durable hydraulic system (based on that used in the IOS Sea Soar: Collins et al., 1983) drives the tilting of the wings. This system is designed to allow long tows (approximately 1000 hours between routine services), and due to the high oil pressure of up to 7 MPa, an immediate response to the command signal generates sharp turning points in the fish profiles. The oil pressure is provided by a pump driven by an impeller at the back of the fish turned by the water flowing past it.

The generation and transmission of the command signal is one task of the control system on board the ship, which also monitors the attitude of the fish and uses the data supplied by the payload (CTD-probe), to calculate salinity and density. The system described and its software is developed from those of the FWG-controller. There are two operating modes, manual and automatic. In manual mode, used only during deployment and recovery of the fish, the wing angle is adjusted by the setting of a hand-operated potentiometer. In automatic mode, the controller guides the fish along a sawtooth track between maximum and minimum depth with a constant dive- and climb-rate, all chosen by the operator. The control algorithm tries to minimize any deviation from the desired track. In order to control the fish independently from the payload (CTD) a separate pressure gauge is used, which is part of the control electronics.

The fish was towed on a 10 mm diameter single core towing cable, fixed by a bridle to the fish. This cable was unfaired and has a nominal breaking strain of six tonnes. All signal transfer to and from the underwater unit and the current supply was carried along this cable. Three frequency bands were used, one for the control signal to the fish, one for the fish parameter to the ship and one for the CTD data to the ship. The cable was paid out from the towing winch on FS "Poseidon" using the A-Frame and the Geological Boom as shown in figure 2.2.2. In normal towing operation the boom is in its resting position. Only during deployment and recovery the boom is extended and the cable removed from the snatch block on the port side of the A-Frame.

The payload in 1981

The CTD-probe in the towed fish was a slightly modified ME-Kompakt-Sonde from "Meerestechnik Elektronik GmbH, Trappenkamp". In order to resolve small-scale temperature and salinity gradients, the sensors should have high resolution and accuracy, and a quick response. For quality control of the data two thermometers and conductivity cells plus the possiblity to display the measured differences were needed. Table 1 shows the specifications of the sensors as given by the manufacturers.

Table 1 - Table of sensor specification ME-Multisonde

PARAMETER	SPECIFICATION
PRESSURE	Principle : Strain-gauge pressure cell Range : 0 - 600 dbar Resolution : 0.01 dbar Accuracy : 0.25 % of range
TEMPERATURE	Principle : Platinum resistance Range : -2 - +40 °C Resolution : 0.001 °C Accuracy : 0.005 °C
CONDUCTIVITY	Principle : Symmetric electrode cell Range : 5 - 55 mS/cm Resolution : 0.001 mS/cm Accuracy : 0.005 ms/cm

Temperature and conductivity sensors were mounted in pairs on the lower tail plane of the fish, figure 2.2.3, whereas the strain-gauge pressure cell is directly fixed to the CTD-vessel inside the towed fish. The sampling rate, which was used in the NOA'81 experiment was 16 cycles per second, equivalent to a time interval of 62.5 ms between each data cycle, each of which consists of one pressure, two temperature and two conductivity measurements.

The raw data from the CTD-probe were converted into 16-bit words by the microprocessor controller and then archived on a nine-track digital tape, followed by trailer information about time and dive-climb orientation after every 50 data cycles.

To allow quick-look analysis of the data, every sixteenth cycle (i.e. one cycle per second) was transformed into physical units, and salinity and

density were calculated. All values were displayed on the front panel of the controller, and a subsample, chosen by the operator, was available on analogue output channels.

2.3 The "Poseidon" Navigation System

The NOA'81 expedition was the first expedition in which the "Poseidon" navigation system was used to collect and store navigation data. This system serves exclusively as a scientific aid and is not used for the routine ship navigation. The system is based on a Hewlett-Packard HP1000 minicomputer to which many of the ship's navigational instruments are interfaced as shown in figure 2.3.1. During this cruise the computer was running under a version of the RTE-MIII operating system with 64K memory. This allowed a maximum of three partitions which in turn limited the number of programs which could run in parallel to three. So three tasks could be performed in real-time: first the acquisition of satellite-navigation positions from the Magnavox MX1105, second the integration of the ship's position relative to the water using the Colnbrook electromagnetic log, and third displaying the navigation in alphanumeric and graphic form on the system's graphic terminals.

Spot values of all the available navigational parameters were printed out and stored on disc every two minutes. The data on disc were then transferred to magnetic tape two or three times a day as necessary for merging with the data from the towed fish.

The electromagnetic log was calibrated off the Azores on 18th July 1981 using a drifting radar-buoy with a sail centred at the depth of the log (ca. 4.5 m). The fore-aft and port-starboard components were calibrated separately. The details of the method used are contained in Leach, 1984. This was a third set of coefficients obtained which were accordingly stored in a file named #KAL3.

Table 2.3.1 lists the programs used during the NOA '81 expedition.

Table 2.3.1 - Programs used on the "Poseidon" navigation system during NOA'81

SATNA	acquisition of satellite navigation data
EMLOG/EMLO2(TE)	acquisition and integration of electromagnetic log signal
PLOTT/PLOT2(TE)/PLOT3(TE)	output of alphanumeric and graphic data to terminals
CHK2M	correction of 2-minute data on disc
H2MTP H2MTQ H2MTR	transfer of 2-minute data from disc to tape
EMKAL	calibration of electromagnetic log
DECCA/DECC2(TE)	Decca navigation

Note: Those programs followed by the letters (TE) ran under timed execution and were scheduled by the operating system whereas the others were free-running.

2.4 Data acquisition and real-time monitoring

To conduct an experiment for mesoscale frontal studies means not only to have a suitable measurement system, but to obtain information about the spatial structure of the phenomenon in almost real-time. This led to the real-time data processing scheme, shown in figure 2.4.1. "Real-time" in this context means to get the desired results, for example, plots of temperature distribution on density surfaces, in a time interval, which is equivalent to that of data acquisition. In the first stage, the raw fish data and the navigation data were merged and interpolated to the same time interval. The data were then separated into ascending and descending profiles. For the real-time analysis only the descending part was used for further block averaging and transformation to physical units. In addition salinities and densities were calculated, and the result is stored on digital tape.

In the third stage the variables were interpolated onto standard surfaces, e.g. temperature and pressure on constant density (σ_t) and density on temperature.

These products were plotted afterwards, to allow necessary data analysis.

POSEIDON TOWED FISH SYSTEM

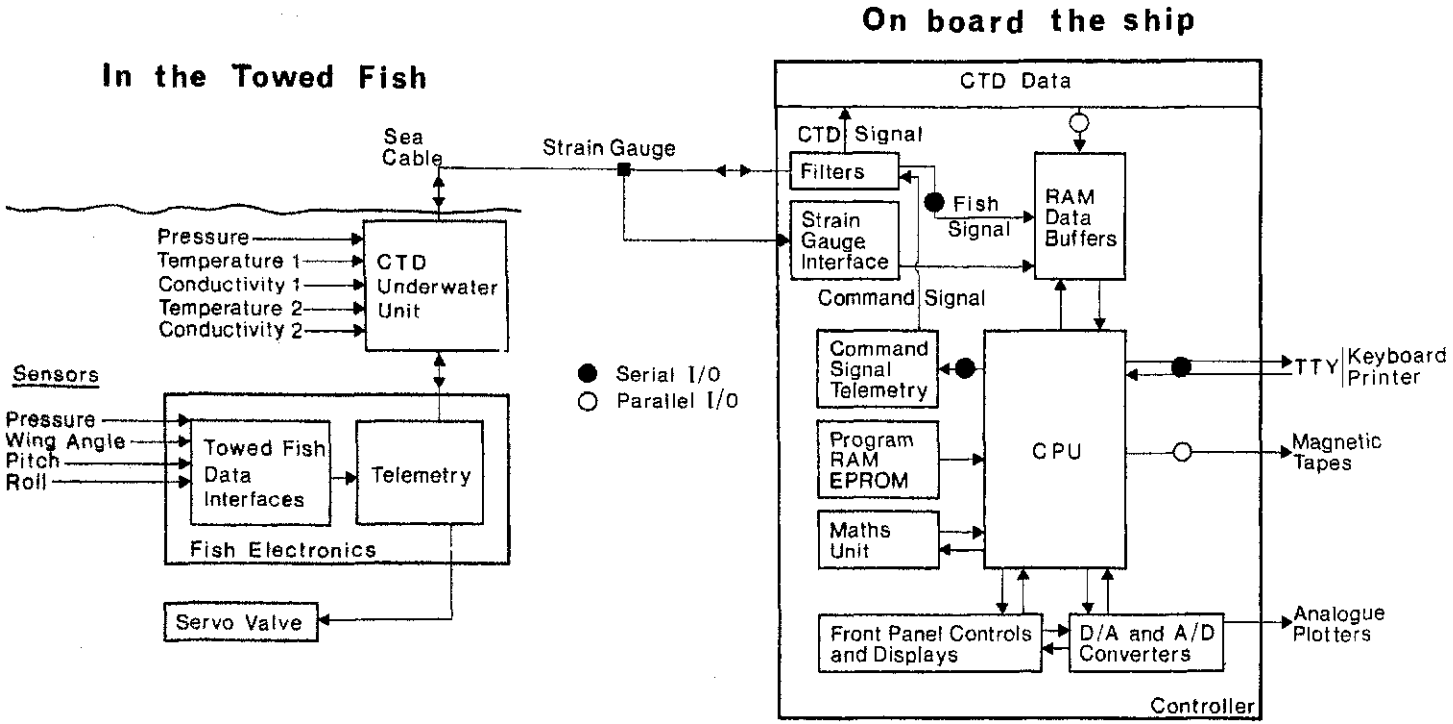

Fig. 2.2.1: Sketch of the main components in the towed fish system, including the flow of control signals and scientific data.

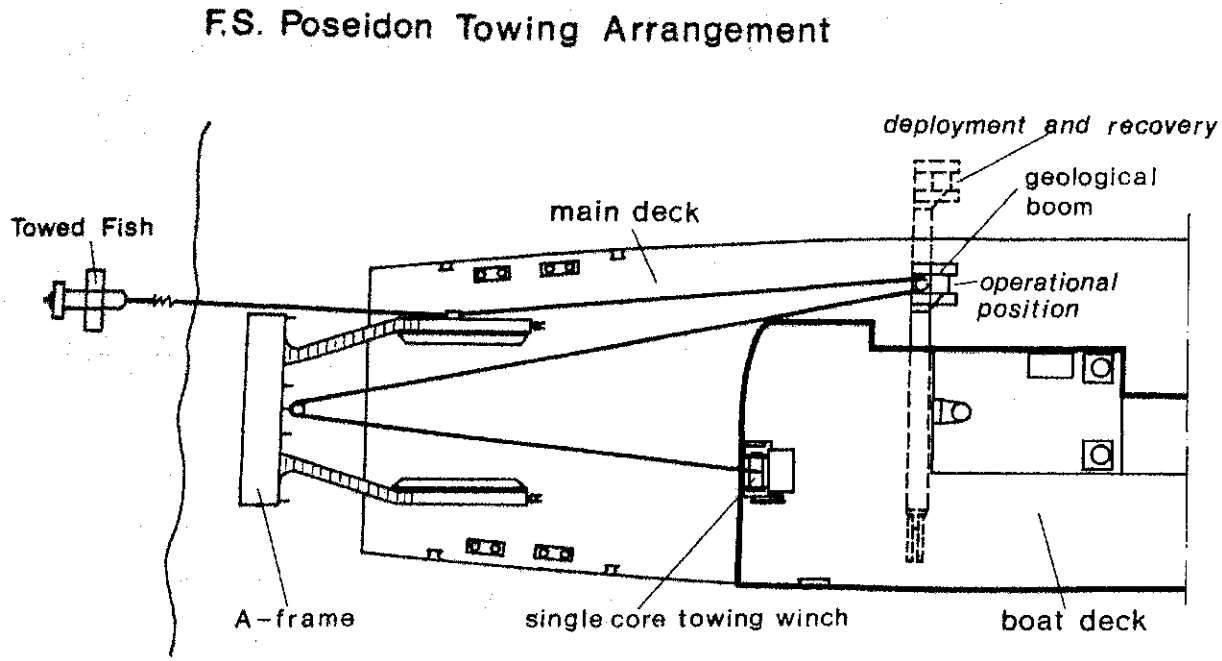

Fig. 2.2.2: "Schleppfisch" towing arrangement viewed from above on board FS "Poseidon" using the towing winch (10 mm single core cable), the geological boom and the A-Frame.

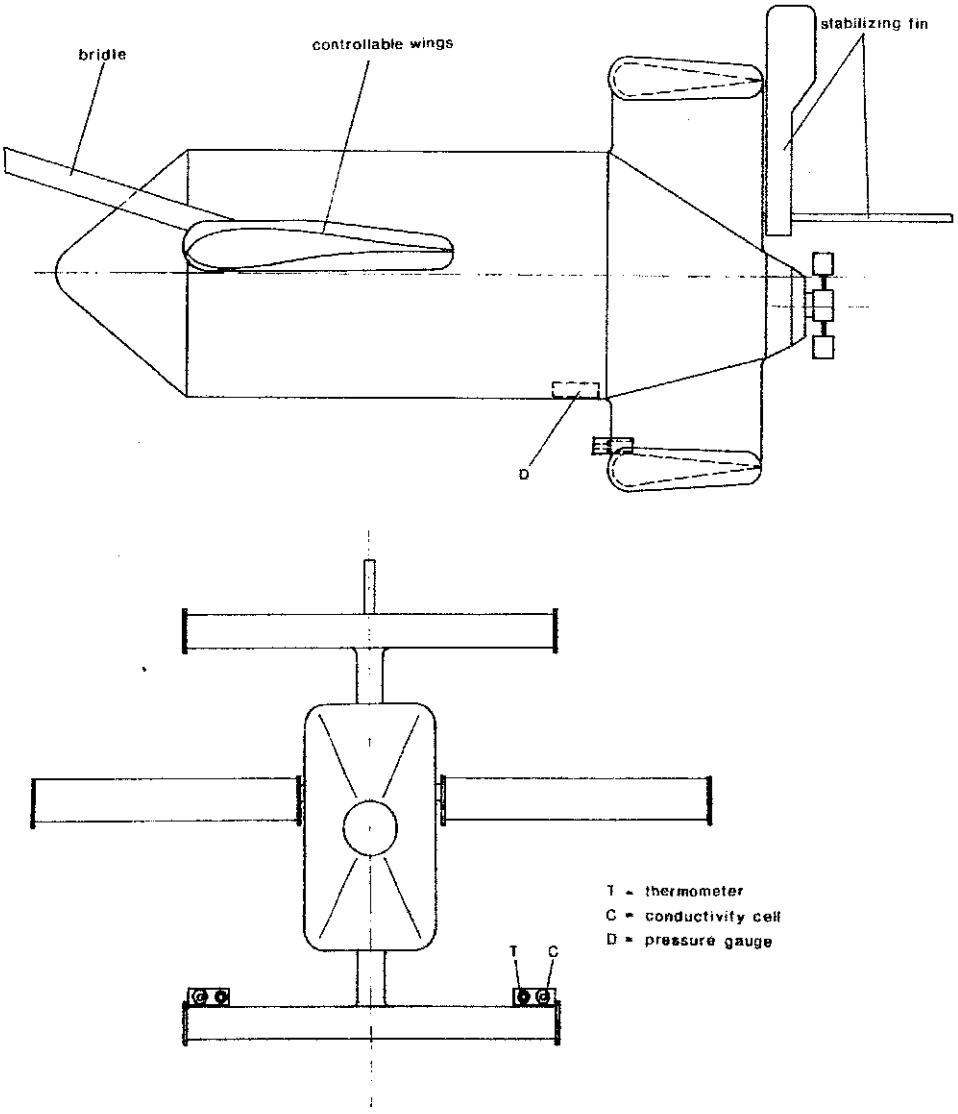

Fig. 2.2.3: Front- and side view of the towed fish, showing the main components of the fish and the scientific sensor configuration during the experiment NOA'81.

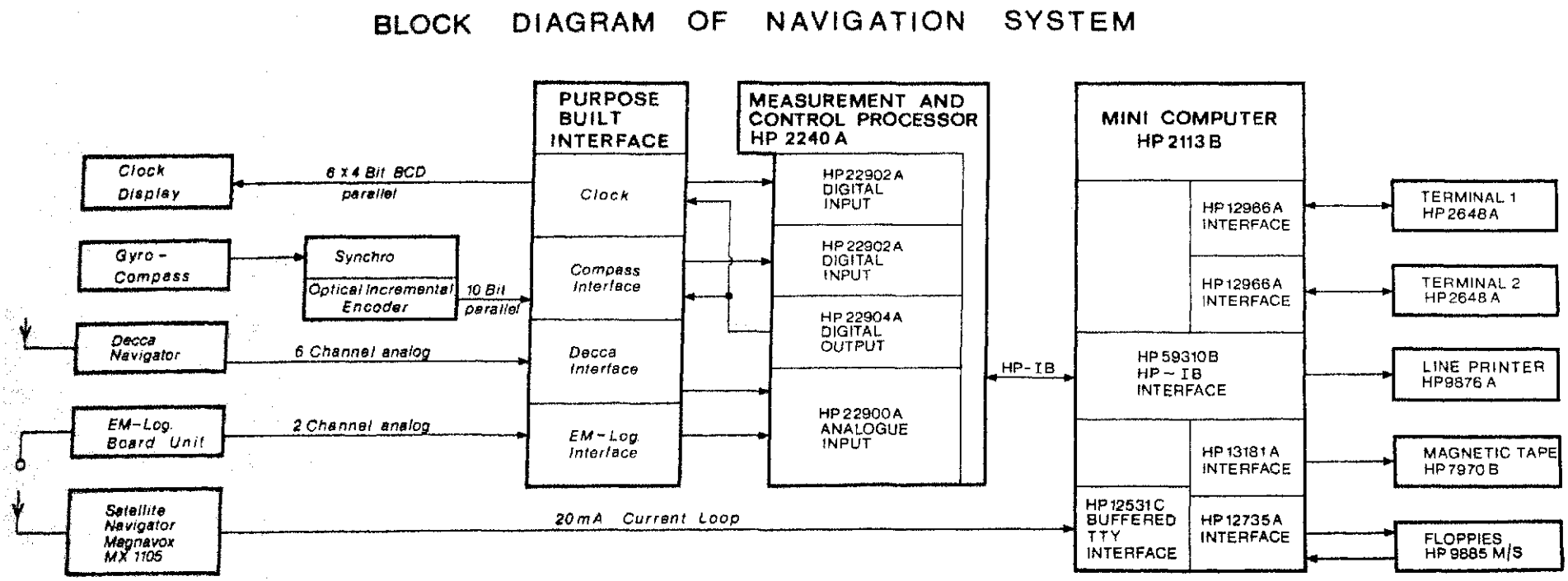

Fig. 2.3.1: Blockdiagram of the scientific navigation system, including data sources, main computer and data storage peripherals.

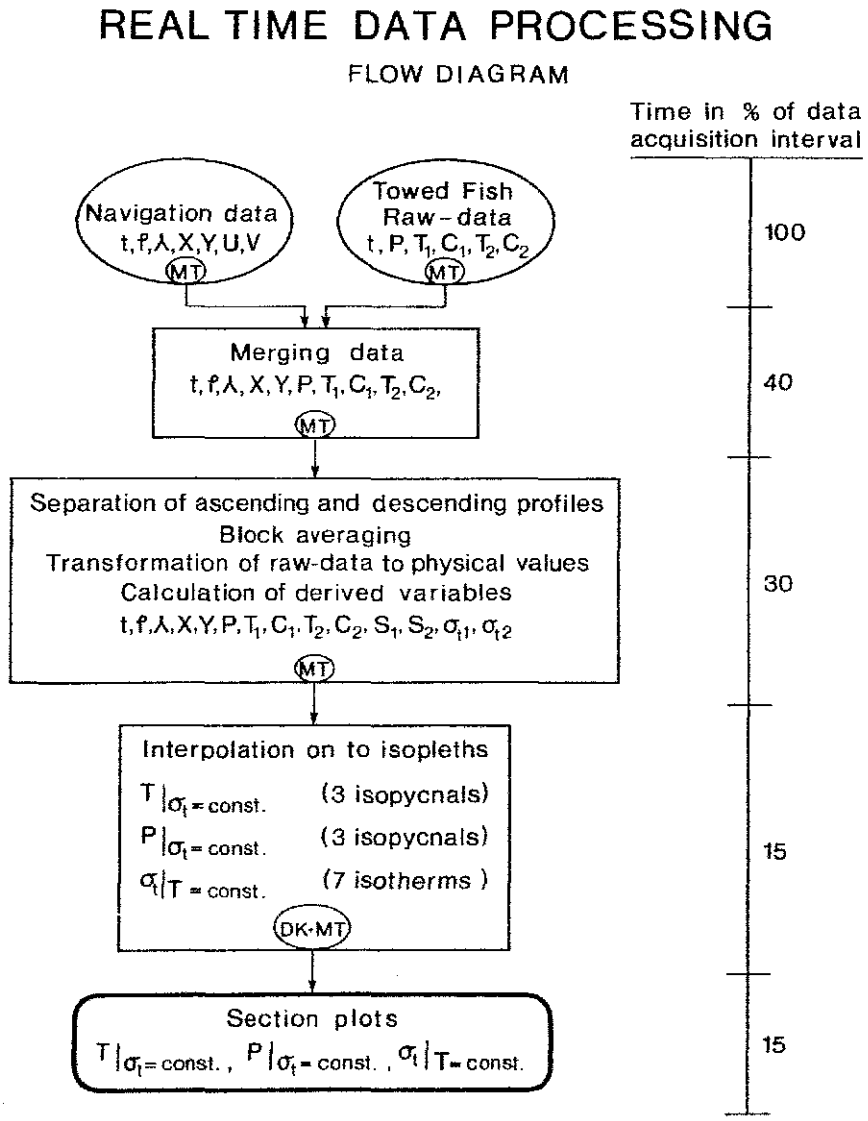

Fig. 2.4.1: Blockdiagram of on-board real-time data processing and timing diagram. The final output was used to control the survey pattern.

3. THE EXPERIMENT

The long-term field programme was designed to make a series of long sections measuring the temperature, salinity and density field in the seasonal boundary layer during different seasons of the year. A detailed study of the three-dimensional thermohaline variability at the North Atlantic Polar Front was incorporated in these long sections.

The undulation of the fish was set to a sawtooth waveform with turning points close to the surface and at 80 metres. A ship's speed of about 4 - 5 metres per second and a mean ascent/descent rate of 2 metres per second gave a wavelength of about 500 metres. A typical example of the track is shown in figure 3.1.

The data sampling rate (16 data cycles per second) gave a mean vertical resolution of 12.5 cm.

3.1 The Long Sections

For the long sections we chose two standard tracks which were planned to be surveyed in different years and at different seasons (figure 3.1.1).

The Azores - English Channel section starts at the shelf edge of the western approaches to the English Channel at about 48°15' N, 10°40' W, passes through the position of Ocean Weather Ship "R" at 47° N, 17° W and finishes at the eastern end of the Azores' island São Miguel at 37°50' N, 24°50' W.

The section Azores - Greenland starts at the western end of São Miguel at 37°50' N, 25°55' W heading towards the southern end of Greenland, avoids the direct pass over of the relatively shallow Chaucer Bank at 43° N, 29° W, by passing through the point 43° N, 30° W and passes Ocean Weather Ship "C" at 52°40' N, 35°30' W and continues in the same direction until the 10 °C isotherm reaches the surface, which was found in 1981 at 55° N, 37° W.

The high spatial resolution covers a spectral range from 2500 km which is the length of a standard section to the Nyquist wave length of 1 km, which was twice the distance between single profiles. With this range gyre-scale, eddy-scale as well as mesoscale structures are resolved.

The depth range from 0 - 80 m includes the mixed layer and the diurnal thermocline and at least in the summer the upper part of the seasonal

thermocline. As the system works at full ship's speed of about 5 ms^{-1} the measurements are as synoptic as reasonably possible. The high data density ensures the observed structures a high statistical significance.

The timetable of the 1981 expedition allowed comparison of measurements of the same area in a time range of single days to 2 months (figure 3.1.2). The time interval between the northward and southward leg of the Azores-Greenland section is only some days north of the Polar Front and about 2 weeks south of it. The return leg from the Azores towards the English Channel (10th to 18th September) was made 2 months later than the outward leg (14th to 18th July).

3.2 The Polar Front Survey

The area for the frontal survey was roughly fixed during the long section B102 from the Azores to the outcrop of the 10 °C isotherm at about 55° N. The region of strongest horizontal thermohaline contrast was found near 51° N, 35° W in the vicinity of OWS "C". This region was thought to be the edge of the warm water sphere, separating the relatively warm water of about 15° C at the surface from the relatively cold water with 11 °C or less. The sea surface salinity decreased from 35.4 x 10^{3} to less than 34.8 x 10^{3} within 50 kilometres.

A set of two east-west sections (C301, C305 combined with C303) each about 400 kilometres long (figure 3.2.1) should give some information about the principle synoptic-scale structures in this region. These sections form a nearly rectangular box of 400 km x 200 km, 5° W of the Mid-Atlantic Ridge south of the Gibbs-Fracture-Zone.

A more detailed study of the frontal structures was carried out at 51° N, 35° W. This part of the experiment consists of 10 sections, each about 75 km long and about 10 km apart. These sections were orientated almost perpendicular to the axis of the front. Unfortunately the original orientation had to be changed after section C312 due to bad weather conditions.

Table 3.1 shows a summary of all NOA'81 sections with start and end position, start and end time and the mean ship's heading.

In addition to the sections, a deep (600 m) section with conventional CTD dips was carried out to explore the vertical extension of the observed features.

Table 3.1: List of all NOA'81 SEA ROVER sections with start and end time, start and end position, and the nominal ship's heading.

Section	Start of Section			End of Section			Orientation
	Day no. (GMT)	Longitude (W)	Latitude (N)	Day no. (GMT)	Longitude (W)	Latitude (N)	
B101	195/0810	11°28.02'	48°29.94'				
B101	196/0932	16°59.73'	47°00.48'				OWS "R"
B101				199/0708	24°56.55'	37°51.43'	
B102	202/1012	25°56.42'	37°50.32'				
B102	206/1303	35°33.90'	52°40.80'				OWS "C"
B102				207/0518	37°00.17'	55°04.02'	northernmost point
B103	207/0518	37°04.02'	55°04.02'	208/1300	34°53.50'	50°19.06'	
C301	208/1300	34°53.50'	50°19.06'	209/0452	31°00.22'	50°15.67'	"90°"
C302	209/0452	31°00.22'	50°15.67'	209/0930	30°55.69'	51°00.48'	"360°"
C303	209/0930	30°55.69'	51°00.48'	210/1000	37°04.36'	51°11.51'	"270°"
C304	210/1000	37°04.36'	51°11.51'	210/1420	37°06.29'	50°44.97'	"180°"
C305A	210/1420	37°06.29'	50°44.97'	210/1934	35°54.65'	50°45.69'	"90°"
C305B	210/1934	35°54.65'	50°45.69'	210/2110	35°58.42'	50°34.92'	"180°"
C305C	210/2110	35°58.42'	50°34.92'	211/0800	33°16.16'	50°39.04'	"90°"
C305D	211/0800	33°26.16'	50°39.04'	211/1116	33°38.94'	50°25.21'	"235"
C306A	211/1330	33°43.89'	50°25.80'	211/1726	34°44.45'	50°28.04'	"270°"
C306B	211/1726	34°44.45'	50°28.04'	211/2118	35°18.89'	50°05.01'	"225°"
C307	211/2134	35°19.83'	50°04.85'	212/0412	35°53.96'	50°33.02'	111 "315°
C308A	212/0142	35°53.96'	50°33.02'				112A "135°"
				212/0526	35°30.55'	50°19.96'	
C308B	212/0841	35°48.58'	50°35.67'	212/1052	35°30.98'	50°24.16'	1L2B "135°"
C309	214/0946	35°21.05'	50°19.61'	214/1125	35°08.02'	50°11.25'	
C310	214/2010	34°55.46'	50°04.82'	215/0340	35°49.00'	50°38.13'	"315°" section
C310A	215/0340	35°49.00'	50°38.13'	215/0436	35°44.10'	50°43.34'	~50° turning point
C311	215/0436	35°44.10'	50°43.34'	215/0914	35°00.09'	50°14.57'	"135" section
C311A	215/0914	35°00.09'	50°14.57'	215/1002	34°53.39'	50°19.26'	~25° turning point
C312	215/1002	34°53.39'	50°19.26'	215/1500	35°39.45'	50°45.25'	"315° section
C312A	215/1500	35°39.45'	50°45.25'	215/1542	35°37.71'	50°49.72'	~25° turning point
C313	215/1542	35°37.71'	50°49.72'	215/2024	34°39.73'	50°35.52'	"110°" section
C313A	215/2024	34°39.73'	50°35.52'	215/2106	34°36.58'	50°40.37'	~10° turning point
C314	215/2106	34°36.58'	50°40.37'	216/0158	35°40.96'	50°58.03'	"290°" section
C314A	216/0158	35°40.96'	50°58.03'	216/0222	35°38.80'	51°00.42'	~10° turning point
C315	216/0222	35°38.80'	51°00.42'	216/0708	34°34.92'	50°45.39'	"110°" section
C315A	216/0708	34°34.92'	50°45.39'	216/0752	34°32.83'	50°50.87'	~20° turning point
C316	216/0752	34°32.83'	50°50.87'	216/1200	35°29.12'	51°03.96'	"290°" section
C316A	216/1200	35°29.12'	51°03.96'	216/1236	35°27.58'	51°08.94'	~20° turning point
C317	216/1236	35°27.58'	51°08.94'	216/1802	34°05.39'	50°50.16'	"108°" section
B104	216/1802	34°05.39'	50°50.16'	220/0852	25°55.48'	38°00.21'	Polar Front - Azores
B105	253/1508	24°29.28'	38°56.20'	257/1042	11°22.08'	48°29.86'	Azores - Lands End

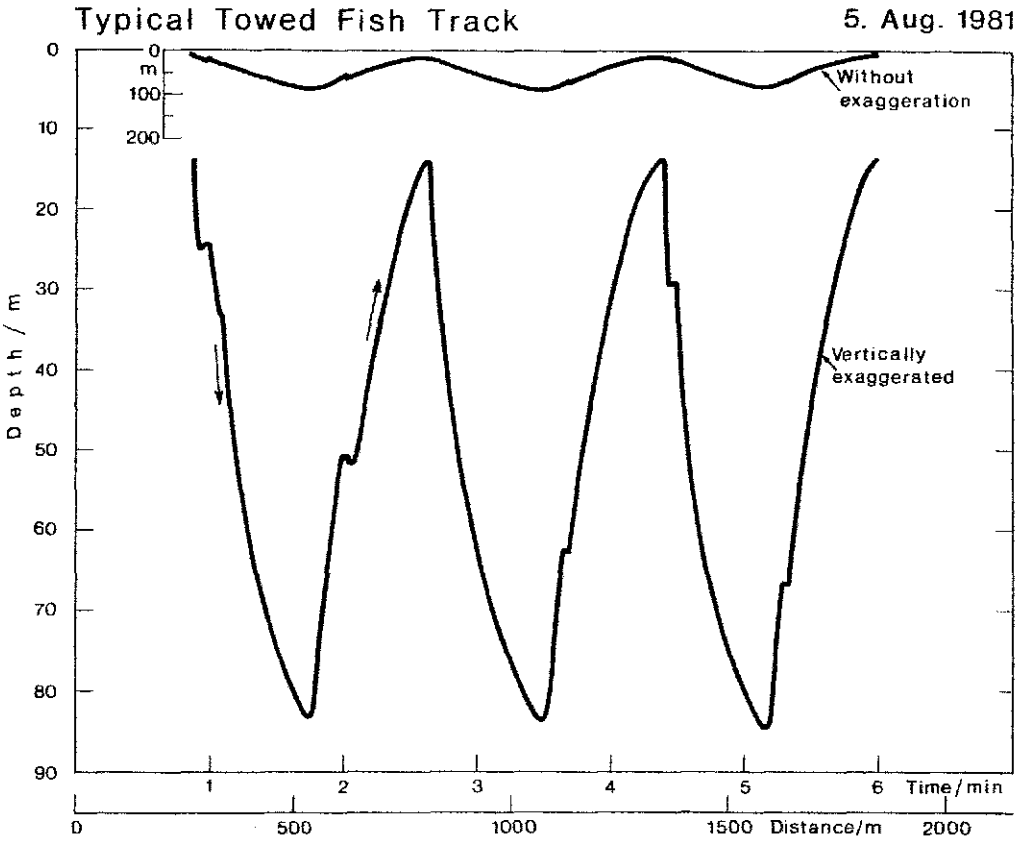

Fig. 3.1: Three cycles of the towed fish undulations showing the period and horizontal resolution of the measurements. The non-exaggerated version gives an impression of the slope of the track.

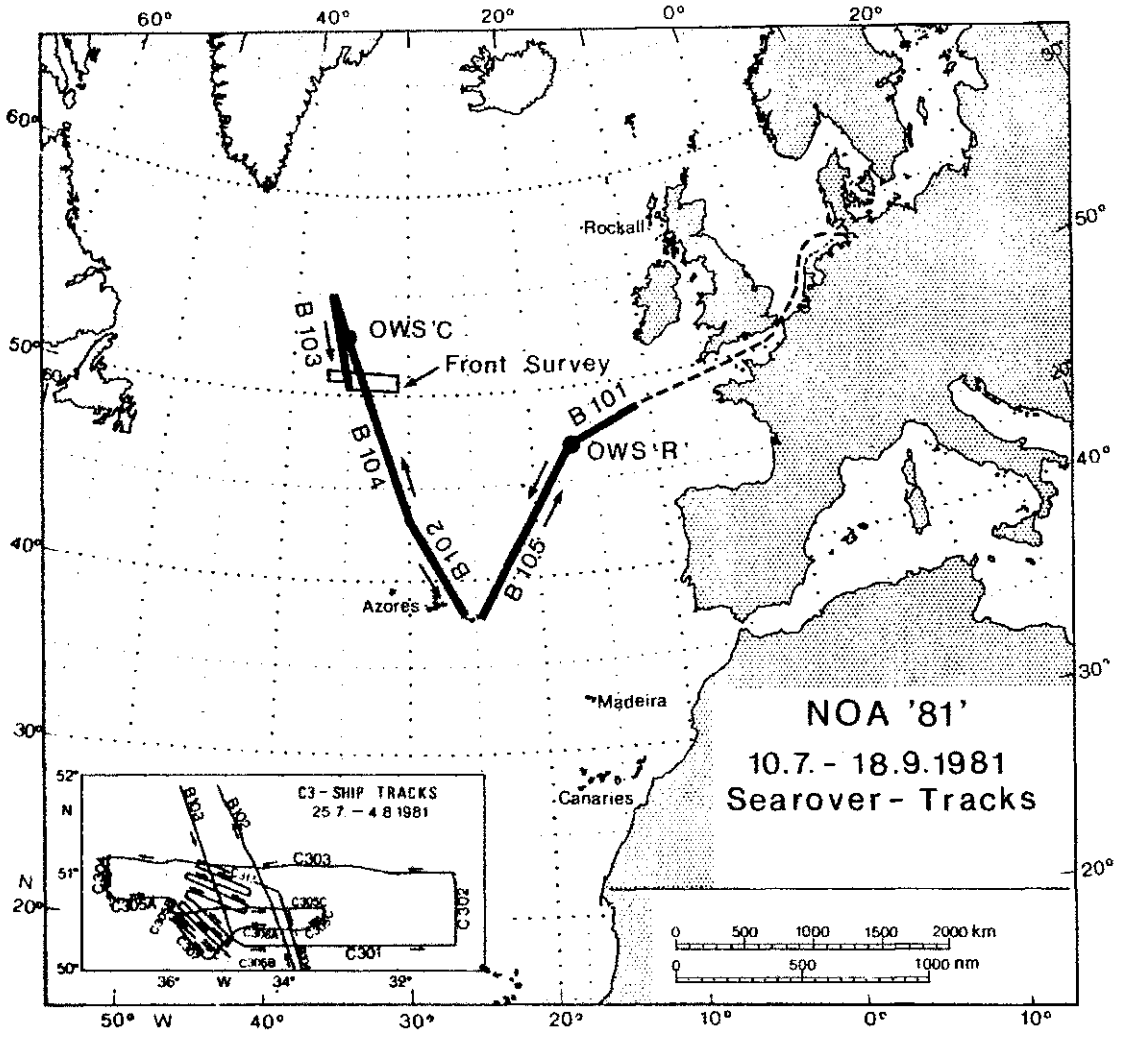

Fig. 3.1.1: Ship's track during the SEA ROVER experiment in summer 1981. In the lower left corner an expanded part of the frontal survey region is shown (see also figure 3.2.1).

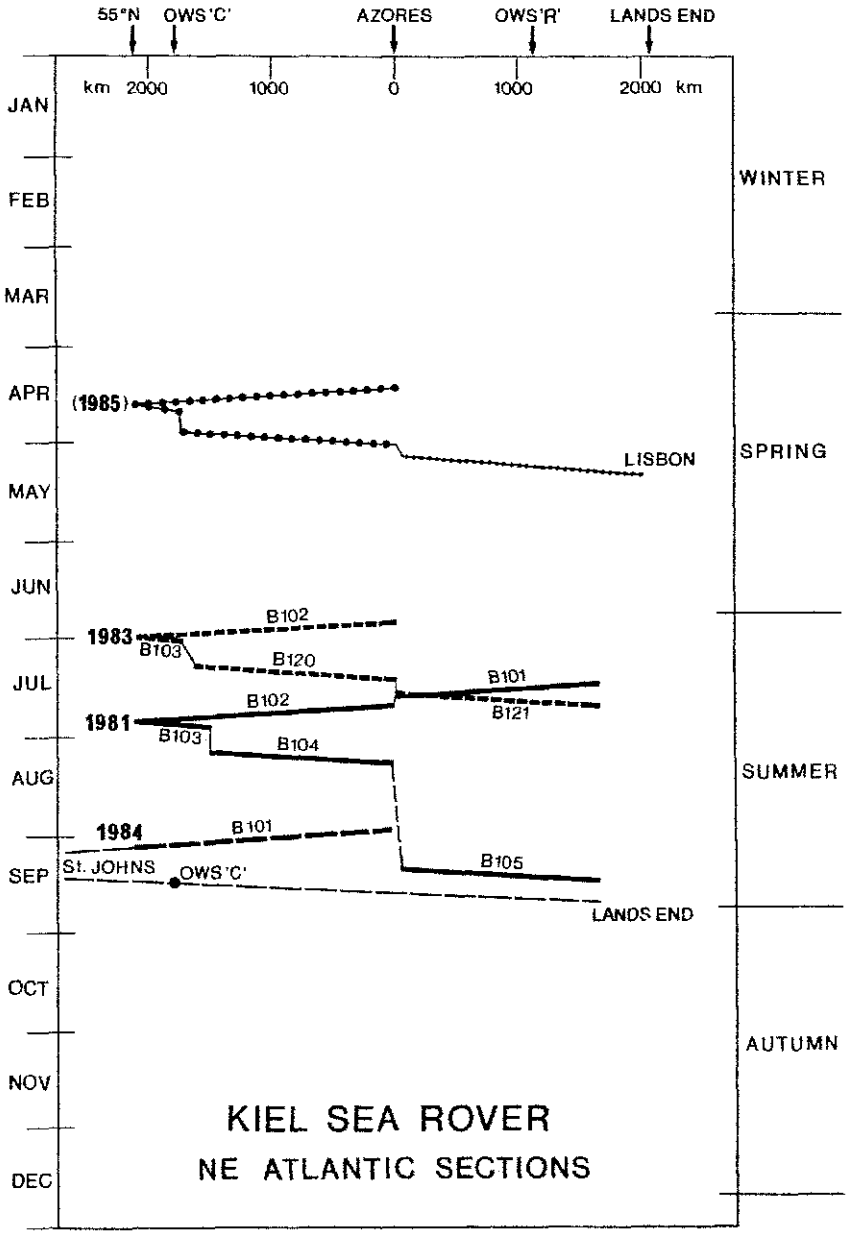

Fig. 3.1.2: Seasonal distribution of long SEA ROVER sections 1981 to 1985. The time of year is presented versus the distance from the Azores (Sao Miguel) along the standard sections. Thin lines indicate SEA ROVER sections which do not follow the standard tracks.

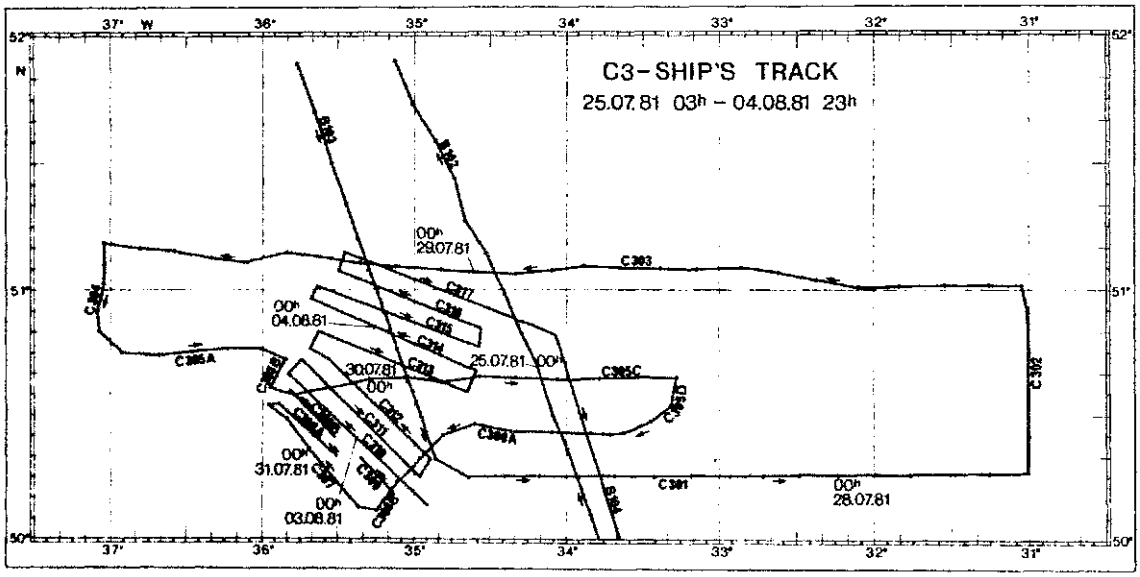

Fig. 3.2.1: Ship's track during the frontal survey in summer 1981.

4. PROCESSING AND REDUCTION OF HYDROGRAPHIC DATA

A flow diagram of the data processing and its products is presented in figure 4.1. The processing described in this chapter is that used on land after the experiment.

4.1 CTD raw data recording

The signals from the pressure sensor, the two temperature and the two conductivity sensors of the CTD-payload were digitized in the underwater unit and written on tape in blocks of 256 16-bit words. 250 words contain 50 cycles with raw numbers from the five sensors stored at the interval of 62.5 ms followed by a 6-word trailer containing the start time of the block and an up/down flag indicating whether the fish was climbing or diving.

4.2 Navigation data recording and correction

On the navigation computer a permanent random access file was arranged with 720 records, one for each 2-minute interval of the day. Every 2 minutes the file was updated with the current navigation data. Absolute and relative navigation data stored in this day-file were dumped onto magnetic tape twice a day for archiving. The ship's drift between satellite fixes was uniformly distributed over the track integrated by the EM-log. Program NAGUT corrected the navigation data between satellite fixes.

4.3 Merging navigation and CTD raw data (1st processing)

The program for the first processing stage called VMRAN formed a time basis by extrapolating the start time of a CTD raw data block for the next 50 cycles by integrating the sampling interval. It searched for the matching 2-minute interval in the navigation files and interpolated the positions linearly. Thus for every 62.5 ms a cycle was created containing explicitly the time, the raw values from the CTD-sensors, the navigation values and the up/down flag.

4.4 Calibration, editing, data reduction, and calculation of derived variables (2nd processing)

In order to minimize the number of output tapes calibration of CTD raw values, editing spikes, data reduction and calculation of derived values were handled by one program called MEDIT.

A time constant correction was applied to the temperature values in order to minimize the mismatch between the temperature and conductivity measurements. Empirical tests yielded a time constant of 85 ms needed to reduce the salinity spikes caused by this mismatch. A description of these tests is given in section 5.2. Then the raw values from the CTD sensors were transformed into physical units using laboratory calibration coefficients in a second order polynomial.

Salinity was calculated from pressure, temperature and conductivity and then filtered with a median-filter (Sy, 1985) with a 5-cycle window to remove spikes without eliminating strong gradients. The data was then averaged over five cycles. The averaged temperatures and salinities were used for the calculation of σ_t for each sensor pair respectively.

4.5 Pressure monotonisation and up-down splitting (3rd processing)

Experience from former Batfish experiments (GATE, Leach et al., 1985) showing significant differences in the signals of the ascending and descending parts of the fish track which suggests separating them. As the fish did not follow exactly the control signal, the turning points had to be determined from the data. Program TURNP performed the following processing.

The up/down-flag, which changed when the control signal switched from dive to climb up or vice versa, could be used as a criterion for starting the search for the next pressure maximum or minimum within a limited number of cycles. During the separation of ascents and descents, cycles which were not monotonous in pressure were dropped. A plausibility check of the hydrographic data also removed single senseless values caused by parity errors in the raw data and substituted them by the preceding value.

The profiles were counted and the number was stored as a label in each data cycle, even numbers for descents, odd numbers for ascents. Ascents and descents were stored in separate files.

4.6 Calibration correction of salinity and pressure (4th processing)

The calibration of the conductivity sensors in the laboratory was not sufficiently exact. The salinities of the hourly samples had to be used for a correction of the calibration. The water sample salinities were compared with CTD salinities in space and time. Using a linear regression performed by program LINREG, correction parameters for a linear transformation were calculated (figure 4.6.1). The calibration of pressure also had to be corrected. This was achieved by using the distribution of pressure at the upper turning point (figure 4.6.2). The pressure values showed a temperature dependent negative offset $\Delta P(T)$.

$$P_{corr} = P + \Delta P(T)$$

The pressure was corrected by adding the offset for the mean surface temperature of a 4-hour file. Using program EICH3 salinity and pressure were corrected and density was recalculated within the new calibrated salinities.

4.7 Elimination of small density inversions (5th processing)

At this stage density was contaminated by inversions due to salinity spikes which could not be removed by the preceding editing methods. A median-filter with a 5-cycle window on density was used to reduce as much of the small-scale noise as possible. Bigger inversions which were observed mainly at the bottom end of the profiles were thought to be an artifact of the slope of the fish-track and therefore they should be eliminated in the 6th processing. For consistancy the salinity was recalculated from temperature and the filtered density. The filtering was done with program MEDFIL and yielded the clean data set, the basis for various further analysis.

4.8 Monotonisation and vertical interpolation (6th processing)

For isopycnic analysis the profiles were monotonized in density and interpolated on constant σ_t-intervals of 0.025 kg m^{-3} with program MONINT. Vertical interpolation onto constant pressure values was performed at intervals of 1.0×10^4 Pa. Isopycnal or isobaric surfaces were extracted from the vertically interpolated profiles by appending and extraction routines EDIT2 and EXTRAC.

4.9 Calculation of spacing between isopycnals (7th processing)

Using program PRESDF isopycnal spacing was determined by calculating the pressure differences between σ_t surfaces which were 0.1 kg m^{-3} apart, within the same routine the depth of each isopycnal relative to a chosen reference isopycnal was calculated.

4.10 Objective analysis (8th processing)

The objective analysis method applied to this data set is described in Woods et al. (1981). Briefly, the method works as follows: Firstly the two-dimensional auto-correlation function (biased) of the data to be analysed was computed. A weighting function (fig. 4.10) was derived by smoothing this raw auto-correlation function, multiplying it by a conical taper and setting negative values to zero. This weighting function would reach a value of zero within a finite number of grid lengths, normally less than eight, depending on the correlation distance. The weighting function was then used in a successive-correction objective analysis scheme. In order to avoid influencing the results by statistics with different characteristics the computation of the weighting function carried out separately for each parameter and each surface. The appplied program for objective analysis was called OBANA.

DATA PROCESSING FLOW DIAGRAM

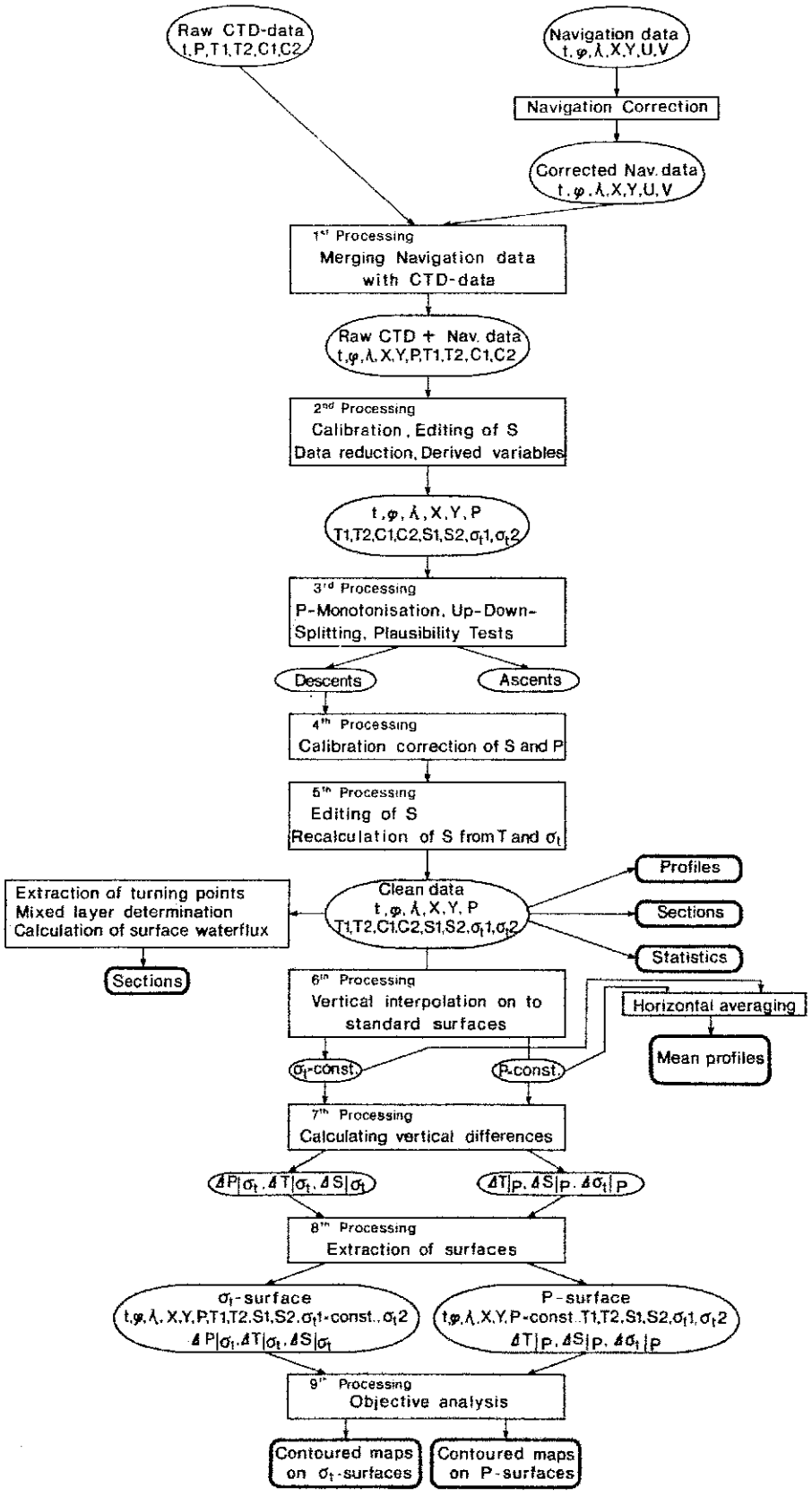

Fig. 4.1: Flow diagram of the data processing of the towed fish - CTD - data. Ovals contain stored processing stages, rectangles are programs and rounded boxes indicate standard products.

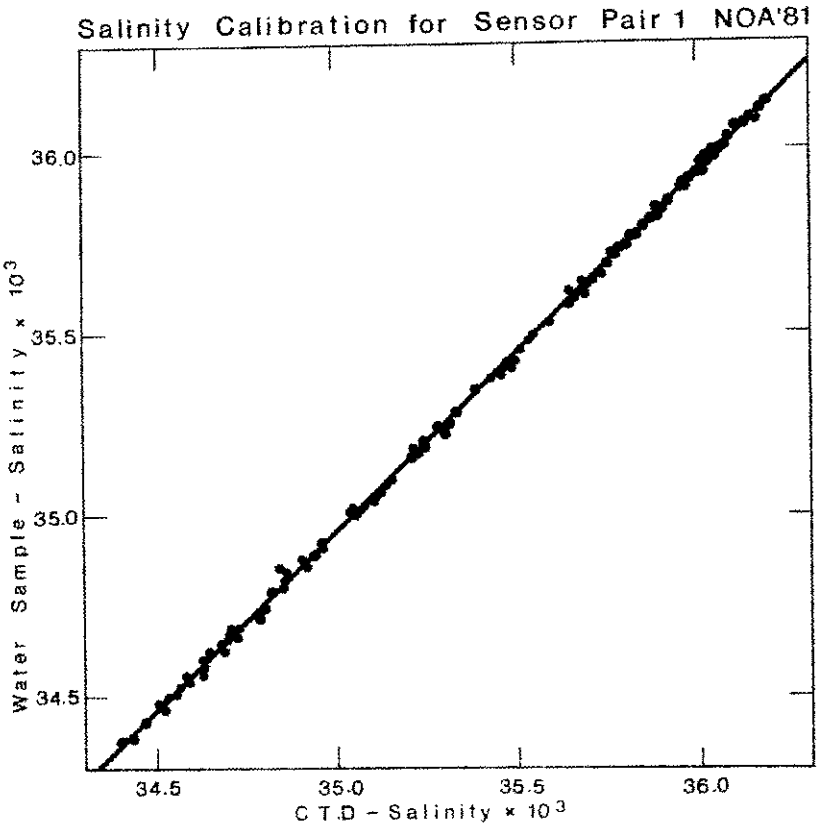

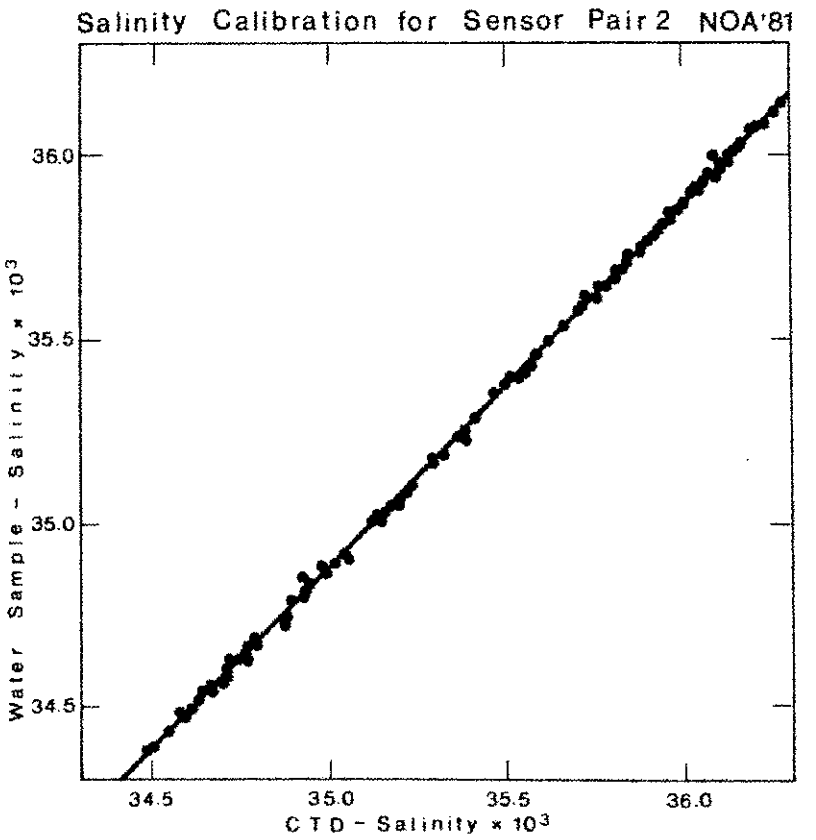

Fig. 4.6.1: Linear regression of salinities of salinometered water samples and raw calibrated CTD-data presented separately for each sensor pair. The slope and offset of the regression curve ⟶ the final calibration of CTD-salinities.

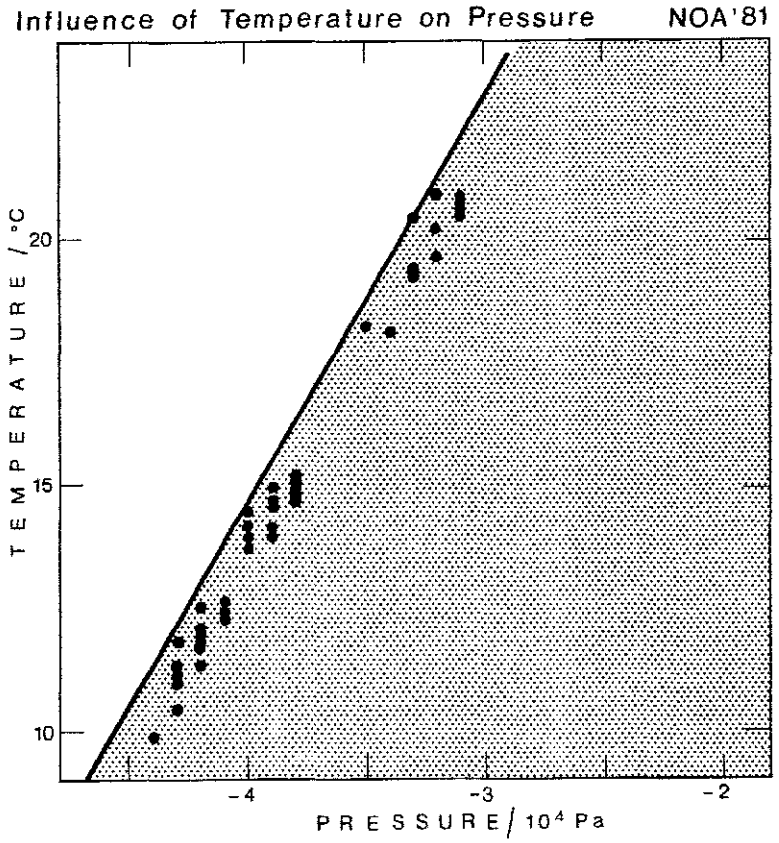

Fig. 4.6.2: Sea surface temperatures and displayed pressure values where the fish reached the sea surface. The tangential line was used to correct the temperature-dependent offset of the pressure gauge.

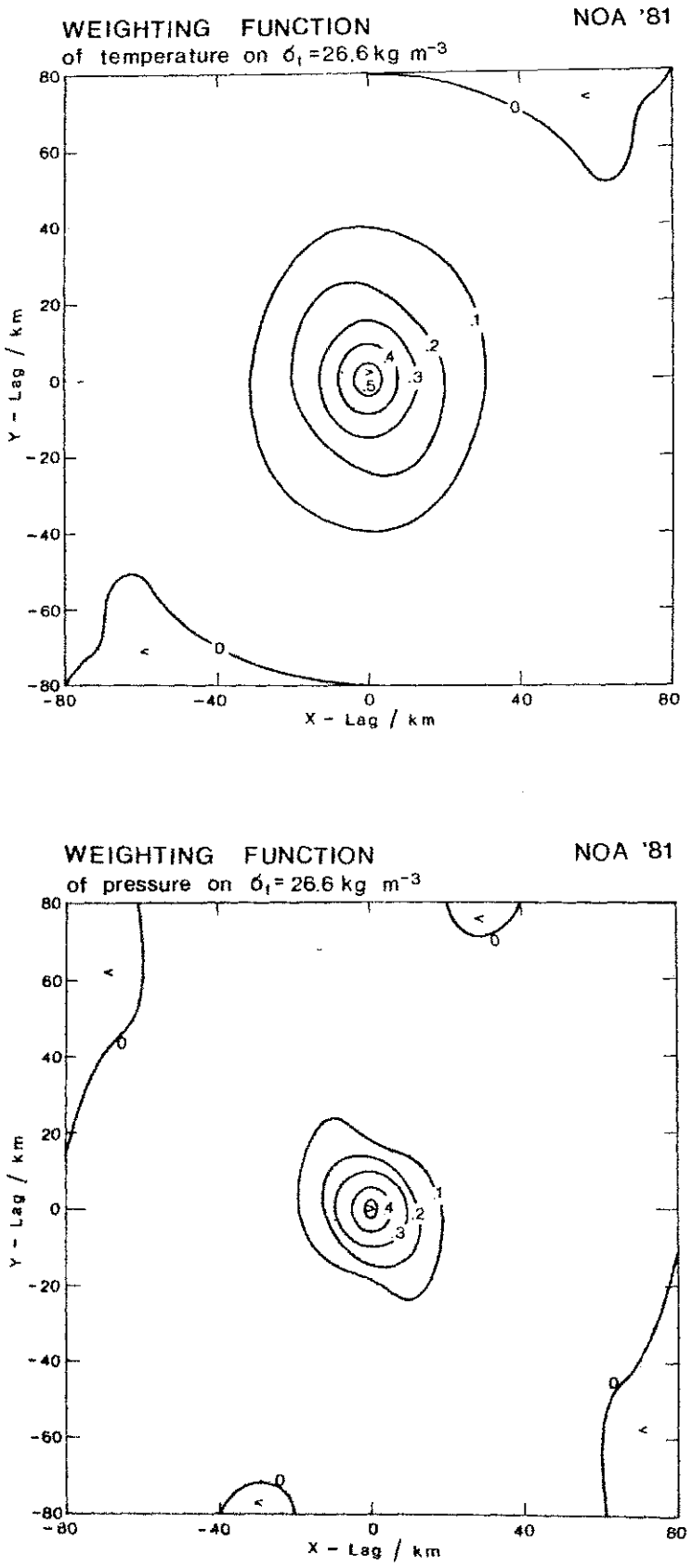

Fig. 4.10: Examples of weighting functions of temperature and depth of isopycnal σ_t = 26.5 kg m^{-3}, derived from raw autocorrelation functions of the frontal survey.

5. ANALYSIS OF ERRORS

Before starting to present the results of the data analysis, the careful error analysis carried out is discussed in this chapter.

5.1 Measurement errors and corrections applied during data processing

In all CTD measurements, random errors arise from the electronic noise and the digitizing interval. Systematic errors have been caused by the response time of the sensors due to rapidly changing fields and by the inaccuracies involved in the calibration of the sensors.

An ME-Multisonde was used (MS 38) which was equipped with one pressure gauge and pairs of thermometers (Rosemount PT 200) and large conductivity cells. The accuracies guaranteed by the manufacturer are listed in table 1. Due to technical reasons we reduce the orginal 16-bit resolution to 15 bit, which led to a digitizing interval of 2 mK, 0.002 mS/cm and 0.02 dbar for the thermometers, conductivity cells and the pressure gauge.

The systematic errors occuring turned out to be much more important then these random inaccuracies, which we can therefore neglect in our error analysis.

A major problem for the accuracy of the measurements was the inefficient calibration. The sensor calibrations were carried out by the manufacturer and it turns out, that they over-estimated the accuracy. For pressure and salinity a way was found to improve the calibration, for temperature no correction could be found for the inaccuracies detected by comparing both sensors with each other.

The other important source of inaccuracy was the heat flow, especially in the thermometers and the pressure gauge.

Temperature and conductivity were measured with two sensors each. As both sensor pairs can be treated as independent measurements of the same water, the analysis of the difference between them gave us additional information about the accuracies and the impact of applied correction and editing methods upon the measurements.

In the following sections the problems and the attempt to solve them are described for each parameter respectively.

Pressure

A systematic error of the pressure measurement is caused by the rapid change of temperature of the surrounding water. The pressure strain gauge of the CTD-probe is mounted inside the fish's hull. Its good thermal contact to the pressure vessel which has a much larger thermal capacity than the sensor itself damp the temperature change of the sensor.

Small holes on the side of the fish's body provide the contact of water inside with the outside. Although we have no quantitative measurement of the temperature in the interior of the fish, we assume the temperature range outside the fish of 5 to 8 K between the turning points of a profile to be suppressed by a factor of three, which is supported by the results of an earlier test cruise. The error in the pressure signal could be estimated to approximately 0.1×10^{4} Pa/K.

We decided to treat the ascending and descending parts of the fish track separately to get consistant data sets which are not affected relatively by this systematic error.

The effect of dynamic pressure, caused by the passage of the fish through the water is also a systematic error estimated for a towing speed of 5 m s^{-1}, according to $p = 1/2\ \rho u^{2}$ is of order 1×10^{4} Pa.

The calibration of the pressure sensor done by the manufacturer turned out to be incorrect. It showed a negative offset. The fact that the towed fish often reached the sea surface allowed this error to be corrected. A scatter diagram of the pressure at the upper turning points versus the temperature along the sections was plotted (figure 4.6.2). It was assumed, that the minimum pressure at different temperature values is the sea surface pressure, a statement which is supported by frequent sightings of the fish at the surface. The solid line in this graph was used to correct the data by shifting the whole profile according to its sea surface temperature value. To overcome the difficulty that not all profiles reached the surfaces the profiles of each four-hour section were shifted equally according to the four-hour mean surface temperature. We also took account of the fact, that the pressure sensor is 0.7 m below the top of the fish.

Taking these details into account yields an absolute error of $\pm 0.2 \times 10^{4}$ Pa around the upper turning point where the sea surface is a relatively well-defined reference level. In the deeper layers the uncertainties increase towards the lower turning point where the combination of

thermal effects, sensor-lag, calibration uncertainties, and dynamical pressure add up to an error of $\pm$ 1.6 x 10^4 Pa.

Temperature

Before the calibration of the temperature signal in the 2nd processing stage, a simple time constant correction for the thermometers was carried out. The algorithm applied to the data is shown in the following equation;

$$T = T_m + \tau \frac{\Delta T_m}{\Delta t}$$

where T_m is the measured temperature and τ the time constant of the thermometer. This time constant was estimated empirically by trying to reduce the spikes in the computed salinity signal. A time constant of about 85 ms (1.36 raw data cycles) was found to be most appropriate. This value is supported by the values given by the Rosemount company of about 120 ms. Nevertheless it was not possible to get rid of all salinity spikes and so it was decided to edit salinity separately.

By horizontally averaging mean and standard deviation profiles of the difference $T_1 - T_2$ were calculated. They are presented in fig. 5.1.1a using raw data and in fig. 5.1.1d calculated from data that had passed all data processing stages. A systematic mean difference of - 10 mK limits the quality of the calibration. Why the difference becomes positive in the high gradient zone around 20 m is not understood. Randomly distributed differences were found along the whole profile, increasing proportionally with the local vertical temperature gradient.

These differences can be produced alone by rolling movements of the fish, because their magnitude is consistent with the observed roll angles and the vertical temperature gradient.

The comparison of fig. 5.1.1a and fig. 5.1.1d show that the data processing did not change the statistics of the temperature measurement. The mean profiles are identical considering the depth shift due to correction of the pressure offset. The standard deviation is slightly diminished after block averaging.

It is not clear how the temperature changes along the sensor cables, which were partly inside the fish, will effect the measurements, but it was

assumed to be negligible. From the manufacturer of the CTD sonde we received the following accuracies:

Absolute accuracy	± 10 mK
relative accuracy	± 3 mK

Conductivity

The main source of error in the conductivity signal is due to calibration inaccuracies. It was assumed, that the temperature effect was negligible and fouling by drifting material does not occur. We did not try to correct the conductivity itself, but the salinity as described in the following section.

Salinity

It was mentioned above that the calibration of the conductivity sensors turned out to be inaccurate. To improve the accuracy we compared salinities of water samples, taken every hour at hull depth with CTD-salinities matching in time and space. Data pairs from regions with high vertical or horizontal gradients were rejected. Data from low variability regions were used for a linear regression (fig. 4.6.1) calculating the coefficients for a linear transformation to correct the measured salinity values. The residual of the regression analysis was 0.023×10^{-3}.

The mismatch in the response of the thermometers and conductivity cells was the most severe problem in the data set. The time lag of the thermometer caused by a time-constant of about 120 ms (a value given by the manufacturer) is an intrinsic property of the sensor, whereas the water-exchange time in the conductivity cell is a function of electrode spacing and the speed at which the fish penetrates the water. We decided to use an empirical method to minimize these effects by applying a temperature time constant correction of $\tau = 0.085$ s. This value was determined by minimizing the difference in temperature and salinity at those parts of the ascending and descending parts of the profiles, which were close to the turning points of the fish. In these regions, horizontal differences in the parameters should be small. The second criterion for the choice of this value was the symmetrical distribution of the remaining salinity spikes along the mean profiles.

This correction also reduced the size of salinity spikes but could not eliminate them all. We decided to use a median filter (Sy, 1985), a technique

which eliminates spikes but does not affect sharp gradients. The width of this filter was chosen to have a minimum effect on the statistics of the profiles. Furthermore we block-averaged the data over the range of the filter width.

Another use of the median filter upon density and a re-iteration of salinity from temperature and filtered density did not have much effect in the improvement of the data.

In spite of this editing scheme there are still remaining single spikes mainly in the zone of high vertical gradients just below the mixed layer which was also the region of maximum diving speed. Most of the remaining spikes have magnitudes less than 0.02×10^{-3} and only very few spikes exceed 0.07×10^{-3}.

The effect of all the correction procedures on the salinity data can be seen by comparing raw data and ready processed average profiles of the difference $S_1 - S_2$ (fig. 5.1.1b and fig. 5.1.1.e). The recalibration shifted the mean profile towards the zero line. Its vertical structure was not changed significantly. The deviation from zero remains less than 0.01×10^{-3} at the upper boundary of the thermocline and values between 0.02 and 0.015 at the deeper parts to values around 0.01×10^{-3}, which is in the order of magnitude which could be expected for differences due to rolling of the instrument.

The comparison of water sample salinities with the edited CTD-salinities along section B102 (figure 5.1.2) shows to which extent the absolute accuracy of salinity could be improved. The difference between sensor pair 1 and sensor pair 2 remains mainly within the limits of $\pm 0.01 \times 10^{-3}$. The water sample-CTD-differences do not exceed $\pm 0.01 \times 10^{-3}$, except in regions of high horizontal gradients, where the non-perfect synchronization of sampling and CTD-measurements may have led to a mismatch in the resulting salinities.

Density

The errors in the density (σ_t) are an accumulation of the errors of temperature and salinity since density is a function of salinity and temperature

$$\varepsilon_{\sigma_t} = \frac{\partial \sigma_t}{\partial s} \varepsilon_s + \frac{\partial \sigma_t}{\partial T} \varepsilon_T ,$$

with $\varepsilon_s = 0.02 \times 10^{-3}$ and $\varepsilon_T = 0.01$ K the errors in salinity and temperature. Tests for different regions and different vertical gradients reveal values of ε_{σ_t} to be less than 0.005 kg m^{-3}.

As for temperature and salinity mean profiles of the differences $\sigma_{t1} - \sigma_{t2}$ are presented in fig. 5.1.1c and 5.1.1f. As with salinity the editing reduces the variability of the sensor differences to the rolling range.

5.2 Numerical estimation of uncertainties in derived quantities.

Derived quantities such as salinity and density were influenced by the different time response of thermometers and conductivity sensors. Following various non-analytical stages in the data processing scheme, the uncertainties in the derived variables can only be estimated by a numerical experiment. Therefore a synthetic set of profiles of temperature and salinity were generated and from these the corresponding conductivity profile was derived. The shape of the profiles were as close to the observed profiles as possible, although they are simplified due to their analytical construction. The salinity profile was constant with depth and the initial temperature profile has a mixed layer and decays exponentially below 20 m with realistic vertical gradients. The initial set of profiles is shown in figure 5.2.1.

The time constant of the thermometer was given by the Rosemount Company to 120 milliseconds and in a simple laboratory test this value was proved to be accurate.

The flushing time of the conductivity cell varies with the penetration speed of the fish. Typical parameters were a towing speed of 5 m s^{-1} and a diving rate of 2 m s^{-1} resulting in a flushing time of about 10 milliseconds.

With these values in mind, we filtered the initial temperature profile according to:

$$T = T_m + \tau_T \frac{\partial T_m}{\partial t} \qquad (5.2.1)$$

where T is the initial temperature, τ_T = 110 milliseconds the difference in the response characteristic between temperature and conductivity and T_m the resulting (measured) temperature.

In finite differences this equation is written as

$$T_{(i)} = T_{m(i)} + \frac{\tau_T}{\Delta t} \left(T_{m(i)} - T_{m(i-1)} \right) \qquad (5.2.2)$$

with Δt = 62.5 milliseconds given by the sampling rate of the CTD. From this equation an expression for $T_{m(i)}$ was derived:

$$T_{m(i)} = \frac{1}{1+\alpha} T_{(i)} + \frac{\alpha}{1+\alpha} T_{m(i-1)} \qquad (5.2.3)$$

with $\alpha = \frac{\tau}{\Delta t}$ = constant.

The initial condition for $T_{m(i)}$ with i=1 is given by $T_{m(1)} = T_{(1)}$, which is true for the mixed layer. The conductivity profile remains unchanged. The data were processed following the scheme of the data processing flow diagram (figure 4.1) and at each stage the resulting salinity and density profile was compared with the initial profiles. Two numerical experiments were carried out, the first with a constant diving rate of 2 m s^{-1} and the second with a non-uniform diving rate, which varies between 1 m s^{-1} and 4 m s^{-1} with the maximum speed in the region of the strongest vertical gradient (at 20 m). The diving rate in the second experiment was tuned to be similar to the diving characteristics of the fish during the NOA'81 expedition. The first step in the data processing was the application of the empirically estimated time constant τ = 85 milliseconds to the temperature data. Figure 5.2.2 shows the salinity difference between the initial profile and the derived salinity for both experiments. In this stage (Ia for constant diving speed) the variable diving rate (IIa) led to an increase of the maximum salinity error by a factor of two. The range, in which the salinity error exceeds 0.01 x 10^{-3} is concentrated in the top 8 m

of the thermocline for case (Ia) and about 15 m for case (IIa). The median filter (Ib, IIb) had no effect on these profiles, but the following block average (figure Ic, IIc) can shift the 'error region' into the mixed layer which might lead to an error in the determination of mixed layer depth.

Remaining inversions in the density profile caused by the weak slope of the fish-track at the lower turning points were eliminated by applying the median filter also to the density profile, and salinity was re-iterated from the resulting density and the temperature profile (figures Id, IId). The results of this experiment are shown in figure 5.2.3 where ε_s, the error in salinity is plotted as a function of $\partial T/\partial z$. For case (I) with a constant diving rate of 2 m s^{-1} the error in salinity is a linear function of the rate of change of temperature, and ε_s is only greater than 0.02 in regions, where $\partial T/\partial z$ exceeds 0.45°K m^{-1}. For case (II) the salinity error exceeds 0.02 at $\partial T/\partial z$ greater than 0.25°K m^{-1}.

Temperature gradients of this magnitude (0.25°K m^{-1}) were observed not only at the top of the pycnocline, but the anomalously high diving rates were only at present in the top 30 m of the fish track, whereas in the remaining parts of the profile the diving speed was about 2 m s^{-1}. Therefore errors in salinity caused by the nonperfect time-constant correction were estimated to be less than 0.02 x 10^{-3} for the major fraction of the profiles, and only very close to the top of the seasonal thermocline the error may reach 0.05 x 10^{-3}.

Where temperature inversions occur, the error in salinity is expected to be less than 0.02 x 10^{-3}, assuming that the diving rate was about 2 m s^{-1} over the depth range of the inversion.

The density profile is also influenced by the mismatch in the time response of the thermometer and conductivity cell. Therefore the same procedure was carried out for density and the result is shown in figure 5.2.4. The errors in density were remarkably reduced during the processing stages; nevertheless the maximum error in density is 0.025 kg m^{-3} at constant diving speed (figure 5.2.3 case Id) and about 0.05 kg m^{-3} at variable diving speed. This error is limited to the top of the pycnocline and case IId can be treated as a worst case example for the top 10 metres of the pycnocline. Everywhere else the error in density would be less than 0.01 kg m^{-3}.

The errors in the density profile would also influence the spacing between pairs of isopycnals, which were derived in the 7th processing stage

(figure 4.1). Firstly the interpolation onto standard density surfaces being 0.025 kg m^{-3} apart was carried out for the initial density profile and the final editing stage. Afterwards the pressure difference between density surfaces being 0.1 kg m^{-3} apart was determined, and the resulting difference between the true isopycnic spacing and the final product (after editing) is presented in figure 5.2.5 and 5.2.6. Except for the top of the seasonal pycnocline, the error in isopycnic spacing in this model is close to the vertical resolution (12.5 cm). Nevertheless, in the region of strongest vertical gradients this error may exceed 20 % of the true spacing for the case of non-uniform diving speed. Below this region the error in isopycnic spacing is less than 5 %. The accuracy of isopycnic spacing resulting from the mismatch in the time response of our sensors is $\epsilon_{\Delta p} = 0.2$ m.

This numerical study has also shown that a reduction of the errors in salinity requires a reduction of the diving rate, which should be constant over the total depth range. On the other hand, a reduction of the diving speed will result in a weaker slope of the fish track and the occurrence of density inversions due to internal waves is more likely.

The apparent thickness, caused by the slope of the internal waves compared to inclination of the fish track, will be increased, if the diving rate is reduced. Therefore one has to choose a compromise according to the scientific objectives of the data set.

5.3 Estimating the errors in the objectively analysed fields

As described above (section 4.10) the objective analysis is carried out using a tempered version of the autocorrelation function of the data to be analysed as the weighting function in the method of successive correction. The error field is calculated by considering the irregularly spaced input data which contributes to each grid point. Mathematically the objective analysis can be written as

$$\hat{u}(\underset{\sim}{x}) = \int_S w(\underset{\sim}{r}) u(\underset{\sim}{x}+\underset{\sim}{r}) d\underset{\sim}{r} \qquad (5.3.1)$$

where u is the input data, w the weighting function and $\hat{u}$ the objectively analysed field. Since the weighting function tends to zero within a finite

$\underset{\sim}{r}$ the area of integration s is simply the area within which the weighting function is non-zero.

Equation 5.3.1 can be rewritten in the discrete form

$$\hat{u}_{ij} = \frac{1}{n} \sum_{k=1}^{n} w \, (\underset{\sim}{x}_k - \underset{\sim}{x}_{ij}) \, u_k \qquad (5.3.2)$$

$$\text{or} \quad \hat{u}_{ij} = \frac{1}{n} \sum_{k=1}^{n} w_k \, u_k \qquad (5.3.3)$$

for short, where n data points contribute to the grid point (i,j) and w_k is taken to be the weighting appropriate to the position of u_k relative to (i,j).

In order to describe the statistics of the data contributing to each grid point we have introduced two quantities, the weighted number of contributions (WNC) und the weighted root-mean-square error (WRMSE). These quantities are defined thus

$$\text{WNC} = \sum_{k=1}^{n} \left| \, w_k \, \right| \qquad (5.3.4)$$

$$(\text{WRMSE})^2 = \frac{1}{n} \sum_{k=1}^{n} \left[\, w_k \, (\, u - \hat{u}_{ij} \,) \, \right]^2 \qquad (5.3.5)$$

The weighted number of contributions is therefore simply the sum of the magnitudes of the weights appropriate to such data points as are available to contribute to the grid-point in question. Since in the objective analysis, equation 5.3.2, data points only contribute according to their w_k to the grid point field it was felt to be necessary to estimate in this way the number of contributions received by each grid point rather than consider the unweighted, integer number of data points contributing, which might be far away from the grid point and not influencing it significantly. In the case of the NOA'81 data set, where the data were collected by a rather irregular survey pattern, it was particularly necessary to develop a criterion for distinguishing between those areas where sufficient data were available to be able to make a reliable objective analysis and those areas

where the data coverage was too low. It might reasonably be argued that a value of WNC = 1.0 could be used to distinguish between well-measured and poorly-measured areas, since this value means that there is the equivalent of one data point contributing to each grid point. In figure 5.3.1 a map of the ship's track with the WNC field for temperature on sigma-t is shown.

In calculating the WRMSE it was likewise felt to be better to use the weighting function to modify the estimate of the fluctuations of the data relative to the grid points rather than use the unweighted variance of the data because the data points farther away from the grid point would naturally be expected to deviate further from the grid point value and in the sum of squares would dominate the calculation. The meaning of this quantity should be interpreted with caution however. Although we have loosely termed it an "error" it is not an inaccuracy in the same way as an instrumentation or calibration limitation. It should be seen as an estimate of that part of the spatial spectrum which cannot be represented on the chosen grid due to the, relatively, poor spectral window of the grid. Figure 5.3.2 shows $T)_{\sigma_t}$ and its WRMSE, figure 5.3.3.

Using the WNC and the WRMSE it was also possible to derive a weighted confidence limit (WCL) field using the well-known t-test formula (Kreyszig, 1968; Jenkins and Watts, 1968)

$$t_\nu \left(1 - \frac{\alpha}{2} \right) \frac{\sigma}{\sqrt{n}} \tag{5.3.6}$$

where σ is the standard deviation of n data points and $t_\nu (1-\frac{\alpha}{2})$ is a factor depending on the number of degrees of freedom $\nu (= n-1)$. Our version of this formula is

$$\mathrm{WCL} = t_\nu \left(1 - \frac{\alpha}{2} \right) \cdot \mathrm{WRMSE} \; / \; (\mathrm{WNC})^{1/2} \tag{5.3.7}$$

where the number of degrees of freedom ν is also taken to be WNC. For WNC less than unity WCL is not defined. The WCL for temperature on sigma-t is shown in figure 5.3.4.

5.4 Synopticity

The survey of the polar front took eight days and furthermore it was not conducted in a spatially systematic way. Little is known about the time scales of the synoptic and mesoscale turbulence in this area and due to the high cloudiness satellite images also fail to give the necessary information. It is however possible that the structures under observation were changing and developing during the period of the survey. In order to estimate the asynopticity for each part of the field, the time of the measurements was objectively analysed using the velocity component weighting functions and the statistics of the data points contributing to each grid point calculated as described in section 5.3. Within the area with WNC greater than 1.0 both the WRMSE and the WCL gave values of about 0.5 d. Thus the time scale for the lack of synopticity of the well-supported grid points was approximately half a day. This is probably shorter than the likely time scale of development of such meander structures in the ocean and therefore the lack of synoptic measurement and also the lack of systematic measurement would not seem to be too serious.

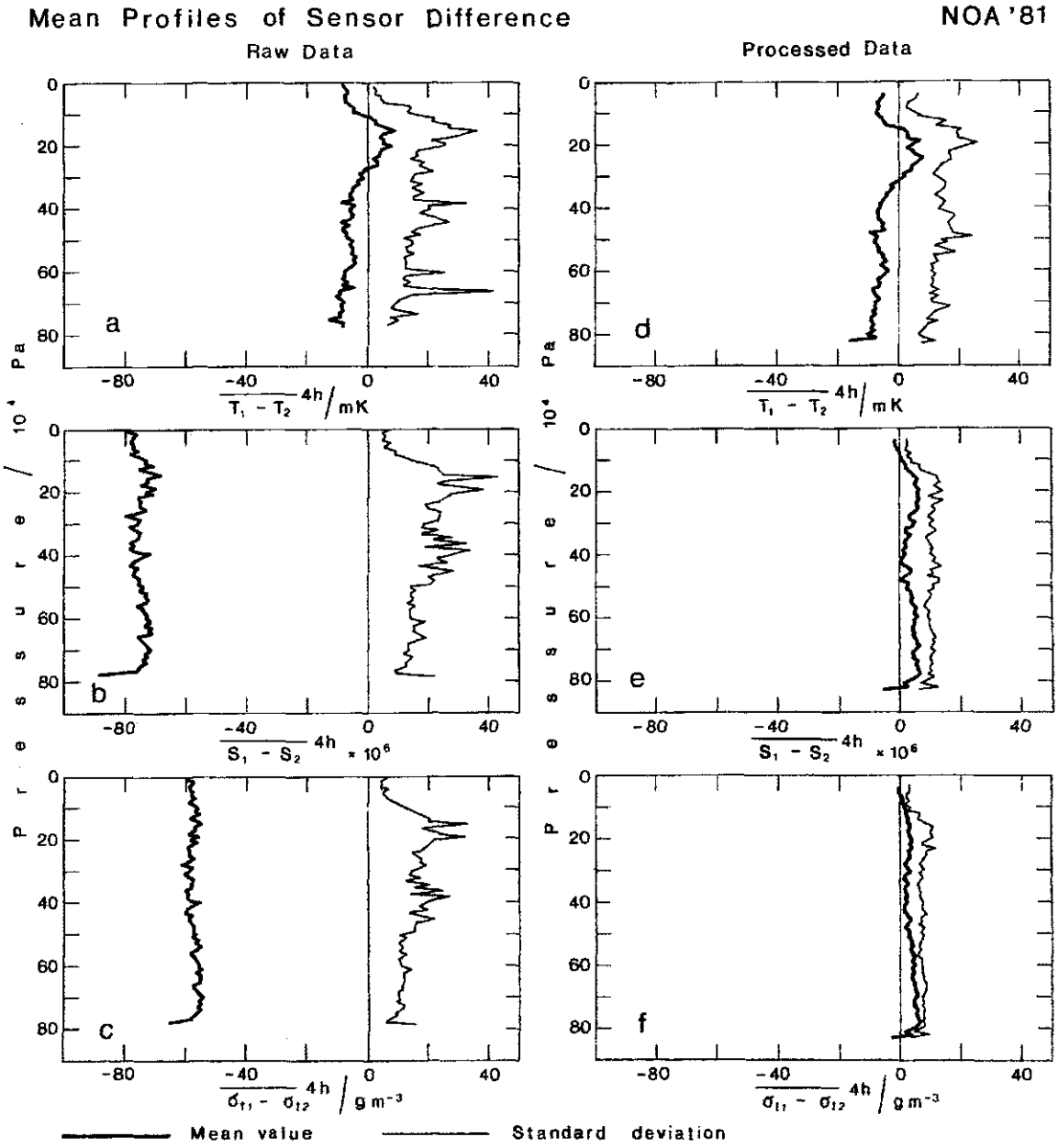

Fig. 5.1.1: Mean and standard deviation profiles of differences between the towed fish sensors averaged horizontally over 4 hours.
a) temperature d) temperature
b) salinity e) salinity
c) σ_t of raw data f) σ_t of data after 5th processing.

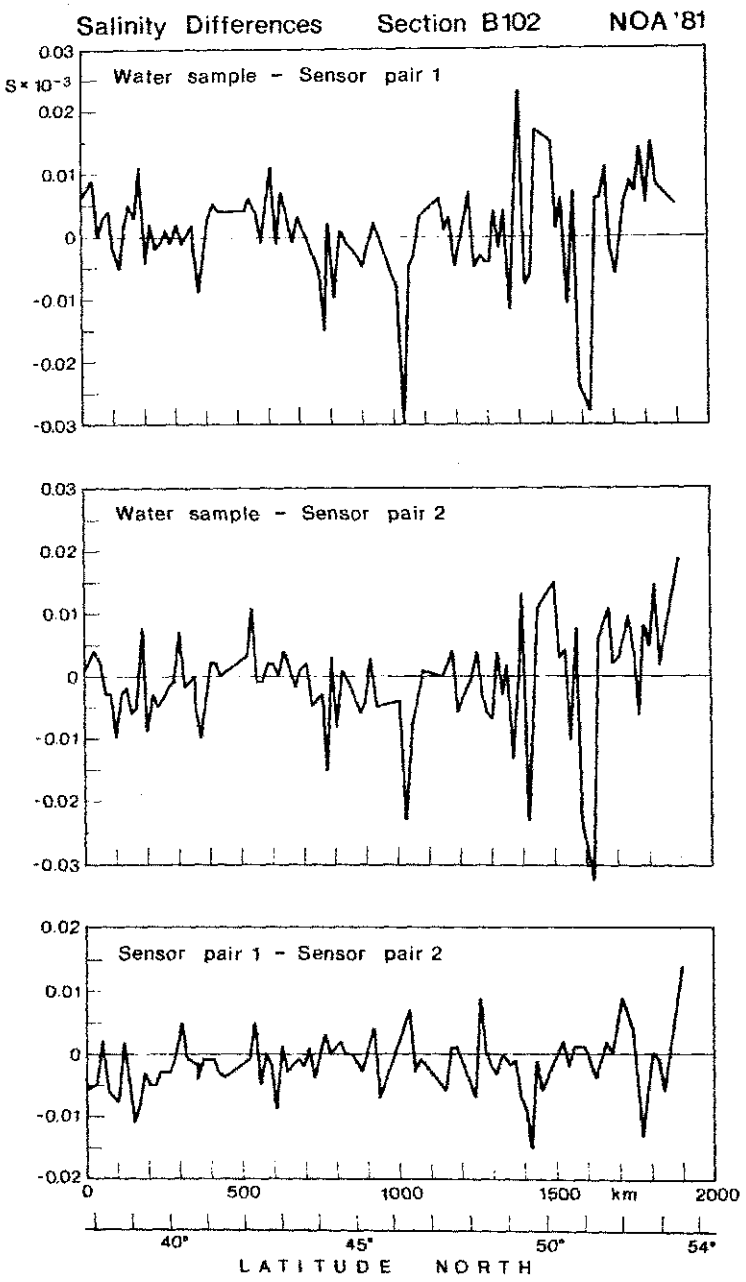

Fig. 5.1.2: Comparison of salinity values along section B102 salinity difference a) water sample - CTD-salinity pair 1
b) water sample - CTD-salinity pair 2
c) CTD-salinity pair 1 - CTD-salinity pair 2

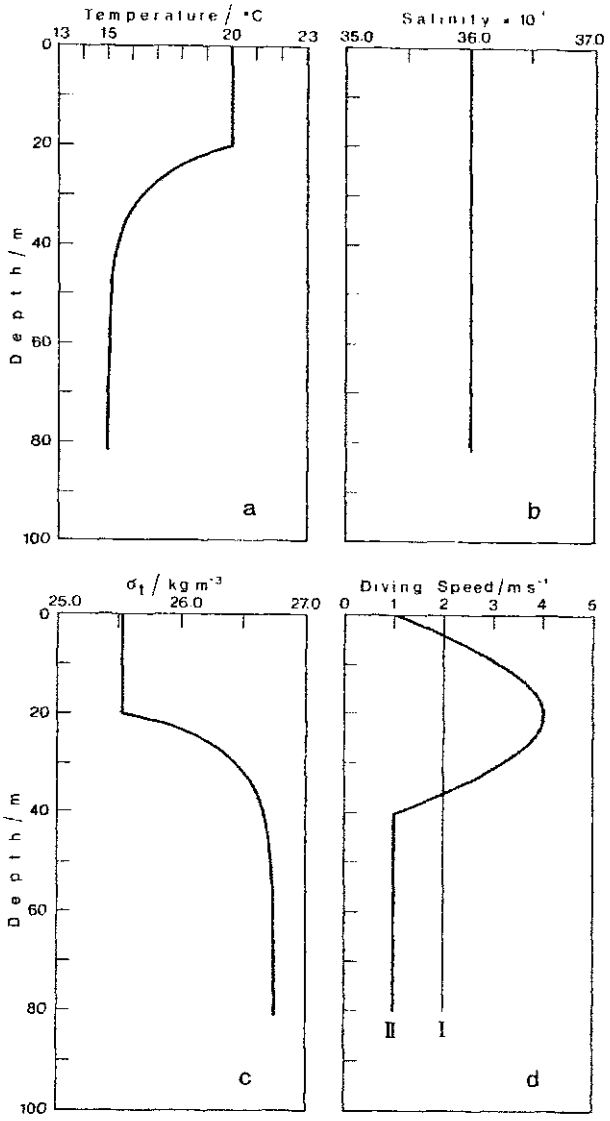

Fig. 5.2.1: Artificially generated, initial profiles for the numerical estimation of uncertainties in derived quantities.
a) temperature b) salinity c) σ_t,
d) I : constant diving speed (2 m s^{-1})
II: variable diving speed

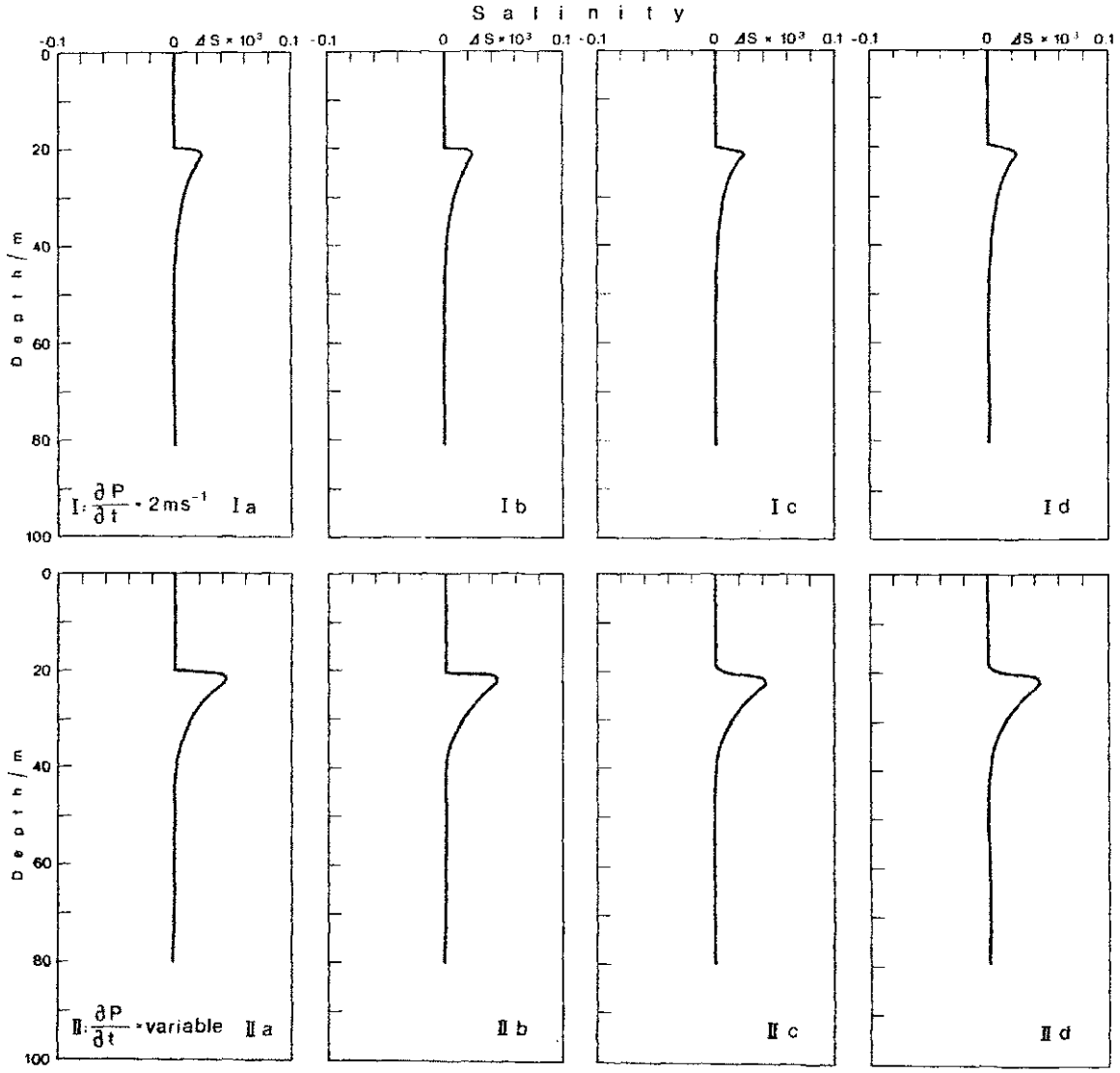

Fig. 5.2.2: Salinity difference between the initial profile and the derived profile after various processing stages.
I : constant diving speed (2 m s^{-1})
II: variable diving speed
a) after time constant correction of temperature
b) after median filtering in salinity
c) after block averaging
d) after median filtering of density

14.3 Coefficients for pressure calibration correction

$$P_c = P + a_o + a_1 Tu$$

P_c: corrected pressure value

P : CTD-pressure

Tu: 4-hour mean of upper turning point temperature

$a_o = 5.79\ 10^4 Pa$

$a_1 = -0.1212\ 10^4 PaK^{-1}$

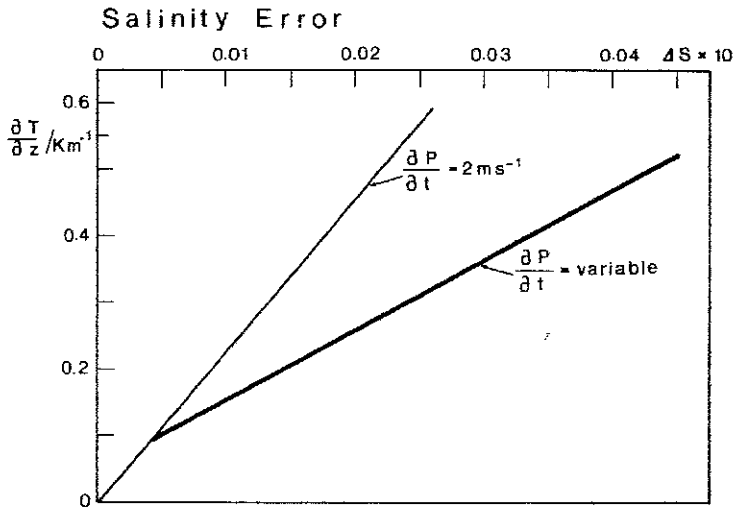

Fig. 5.2.3: Dependence of salinity error of the vertical temperature gradient $\frac{\partial T}{\partial z}$ and the diving speed of the towed fish $\frac{\partial P}{\partial t}$.

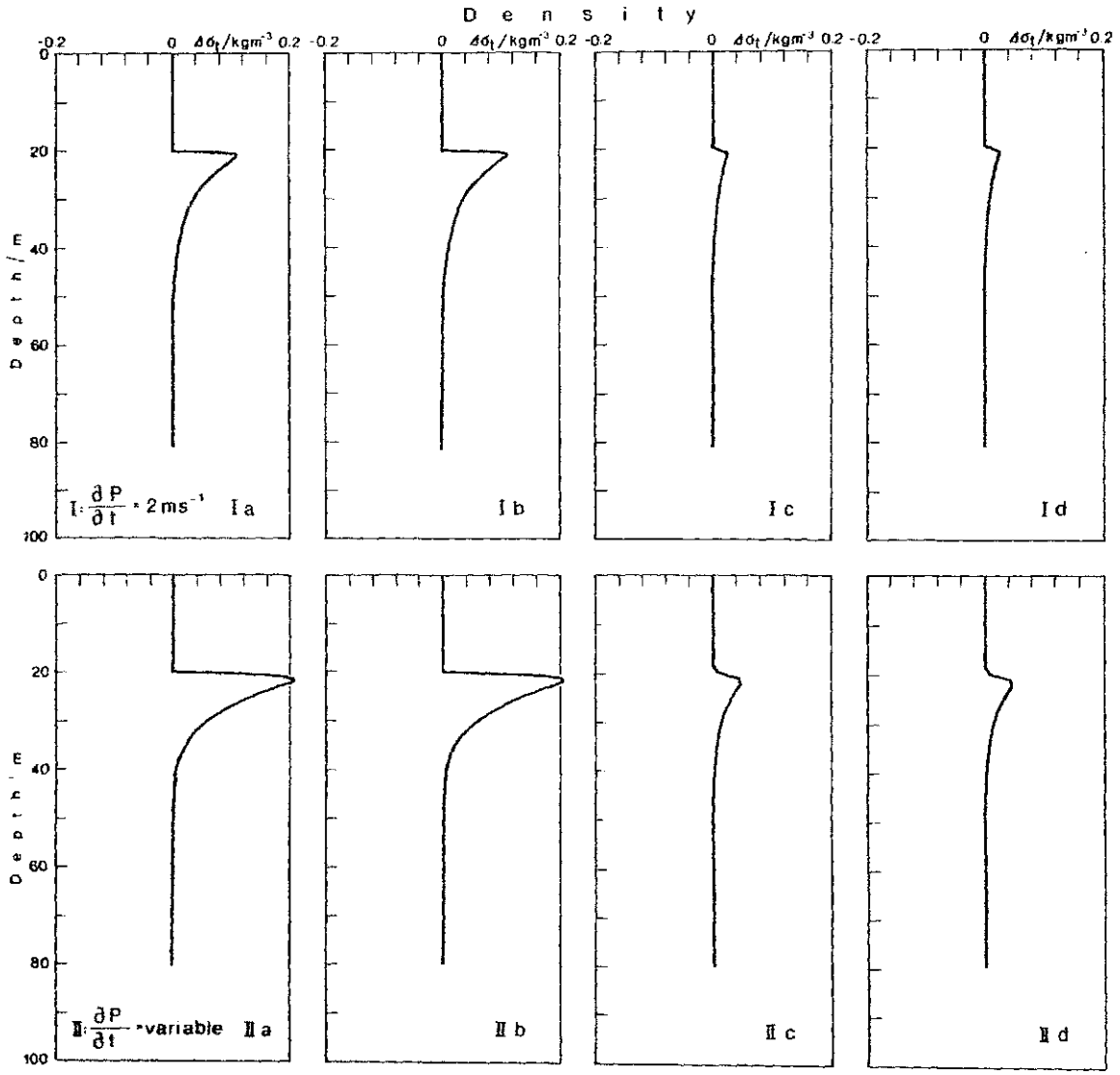

Fig. 5.2.4: Density difference between the initial profile and the derived profile after various processing stages.
I : constant diving speed (2 m s^{-1})
II: variable diving speed
a) after time constant correction of temperature
b) after median filtering in salinity
c) after block averaging
d) after median filtering of density

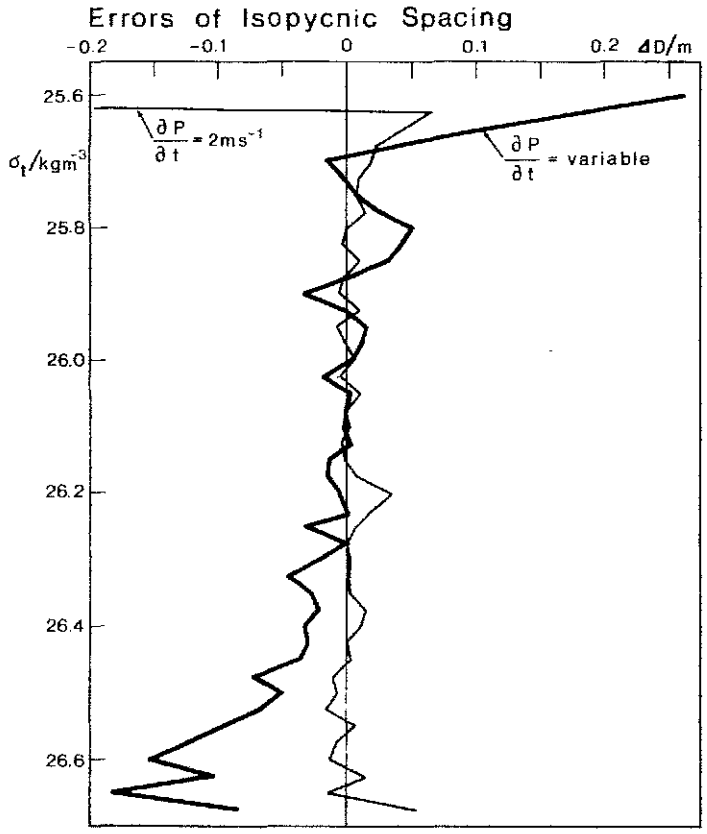

Fig. 5.2.5: Error profile of isopycnic spacing from a numerical experiment as a function of different diving speeds of the fish.

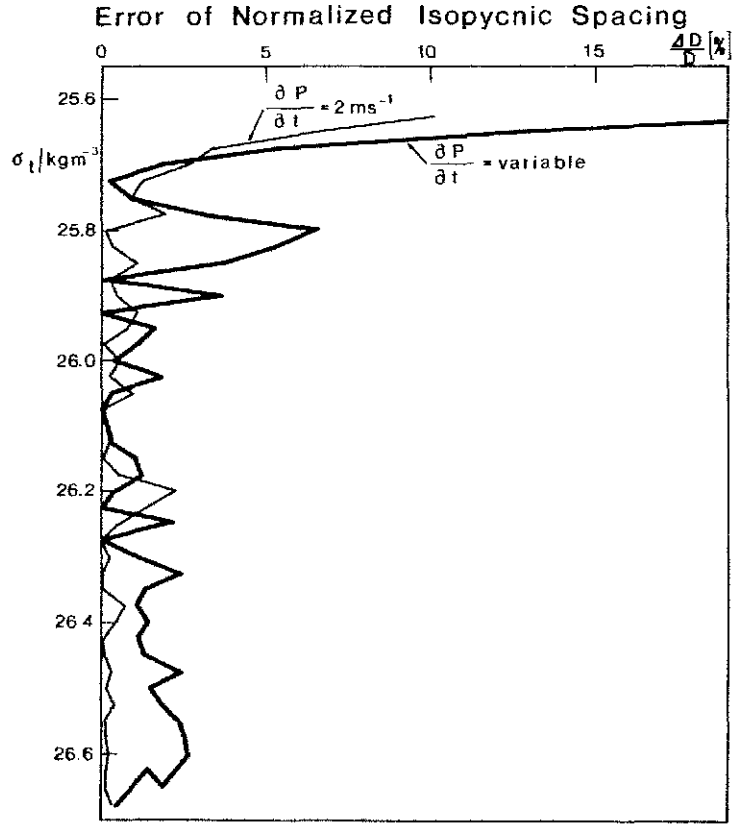

Fig. 5.2.6.: Error profile of isopycnic spacing relative to the true isopycnic spacing.

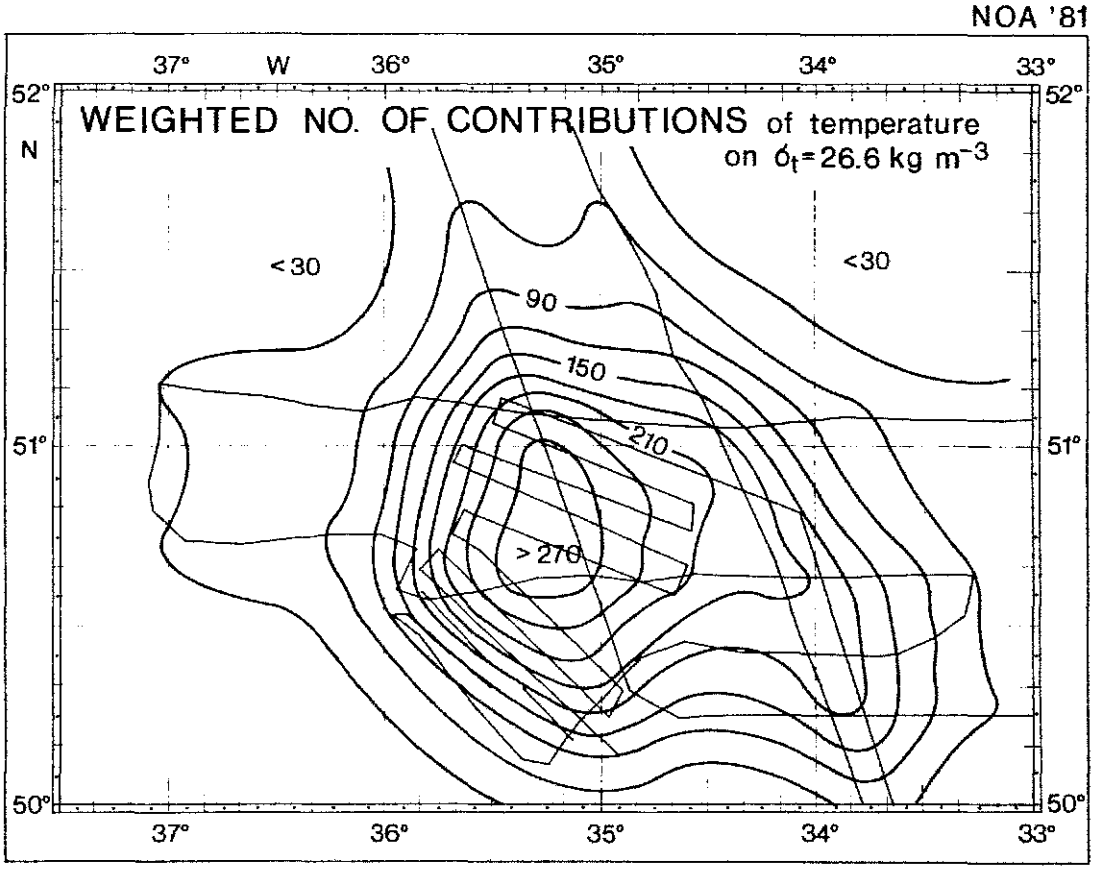

Fig. 5.3.1: Weighted number of contributions of temperature on σ_t=26.6 kg m^{-3}, including the ship's track during the frontal survey.

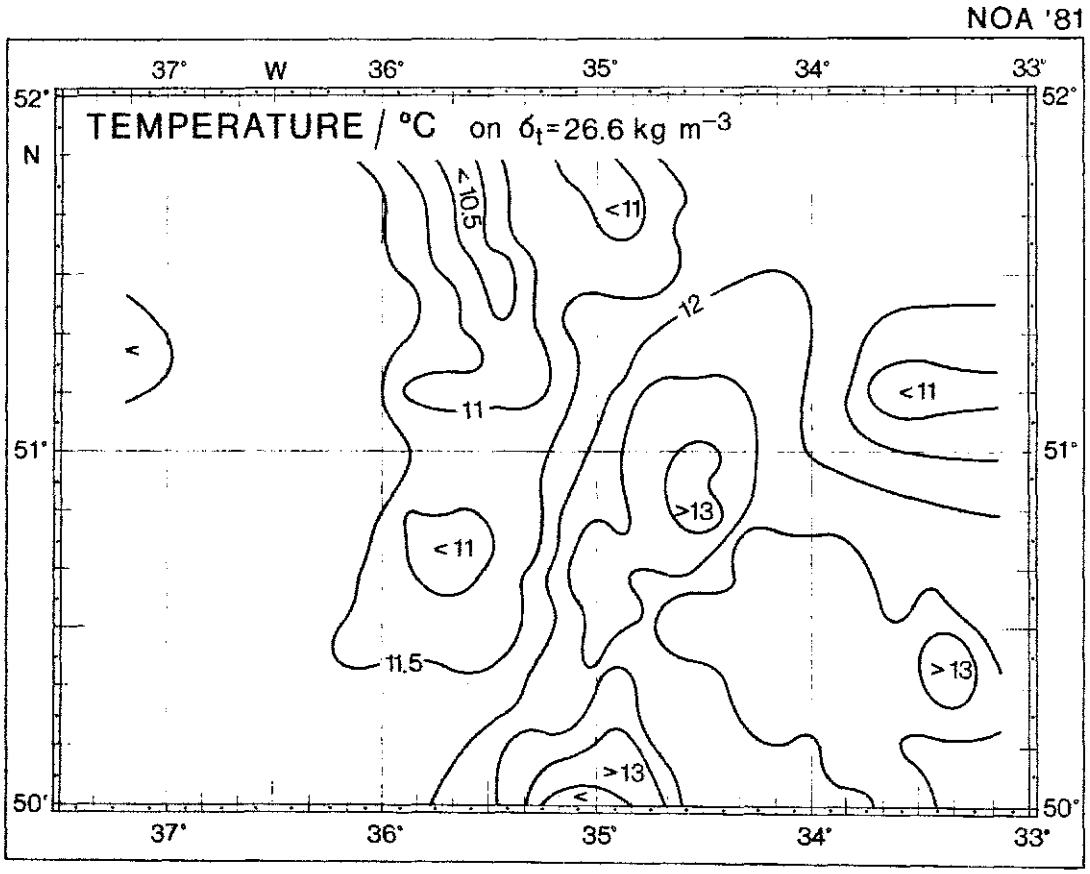

Fig. 5.3.2: Temperature distribution on σ_t = 26.6 kg m^{-3} in the frontal area.

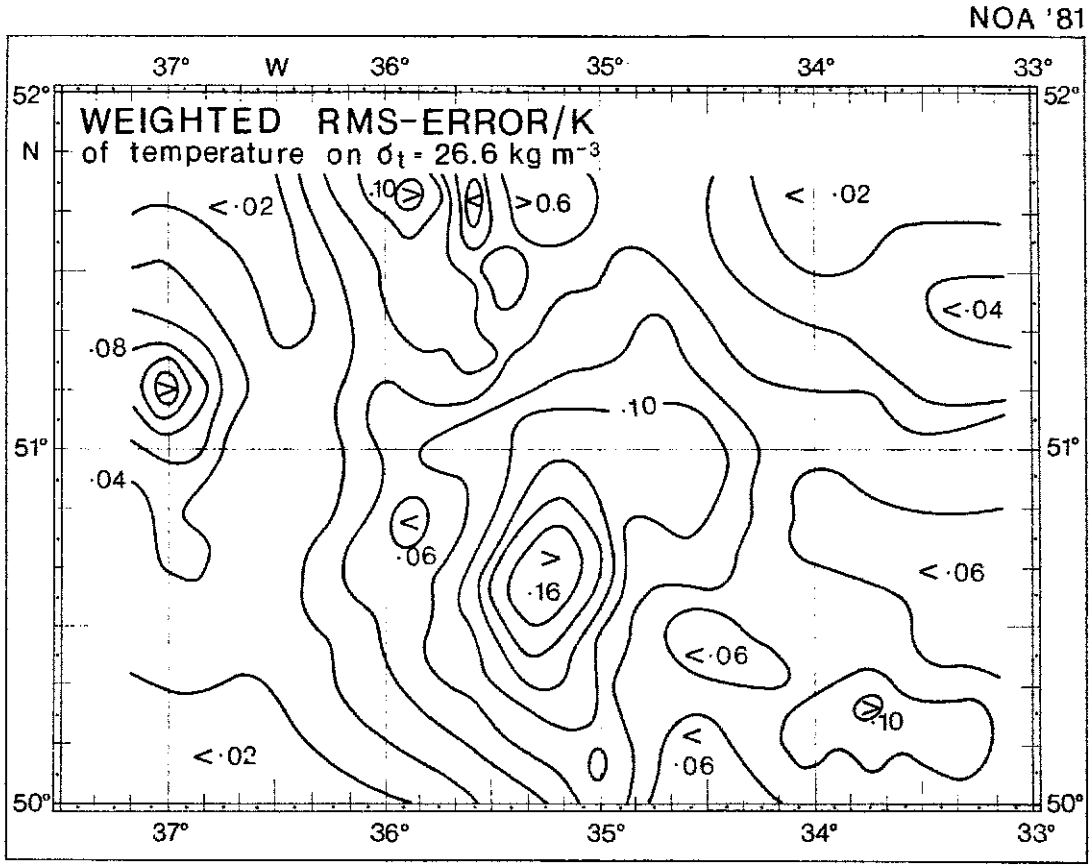

Fig. 5.3.3: Weighted RMS-error of temperature on σ_t = 26.6 kg m^{-3} in the frontal area.

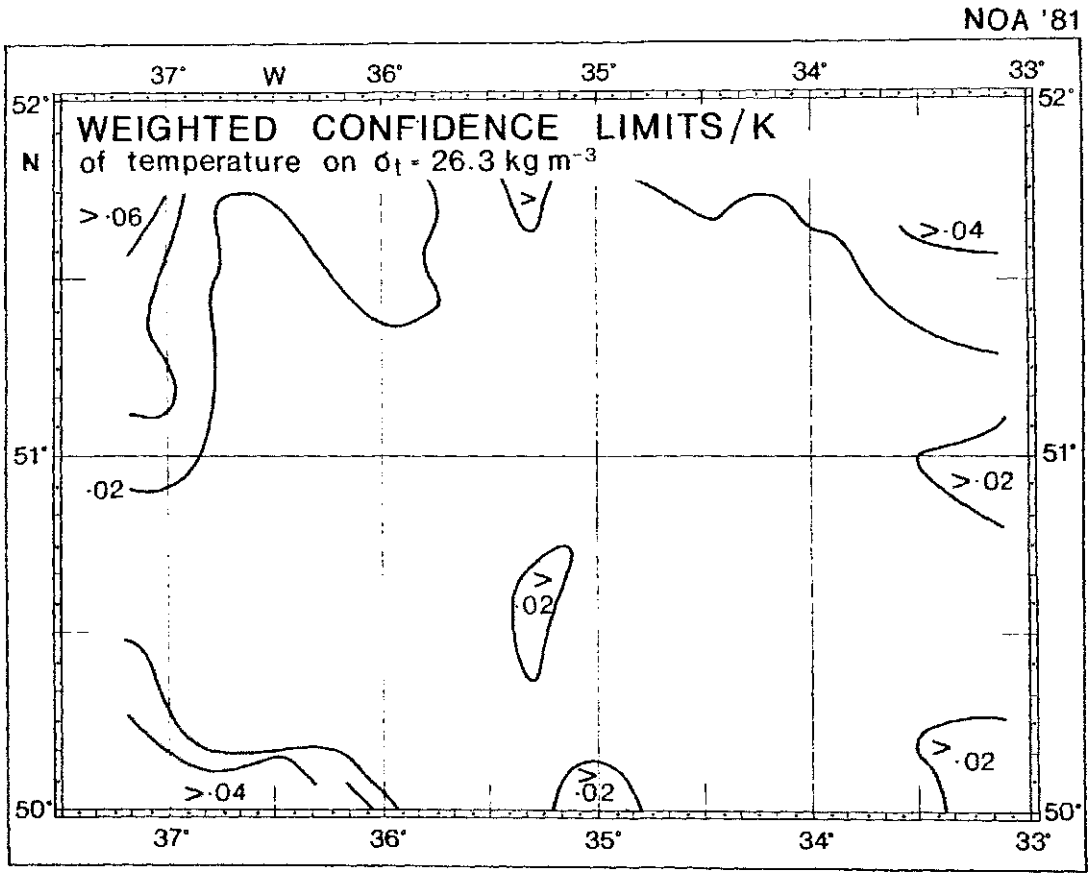

Fig. 5.3.4: Weighted confidence limits of temperature on σ_t = 26.6 kg m^{-3} in the frontal area.

6. STANDARD PRODUCTS - OFFSET PROFILES

As mentioned in the introduction only a subsample of the total data set will be presented here. These data were edited to stage 5 as shown in the flow diagram (fig. 4.1).

6.1 Profiles from the Long Sections

To give an impression of the variety of features along the 2500 km track, with approximately 5000 profiles, 5 sets of 21 successive profiles were chosen for more detailed presentation. The start and end positions of each set is listed in table 6.1. To present the location of the sets their numbers are marked in figure 7.1.6 showing the variability of temperature on constant σ_t surfaces along the whole section.

Table 6.1: Location of 5 selected regions of long section B102

Set No.	Characteristic	Start		End	
		Latitude N	Longitude W	Latitude N	Longitude W
1	horizontally homogeneous warm water	40°38.58'	28° 6.36'	40°43.98'	28°10.38'
2	edge of an eddy	42°23.59'	29°28.01'	42°28.50'	29°32.00'
3	strong front	47°52.50'	32°33.18'	47°56.64'	32°36.00'
4	polar front	51° 1.08'	34°28.08'	51° 5.88'	34°31.80'
5	homogeneous cold water	53° 6.54'	35°50.52'	53°11.32'	35°53.10'

Figure 6.1.1 shows profiles of set 1 in the warm water sphere (NACW) at 40°30' N, belonging to a fairly uniform water mass.

Figure 6.1.2 shows profiles of set 2 cutting a frontal structure at 42°20' N. Especially in the salinity profiles it is apparent how the section crosses the front within 6 km. In this range colder lower salinity water is lying under the warmer water of profiles 100 to 112.

Figure 6.1.3 shows a region where the section cuts a tongue of warm, saline water embedded in a colder surrounding. Below 40 m depth the boundary between the water masses is much sharper than in the overlying water.

Set 4 is not presented here because the Polar Front is described in detail in section 6.2.

Figure 6.1.4 shows profiles of set 5 lying in the horizontally relatively uniform cold water north of the Polar Front.

6.2 Profiles from the Frontal Survey - sections C311 and C312

The following examples each show approximately 7 - 8 km of a typical region in the frontal area taken from sections "C311" and "C312" which were about 10 km apart. The start and end positions of these regions are listed in table 6.2. Each figure consists of twenty successive profiles of temperature, salinity and density. The even numbers by the profiles indicate that the profiles were taken from the descending sections of the fish track.

Table 6.2: Selected regions in sections C311, C312

Section	Region	Start		End	
		Latitude N	Longitude W	Latitude N	Longitude W
C311	warm	50°14.28'	34°59.70'	50°17.64'	35° 2.94'
C311	front	50°26.34'	35°13.14'	50°29.04'	35°17.70'
C311	cold	50°37.98'	35°37.20'	50°40.86'	35°42.12'
C312	warm	50°19.38'	34°53.58'	50°21.72'	34°57.78'
C312	front	50°30.06'	35°11.04'	50°32.34'	35°15.54'
C312	cold	50°42.96'	35°35.28'	50°44.40'	35°40.38'

These regions are presented in a set of offset profiles, they are marked in the section plots as "W", "F", "C" with a black bar (chapter 7.2); and they were also used (paragraph 7.1) for the average conditions in each of the areas.

The definition "warm" refers to the warmer part, "front" to the thermoclinicity maximum and "cold" to the colder part of the section in question.

Figures 6.2.1 and 6.2.2 were taken from the warm side, figure 6.2.3 and 6.2.4 from the region of highest horizontal temperature gradient and figures 6.2.5 and 6.2.6 from the cold side of the front.

Plots of temperature versus σ_t reveal that thermohaline fine-structure was masked by the internal wave field. Again a set of figures (6.2.7 - 6.2.10) from both sides of the thermohaline front as well as the maximum gradient region is presented.

By comparing the profiles of temperature versus density the obvious difference in the three regions is the lack of fine-structure on the cold side, while the regions "W" and "F" show coherent temperature inversions over some kilometres with vertical scales of a few metres.

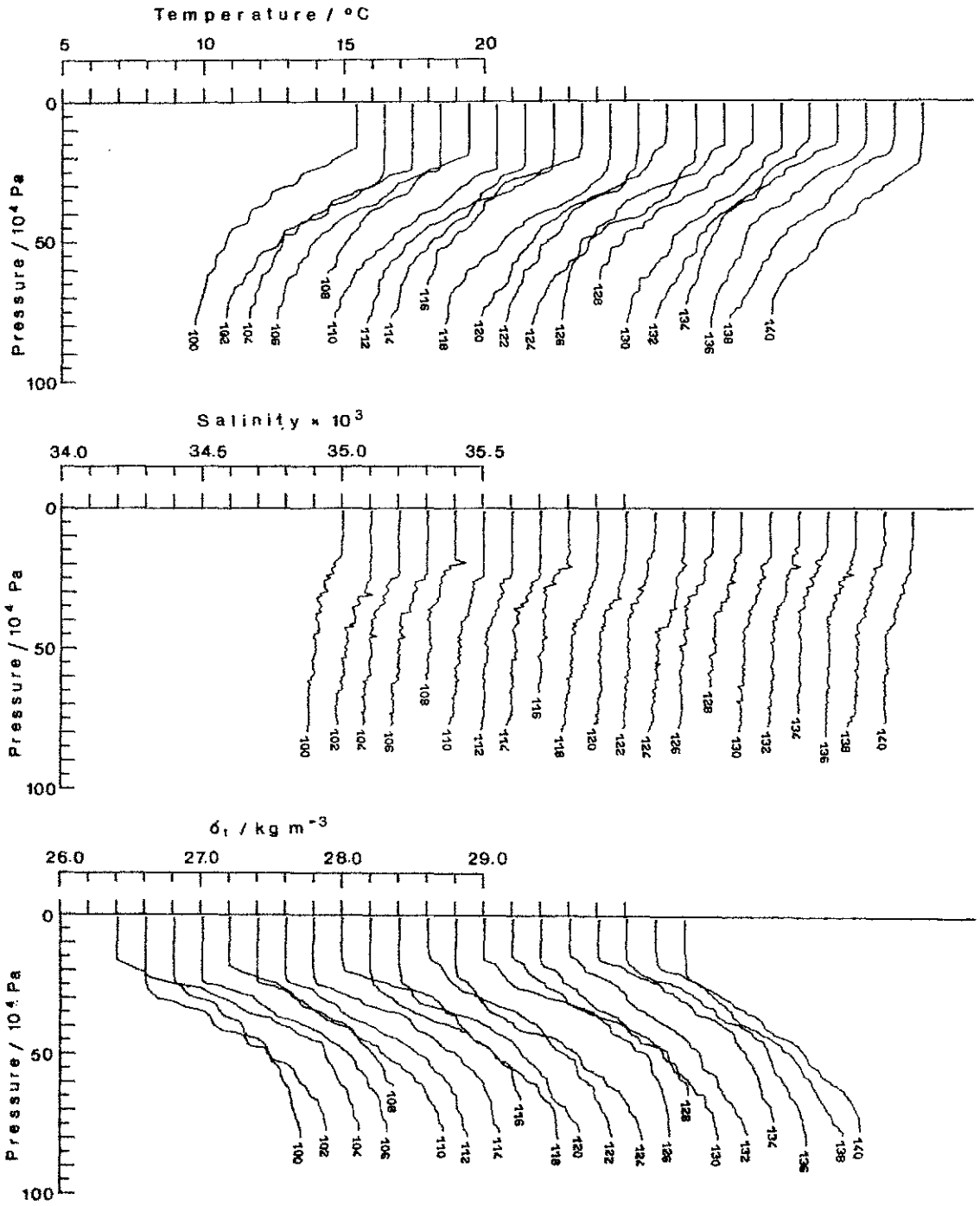

Fig. 6.1.1: 20 offset profiles from section B102 set no. 1 in horizontally relatively homogeneous warm water covering approximately 8 km.

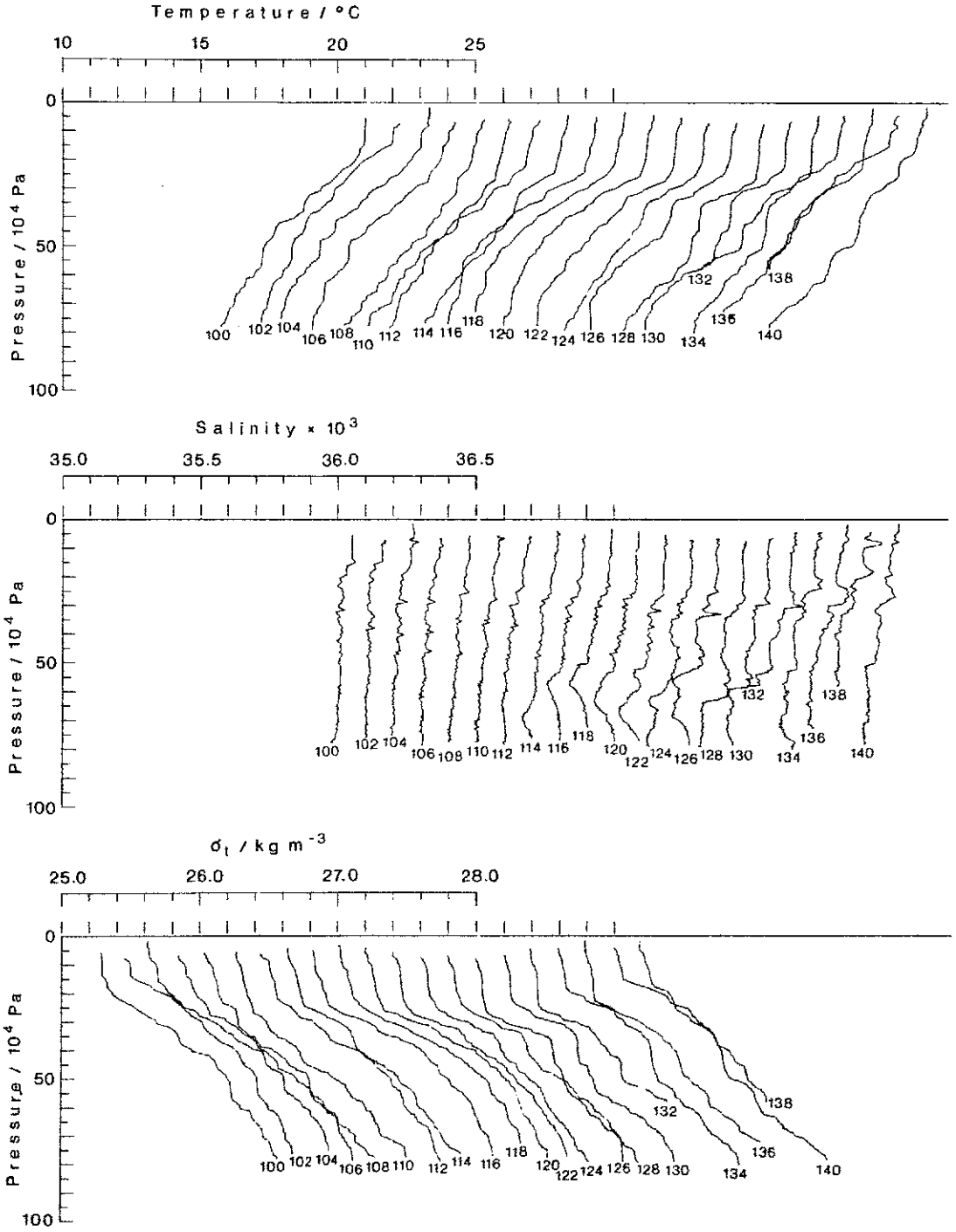

Fig. 6.1.2: 20 offset profiles from section B102, set no. 2 at a mesoscale front leading into lower saline water.

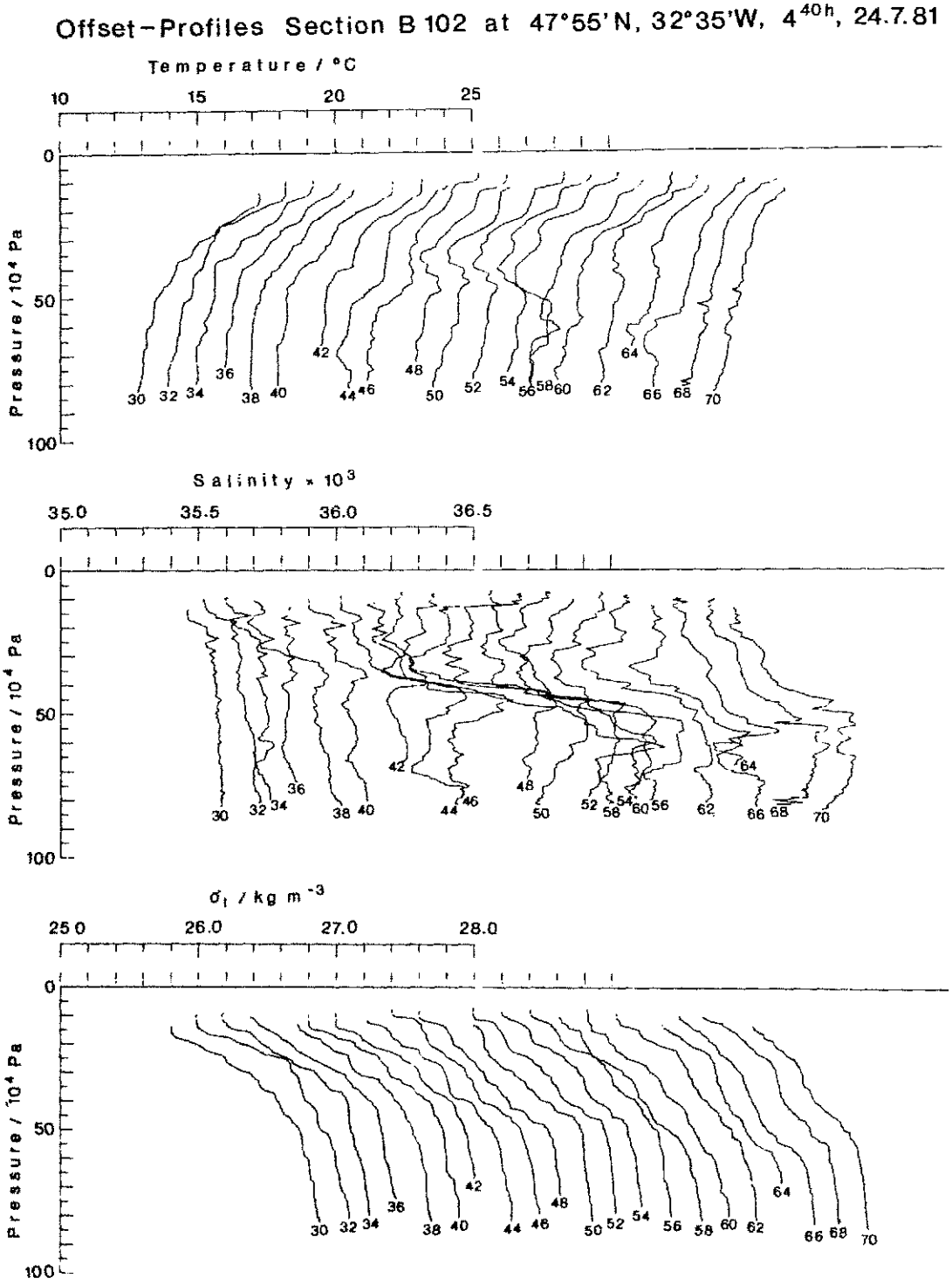

Fig. 6.1.3: 20 offset profiles from section B102, set no. 3 at a strong front where low saline water is covering subtropical waters with higher salinity.

NOA '81

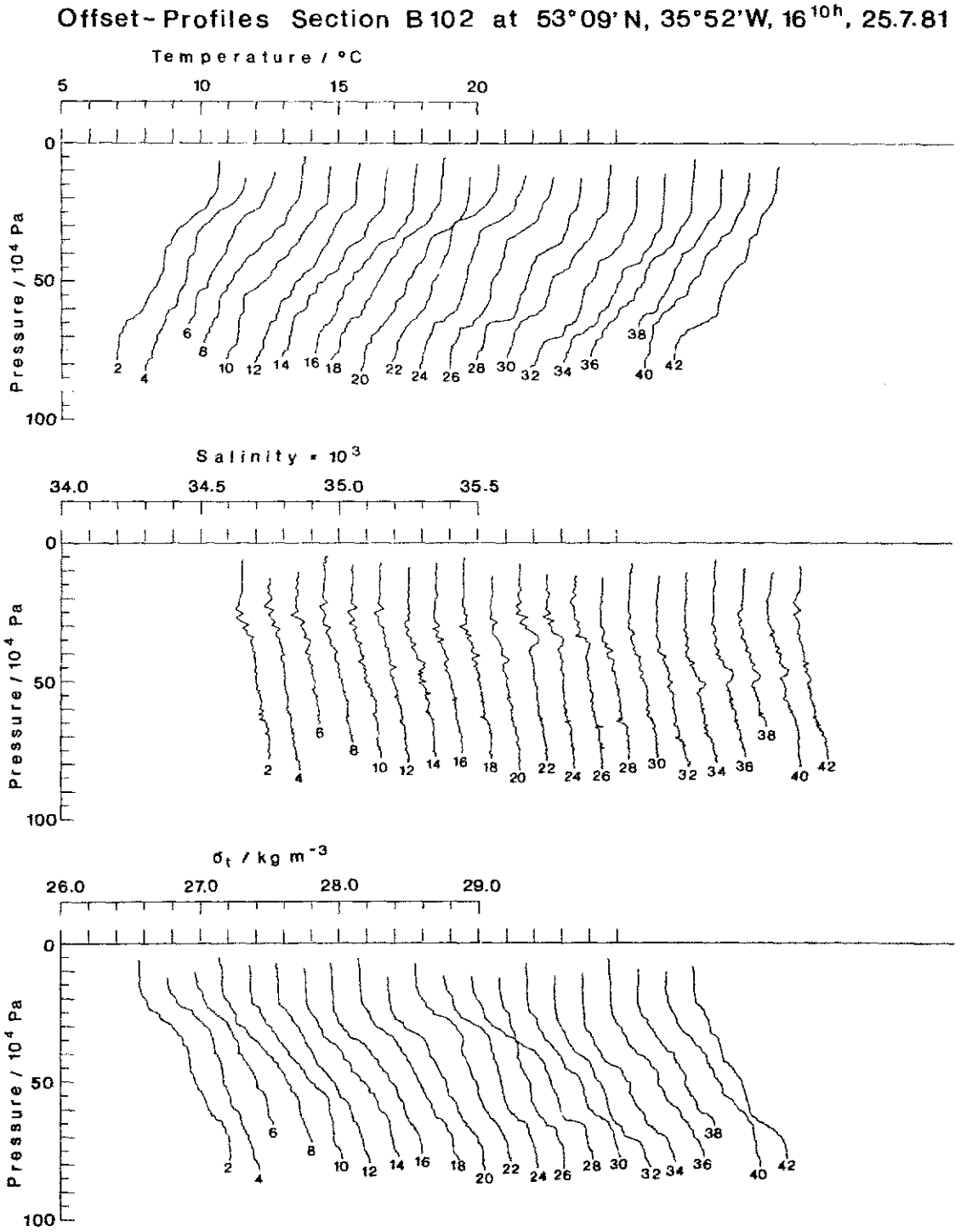

Fig. 6.1.4: 20 offset profiles from section B102, set no. 5 in horizontally relatively homogeneous cold water north of the polar front.

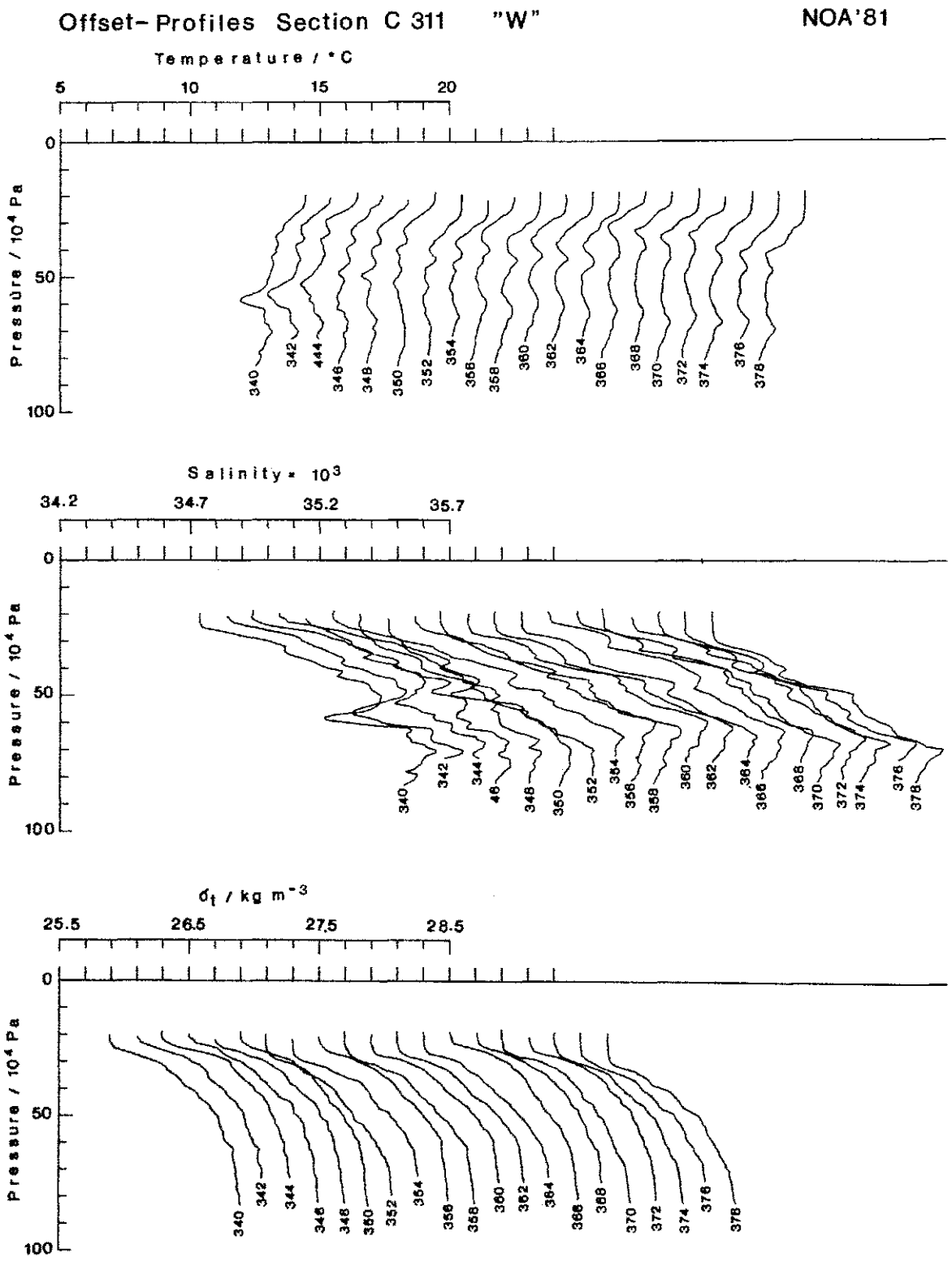

Fig. 6.2.1: 20 offset profiles from the warm part of section C311 covering approximately 8 km. The numbers at the lower end of the profiles indicate the position in the section.

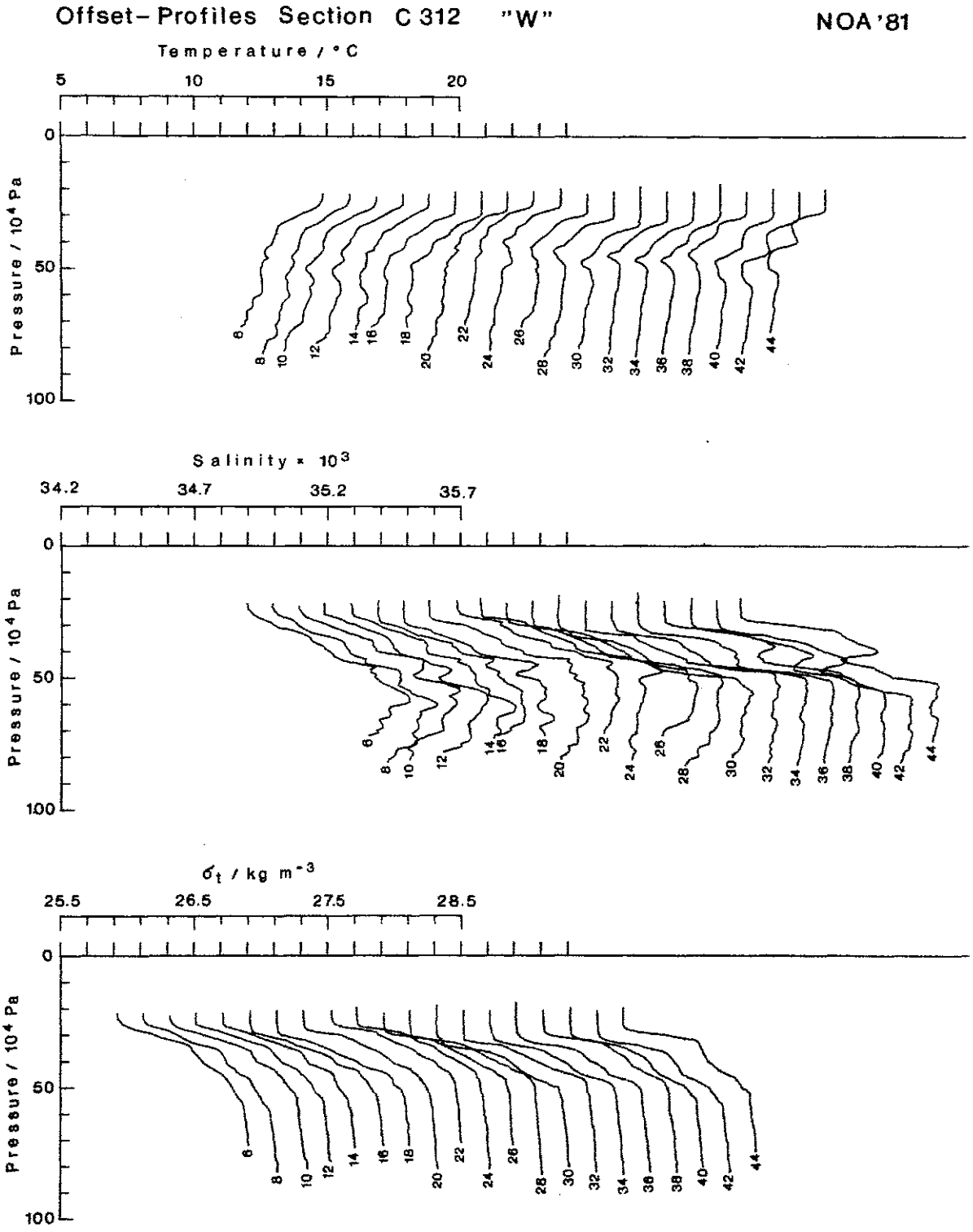

Fig. 6.2.2: 20 offset profiles from the warm part of section C312 covering approximately 8 km.

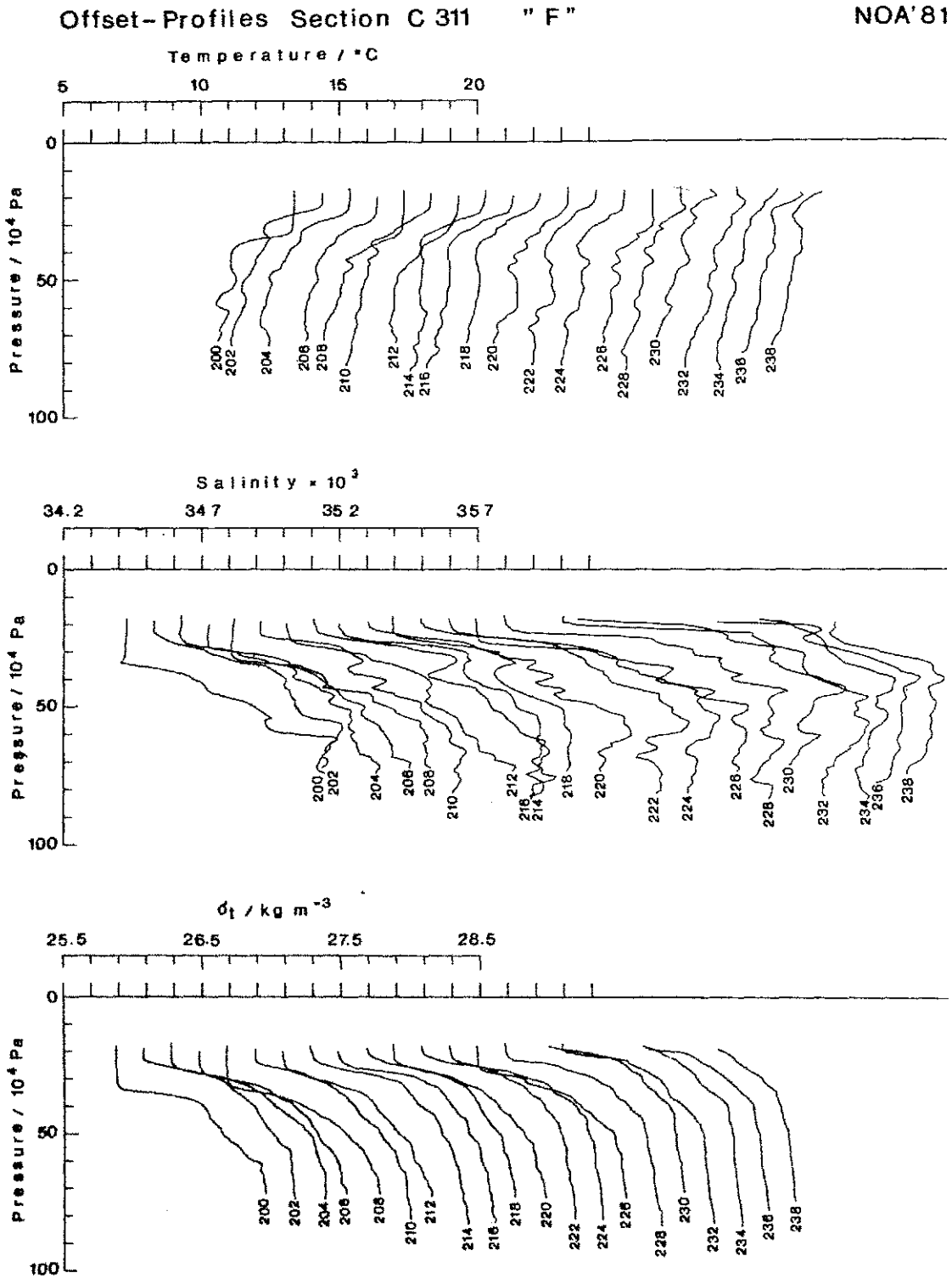

Fig. 6.2.3: 20 offset profiles from the region of the thermoclinicity maximum of section C311.

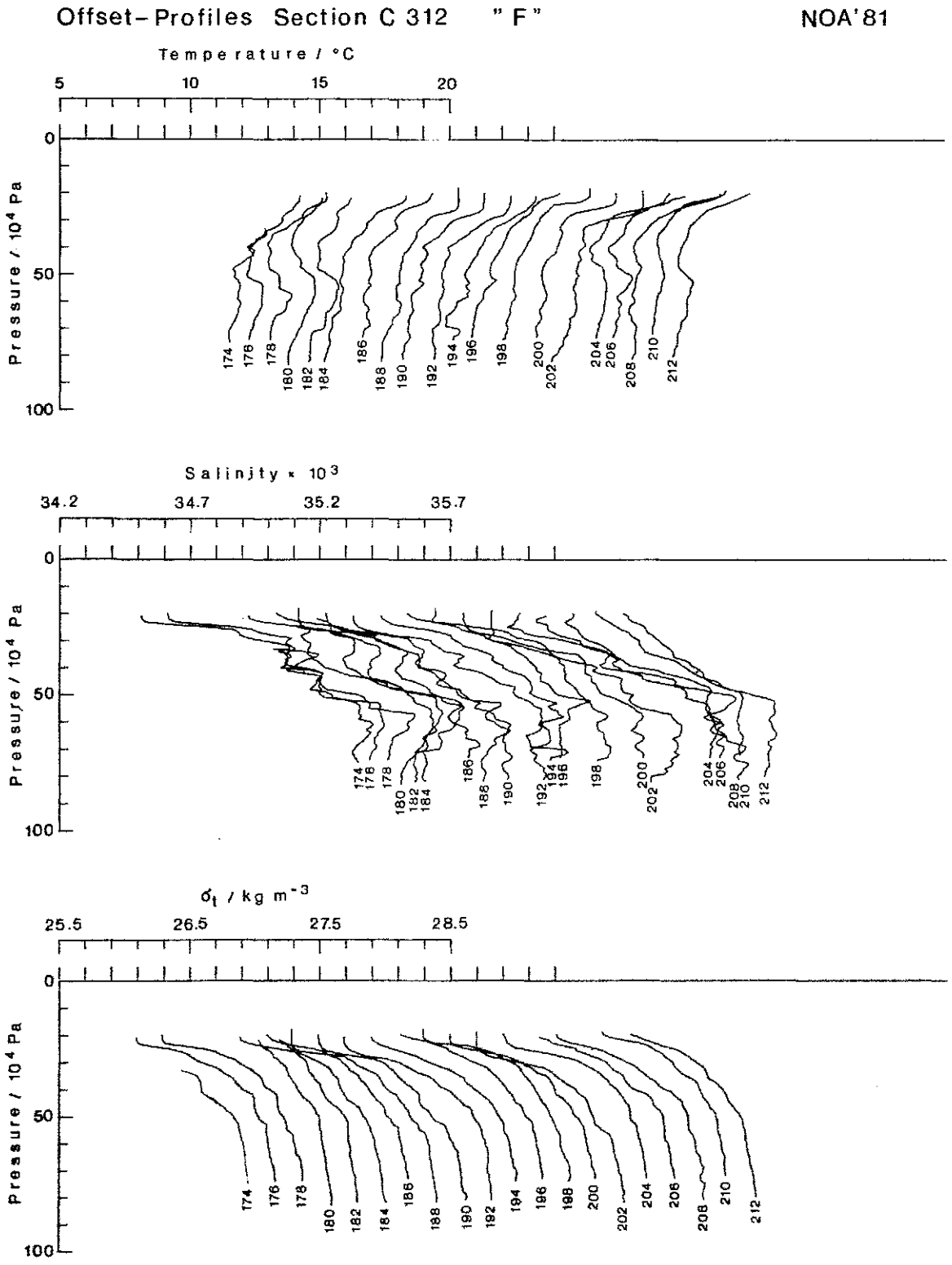

Fig. 6.2.4: 20 offset profiles from the region of the thermoclinicity maximum of section C312.

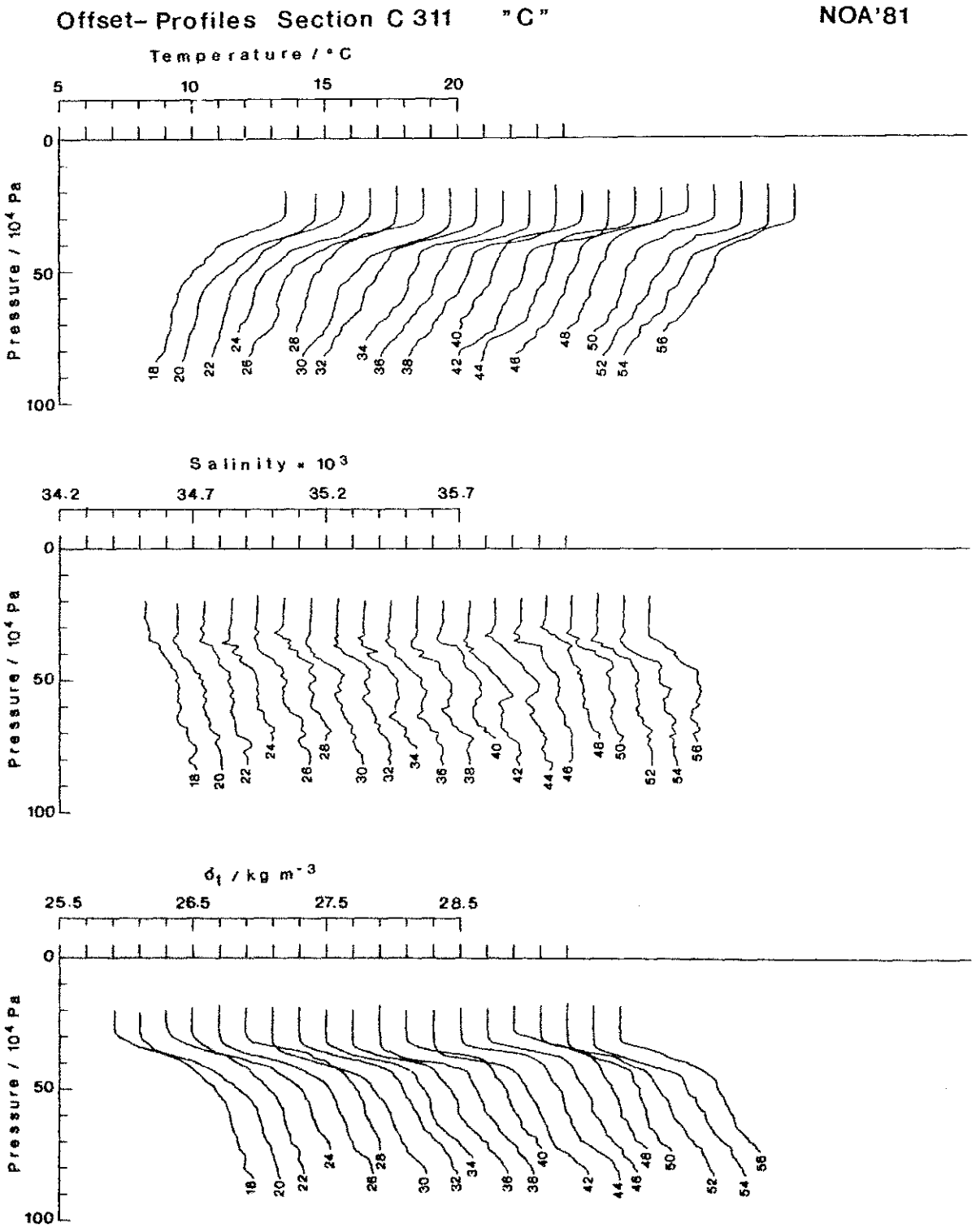

Fig. 6.2.5: 20 offset profiles from the cold part of section C311.

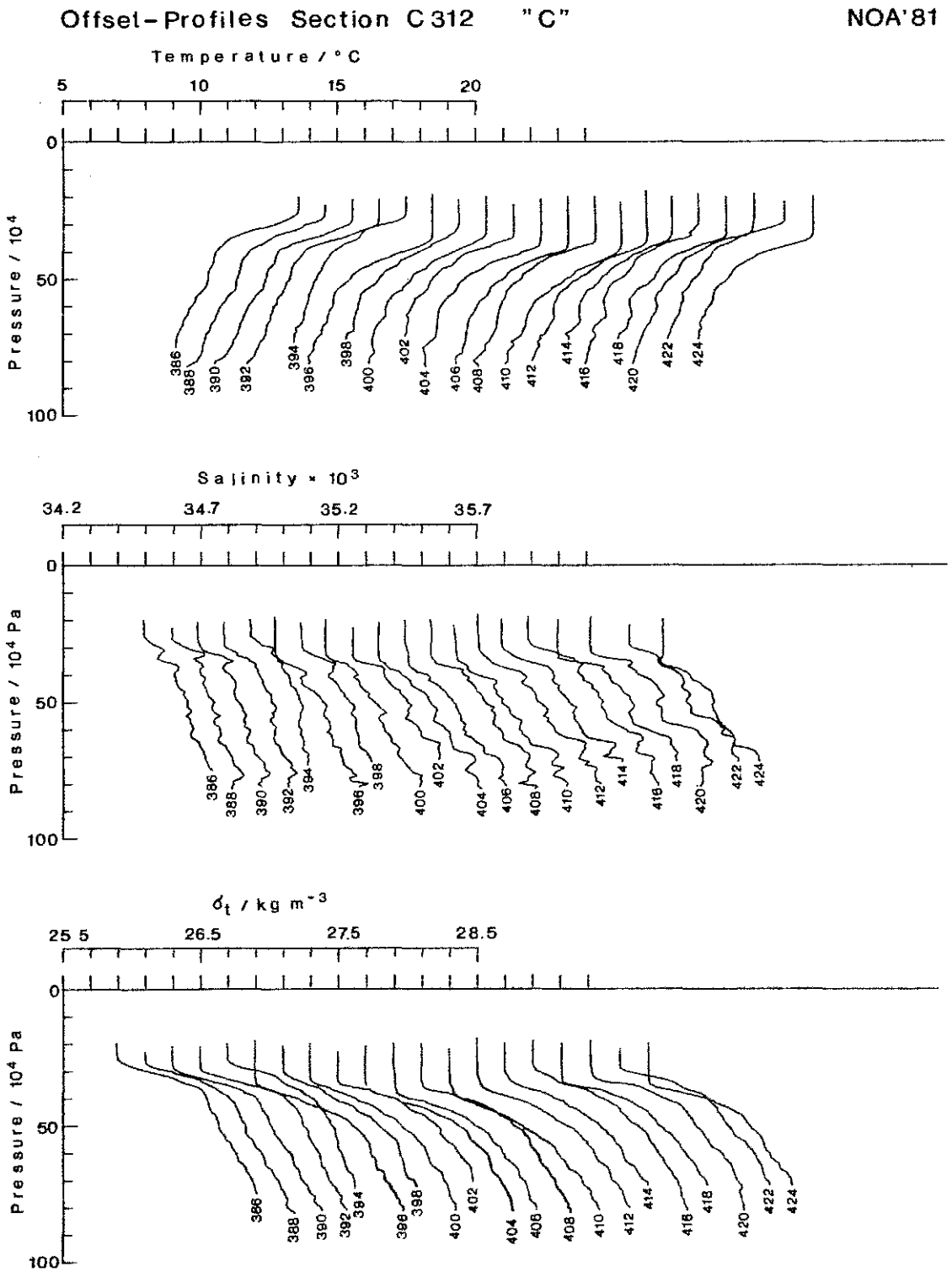

Fig. 6.2.6: 20 offset profiles from the cold part of section C312.

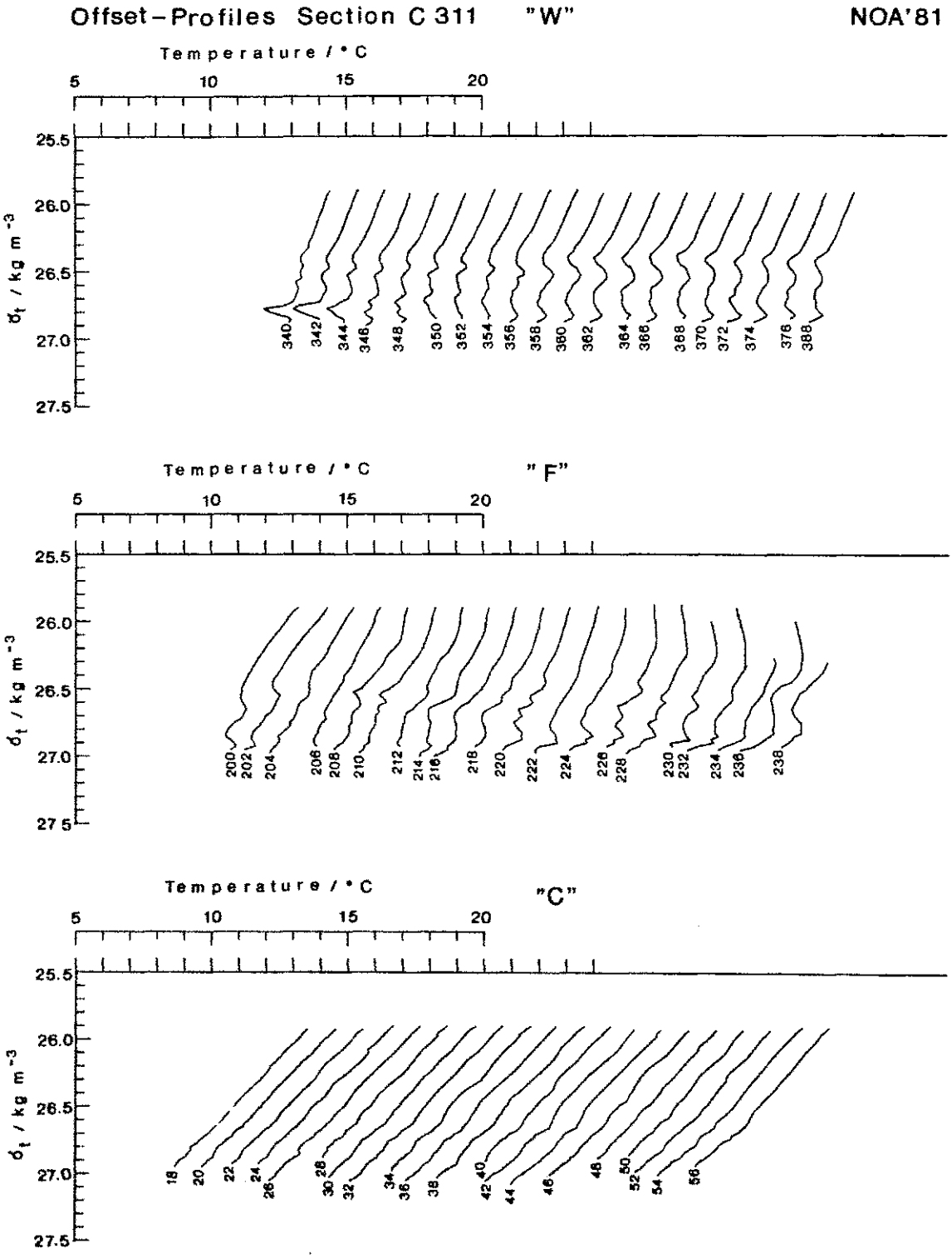

Fig. 6.2.7: Offset profiles from section C311, showing temperature versus σ_t from three selected regions ("W", "F", "C").

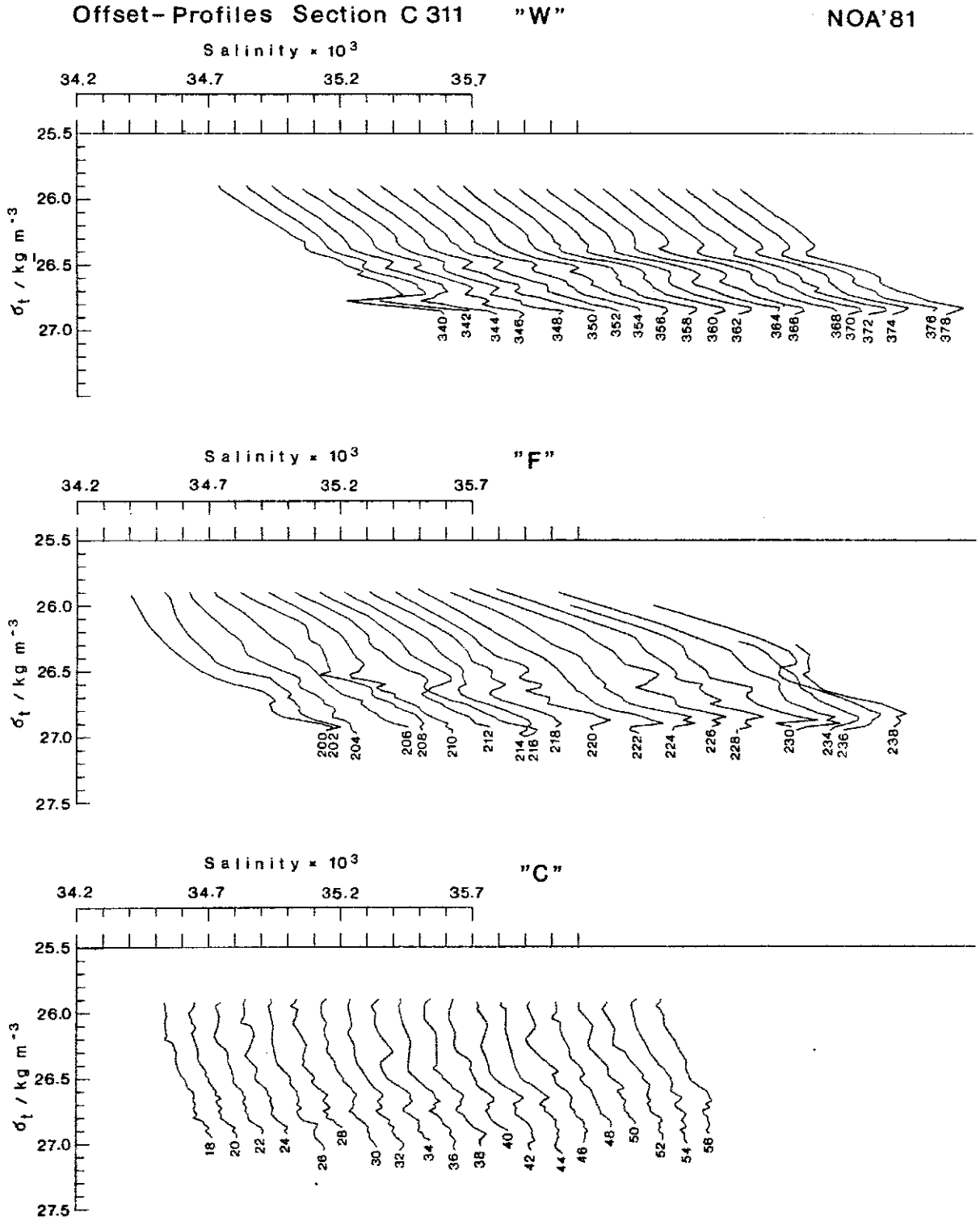

Fig. 6.2.8: Offset profiles from section C311, showing salinity versus σ_t from three selected regions ("W", "F", "C").

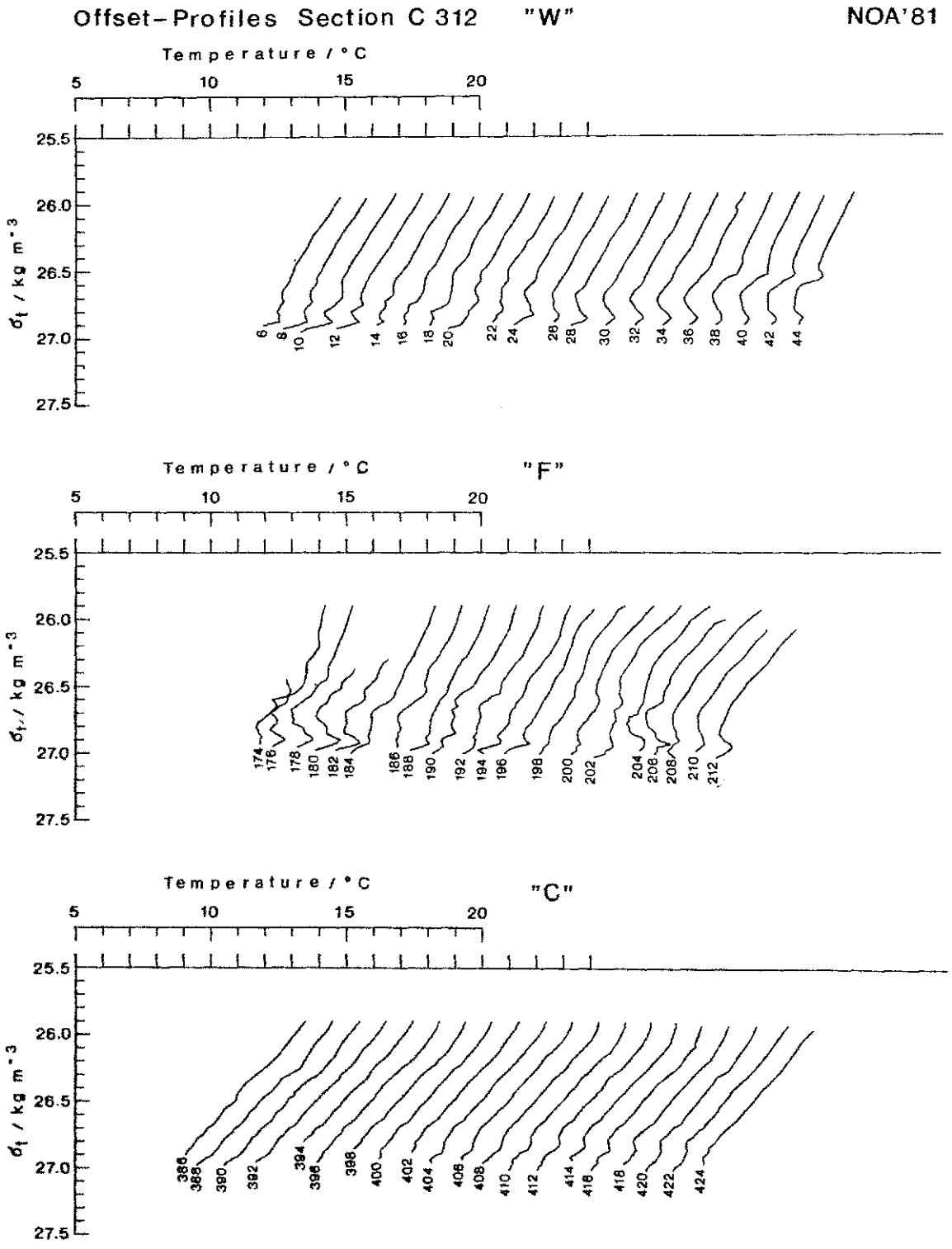

Fig. 6.2.9: Offset profiles from section C312, showing temperature versus σ_t from three selected regions ("W", "F", "C").

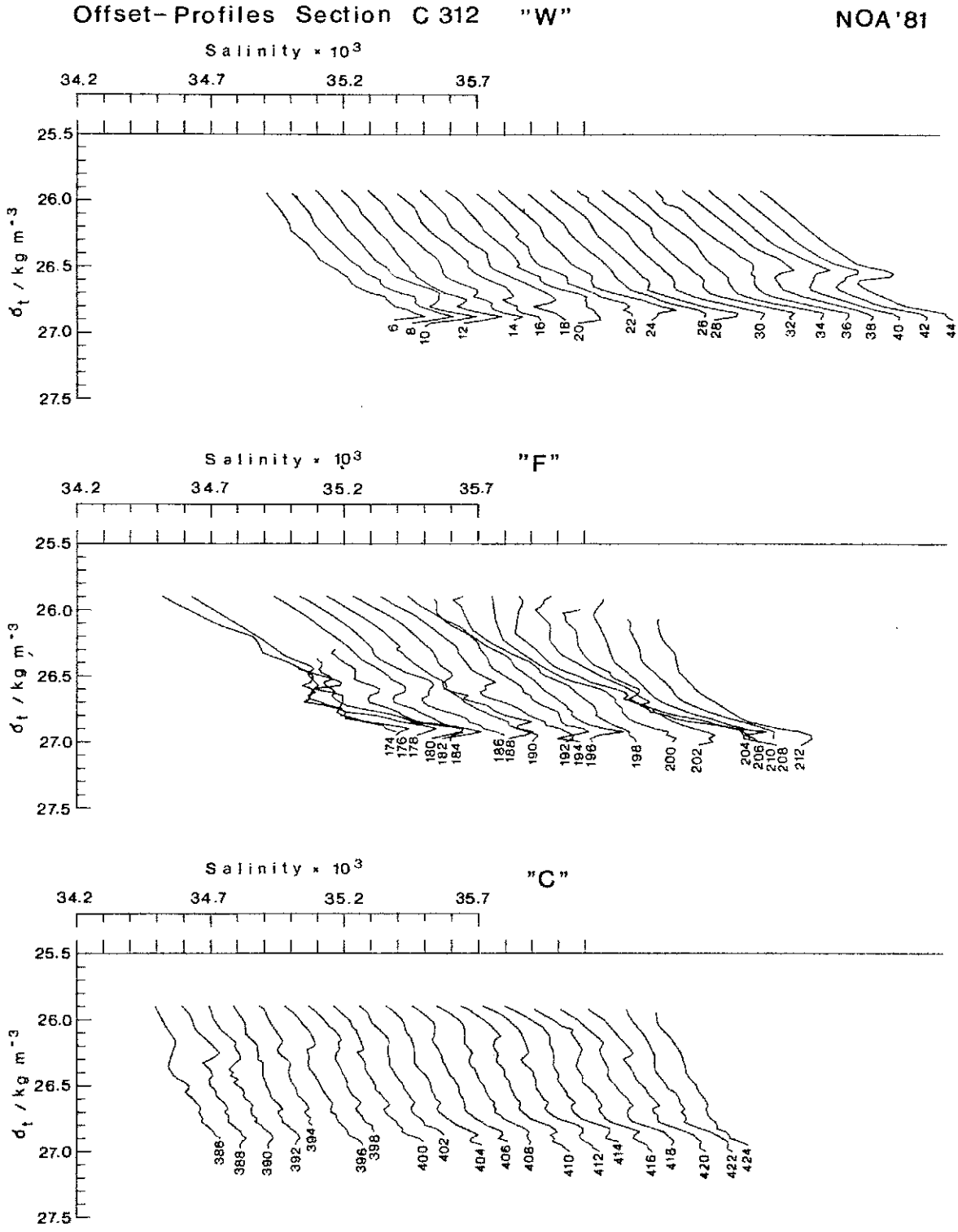

Fig. 6.2.10: Offset profiles from section C312, showing salinity versus σ_t from three selected regions ("W", "F", "C").

7. STANDARD PRODUCTS - SECTIONS

7.1 Long Section

After processing stage 5 time series of values of temperature, salinity, σ_t and pressure measured at the upper and lower turning points of the towed fish give a comprehensive overview of the range reached by the instrument along a whole long section. They also reveal immediately a number of structures which can be analysed in detail in further analysis.

The pressure values at the upper and lower turning points (fig. 7.1.1) show that the fish scanned on average the water column between 5 m and 75 m. From the 24th July the upper turning point was shifted to about 10 m due to bad weather conditions (fig. 10.1). A comparison with the mixed layer depth (fig. 7.1.2), determined by the sharp change of gradient of the temperature profile, shows that the fish always reached the "mixed layer" so that the upper turning point values represent the hydrographic conditions in the "mixed layer".

The temperatures of upper and lower turning points (fig. 7.1.3) show at first look similar patterns. However the surface temperatures show a somewhat smoother curve compared with the step-like variations at 75 m.

This difference between both curves is even more obvious in the salinities (fig. 7.1.4) where very sharp horizontal gradients underlie smoother gradients at the sea surface. Near the Azores saltier water is lying over fresher water at 75 m. Going north the surface salinity decreases compared to the 75-m-level, and stays consistently lower in the northern half of the section. The differences are notably larger around the main fronts.

The large-scale slope of the density distribution (fig. 7.1.5) shows the gyre-scale baroclinicity. The increased variability at the lower turning points between the 21st and 25th July seems to be correlated with the changing wind during these days (figure 11.1).

According to the data processing flow diagram (figure 4.1) sections were plotted after interpolation onto constant intervals of either pressure or σ_t. The results of this processing stage are presented in form of contoured sections of the different variables with pressure or σ_t as the vertical coordinates, and additionally as sections showing the horizontal distribution of a variable on a surface of constant density or pressure.

The presentation of temperature variations on equally spaced density surfaces avoids the distortion of the water column by internal waves. As temperature changes on an isopycnal must be compensated by salinity, they indicate water mass changes. Figure 7.1.6 gives a comprehensive view of the horizontal as well as vertical water mass changes along the whole section.

Between 38° and 46° N the water mass remains relatively uniform. Some synoptic-scale structures bounded by sharp fronts can be distinguished from large regions with length scales 40 - 300 km of uniform distribution.

From 46° to 53° N temperature decreases stepwise. Only at a few sites the water mass changes are distributed continously over some tens of kilometres. At the majority of this extent narrow frontal regions of some kilometres width, perceptible by strong temperature steps and inversions are embedded in horizontally relatively homogeneous regimes.

The cold water region north of 53° N seems to have less horizontal water mass variability than the subtropical region.

The spacing between the isotherms indicates how much the stability of stratification is due to the temperature gradient. South of 45° N where a positive vertical salinity gradient (compare fig. 7.1.4) reduces the stability of the water column the spacing of isotherms is smaller than at 50° N or north of 53° N regions with stabilizing negative salinity gradient.

In frontal regions, where even temperature inversions are found, the much lower salinity of the overlying water keeps the stratification stable.

7.2 Frontal Survey

In order to show the large horizontal and vertical variability in the frontal area sections C311 and C312 were again chosen. From experience with the GATE Batfish data, Woods & Minnett (1979) and Leach, Minnett and Woods (1985), it seems obvious to present the data in isopycnic coordinates, which should remove the strong internal wave signal. A set of standard isopycnals σ_t = 26.0 kg m^{-3} to σ_t = 27.0 kg m^{-3} with 0.1 kg m^{-3} increment was thought to be representative for that part of the seasonal thermocline which lies in the range of the towed fish. This also means, that there is almost no information about the "mixed layer". For a better comparison of the two sections, which originally have had reversed orientation, section C311 was reversed, and both sections were projected onto straight lines

defined by their start and end positions. Additionally the data were interpolated linearly to a standard horizontal spacing of Δx = 0.4 km, which corresponds to the mean wavelength of the towed fish during the front experiment.

In figure 7.2.1 the temperature on isopycnals is shown, and because the temperature will be compensated by salinity on any particular isopycnal, this parameter is an indicator of the water masses at the front. The most striking feature in both sections are the warm (salty) water at the southeast end and the cold (fresh) water at the northwest end, separated by a region of strong thermoclinicity, the temperature gradient on an isopycnal, which is only a few kilometres wide. Temperature inversions are observed in the warmer part of the sections, which is mostly dominated by salinity, whereas at the cold side, which is temperature dominated, almost no inversions occur.

Unfortunately in the case of the most important quantity for dynamical studies, namely the depth of the isopycnals, it is not possible to remove internal waves by such a simple method. Figure 7.2.2 is therefore a mixture of the internal wave signal and frontal baroclinicity. Nevertheless both sections show similarities which are unlikely to be due to internal waves. So the upper isopycnals on the warm side are closer to the surface than on the cold side, which is in contrast to the large-scale baroclinicity with the isopycnals sloping up to the cold (fresh) water in the north. This trend is reversed in the deeper part of the section, where σ_t = 27.0 kg m^{-3} is found only in the cold and fresh region and is outside the fish's range in the warmer part.

Isopycnal spacing is presented in figure 7.2.3 as the depth difference between successive isopycnals and σ_t = 26.5 kg m^{-3}. This should remove most of the internal wave signal, namely the lowest mode, which moves isopycnals up and down together. The higher modes, though less energetic, are still present. This plot should at least give an indication of the vortex stretching (Fischer, Leach and Woods, 1985). The maximum spacing above σ_t = 26.5 kg m^{-3} is found at about 50 km from the origin of the sections accompanied by a minimum below the reference surface. Strong similarities in the isopycnal spacing can be seen in both sections.

In order to illuminate the advantage of isopycnic analysis the temperature distribution on surfaces of constant pressure is also shown (figure 7.2.4). Here the standard surfaces were from 20 m to 80 m being 10 m apart. In this

diagram the "mixed layer" signal is present in the uppermost surface of 20 m, and the temperature distribution is due to internal waves as well as frontal structures. From the mean profiles in chapter 8 the magnitude of the internal wave contribution to the observed variability can be estimated.

In order to explore the vertical extent of the observed structures, a standard CTD section across the region of strongest thermohaline contrast was made. The station distance was 5 nautical miles and the CTD was lowered down to 600 m.

Figure 7.2.5 shows the temperature distribution with strong horizontal gradients even in the deepest part of the section, although the strongest gradients were found in the top 200 metres.

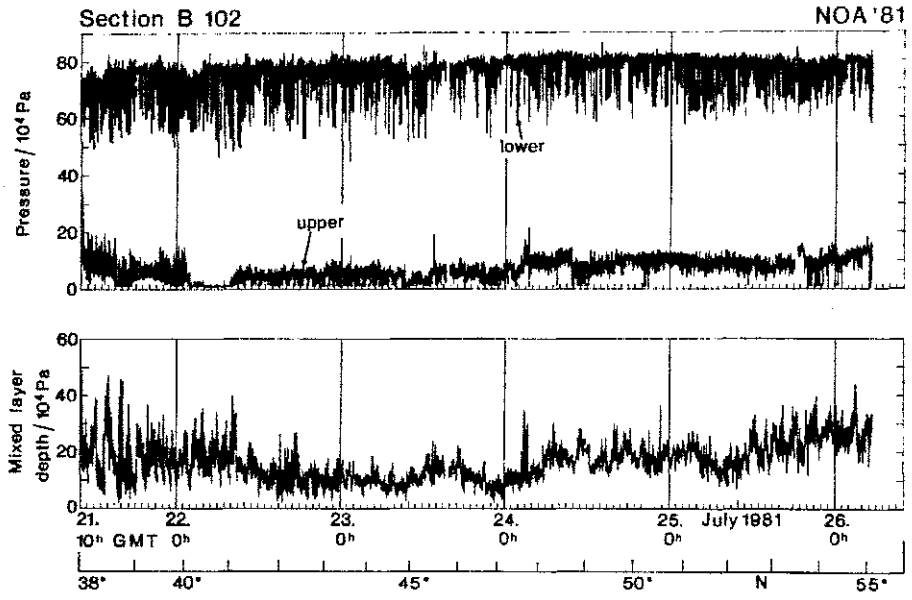

Fig. 7.1.1: Pressure values at the upper and lower turning points of the towed fish's undulations along section B102.

Fig. 7.1.2: Mixed layer depth along section B102 defined by the criterion: the depth where the vertical temperature gradient exceeds $\frac{dT}{dz} = 0.09\ K\ m^{-1}$.

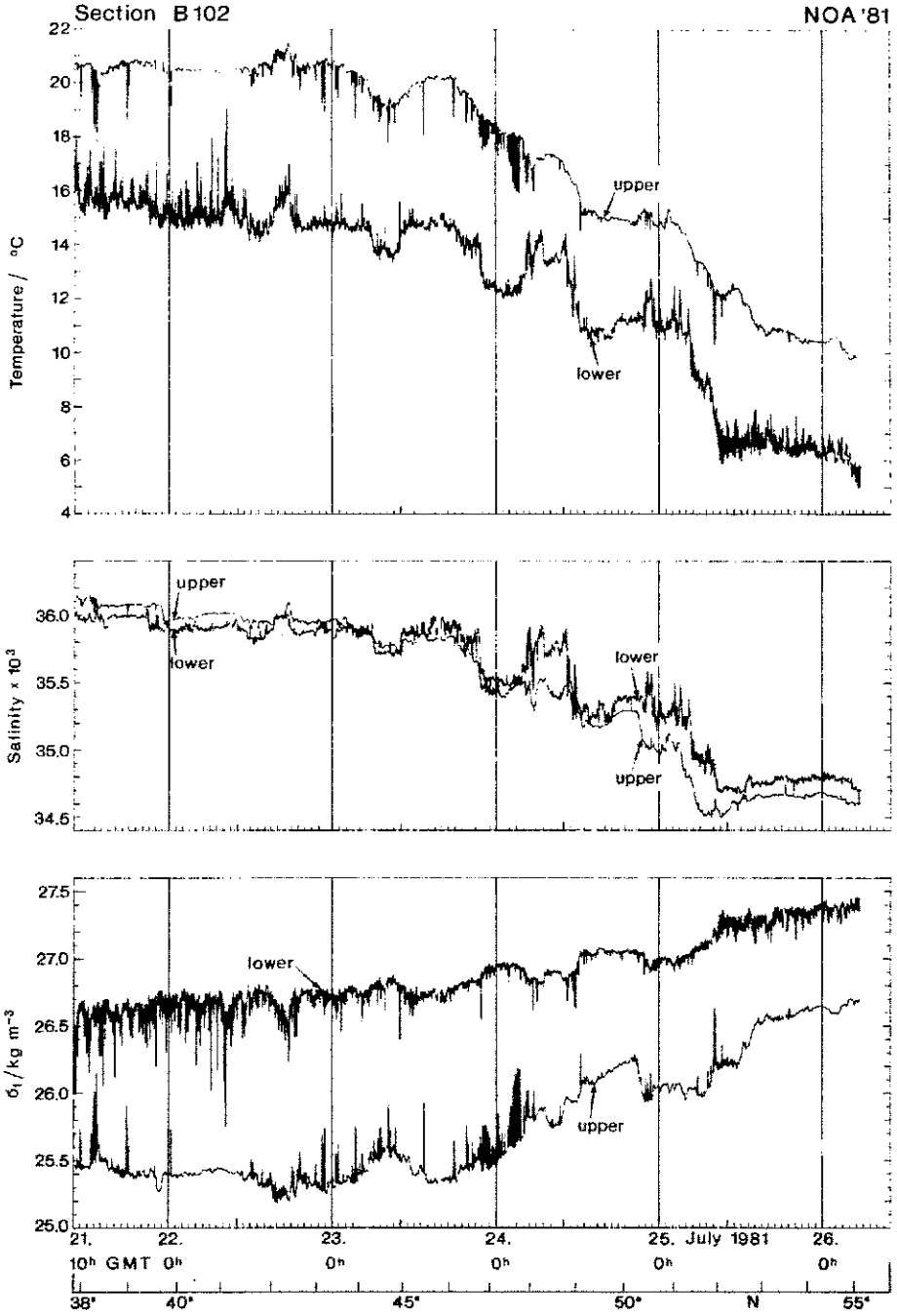

Fig. 7.1.3. - Fig. 7.1.5: Temperature, salinity and σ_t at the upper and lower turning points of the towed fish's undulation along section B102.

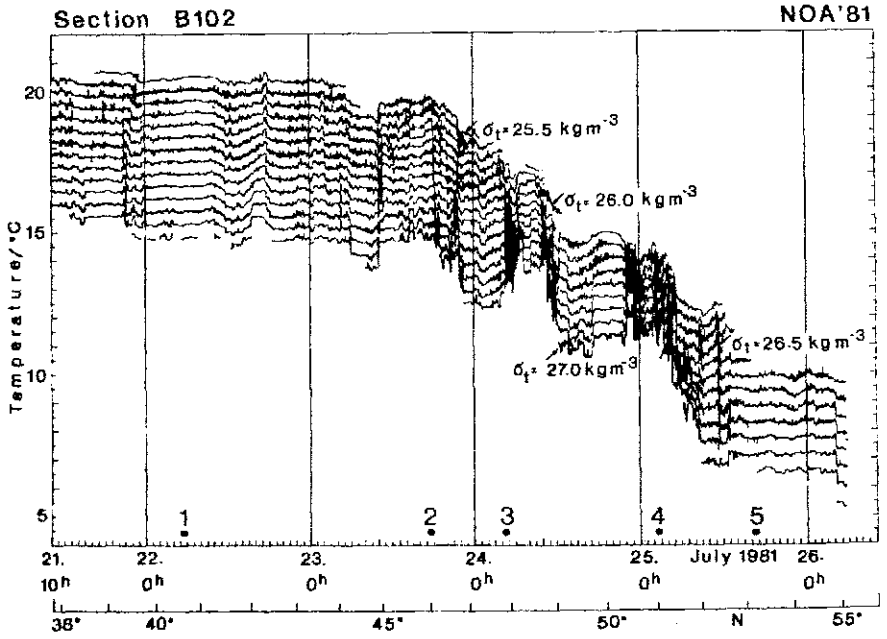

Fig. 7.1.6: Temperature distribution on surfaces of constant σ_t (σ_t = 25.4 to 27.4 kg m^{-3}) of section B102.
The numbered dots indicate the 5 selected sets presented as offset and mean profiles in chapter 6.

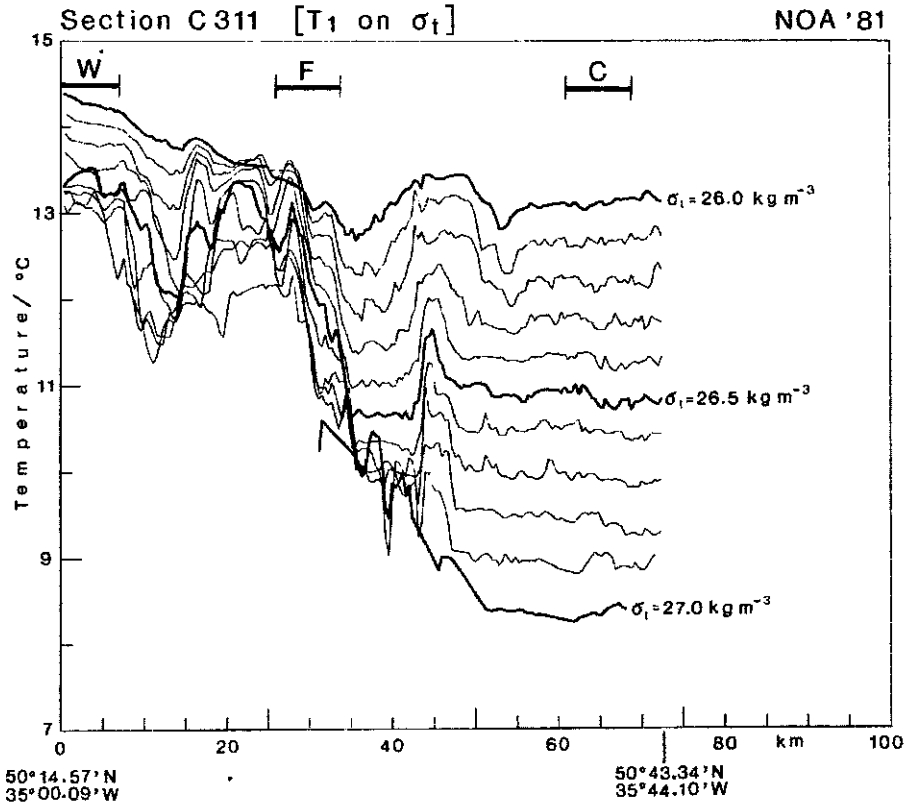

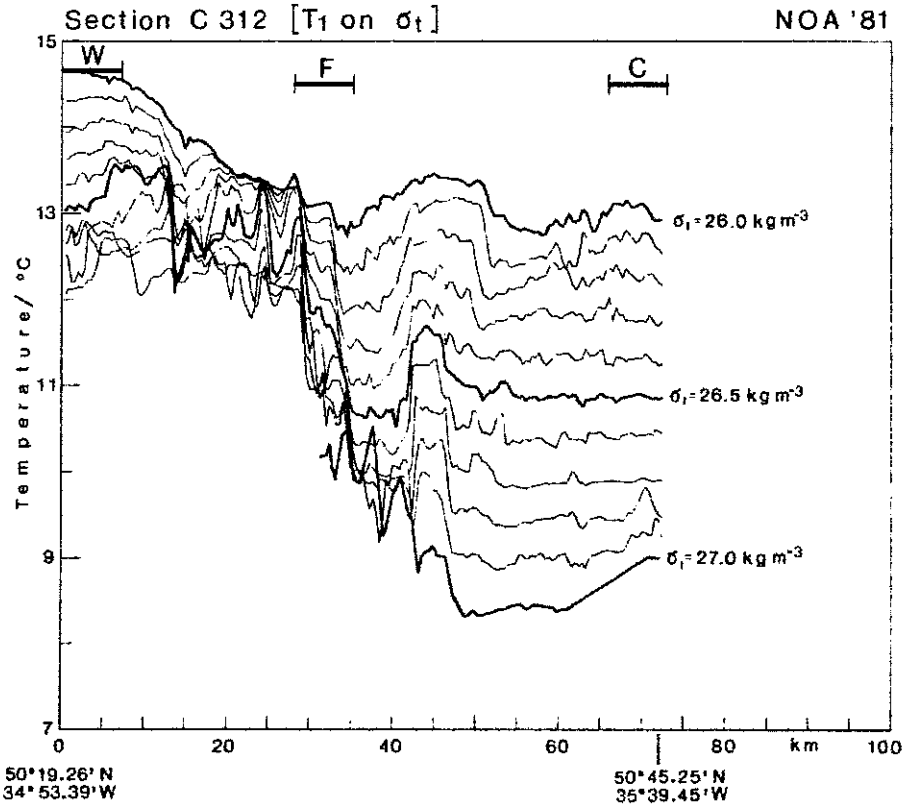

Fig. 7.2.1: Temperature distribution on selected isopycnals (σ_t = 26.0 kg m^{-3} - 27.0 kg m^{-3}) of two parallel sections C311 and C312. Heavy bars indicate selected regions presented as offset profiles.

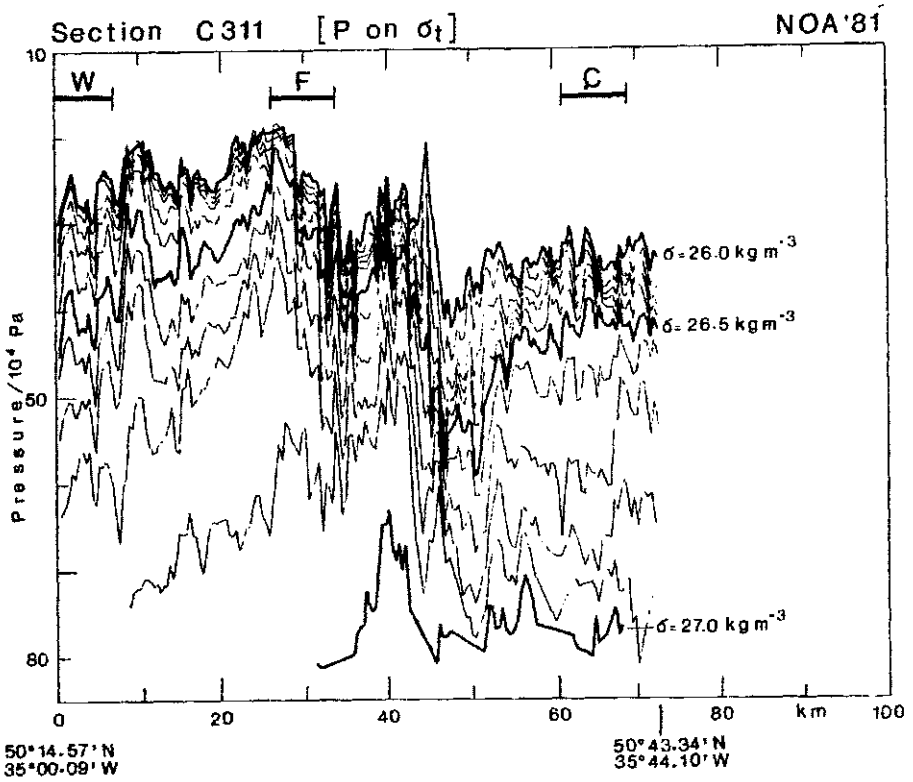

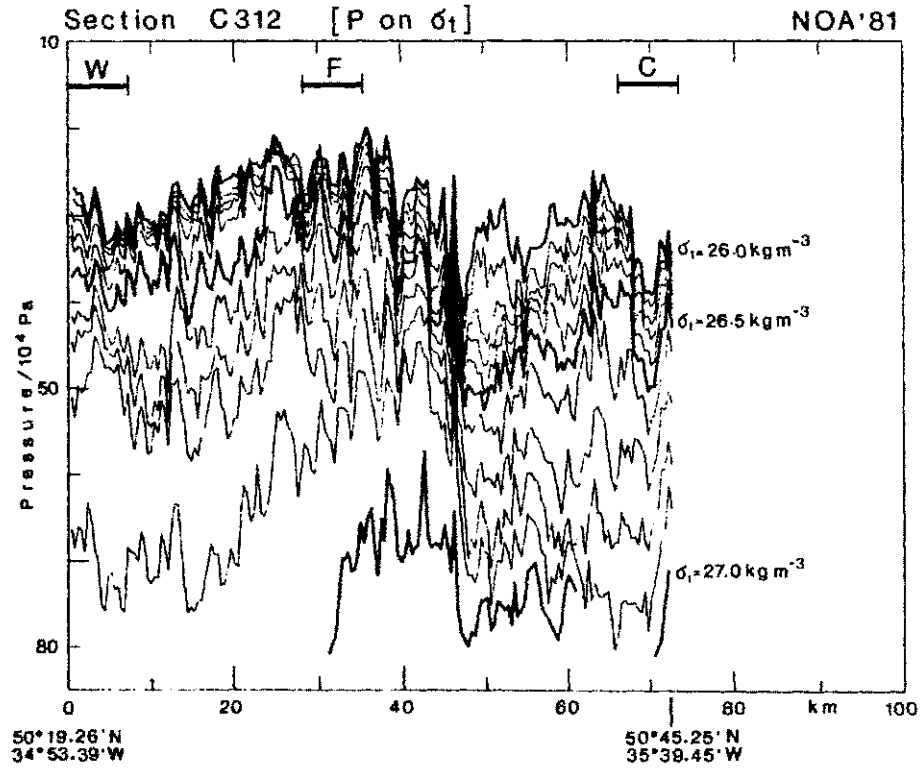

Fig. 7.2.2: Depth of selected isopycnals (σ_t = 26.0 kg m^{-3} - 27.0 kg m^{-3}) of two parallel sections C311 and C312. Heavy bars indicate selected regions presented as offset profiles.

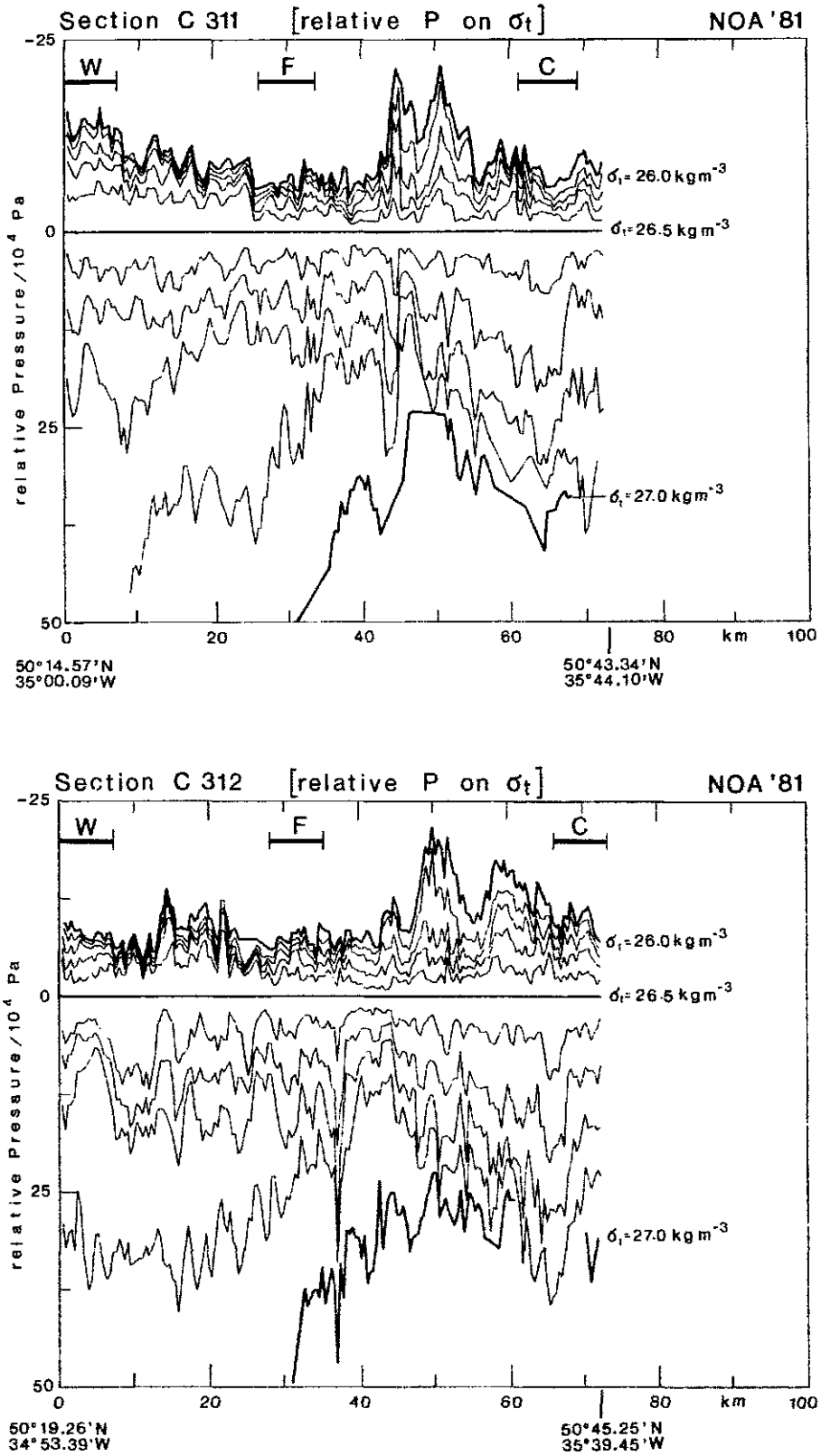

Fig. 7.2.3: Depth of selected isopycnals relative to σ_t = 26.5 kg m^{-3} for two parallel sections C311 and C312. Heavy bars indicate selected regions presented as offset profiles.

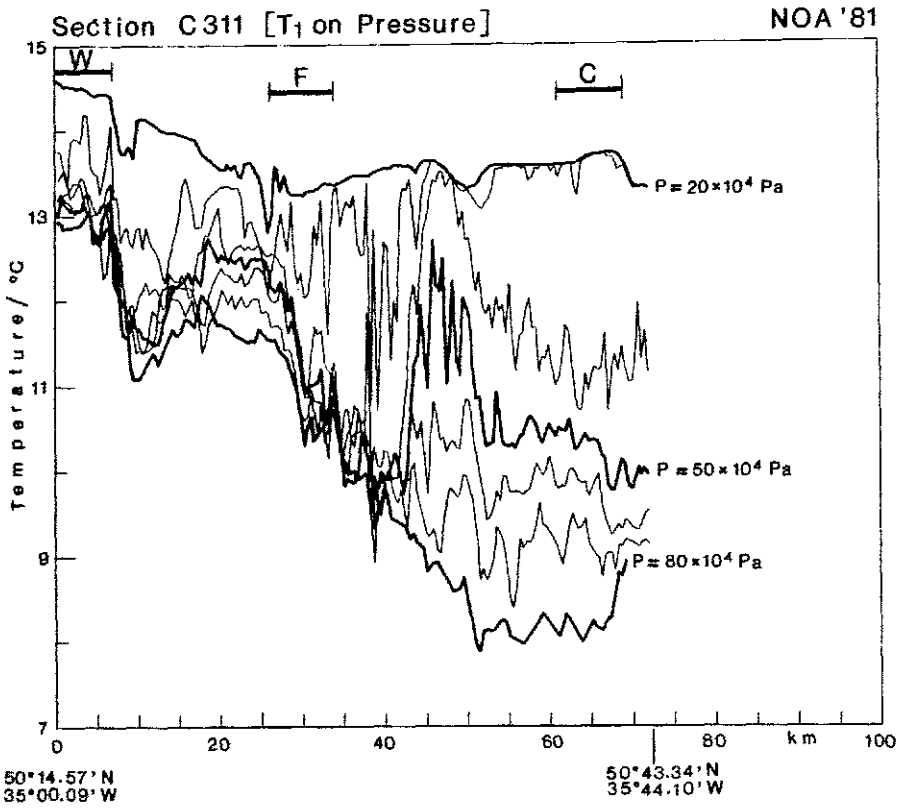

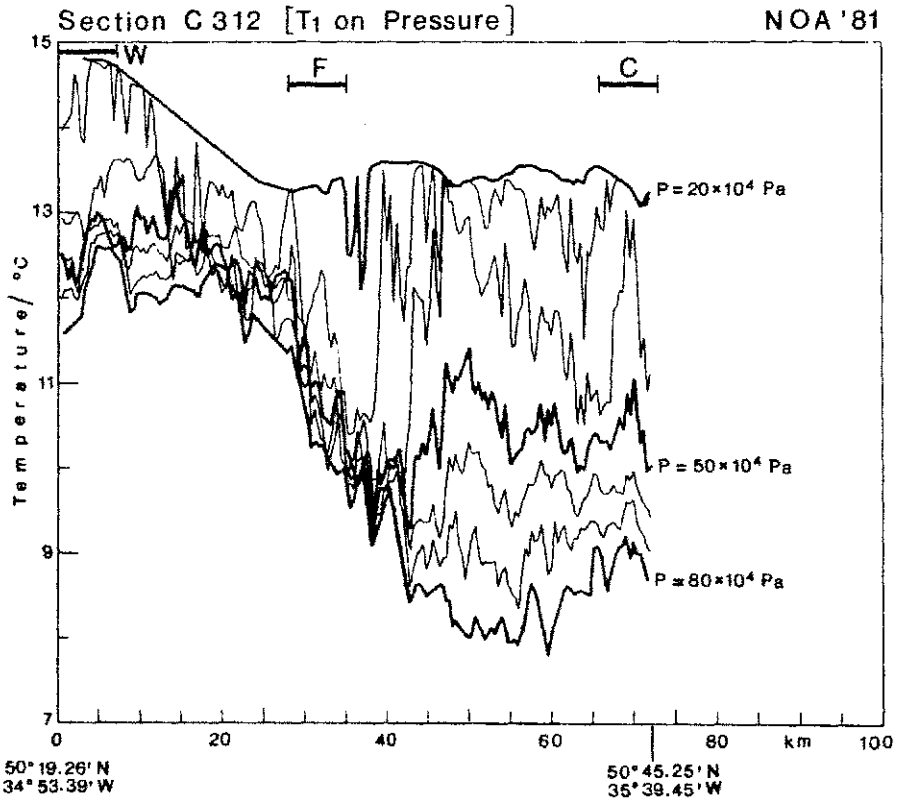

Fig. 7.2.4: Temperature distribution in seven depth layers, being 10 m apart from parallel sections C311 and C312. Heavy bars indicate selected regions presented as offset profiles.

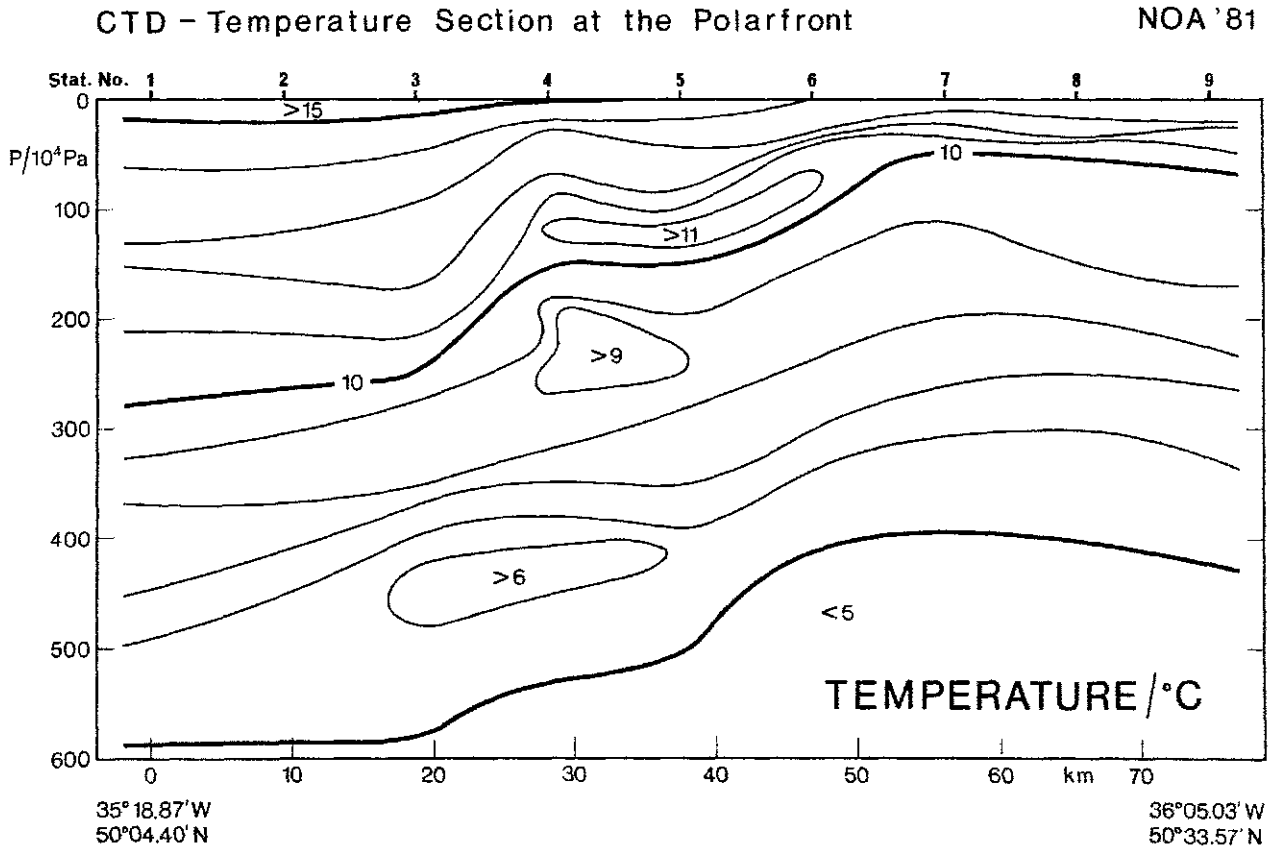

Fig. 7.2.5: Temperature section in the region of strongest horizontal temperature gradients, derived from standard CTD station data.

8. STATISTICS OF THE HYDROGRAPHIC DATA

In this chapter diagrams of mean profiles with their standard deviations will be shown. A comparison between data averaged on constant density with data averaged on constant pressure will be made, to show how much of the observed variability is due to internal waves and how much is due to frontal processes.

Histograms of salinity, temperature and normalized isopycnal spacing on surfaces of constant density are also shown.

T-S diagrams are presented to illustrate water mass characteristics.

8.1 Mean and standard deviation profiles

a) Frontal Survey

From the frontal area sections C311 and C312 are again shown. Mean profiles for the cold and warm side of the front are presented and can be compared with those from the region of maximum thermoclinicity. As in the series of offset profiles shown in paragraph 6.2 the averaging intervals were chosen to be 20 profiles (7 - 8 km).

Figures 8.1.1 and 8.1.2 show mean profiles whith their standard deviations of temperature, salinity and density averaged on constant pressure. The statistical significance of these profiles can be seen from the number of contributions. The variability in these profiles is indicated by their standard deviations, being partly internal wave induced and partly due to the frontal variability. The variability is strongest at the thermoclinicity maximum and it is interesting to note that a well developed mixed layer can only be detected at the warm and cold side of the front.

In order to remove most of the internal wave signal figures 8.1.3 and 8.1.4 show the set of profiles averaged on constant σ_t. Notice the remarkable difference in the standard deviations of the 'front' compared with the other regimes, which means, that there is a very narrow T-S relationship on both sides of the front with a highly variable transition zone in-between. As already mentioned the thermohaline difference between these regions is increasing with depth.

For comparison of the internal wave-induced variability with that of the front, mean and standard deviation profiles of temperature and salinity

were averaged along constant σ_t, but plotted versus the mean pressure of the density layer in question (figures 8.1.5, 8.1.6). This procedure led to a reduction of the variability especially at the cold and warm sides.

b) Long Sections

Large-scale variability along section B102 can be seen from a series of mean profiles and their standard deviations of temperature and salinity (8.1.7., 8.1.8). Each of the profiles represent the average conditions for each degree of latitude, beginning just north of the Azores 38° N up to 55° N. The averaging was performed on surfaces of constant σ_t to reduce the internal wave signal, but temperature and salinity are presented as a function of their mean pressures.

Most of the standard deviations of the averaged profiles are larger or smaller depending on the intensity of eddies and mesoscale fronts in the latitude interval. Only the averages centred at 46.5°, 48.5°, 50.5° and 51.5° N which include the main branches of the Polar Front have clearly larger standard deviations and a different slope of the mean profile.

To show the clear differences of regimes regardless of their situation in geographical intervals, four of the selected sets described in paragraph 6.1 were averaged along isopycnals and presented versus pressure in figure 8.1.10 analogous to the mean profiles of the frontal survey.

The low standard deviations in the averages of set 1 and 5 indicate their situation in isopycnically homogeneous regimes. Set 1 situated in subtropical waters is thermally stronger stratified than set 5 lying in subpolar water. But the positive salinity gradient in set 1 reduces the stability, while the negative salinity gradient in set 5 supports the thermal stratification.

The large standard deviations of set 3 and 4 indicate the high horizontal variability in the regions of maximum thermoclinicity along the section. In both profiles they have maxima at about 30 and 50 m. The drastic decrease at the top of the profiles show how the strong thermoclinicity in the thermocline is hidden from the surface by a horizontally much more horizontally homogeneous mixed layer.

A clearly distinguishable colder and fresher water mass in the upper 45 m leads to the bending of the mean profiles.

Section B102 was averaged along constant densities in intervals of 1° of latitude.

Statistical moments of the isopycnic distribution of pressure, temperature, salinity and the spacing between $\sigma_t = \pm 0.05$ kg m^{-3} are listed in tables 8.1.1 - 17 for isopycnals being 0.1 kg m^{-3} apart.

The uppermost value of any profile was excluded from averaging, to avoid the contamination of the statistics by values of the mixed layer. Unlike temperature and salinity where regions of relatively uniform water mass can clearly be distinguished from regions of varying water masses, the pressure distribution and the isopycnal spacing do not show obvious correlations with the hydrographic features.

The variability of pressure is greatest near the Azores. In the frontal region it increases only in the lower layers at strong fronts. The spacing shows some isolated, heavily skewed distributions with high kurtosis.

8.2 Probability distributions on surfaces of constant density

In this section probability distribution functions (PDF) of temperature (figure 8.2.1), salinity (figure 8.2.2) and pressure (figure 8.2.3) on surfaces of constant density will be shown. Each PDF represents all data points in the frontal region on a distinct σ_t-surface. The number of points in each window is normalized by the total number of points on that surface. The PDF's of salinity and temperature show a bimodal structure indicating the two water masses observed in that area. This bimodal structure is not observed in the pressure distribution, furthermore the pressure distribution is nearly Gaussian, especially on the surfaces $\sigma_t = 26.6$ kg m^{-3} and $\sigma_t = 26.3$ kg m^{-3} where the kurtosis is around three (table 8.2.1) and the skewness is very small. PDF's of normalized thickness (spacing between pairs of isopycnals being 0.1 kg m^{-3} apart) are also shown. To remove the effect of changes in the mean vertical density gradient, the thickness is normalized with regard to its mean value (see table 8.2.1). The resulting PDF's (figure 8.2.4) show a very skewed distribution, up to four times its mean value.

8.3 T-S Diagrams

a) Front Regions

One of the most classic diagrams in oceanography is that of the T-S relationship, which again is presented for typical regions named "C", "F", "W" from sections C311 and C312 (figure 8.3.1, 8.3.2.). The averaging was carried out along density surfaces and the bars in the figures denote standard deviations of typical places in the T-S domain. The total range in salinity is $34.5 \cdot 10^{-3}$ - $35.5 \cdot 10^{-3}$ and 9 °C to about 15 °C. Comparing the T-S diagrams from "C" and "W" it can be seen that the salinities - as well as the temperatures - are closer to each other above σ_t = 26.0 kg m^{-3} and deviate more to about σ_t = 26.9 kg m^{-3}, where the warm side shows a strong salinity maximum. This maximum could also be detected in the region of the thermoclinicity maximum. Furthermore the T-S profile in that region shows strong similarities to that of the warm side although the thermohaline variability, shown by the standard deviation bars is much stronger at the thermoclinicity maximum. Another notable feature is the very fresh water in the top layers of the thermoclinicity maximum region which can be explained by a phase shift of the thermoclinicity signal with depth and the very fresh band of water seen on the cold side of the thermoclinicity maximum in the section plots (figure 7.2.1).

b) Long Sections

The same presentation for the four typical sets of the long section B102 is used in figure 8.3.3. In the regions with relatively uniform water masses, No 1 and No 5, where the standard deviation bars are small, the density stratification is mainly due to the positive temperature gradient. The salinity provides in region No 1 a slight reduction of the stability with its positive gradient and in region No 5 an increase in stability with a weak negative gradient. The two examples, chosen from regions with maximum horizontal temperature and salinity gradients show similarities, too. The upper part is mainly thermally stratified until a clear increase of salinity indicates the transition to a different water mass in which the profile continues again in nearly vertical direction. The mixed layer represented by the uppermost standard deviation bar has a much lower horizontal variability than the thermocline.

Table 8.1.1 - 17

Statistics of dependent variables on isopycnal surfaces from section B102, NOA '81 for one degree intervals.

table 8.1.1:	38° N to 39° N,	26°06' W	to	26°40' W
table 8.1.2:	39° N to 40° N,	26°40' W	to	27°14' W
table 8.1.3:	40° N to 41° N,	27°14' W	to	27°50' W
table 8.1.4:	41° N to 42° N,	27°50' W	to	28°25' W
table 8.1.5:	42° N to 43° N,	28°25' W	to	29°01' W
table 8.1.6:	43° N to 44° N,	29°01' W	to	29°38' W
table 8.1.7:	44° N to 45° N,	29°23' W	to	30°15' W
table 8.1.8:	45° N to 46° N,	30°15' W	to	30°56' W
table 8.1.9:	46° N to 47° N,	30°56' W	to	31°32' W
table 8.1.10:	47° N to 48° N,	31°32' W	to	32°11' W
table 8.1.11:	48° N to 49° N,	32°11' W	to	32°52' W
table 8.1.12:	49° N to 50° N,	32°52' W	to	33°33' W
table 8.1.13:	50° N to 51° N,	33°33' W	to	34°15' W
table 8.1.14:	51° N to 52° N,	34°15' W	to	34°57' W
table 8.1.15:	52° N to 53° N,	34°57' W	to	35°41' W
table 8.1.16:	53° N to 54° N,	35°41' W	to	36°26' W
table 8.1.17:	54° N to 55° N,	36°26' W	to	37°11' W

PRES : Pressure / 10^4 Pa

TEM1 : Temperature / °C of sensor 1

S1 : Salinity x 10^3 of sensor pair 1

PDIF : Pressure difference / 10^4 Pa between isopycnals plus and minus $\Delta\sigma_t$ = 0.05 kg m^{-3} the σ_t-surface in question.

table 8.1.1: 38° N to 39° N, 26°06' W to 26°40' W

Surface	Parameter	Mean	Minimum	Maximum	St.Dev.	Skewness	Kurtosis	Datapoints
Sigmat = 25.500								
	PRES	19.060	4.390	45.540	7.900	0.490	3.056	176.
	TEM1	20.320	20.180	20.480	0.082	0.572	1.786	176.
	S 1	36.077	36.030	36.135	0.029	0.573	1.787	176.
	PDIF	4.090	0.430	36.190	4.922	4.297	25.360	83.
Sigmat = 25.600								
	PRES	21.970	6.060	48.440	8.890	0.505	2.876	245.
	TEM1	19.890	19.780	20.160	0.084	0.807	2.712	245.
	S 1	36.061	36.021	36.154	0.029	0.815	2.731	245.
	PDIF	2.650	0.380	18.120	2.337	2.840	14.900	238.
Sigmat = 25.700								
	PRES	24.580	8.240	57.480	9.380	0.492	2.869	265.
	TEM1	19.450	19.320	19.810	0.085	1.123	4.007	265.
	S 1	36.040	35.995	36.161	0.029	1.135	4.041	265.
	PDIF	2.630	0.370	14.790	2.025	1.861	8.130	261.
Sigmat = 25.800								
	PRES	26.720	9.930	63.580	9.780	0.503	2.982	270.
	TEM1	19.020	18.870	19.380	0.082	1.327	5.598	270.
	S 1	36.024	35.973	36.146	0.028	1.349	5.682	270.
	PDIF	2.340	0.240	13.870	1.851	2.870	14.580	268.
Sigmat = 25.900								
	PRES	29.140	11.350	71.880	10.220	0.492	3.196	270.
	TEM1	18.580	18.410	18.830	0.069	0.741	3.712	270.
	S 1	36.008	35.953	36.090	0.023	0.759	3.759	270.
	PDIF	2.580	0.240	10.990	1.819	1.667	6.440	270.
Sigmat = 26.000								
	PRES	31.930	12.610	73.030	10.590	0.408	2.911	272.
	TEM1	18.150	17.970	18.330	0.062	0.427	3.252	272.
	S 1	35.998	35.939	36.056	0.020	0.444	3.246	272.
	PDIF	3.200	0.380	11.900	2.023	1.313	4.750	272.
Sigmat = 26.100								
	PRES	35.120	13.810	74.680	10.700	0.311	2.917	273.
	TEM1	17.730	17.510	17.900	0.058	0.396	3.449	273.
	S 1	35.991	35.922	36.047	0.019	0.403	3.443	273.
	PDIF	3.740	0.440	19.290	2.407	2.036	10.410	272.
Sigmat = 26.200								
	PRES	39.110	15.150	75.370	10.620	0.229	2.935	273.
	TEM1	17.300	17.160	17.470	0.058	0.037	3.222	273.
	S 1	35.987	35.941	36.040	0.018	0.044	3.219	273.
	PDIF	4.370	0.380	17.220	2.922	1.581	6.000	271.
Sigmat = 26.300								
	PRES	43.390	17.240	70.570	10.540	0.066	2.886	265.
	TEM1	16.870	16.670	17.020	0.058	-0.408	4.141	265.
	S 1	35.980	35.921	36.027	0.018	-0.396	4.135	265.
	PDIF	5.750	0.650	20.890	3.282	1.420	6.200	261.
Sigmat = 26.400								
	PRES	50.070	27.900	76.430	9.720	0.234	2.746	253.
	TEM1	16.440	16.190	16.590	0.070	-1.325	5.229	253.
	S 1	35.979	35.903	36.025	0.021	-1.314	5.199	253.
	PDIF	8.900	0.940	26.080	5.167	1.049	3.790	240.
Sigmat = 26.500								
	PRES	58.310	37.860	80.090	8.590	-0.041	2.245	222.
	TEM1	16.000	15.760	16.140	0.082	-1.093	3.902	222.
	S 1	35.977	35.905	36.018	0.024	-1.084	3.882	222.
	PDIF	10.300	1.310	31.710	5.584	1.066	4.350	180.
Sigmat = 26.600								
	PRES	66.610	51.180	80.810	6.230	-0.096	2.311	111.
	TEM1	15.540	15.280	15.720	0.100	-1.197	3.894	111.
	S 1	35.971	35.895	36.024	0.029	-1.187	3.881	111.
	PDIF	14.850	3.530	30.950	6.612	0.565	2.720	27.

table 8.1.2: 39° N to 40° N, 26°40' W to 27°14' W

Surface	Parameter	Mean	Minimum	Maximum	St.Dev.	Skewness	Kurtosis	Datapoints
Sigmat = 25.400								
	PRES	17.800	6.020	33.940	4.862	0.170	3.122	133.
	TEM1	20.540	20.290	20.690	0.135	-0.555	1.601	133.
	S 1	36.024	35.934	36.077	0.048	-0.555	1.602	133.
	PDIF	1.740	0.373	5.780	1.400	1.341	3.900	3?.
Sigmat = 25.500								
	PRES	20.980	5.040	38.390	5.578	-0.222	3.032	268.
	TEM1	20.130	19.850	20.460	0.151	-0.407	1.577	268.
	S 1	36.012	35.913	36.125	0.053	-0.405	1.577	268.
	PDIF	2.350	0.373	11.800	1.501	2.212	10.640	265.
Sigmat = 25.600								
	PRES	22.610	6.230	40.220	5.663	-0.247	3.092	269.
	TEM1	19.700	19.420	19.950	0.146	-0.213	1.610	269.
	S 1	35.995	35.899	36.081	0.050	-0.208	1.609	269.
	PDIF	1.640	0.383	6.860	0.971	1.992	9.450	268.
Sigmat = 25.700								
	PRES	24.440	6.690	43.810	5.836	-0.220	3.346	270.
	TEM1	19.260	18.970	19.600	0.145	-0.201	1.841	270.
	S 1	35.975	35.876	36.089	0.049	-0.193	1.844	270.
	PDIF	2.070	0.460	7.620	1.246	1.499	5.650	269.
Sigmat = 25.800								
	PRES	26.630	8.310	44.910	5.974	-0.227	3.085	271.
	TEM1	18.830	18.530	19.100	0.139	-0.209	1.849	271.
	S 1	35.961	35.860	36.051	0.046	-0.203	1.847	271.
	PDIF	2.390	0.527	7.240	1.235	0.802	3.220	271.
Sigmat = 25.900								
	PRES	29.250	11.110	48.730	6.003	-0.076	3.084	271.
	TEM1	18.410	18.130	18.700	0.132	-0.255	2.061	271.
	S 1	35.953	35.860	36.047	0.043	-0.246	2.063	271.
	PDIF	2.910	0.405	11.030	1.567	1.708	8.140	271.
Sigmat = 26.000								
	PRES	32.440	12.730	51.450	6.011	-0.104	3.188	271.
	TEM1	17.980	17.720	18.300	0.135	-0.107	1.922	271.
	S 1	35.944	35.860	36.046	0.044	-0.099	1.925	271.
	PDIF	3.390	0.572	11.560	1.968	1.467	5.400	271.
Sigmat = 26.100								
	PRES	35.920	15.690	54.430	6.289	0.055	3.182	271.
	TEM1	17.550	17.300	17.870	0.138	0.094	1.750	271.
	S 1	35.935	35.857	36.036	0.044	0.100	1.754	271.
	PDIF	3.640	0.614	12.180	2.232	1.379	4.820	271.
Sigmat = 26.200								
	PRES	39.930	18.470	61.080	7.056	0.133	2.944	270.
	TEM1	17.120	16.870	17.460	0.155	0.115	1.673	270.
	S 1	35.930	35.852	36.038	0.049	0.121	1.678	270.
	PDIF	4.810	1.074	18.590	2.434	1.398	6.690	270.
Sigmat = 26.300								
	PRES	45.170	26.410	71.240	7.337	0.302	3.271	268.
	TEM1	16.710	16.440	17.070	0.164	0.175	1.731	268.
	S 1	35.931	35.850	36.045	0.051	0.182	1.738	268.
	PDIF	5.340	1.501	20.650	2.865	1.819	7.890	266.
Sigmat = 26.400								
	PRES	51.080	31.950	75.790	7.174	0.593	3.571	263.
	TEM1	16.290	16.010	16.660	0.170	0.178	1.599	263.
	S 1	35.933	35.851	36.046	0.052	0.184	1.604	263.
	PDIF	6.940	1.586	17.940	3.010	0.878	3.560	257.
Sigmat = 26.500								
	PRES	58.050	38.330	75.560	6.944	0.252	2.815	250.
	TEM1	15.870	15.600	16.210	0.165	0.124	1.467	250.
	S 1	35.937	35.857	36.041	0.049	0.129	1.469	250.
	PDIF	8.640	1.414	18.880	3.230	0.529	3.130	226.
Sigmat = 26.600								
	PRES	66.160	51.160	79.720	5.771	-0.127	2.504	190.
	TEM1	15.420	15.190	15.790	0.164	0.321	1.580	190.
	S 1	35.935	35.869	36.044	0.048	0.326	1.588	190.
	PDIF	11.770	4.809	27.510	3.888	0.929	4.360	115.

table 8.1.3: 40° N to 41° N, 27°14' W to 27°50' W

Surface	Parameter	Mean	Minimum	Maximum	St.Dev.	Skewness	Kurtosis	Datapoints
Sigmat = 25.500								
	PRES	21.160	8.660	38.910	5.482	0.397	3.048	248.
	TEM1	20.040	19.940	20.220	0.047	0.007	3.238	248.
	S 1	35.981	35.945	36.043	0.016	0.009	3.253	248.
	PDIF	2.410	0.360	13.200	1.736	3.106	16.450	231.
Sigmat = 25.600								
	PRES	23.270	9.830	41.980	5.573	0.295	3.139	248.
	TEM1	19.630	19.470	19.790	0.049	-0.111	3.155	248.
	S 1	35.970	35.915	36.024	0.017	-0.110	3.168	248.
	PDIF	2.270	0.360	9.030	1.401	1.389	5.330	248.
Sigmat = 25.700								
	PRES	25.760	11.700	45.020	5.868	0.275	3.170	248.
	TEM1	19.210	19.060	19.330	0.054	-0.428	2.902	248.
	S 1	35.957	35.907	35.999	0.018	-0.418	2.898	248.
	PDIF	2.410	0.360	10.050	1.437	1.637	7.290	248.
Sigmat = 25.800								
	PRES	28.120	12.720	46.470	6.144	0.237	3.077	248.
	TEM1	18.800	18.640	18.970	0.053	-0.313	3.753	248.
	S 1	35.949	35.898	36.008	0.018	-0.300	3.749	248.
	PDIF	2.480	0.620	7.390	1.386	1.157	4.100	248.
Sigmat = 25.900								
	PRES	30.770	13.670	51.360	6.582	0.157	3.068	248.
	TEM1	18.370	18.150	18.480	0.051	-1.101	5.112	248.
	S 1	35.938	35.868	35.974	0.017	-1.089	5.081	248.
	PDIF	2.860	0.640	11.790	1.600	1.417	6.640	248.
Sigmat = 26.000								
	PRES	33.860	14.870	53.780	6.966	0.130	3.153	247.
	TEM1	17.940	17.720	18.060	0.045	-1.229	5.952	247.
	S 1	35.931	35.859	35.968	0.014	-1.217	5.896	247.
	PDIF	3.100	0.400	8.720	1.634	1.000	3.610	247.
Sigmat = 26.100								
	PRES	36.890	16.180	57.090	6.959	0.114	3.274	247.
	TEM1	17.510	17.400	17.610	0.036	-0.710	4.314	247.
	S 1	35.923	35.887	35.954	0.011	-0.700	4.298	247.
	PDIF	3.140	0.640	10.870	1.633	1.265	5.400	246.
Sigmat = 26.200								
	PRES	39.850	17.610	59.840	6.918	0.063	3.208	245.
	TEM1	17.080	16.940	17.180	0.033	-0.717	5.111	245.
	S 1	35.917	35.873	35.948	0.010	-0.707	5.196	245.
	PDIF	3.370	0.650	9.800	1.846	0.946	3.620	245.
Sigmat = 26.300								
	PRES	43.970	24.590	63.000	7.294	0.032	2.807	245.
	TEM1	16.650	16.560	16.730	0.026	0.019	4.088	245.
	S 1	35.914	35.886	35.939	0.008	0.025	3.934	245.
	PDIF	4.790	0.990	14.300	2.669	1.200	4.400	243.
Sigmat = 26.400								
	PRES	49.070	30.090	67.070	7.153	0.028	2.795	243.
	TEM1	16.220	16.150	16.300	0.024	0.005	3.541	243.
	S 1	35.912	35.890	35.936	0.007	0.009	3.827	243.
	PDIF	5.790	1.040	20.850	3.355	1.318	5.480	237.
Sigmat = 26.500								
	PRES	54.880	33.570	72.190	7.483	-0.196	2.631	228.
	TEM1	15.780	15.700	15.880	0.033	0.236	3.488	228.
	S 1	35.910	35.888	35.939	0.010	0.240	3.485	228.
	PDIF	6.940	2.210	18.460	3.206	1.167	4.180	220.
Sigmat = 26.600								
	PRES	62.540	43.650	78.930	7.963	-0.370	2.441	205.
	TEM1	15.310	15.200	15.520	0.048	0.851	4.877	205.
	S 1	35.904	35.871	35.963	0.014	0.861	4.913	205.
	PDIF	9.700	2.160	27.660	3.712	1.146	6.370	148.

table 8.1.4: 41° N to 42° N, 27°50' W to 28°25' W

Surface	Parameter	Mean	Minimum	Maximum	St.Dev.	Skewness	Kurtosis	Datapoints
Sigmat = 25.500								
	PRES	17.890	5.260	39.830	5.881	0.949	3.990	248.
	TEM1	19.960	19.740	20.180	0.109	-0.135	1.833	248.
	S 1	35.951	35.876	36.028	0.038	-0.132	1.834	248.
	PDIF	2.680	0.605	16.520	1.948	2.663	14.690	243.
Sigmat = 25.600								
	PRES	20.460	8.360	42.900	6.598	0.950	3.627	249.
	TEM1	19.510	19.250	19.720	0.122	-0.187	1.755	249.
	S 1	35.927	35.840	35.999	0.042	-0.183	1.752	249.
	PDIF	3.000	0.735	16.580	2.067	2.750	14.620	249.
Sigmat = 25.700								
	PRES	23.550	9.720	49.250	7.629	1.143	4.006	249.
	TEM1	19.090	18.790	19.310	0.134	-0.299	1.806	249.
	S 1	35.917	35.816	35.990	0.045	-0.294	1.802	249.
	PDIF	2.930	0.621	10.630	1.869	1.533	5.740	248.
Sigmat = 25.800								
	PRES	26.250	13.110	53.740	7.995	1.123	3.960	248.
	TEM1	18.670	18.380	18.880	0.142	-0.256	1.755	248.
	S 1	35.906	35.810	35.976	0.047	-0.252	1.752	248.
	PDIF	2.900	0.566	11.770	1.702	1.715	7.210	248.
Sigmat = 25.900								
	PRES	29.200	14.820	58.400	8.398	1.051	3.894	247.
	TEM1	18.250	17.980	18.510	0.142	-0.195	1.602	247.
	S 1	35.899	35.811	35.984	0.046	-0.190	1.601	247.
	PDIF	2.880	0.560	8.060	1.535	1.231	4.650	247.
Sigmat = 26.000								
	PRES	32.170	16.020	61.370	8.763	1.026	3.972	247.
	TEM1	17.820	17.560	18.100	0.147	-0.139	1.520	247.
	S 1	35.892	35.809	35.982	0.047	-0.134	1.519	247.
	PDIF	3.390	0.574	10.810	1.933	1.264	4.770	247.
Sigmat = 26.100								
	PRES	35.850	18.420	63.900	8.799	0.799	3.562	246.
	TEM1	17.390	17.140	17.620	0.142	-0.065	1.429	246.
	S 1	35.884	35.805	35.957	0.045	-0.061	1.429	246.
	PDIF	3.900	0.670	12.900	2.340	1.115	3.920	246.
Sigmat = 26.200								
	PRES	39.790	21.520	67.560	9.124	0.595	3.035	246.
	TEM1	16.950	16.670	17.190	0.148	-0.021	1.373	246.
	S 1	35.877	35.791	35.953	0.046	-0.018	1.374	246.
	PDIF	4.020	0.781	17.890	2.425	1.793	8.040	246.
Sigmat = 26.300								
	PRES	44.090	26.230	70.300	9.210	0.675	3.238	246.
	TEM1	16.520	16.270	16.800	0.158	0.023	1.371	246.
	S 1	35.875	35.797	35.959	0.048	0.027	1.373	246.
	PDIF	4.810	0.755	15.160	2.553	0.857	3.660	245.
Sigmat = 26.400								
	PRES	48.930	28.970	73.360	9.063	0.592	3.240	241.
	TEM1	16.090	15.780	16.370	0.161	-0.053	1.505	241.
	S 1	35.873	35.782	35.958	0.048	-0.048	1.504	241.
	PDIF	5.680	0.724	18.700	3.531	1.120	3.970	236.
Sigmat = 26.500								
	PRES	54.720	33.380	77.230	9.154	0.236	2.939	227.
	TEM1	15.640	15.340	15.980	0.169	0.087	1.588	227.
	S 1	35.869	35.782	35.969	0.050	0.093	1.588	227.
	PDIF	7.380	2.316	18.600	3.325	0.905	3.670	213.
Sigmat = 26.600								
	PRES	60.860	39.330	76.270	8.059	-0.487	2.749	189.
	TEM1	15.180	14.880	15.520	0.170	0.380	1.842	189.
	S 1	35.864	35.779	35.964	0.049	0.388	1.849	189.
	PDIF	9.710	1.994	24.950	4.259	0.981	4.100	157.
Sigmat = 26.700								
	PRES	68.440	49.000	80.160	7.666	-0.862	2.943	103.
	TEM1	14.700	14.410	15.040	0.153	0.351	1.822	103.
	S 1	35.858	35.777	35.953	0.043	0.359	1.830	103.
	PDIF	15.480	2.982	24.750	5.770	-0.262	2.150	30.

table 8.1.5: 42° N to 43° N, 28°25' W to 29°01' W

Surface	Parameter	Mean	Minimum	Maximum	St.Dev.	Skewness	Kurtosis	Datapoints
Sigmat = 25.300								
	PRES	13.320	5.110	27.580	5.030	0.758	3.115	99.
	TEM1	20.820	20.680	21.090	0.108	1.307	3.426	99.
	S 1	35.993	35.943	36.088	0.039	1.311	3.430	99.
	PDIF	7.390	1.920	16.380	3.557	0.489	2.760	50.
Sigmat = 25.400								
	PRES	15.740	3.500	30.150	5.450	0.455	2.709	177.
	TEM1	20.380	20.240	20.680	0.098	1.426	4.582	177.
	S 1	35.968	35.919	36.074	0.035	1.432	4.600	177.
	PDIF	3.780	0.670	14.700	2.447	1.430	5.350	146.
Sigmat = 25.500								
	PRES	18.000	5.210	32.560	5.740	0.465	2.633	190.
	TEM1	19.970	19.810	20.300	0.103	1.534	4.739	190.
	S 1	35.955	35.901	36.071	0.036	1.541	4.760	190.
	PDIF	2.560	0.680	12.580	1.523	2.598	14.150	187.
Sigmat = 25.600								
	PRES	20.260	6.250	36.020	5.870	0.452	2.762	195.
	TEM1	19.550	19.390	19.880	0.104	1.366	4.814	195.
	S 1	35.942	35.887	36.056	0.036	1.376	4.840	195.
	PDIF	2.710	0.710	7.990	1.438	1.219	4.230	193.
Sigmat = 25.700								
	PRES	23.110	8.880	41.700	6.260	0.361	2.839	195.
	TEM1	19.140	18.970	19.500	0.108	1.089	4.242	195.
	S 1	35.935	35.876	36.057	0.037	1.103	4.280	195.
	PDIF	2.880	0.700	12.450	1.874	1.768	7.280	195.
Sigmat = 25.800								
	PRES	25.970	10.510	47.080	7.290	0.606	3.445	195.
	TEM1	18.740	18.550	19.090	0.117	0.874	3.284	195.
	S 1	35.930	35.868	36.048	0.039	0.884	3.310	195.
	PDIF	2.820	0.540	14.490	2.001	2.211	10.300	195.
Sigmat = 25.900								
	PRES	28.940	11.800	55.900	8.180	0.719	3.828	195.
	TEM1	18.340	18.140	18.680	0.133	0.740	2.810	195.
	S 1	35.929	35.863	36.039	0.044	0.750	2.830	195.
	PDIF	2.850	0.520	14.830	1.894	2.209	11.410	195.
Sigmat = 26.000								
	PRES	31.630	16.440	60.110	8.420	0.748	3.794	195.
	TEM1	17.920	17.640	18.260	0.154	0.561	2.246	195.
	S 1	35.924	35.832	36.032	0.050	0.570	2.250	195.
	PDIF	2.830	0.580	8.880	1.521	0.935	3.780	195.
Sigmat = 26.100								
	PRES	34.690	18.610	64.340	9.050	0.844	3.941	195.
	TEM1	17.500	17.240	17.830	0.165	0.557	2.051	195.
	S 1	35.919	35.838	36.025	0.052	0.565	2.060	195.
	PDIF	3.420	0.650	10.310	1.747	0.899	3.650	195.
Sigmat = 26.200								
	PRES	38.520	19.840	68.950	9.070	0.871	4.119	194.
	TEM1	17.080	16.770	17.400	0.177	0.417	1.813	194.
	S 1	35.916	35.819	36.016	0.055	0.424	1.820	194.
	PDIF	4.380	0.960	13.600	2.419	1.155	4.240	194.
Sigmat = 26.300								
	PRES	43.060	22.160	74.030	10.190	0.722	3.368	194.
	TEM1	16.640	16.310	16.970	0.196	0.271	1.498	194.
	S 1	35.912	35.809	36.013	0.060	0.276	1.500	194.
	PDIF	4.910	1.160	16.350	2.992	1.176	4.220	193.
Sigmat = 26.400								
	PRES	48.810	25.750	78.360	10.570	0.377	2.906	189.
	TEM1	16.220	15.910	16.520	0.208	0.207	1.376	189.
	S 1	35.913	35.820	36.004	0.063	0.211	1.380	189.
	PDIF	7.330	1.580	17.210	3.464	0.663	3.130	184.
Sigmat = 26.500								
	PRES	55.060	32.310	76.890	9.520	-0.059	2.591	173.
	TEM1	15.780	15.530	16.100	0.216	0.279	1.291	173.
	S 1	35.911	35.837	36.006	0.064	0.282	1.290	173.
	PDIF	8.910	3.790	22.140	3.273	1.183	4.870	158.
Sigmat = 26.600								
	PRES	63.510	42.810	81.920	8.200	-0.484	2.775	135.
	TEM1	15.290	15.080	15.620	0.191	0.695	1.763	135.
	S 1	35.898	35.837	35.992	0.056	0.699	1.770	135.
	PDIF	12.290	4.640	29.910	5.002	1.181	4.750	90.
Sigmat = 26.700								
	PRES	70.310	55.940	80.090	5.850	-0.329	2.201	48.
	TEM1	14.750	14.670	14.880	0.059	0.788	1.945	48.
	S 1	35.871	35.850	35.908	0.017	0.789	1.950	48.
	PDIF	22.310	19.660	26.850	2.513	0.722	2.030	6.

table 8.1.6: 43° N to 44° N, 29°01' W to 29°38' W

Surface	Parameter	Mean	Minimum	Maximum	St.Dev.	Skewness	Kurtosis	Datapoints
Sigmat = 25.400								
	PRES	12.080	4.640	21.670	3.309	0.397	2.876	214.
	TEM1	20.280	20.060	20.500	0.081	-0.628	3.093	214.
	S 1	35.933	35.855	36.010	0.028	-0.621	3.087	214.
	PDIF	2.290	0.270	13.590	1.818	2.735	14.070	139.
Sigmat = 25.500								
	PRES	13.770	3.390	24.030	3.526	0.322	3.022	224.
	TEM1	19.850	19.570	20.100	0.089	-0.407	3.089	224.
	S 1	35.915	35.818	36.000	0.031	-0.396	3.085	224.
	PDIF	1.810	0.460	6.450	1.049	1.714	6.740	222.
Sigmat = 25.600								
	PRES	15.650	5.440	25.530	4.076	0.345	2.573	229.
	TEM1	19.420	19.220	19.720	0.097	-0.061	2.925	229.
	S 1	35.898	35.829	36.001	0.033	-0.048	2.951	229.
	PDIF	2.230	0.290	8.970	1.272	1.533	6.740	228.
Sigmat = 25.700								
	PRES	18.120	7.840	31.520	4.528	0.368	2.722	232.
	TEM1	19.000	18.760	19.230	0.099	-0.320	2.103	232.
	S 1	35.887	35.808	35.963	0.033	-0.314	2.104	232.
	PDIF	2.650	0.550	8.540	1.472	1.503	5.730	230.
Sigmat = 25.800								
	PRES	20.710	10.260	35.650	4.894	0.336	2.787	235.
	TEM1	18.600	18.380	18.780	0.097	-0.327	2.103	235.
	S 1	35.883	35.812	35.944	0.032	-0.321	2.099	235.
	PDIF	2.720	0.550	10.600	1.447	1.606	8.240	233.
Sigmat = 25.900								
	PRES	23.230	11.050	37.010	5.439	0.279	2.550	236.
	TEM1	18.200	17.980	18.400	0.091	-0.149	2.192	236.
	S 1	35.884	35.813	35.950	0.030	-0.144	2.192	236.
	PDIF	2.500	0.470	7.540	1.306	1.159	4.680	236.
Sigmat = 26.000								
	PRES	25.780	13.320	40.600	5.564	0.243	2.490	236.
	TEM1	17.790	17.620	18.060	0.089	0.030	2.298	236.
	S 1	35.880	35.828	35.967	0.029	0.038	2.302	236.
	PDIF	2.580	0.600	6.810	1.269	0.758	3.300	236.
Sigmat = 26.100								
	PRES	28.410	16.760	41.640	5.612	0.158	2.272	236.
	TEM1	17.370	17.170	17.650	0.097	0.114	2.205	236.
	S 1	35.877	35.816	35.966	0.031	0.123	2.214	236.
	PDIF	2.720	0.580	9.100	1.448	1.457	5.820	236.
Sigmat = 26.200								
	PRES	31.410	19.330	48.510	5.768	0.151	2.547	236.
	TEM1	16.940	16.750	17.110	0.082	-0.150	2.066	236.
	S 1	35.873	35.814	35.925	0.026	-0.144	2.064	236.
	PDIF	3.320	0.590	10.830	1.655	1.309	5.000	236.
Sigmat = 26.300								
	PRES	34.990	22.290	54.840	6.028	0.099	2.469	237.
	TEM1	16.520	16.290	16.730	0.086	-0.172	2.233	237.
	S 1	35.873	35.803	35.940	0.026	-0.166	2.232	237.
	PDIF	3.980	1.170	10.590	1.861	0.872	3.740	237.
Sigmat = 26.400								
	PRES	39.660	27.790	55.970	6.261	0.039	2.238	237.
	TEM1	16.080	15.900	16.240	0.080	-0.383	2.354	237.
	S 1	35.871	35.815	35.919	0.024	-0.377	2.345	237.
	PDIF	6.000	1.300	21.720	3.473	1.805	7.160	236.
Sigmat = 26.500								
	PRES	47.020	31.790	62.130	6.994	-0.148	2.226	235.
	TEM1	15.640	15.470	15.820	0.075	-0.228	2.540	235.
	S 1	35.871	35.821	35.922	0.022	-0.220	2.538	235.
	PDIF	8.140	2.510	18.760	2.931	0.713	3.590	234.
Sigmat = 26.600								
	PRES	55.970	40.450	77.620	6.943	0.013	2.627	231.
	TEM1	15.200	15.030	15.400	0.078	-0.215	2.516	231.
	S 1	35.870	35.821	35.929	0.022	-0.207	2.518	231.
	PDIF	11.210	3.980	24.370	3.789	0.947	4.020	214.
Sigmat = 26.700								
	PRES	68.770	53.360	80.300	5.761	-0.203	2.414	164.
	TEM1	14.800	14.590	15.010	0.084	-0.465	3.190	164.
	S 1	35.884	35.826	35.946	0.024	-0.454	3.185	164.
	PDIF	19.430	11.210	29.690	4.932	0.383	2.450	42.

table 8.1.7: 44° N to 45° N, 29°23' W to 30°15' W

Surface	Parameter	Mean	Minimum	Maximum	St.Dev.	Skewness	Kurtosis	Datapoints
Sigmat = 25.500								
	PRES	11.750	3.250	20.220	3.195	0.196	3.403	68.
	TEM1	19.700	19.220	19.940	0.168	-1.321	4.055	68.
	S 1	35.864	35.699	35.946	0.058	-1.309	4.030	68.
	PDIF	1.600	0.350	7.870	1.390	2.514	10.380	47.
Sigmat = 25.600								
	PRES	11.070	4.170	21.370	3.274	0.352	2.715	203.
	TEM1	19.140	18.810	19.570	0.172	0.195	2.164	203.
	S 1	35.804	35.691	35.949	0.058	0.208	2.160	203.
	PDIF	1.510	0.310	4.450	0.845	1.322	4.670	146.
Sigmat = 25.700								
	PRES	12.330	4.340	22.290	3.517	0.391	2.544	231.
	TEM1	18.710	18.330	19.140	0.165	0.134	2.485	231.
	S 1	35.792	35.663	35.935	0.055	0.152	2.480	231.
	PDIF	1.660	0.350	5.360	0.941	1.038	4.040	227.
Sigmat = 25.800								
	PRES	13.880	5.070	24.020	3.863	0.382	2.467	237.
	TEM1	18.290	17.820	18.810	0.174	0.115	2.941	237.
	S 1	35.782	35.630	35.954	0.057	0.133	2.940	237.
	PDIF	1.890	0.360	5.680	1.044	0.858	3.350	234.
Sigmat = 25.900								
	PRES	16.170	7.010	30.440	4.730	0.554	2.744	238.
	TEM1	17.870	17.400	18.190	0.174	-0.036	2.439	238.
	S 1	35.776	35.625	35.878	0.056	-0.025	2.420	238.
	PDIF	2.670	0.430	14.040	2.060	2.497	11.540	238.
Sigmat = 26.000								
	PRES	19.180	8.760	35.410	5.832	0.617	2.535	239.
	TEM1	17.450	16.890	17.910	0.189	0.189	2.567	239.
	S 1	35.772	35.598	35.919	0.060	0.206	2.550	239.
	PDIF	3.500	0.540	10.360	1.991	1.198	4.350	239.
Sigmat = 26.100								
	PRES	23.340	12.890	39.550	6.198	0.465	2.317	239.
	TEM1	17.030	16.470	17.510	0.195	0.261	2.740	239.
	S 1	35.773	35.598	35.923	0.061	0.282	2.720	239.
	PDIF	5.090	0.610	14.760	2.700	1.058	4.340	239.
Sigmat = 26.200								
	PRES	28.900	17.190	48.020	6.127	0.252	2.466	239.
	TEM1	16.620	16.220	17.150	0.185	0.447	2.648	239.
	S 1	35.775	35.651	35.938	0.057	0.464	2.650	239.
	PDIF	5.560	0.560	17.640	3.249	0.903	3.540	239.
Sigmat = 26.300								
	PRES	34.320	19.220	51.000	6.121	-0.106	2.617	239.
	TEM1	16.200	15.900	16.750	0.181	0.738	2.553	239.
	S 1	35.776	35.688	35.943	0.055	0.750	2.570	239.
	PDIF	5.130	0.460	15.480	3.007	0.999	3.530	239.
Sigmat = 26.400								
	PRES	38.710	22.420	55.580	6.715	0.060	2.812	238.
	TEM1	15.760	15.420	16.340	0.201	0.694	2.332	238.
	S 1	35.776	35.676	35.948	0.060	0.705	2.350	238.
	PDIF	3.980	1.010	11.070	1.687	1.032	4.520	238.
Sigmat = 26.500								
	PRES	43.010	26.450	63.490	7.021	0.118	2.719	237.
	TEM1	15.300	14.980	15.920	0.219	0.632	2.052	237.
	S 1	35.770	35.679	35.953	0.064	0.642	2.070	237.
	PDIF	5.220	1.020	20.910	2.731	1.741	8.210	237.
Sigmat = 26.600								
	PRES	49.450	30.150	71.020	8.112	-0.011	2.438	236.
	TEM1	14.840	14.460	15.470	0.236	0.474	1.708	236.
	S 1	35.769	35.661	35.951	0.067	0.482	1.720	236.
	PDIF	8.590	2.310	21.790	4.215	0.959	3.380	232.
Sigmat = 26.700								
	PRES	59.310	38.210	78.590	9.395	-0.131	2.205	216.
	TEM1	14.360	13.970	14.910	0.242	0.606	1.797	216.
	S 1	35.763	35.653	35.917	0.068	0.613	1.800	216.
	PDIF	13.180	4.640	28.390	4.081	0.590	3.560	157.

table 8.1.8: 45° N to 46° N, 30°15' W to 30°56' W

Surface	Parameter	Mean	Minimum	Maximum	St.Dev.	Skewness	Kurtosis	Datapoints
Sigmat = 25.500								
	PRES	15.150	8.300	24.240	3.236	0.077	2.464	191.
	TEM1	19.580	19.420	19.770	0.071	0.141	2.480	191.
	S 1	35.820	35.766	35.888	0.024	0.145	2.480	191.
	PDIF	1.200	0.330	7.270	0.797	3.502	23.380	167.
Sigmat = 25.600								
	PRES	16.070	9.290	25.800	3.269	0.191	2.435	216.
	TEM1	19.160	18.890	19.450	0.091	0.482	3.610	216.
	S 1	35.809	35.721	35.909	0.031	0.497	3.610	216.
	PDIF	1.570	0.410	8.120	1.116	2.379	11.030	216.
Sigmat = 25.700								
	PRES	17.980	10.280	26.280	3.421	-0.079	2.234	216.
	TEM1	18.730	18.490	19.140	0.103	0.721	3.950	216.
	S 1	35.797	35.717	35.936	0.034	0.739	3.990	216.
	PDIF	2.290	0.410	9.170	1.423	1.078	4.580	216.
Sigmat = 25.800								
	PRES	20.600	11.190	29.460	4.075	-0.098	2.029	216.
	TEM1	18.360	18.050	18.620	0.100	-0.205	3.490	216.
	S 1	35.805	35.705	35.891	0.033	-0.189	3.460	216.
	PDIF	2.930	0.570	10.580	1.712	1.831	7.730	216.
Sigmat = 25.900								
	PRES	23.630	14.410	34.680	4.288	0.091	2.372	216.
	TEM1	18.010	17.620	18.190	0.103	-1.276	5.620	216.
	S 1	35.820	35.696	35.880	0.033	-1.258	5.560	216.
	PDIF	3.120	0.680	10.040	1.677	1.254	4.570	216.
Sigmat = 26.000								
	PRES	27.160	16.310	38.060	4.017	0.101	2.773	217.
	TEM1	17.670	17.210	17.910	0.098	-1.225	6.770	217.
	S 1	35.841	35.697	35.921	0.031	-1.202	6.670	217.
	PDIF	4.290	0.480	22.600	3.444	2.204	10.590	217.
Sigmat = 26.100								
	PRES	31.660	22.560	45.260	4.197	0.454	3.537	217.
	TEM1	17.300	16.520	17.500	0.122	-2.569	16.430	217.
	S 1	35.856	35.615	35.918	0.038	-2.504	15.930	217.
	PDIF	3.600	0.370	12.070	2.619	1.230	4.120	217.
Sigmat = 26.200								
	PRES	34.710	23.620	51.830	4.504	0.388	3.870	217.
	TEM1	16.890	16.280	17.080	0.116	-1.815	9.800	217.
	S 1	35.859	35.672	35.916	0.036	-1.775	9.560	217.
	PDIF	2.910	0.670	9.280	1.415	1.344	5.610	217.
Sigmat = 26.300								
	PRES	37.450	25.470	53.160	4.611	0.247	3.508	217.
	TEM1	16.490	16.050	16.740	0.103	-0.723	5.000	217.
	S 1	35.864	35.731	35.943	0.032	-0.700	4.920	217.
	PDIF	3.030	0.700	8.010	1.392	0.819	3.370	217.
Sigmat = 26.400								
	PRES	40.910	29.960	57.980	4.461	0.296	3.674	217.
	TEM1	16.060	15.740	16.300	0.112	-0.304	3.350	217.
	S 1	35.866	35.768	35.936	0.034	-0.288	3.320	217.
	PDIF	4.060	0.360	10.800	1.847	0.708	3.360	217.
Sigmat = 26.500								
	PRES	46.440	35.430	60.440	4.016	0.255	3.405	217.
	TEM1	15.640	15.360	15.890	0.125	0.324	2.340	217.
	S 1	35.869	35.788	35.945	0.037	0.334	2.340	217.
	PDIF	7.540	1.220	15.920	3.170	0.270	2.440	215.
Sigmat = 26.600								
	PRES	56.150	43.890	68.640	4.588	-0.076	2.682	213.
	TEM1	15.190	15.010	15.500	0.128	0.929	2.690	213.
	S 1	35.869	35.817	35.958	0.037	0.937	2.700	213.
	PDIF	12.920	4.620	21.950	3.478	0.103	2.760	204.
Sigmat = 26.700								
	PRES	70.700	57.870	82.000	4.546	-0.291	2.738	131.
	TEM1	14.830	14.610	15.150	0.165	0.613	1.870	131.
	S 1	35.893	35.832	35.987	0.047	0.619	1.880	131.
	PDIF	14.320	9.490	18.770	2.132	-0.370	3.040	19.

table 8.1.9: 46° N to 47° N, 30°56' W to 31°32' W

Surface	Parameter	Mean	Minimum	Maximum	St.Dev.	Skewness	Kurtosis	Datapoints
Sigmat = 25.500								
	PRES	12.510	4.560	25.290	3.706	0.774	3.885	171.
	TEM1	19.340	18.150	19.850	0.363	-1.356	4.304	171.
	S 1	35.739	35.344	35.913	0.122	-1.325	4.228	171.
	PDIF	1.610	0.100	4.820	0.909	1.238	4.359	111.
Sigmat = 25.600								
	PRES	13.170	4.630	26.050	3.933	0.570	3.426	209.
	TEM1	18.900	17.890	19.580	0.390	-0.777	2.756	209.
	S 1	35.723	35.391	35.951	0.129	-0.752	2.722	209.
	PDIF	1.460	0.150	4.750	0.890	1.454	5.379	201.
Sigmat = 25.700								
	PRES	14.410	5.370	27.670	4.140	0.530	3.177	222.
	TEM1	18.450	17.630	19.030	0.393	-0.680	2.414	222.
	S 1	35.704	35.438	35.897	0.128	-0.658	2.392	222.
	PDIF	2.080	0.340	9.170	1.428	1.837	7.465	218.
Sigmat = 25.800								
	PRES	16.840	7.200	30.360	4.905	0.641	3.063	230.
	TEM1	18.030	17.180	18.650	0.417	-0.399	2.086	230.
	S 1	35.697	35.428	35.901	0.134	-0.376	2.076	230.
	PDIF	2.860	0.380	12.170	1.838	1.622	7.273	225.
Sigmat = 25.900								
	PRES	19.570	7.350	34.110	5.706	0.502	2.599	230.
	TEM1	17.640	16.730	18.290	0.420	-0.349	2.137	230.
	S 1	35.705	35.419	35.911	0.133	-0.322	2.127	230.
	PDIF	2.630	0.380	10.730	1.801	1.450	5.762	230.
Sigmat = 26.000								
	PRES	22.660	8.560	37.010	6.294	0.044	2.254	230.
	TEM1	17.260	16.410	17.940	0.415	-0.343	2.160	230.
	S 1	35.712	35.452	35.928	0.130	-0.314	2.151	230.
	PDIF	3.850	0.380	15.410	3.009	0.970	3.278	230.
Sigmat = 26.100								
	PRES	26.510	10.310	42.090	7.136	-0.374	2.194	230.
	TEM1	16.850	16.000	17.570	0.433	-0.394	2.147	230.
	S 1	35.716	35.457	35.942	0.133	-0.366	2.136	230.
	PDIF	3.320	0.550	10.240	2.106	1.042	3.639	230.
Sigmat = 26.200								
	PRES	29.620	13.940	49.400	6.948	-0.220	2.305	230.
	TEM1	16.440	15.570	17.080	0.437	-0.440	2.056	230.
	S 1	35.721	35.459	35.917	0.132	-0.416	2.046	230.
	PDIF	3.500	0.500	12.100	2.363	1.029	3.198	230.
Sigmat = 26.300								
	PRES	33.920	20.370	51.810	5.261	0.294	3.186	230.
	TEM1	16.050	15.220	16.700	0.416	-0.423	2.022	230.
	S 1	35.733	35.488	35.931	0.124	-0.400	2.012	230.
	PDIF	4.500	0.620	18.500	3.924	1.362	3.717	230.
Sigmat = 26.400								
	PRES	37.660	21.290	55.030	5.216	0.080	3.504	231.
	TEM1	15.650	14.870	16.320	0.420	-0.418	2.086	231.
	S 1	35.743	35.518	35.943	0.123	-0.393	2.077	231.
	PDIF	3.110	0.470	9.410	1.571	1.012	4.428	230.
Sigmat = 26.500								
	PRES	40.920	23.100	56.030	5.415	-0.093	3.244	230.
	TEM1	15.230	14.320	15.880	0.449	-0.573	2.295	230.
	S 1	35.750	35.493	35.940	0.129	-0.543	2.271	230.
	PDIF	4.040	0.470	13.210	2.583	1.149	3.841	230.
Sigmat = 26.600								
	PRES	45.790	26.110	63.030	6.560	-0.050	2.833	230.
	TEM1	14.790	13.740	15.390	0.474	-0.904	2.669	230.
	S 1	35.756	35.463	35.926	0.133	-0.875	2.630	230.
	PDIF	5.910	1.190	17.740	3.538	1.011	3.259	229.
Sigmat = 26.700								
	PRES	53.940	32.380	74.300	8.843	0.234	2.448	226.
	TEM1	14.380	13.250	15.230	0.513	-0.907	2.692	226.
	S 1	35.768	35.462	36.008	0.141	-0.874	2.653	226.
	PDIF	13.440	4.730	25.970	4.813	0.339	2.383	192.
Sigmat = 26.800								
	PRES	67.210	52.430	80.720	7.031	-0.046	1.872	109.
	TEM1	13.670	12.820	14.430	0.554	-0.326	1.414	109.
	S 1	35.705	35.478	35.910	0.149	-0.313	1.407	109.
	PDIF	14.600	9.420	23.860	3.433	0.449	2.656	38.
Sigmat = 26.900								
	PRES	76.060	72.160	80.690	2.492	0.160	2.005	13.
	TEM1	12.510	12.470	12.520	0.015	-0.838	2.463	13.
	S 1	35.527	35.518	35.531	0.004	-0.837	2.228	13.
	PDIF	NO DATA !						

table 8.1.10: 47° N to 48° N, 31°32' W to 32°11' W

Surface	Parameter	Mean	Minimum	Maximum	St.Dev.	Skewness	Kurtosis	Datapoints
Sigmat = 25.600								
	PRES	10.390	3.720	15.920	2.534	-0.034	3.021	93.
	TEM1	18.031	17.857	18.306	0.104	0.219	2.152	93.
	S 1	35.437	35.381	35.527	0.034	0.229	2.173	93.
	PDIF	1.590	0.220	4.290	0.918	1.252	4.150	54.
Sigmat = 25.700								
	PRES	11.590	5.800	18.550	2.518	0.172	3.100	146.
	TEM1	17.685	17.448	17.919	0.122	-0.357	1.902	146.
	S 1	35.457	35.381	35.531	0.039	-0.352	1.902	146.
	PDIF	1.590	0.280	3.970	0.801	0.822	3.090	122.
Sigmat = 25.800								
	PRES	12.890	6.490	20.820	2.675	0.214	3.122	155.
	TEM1	17.312	16.998	17.711	0.142	-0.057	2.174	155.
	S 1	35.469	35.371	35.596	0.045	-0.040	2.189	155.
	PDIF	1.310	0.170	5.060	0.860	1.473	5.310	152.
Sigmat = 25.900								
	PRES	13.980	7.460	22.260	2.821	0.295	3.053	165.
	TEM1	16.924	16.628	17.348	0.148	-0.214	2.379	165.
	S 1	35.478	35.387	35.611	0.046	-0.197	2.389	165.
	PDIF	1.340	0.200	3.700	0.801	1.103	3.520	158.
Sigmat = 26.000								
	PRES	15.500	7.880	24.110	3.008	0.266	2.885	171.
	TEM1	16.498	16.187	17.014	0.148	-0.161	2.909	171.
	S 1	35.477	35.383	35.637	0.045	-0.141	2.943	171.
	PDIF	1.820	0.230	5.250	0.900	1.008	4.140	170.
Sigmat = 26.100								
	PRES	17.650	10.240	26.440	3.142	0.345	2.902	184.
	TEM1	16.081	15.751	16.334	0.130	-0.854	2.816	184.
	S 1	35.481	35.383	35.557	0.039	-0.845	2.803	184.
	PDIF	3.830	0.660	8.900	1.748	0.915	3.540	178.
Sigmat = 26.200								
	PRES	23.790	14.700	37.980	3.701	0.539	3.660	192.
	TEM1	15.688	15.379	15.850	0.118	-1.078	3.204	192.
	S 1	35.494	35.404	35.542	0.035	-1.070	3.187	192.
	PDIF	7.510	0.980	14.650	2.885	0.015	2.540	187.
Sigmat = 26.300								
	PRES	30.580	20.520	45.600	3.970	0.368	3.668	192.
	TEM1	15.268	14.917	15.445	0.135	-0.958	2.913	192.
	S 1	35.502	35.401	35.553	0.039	-0.950	2.895	192.
	PDIF	5.150	1.110	19.300	2.610	1.407	7.100	192.
Sigmat = 26.400								
	PRES	34.230	21.850	53.410	4.464	0.923	5.532	192.
	TEM1	14.804	14.491	15.031	0.131	-0.864	2.817	192.
	S 1	35.498	35.410	35.563	0.037	-0.854	2.803	192.
	PDIF	2.840	0.690	7.620	1.266	1.192	5.210	192.
Sigmat = 26.500								
	PRES	37.060	24.510	56.480	4.530	0.577	4.841	192.
	TEM1	14.305	14.010	14.568	0.124	-0.577	2.636	192.
	S 1	35.488	35.407	35.561	0.034	-0.564	2.626	192.
	PDIF	2.950	0.930	11.380	1.430	1.893	9.160	192.
Sigmat = 26.600								
	PRES	40.240	27.510	59.340	4.502	0.424	4.497	192.
	TEM1	13.800	13.538	14.176	0.118	-0.211	2.876	192.
	S 1	35.479	35.408	35.582	0.032	-0.195	2.895	192.
	PDIF	3.780	1.230	11.320	1.687	1.023	4.770	192.
Sigmat = 26.700								
	PRES	45.280	33.020	66.400	4.687	0.637	5.030	192.
	TEM1	13.330	13.105	13.627	0.125	0.041	2.371	192.
	S 1	35.482	35.423	35.561	0.033	0.054	2.382	192.
	PDIF	7.410	0.270	16.000	3.088	0.264	2.480	192.
Sigmat = 26.800								
	PRES	55.790	43.570	77.870	5.451	0.874	4.456	191.
	TEM1	12.872	12.679	13.210	0.113	0.205	2.542	191.
	S 1	35.491	35.442	35.579	0.029	0.218	2.563	191.
	PDIF	13.090	5.230	24.670	3.526	0.490	3.750	187.
Sigmat = 26.900								
	PRES	70.570	60.640	81.180	4.652	-0.066	2.292	152.
	TEM1	12.452	12.255	12.874	0.112	0.839	4.249	152.
	S 1	35.513	35.463	35.621	0.028	0.862	4.334	152.
	PDIF	21.560	17.130	27.540	3.509	0.295	1.720	7.

table 8.1.11: 48° N to 49° N, 32°11' W to 32°52' W

Surface	Parameter	Mean	Minimum	Maximum	St.Dev.	Skewness	Kurtosis	Datapoints
Sigmat = 25.900								
	PRES	19.140	10.640	28.780	3.278	0.096	2.847	182.
	TEM1	16.888	16.322	17.122	0.200	-1.203	3.455	182.
	S 1	35.467	35.293	35.539	0.062	-1.191	3.422	182.
	PDIF	2.360	0.530	6.440	1.275	1.231	3.990	131.
Sigmat = 26.000								
	PRES	22.820	13.470	36.460	4.324	0.333	2.938	268.
	TEM1	16.373	15.641	16.821	0.345	-0.426	1.831	268.
	S 1	35.440	35.221	35.576	0.104	-0.413	1.815	268.
	PDIF	4.850	0.663	14.510	3.224	0.807	2.810	228.
Sigmat = 26.100								
	PRES	27.570	15.420	43.630	5.048	0.202	2.912	269.
	TEM1	15.897	14.812	16.456	0.449	-0.538	2.066	269.
	S 1	35.428	35.112	35.594	0.132	-0.515	2.021	269.
	PDIF	4.430	0.983	12.300	2.143	0.977	3.740	269.
Sigmat = 26.200								
	PRES	32.070	19.540	45.540	5.497	-0.089	2.344	269.
	TEM1	15.508	14.297	16.105	0.518	-0.835	2.639	269.
	S 1	35.443	35.097	35.618	0.150	-0.802	2.566	269.
	PDIF	4.050	0.684	12.860	2.250	1.139	4.160	269.
Sigmat = 26.300								
	PRES	35.710	23.990	48.840	5.824	-0.020	2.166	269.
	TEM1	15.148	13.605	15.823	0.608	-1.102	3.189	269.
	S 1	35.469	35.039	35.664	0.172	-1.061	3.089	269.
	PDIF	3.850	0.511	19.260	2.426	2.547	12.960	269.
Sigmat = 26.400								
	PRES	40.210	26.390	58.290	7.267	-0.051	2.032	269.
	TEM1	14.822	13.137	15.500	0.626	-1.129	3.224	269.
	S 1	35.506	35.044	35.699	0.175	-1.087	3.112	269.
	PDIF	4.880	0.644	16.170	3.373	1.045	3.140	269.
Sigmat = 26.500								
	PRES	44.710	28.850	62.950	8.893	-0.045	1.821	269.
	TEM1	14.555	12.984	15.326	0.556	-0.908	2.678	269.
	S 1	35.559	35.133	35.778	0.154	-0.874	2.598	269.
	PDIF	3.960	1.136	11.450	1.864	0.915	3.540	269.
Sigmat = 26.600								
	PRES	48.370	31.330	68.840	9.361	-0.068	1.750	266.
	TEM1	14.282	12.726	15.065	0.585	-1.041	3.243	266.
	S 1	35.613	35.196	35.832	0.160	-0.991	3.128	266.
	PDIF	3.840	0.860	16.280	1.948	2.406	13.790	264.
Sigmat = 26.700								
	PRES	52.630	34.440	71.050	9.850	-0.113	1.671	263.
	TEM1	13.942	12.426	14.898	0.652	-0.706	2.640	263.
	S 1	35.649	35.248	35.914	0.176	-0.650	2.575	263.
	PDIF	5.440	0.977	13.630	2.092	0.624	3.370	261.
Sigmat = 26.800								
	PRES	61.820	41.750	79.220	9.705	-0.285	1.829	248.
	TEM1	13.597	11.839	14.434	0.651	-0.978	3.123	248.
	S 1	35.685	35.231	35.912	0.172	-0.919	3.012	248.
	PDIF	15.090	1.896	33.190	6.461	0.365	2.930	146.
Sigmat = 26.900								
	PRES	76.220	70.880	79.990	2.813	-0.340	1.915	11.
	TEM1	11.893	11.647	13.237	0.454	2.319	7.039	11.
	S 1	35.374	35.313	35.716	0.115	2.330	7.074	11.
	PDIF	6.830	5.435	8.980	1.511	0.516	1.210	4.

table 8.1.12: 49° N to 50° N, 32°52' W to 33°33' W

Surface	Parameter	Mean	Minimum	Maximum	St.Dev.	Skewness	Kurtosis	Datapoints
Sigmat = 26.000								
	PRES	21.880	20.700	22.670	0.756	-0.510	1.454	5.
	TEM1	15.741	15.719	15.777	0.024	0.434	1.309	5.
	S 1	35.250	35.244	35.261	0.007	0.426	1.318	5.
	PDIF	N O	D A T A	!				
Sigmat = 26.100								
	PRES	17.240	11.470	25.080	3.322	0.661	2.723	88.
	TEM1	15.083	14.846	15.290	0.078	0.468	3.404	88.
	S 1	35.189	35.121	35.249	0.022	0.487	3.410	88.
	PDIF	1.560	0.900	3.090	0.687	0.841	2.526	11.
Sigmat = 26.200								
	PRES	19.880	13.230	30.970	3.687	0.548	2.681	214.
	TEM1	14.645	14.340	14.985	0.134	0.146	2.192	214.
	S 1	35.194	35.109	35.291	0.038	0.158	2.193	214.
	PDIF	3.000	0.740	7.530	1.222	0.801	4.385	151.
Sigmat = 26.300								
	PRES	25.000	16.580	37.350	4.676	0.418	2.336	270.
	TEM1	14.232	13.896	14.720	0.216	0.218	1.872	270.
	S 1	35.209	35.117	35.345	0.060	0.231	1.880	270.
	PDIF	5.740	0.600	18.430	4.577	0.765	2.510	270.
Sigmat = 26.400								
	PRES	28.890	18.650	42.230	5.632	0.291	2.123	271.
	TEM1	13.747	13.398	14.235	0.207	0.119	1.893	271.
	S 1	35.206	35.113	35.339	0.056	0.134	1.907	271.
	PDIF	3.160	0.650	12.810	2.097	1.872	7.246	271.
Sigmat = 26.500								
	PRES	32.260	21.720	47.770	5.731	0.271	2.117	271.
	TEM1	13.264	12.892	13.684	0.212	0.145	1.735	271.
	S 1	35.207	35.109	35.318	0.056	0.157	1.737	271.
	PDIF	3.900	0.640	16.020	2.780	1.298	4.209	271.
Sigmat = 26.600								
	PRES	36.080	24.460	54.800	7.101	0.525	2.359	271.
	TEM1	12.833	12.451	13.245	0.222	0.179	1.602	271.
	S 1	35.223	35.126	35.331	0.057	0.189	1.603	271.
	PDIF	3.660	0.570	13.160	2.382	1.429	5.093	271.
Sigmat = 26.700								
	PRES	40.310	26.850	60.590	6.802	0.492	3.069	271.
	TEM1	12.392	12.012	12.764	0.235	0.219	1.590	271.
	S 1	35.240	35.145	35.334	0.059	0.230	1.591	271.
	PDIF	4.040	0.530	13.030	3.077	1.215	3.352	271.
Sigmat = 26.800								
	PRES	43.820	29.700	63.270	6.944	0.255	2.921	271.
	TEM1	11.935	11.506	12.307	0.237	0.030	1.629	271.
	S 1	35.255	35.151	35.347	0.058	0.043	1.626	271.
	PDIF	3.800	1.200	10.740	1.769	1.485	5.368	271.
Sigmat = 26.900								
	PRES	48.720	32.350	69.120	7.383	0.088	2.691	271.
	TEM1	11.474	10.964	11.855	0.242	-0.063	1.769	271.
	S 1	35.272	35.151	35.364	0.058	-0.047	1.762	271.
	PDIF	7.590	1.730	18.380	2.764	0.896	4.217	269.

table 8.1.13: 50° N to 51° N, 33°33' W to 34°15' W

Surface	Parameter	Mean	Minimum	Maximum	St.Dev.	Skewness	Kurtosis	Datapoints
Sigmat = 26.000								
	PRES	16.590	10.790	24.980	2.960	0.408	3.125	52.
	TEM1	15.038	14.926	15.209	0.069	0.351	2.200	52.
	S 1	35.046	35.014	35.095	0.020	0.353	2.200	52.
	PDIF	2.030	1.060	3.310	0.827	0.457	1.590	9.
Sigmat = 26.100								
	PRES	19.640	10.410	27.060	2.850	-0.173	3.320	182.
	TEM1	14.615	14.283	15.070	0.188	0.063	1.830	182.
	S 1	35.057	34.964	35.185	0.053	0.073	1.840	182.
	PDIF	2.030	0.570	4.920	0.860	0.481	2.870	117.
Sigmat = 26.200								
	PRES	21.080	10.620	30.860	3.640	-0.489	3.318	200.
	TEM1	14.246	13.741	14.894	0.327	0.332	1.810	200.
	S 1	35.084	34.946	35.264	0.090	0.347	1.820	200.
	PDIF	2.320	0.490	6.650	1.233	0.879	3.200	195.
Sigmat = 26.300								
	PRES	22.800	12.740	35.020	4.460	-0.123	2.307	259.
	TEM1	14.005	13.257	14.599	0.438	-0.072	1.430	259.
	S 1	35.148	34.946	35.311	0.119	-0.059	1.420	259.
	PDIF	3.520	0.640	10.400	1.957	1.159	4.340	236.
Sigmat = 26.400								
	PRES	27.090	14.450	38.540	5.190	-0.155	2.203	260.
	TEM1	13.620	12.764	14.237	0.413	-0.117	1.460	260.
	S 1	35.173	34.948	35.340	0.111	-0.102	1.450	260.
	PDIF	5.920	1.500	12.560	2.470	0.343	2.320	260.
Sigmat = 26.500								
	PRES	33.570	20.500	47.360	5.640	-0.010	2.374	260.
	TEM1	13.237	12.263	13.799	0.397	-0.360	1.740	260.
	S 1	35.200	34.950	35.349	0.104	-0.341	1.700	260.
	PDIF	5.440	1.080	15.410	2.659	0.968	3.750	260.
Sigmat = 26.600								
	PRES	38.180	24.800	53.710	6.040	-0.090	2.496	260.
	TEM1	12.886	12.062	13.728	0.398	-0.120	2.150	260.
	S 1	35.238	35.029	35.459	0.103	-0.084	2.150	260.
	PDIF	4.470	0.740	18.640	2.911	2.177	9.250	260.
Sigmat = 26.700								
	PRES	43.140	30.300	59.460	6.230	0.136	2.596	260.
	TEM1	12.517	11.625	13.794	0.450	0.290	2.940	260.
	S 1	35.273	35.051	35.606	0.115	0.358	3.030	260.
	PDIF	4.940	0.890	12.720	2.428	0.871	3.280	260.
Sigmat = 26.800								
	PRES	47.970	31.850	65.130	6.390	0.099	2.860	260.
	TEM1	12.155	11.291	13.675	0.517	0.581	3.110	260.
	S 1	35.311	35.099	35.703	0.130	0.656	3.230	260.
	PDIF	6.830	1.470	22.400	4.154	1.199	3.950	259.
Sigmat = 26.900								
	PRES	58.380	36.030	77.720	8.150	-0.221	2.711	247.
	TEM1	11.706	11.161	12.589	0.285	0.223	3.130	247.
	S 1	35.328	35.197	35.547	0.069	0.274	3.200	247.
	PDIF	14.470	2.050	34.390	7.346	0.255	2.290	199.
Sigmat = 27.000								
	PRES	64.870	49.050	81.040	8.220	-0.120	1.982	87.
	TEM1	11.318	10.555	11.468	0.138	-2.588	12.520	87.
	S 1	35.363	35.185	35.398	0.032	-2.530	12.080	87.
	PDIF	33.890	30.730	36.380	2.123	-0.334	1.380	5.

table 8.1.14: 51° N to 52° N, 34°15' W to 34°57' W

Surface	Parameter	Mean	Minimum	Maximum	St.Dev.	Skewness	Kurtosis	Datapoints
Sigmat = 26.100								
	PRES	17.540	9.130	28.170	3.830	0.289	2.563	146.
	TEM1	13.160	12.610	14.120	0.499	0.621	1.730	146.
	S 1	34.666	34.522	34.920	0.131	0.635	1.746	146.
	PDIF	2.190	0.420	6.630	1.185	1.272	4.631	132.
Sigmat = 26.200								
	PRES	18.950	10.680	29.670	3.920	0.267	2.564	162.
	TEM1	12.760	12.170	13.920	0.557	0.774	1.936	162.
	S 1	34.691	34.539	34.995	0.144	0.788	1.957	162.
	PDIF	1.720	0.470	4.060	0.688	0.639	3.187	153.
Sigmat = 26.300								
	PRES	20.080	8.270	32.500	4.730	0.053	2.683	176.
	TEM1	12.340	11.710	13.680	0.601	0.901	2.093	176.
	S 1	34.715	34.556	35.059	0.152	0.915	2.116	176.
	PDIF	2.140	0.390	7.420	1.314	1.689	6.225	171.
Sigmat = 26.400								
	PRES	22.680	9.010	35.940	5.930	0.121	2.517	178.
	TEM1	11.940	11.240	13.330	0.675	0.919	2.084	178.
	S 1	34.745	34.574	35.096	0.168	0.933	2.106	178.
	PDIF	2.940	0.510	13.330	2.418	1.597	5.519	177.
Sigmat = 26.500								
	PRES	25.480	8.600	40.610	7.220	0.047	2.323	180.
	TEM1	11.500	10.750	13.290	0.722	1.108	2.829	180.
	S 1	34.766	34.588	35.213	0.176	1.145	2.930	180.
	PDIF	2.980	0.710	8.410	1.468	1.271	4.648	179.
Sigmat = 26.600								
	PRES	28.630	11.980	43.190	7.220	-0.013	2.331	182.
	TEM1	10.910	10.260	13.040	0.658	1.629	5.152	182.
	S 1	34.756	34.605	35.277	0.157	1.716	5.485	182.
	PDIF	4.390	0.600	17.780	2.346	1.631	8.859	180.
Sigmat = 26.700								
	PRES	34.490	18.090	47.990	6.770	-0.171	2.329	183.
	TEM1	10.490	9.860	12.630	0.657	1.732	5.661	183.
	S 1	34.788	34.647	35.301	0.153	1.831	6.049	183.
	PDIF	6.160	1.360	16.580	3.357	1.132	3.572	183.
Sigmat = 26.800								
	PRES	39.190	21.190	57.740	8.010	-0.162	2.167	183.
	TEM1	10.340	9.380	12.350	0.746	1.028	3.236	183.
	S 1	34.884	34.673	35.358	0.171	1.110	3.421	183.
	PDIF	4.050	1.200	12.090	2.083	1.207	4.231	183.
Sigmat = 26.900								
	PRES	44.150	23.340	67.800	9.710	-0.077	1.992	183.
	TEM1	10.140	8.810	12.000	0.782	0.568	2.804	183.
	S 1	34.967	34.681	35.399	0.175	0.679	2.948	183.
	PDIF	7.070	1.630	20.860	4.827	1.088	3.108	180.
Sigmat = 27.000								
	PRES	53.160	27.410	80.830	13.550	0.311	2.103	169.
	TEM1	9.470	8.240	11.040	0.615	0.582	3.405	169.
	S 1	34.950	34.697	35.297	0.132	0.710	3.523	169.
	PDIF	17.400	4.230	31.970	6.818	-0.213	2.229	120.
Sigmat = 27.100								
	PRES	66.760	44.750	82.700	10.690	-0.348	1.837	59.
	TEM1	8.470	7.580	9.280	0.452	-0.298	1.872	59.
	S 1	34.871	34.700	35.034	0.089	-0.257	1.848	59.
	PDIF	28.040	19.140	33.630	4.281	-0.583	2.192	20.

table 8.1.15: 52° N to 53° N, 34°57' W to 35°41' W

Surface	Parameter	Mean	Minimum	Maximum	St.Dev.	Skewness	Kurtosis	Datapoints
Sigmat = 26.300								
	PRES	18.660	8.850	29.820	4.082	0.278	2.992	132.
	TEM1	11.810	11.510	12.160	0.153	0.058	2.090	132.
	S 1	34.581	34.509	34.668	0.037	0.075	2.100	132.
	PDIF	2.250	0.466	14.240	1.671	3.830	25.700	111.
Sigmat = 26.400								
	PRES	21.460	10.040	33.250	4.821	0.232	2.805	181.
	TEM1	11.380	10.570	11.920	0.176	-0.681	5.420	181.
	S 1	34.607	34.419	34.737	0.042	-0.620	5.250	181.
	PDIF	2.060	0.466	13.070	1.629	3.646	20.850	140.
Sigmat = 26.500								
	PRES	23.670	11.770	36.940	5.163	0.297	2.702	201.
	TEM1	10.890	10.360	11.430	0.168	-0.201	3.160	201.
	S 1	34.620	34.501	34.747	0.039	-0.167	3.160	201.
	PDIF	3.420	0.813	8.760	1.469	0.948	4.200	188.
Sigmat = 26.600								
	PRES	27.370	14.610	46.910	5.117	0.267	3.332	248.
	TEM1	10.410	9.950	10.750	0.112	-0.571	4.470	248.
	S 1	34.639	34.538	34.716	0.025	-0.533	4.410	248.
	PDIF	5.790	1.090	13.300	2.590	0.655	2.840	247.
Sigmat = 26.700								
	PRES	33.690	20.490	52.690	4.965	0.171	3.297	248.
	TEM1	9.880	9.290	10.180	0.113	-1.109	6.510	248.
	S 1	34.650	34.526	34.717	0.024	-1.061	6.340	248.
	PDIF	5.640	1.071	17.860	3.049	1.007	3.670	248.
Sigmat = 26.800								
	PRES	38.750	26.830	56.550	4.303	0.257	3.792	248.
	TEM1	9.380	8.510	9.590	0.117	-2.549	16.720	248.
	S 1	34.673	34.495	34.716	0.024	-2.439	15.700	248.
	PDIF	4.610	0.962	19.710	3.029	1.533	5.760	248.
Sigmat = 26.900								
	PRES	42.990	32.340	59.770	4.213	0.206	3.459	248.
	TEM1	8.820	8.080	9.160	0.153	-1.153	6.590	248.
	S 1	34.684	34.539	34.753	0.031	-1.083	6.310	248.
	PDIF	4.090	1.280	16.740	2.202	1.646	7.810	248.
Sigmat = 27.000								
	PRES	47.350	36.740	63.760	4.575	0.279	3.257	248.
	TEM1	8.260	7.770	8.760	0.123	0.142	4.380	248.
	S 1	34.701	34.607	34.799	0.024	0.189	4.390	248.
	PDIF	5.550	1.532	17.590	2.478	1.689	7.320	248.
Sigmat = 27.100								
	PRES	55.200	43.240	72.320	4.626	0.442	3.605	245.
	TEM1	7.690	7.310	8.190	0.134	0.767	4.200	245.
	S 1	34.719	34.649	34.814	0.025	0.809	4.320	245.
	PDIF	11.760	3.063	23.790	3.822	0.180	3.120	236.
Sigmat = 27.200								
	PRES	68.690	52.890	81.450	4.761	0.020	2.903	208.
	TEM1	6.990	6.680	7.290	0.158	0.107	1.740	208.
	S 1	34.721	34.667	34.774	0.028	0.122	1.750	208.
	PDIF	13.090	3.688	25.640	3.842	0.434	3.670	145.

table 8.1.16: 53° N to 54° N, 35°41' W to 36°26' W

Surface	Parameter	Mean	Minimum	Maximum	St.Dev.	Skewness	Kurtosis	Datapoints
Sigmat = 26.600								
	PRES	23.520	12.320	36.330	4.518	0.117	2.736	165.
	TEM1	10.470	10.380	10.670	0.046	0.820	4.541	165.
	S 1	34.654	34.633	34.698	0.010	0.835	4.590	165.
	PDIF	7.770	2.850	18.750	4.819	0.816	2.469	21.
Sigmat = 26.700								
	PRES	29.080	14.260	43.880	4.863	0.011	3.257	241.
	TEM1	9.900	9.660	10.090	0.058	-0.384	5.028	241.
	S 1	34.654	34.603	34.696	0.013	-0.362	5.020	241.
	PDIF	5.540	1.401	14.390	2.352	0.990	4.167	237.
Sigmat = 26.800								
	PRES	34.220	22.260	46.000	4.878	0.023	2.607	242.
	TEM1	9.380	9.130	9.580	0.079	-0.813	3.367	242.
	S 1	34.671	34.621	34.714	0.016	-0.801	3.340	242.
	PDIF	5.110	0.737	15.820	2.551	1.178	5.030	242.
Sigmat = 26.900								
	PRES	40.220	25.400	55.540	5.507	-0.033	3.247	242.
	TEM1	8.830	8.660	9.010	0.062	-0.522	4.117	242.
	S 1	34.687	34.653	34.723	0.013	-0.501	4.090	242.
	PDIF	6.410	0.733	21.330	3.214	1.301	5.498	242.
Sigmat = 27.000								
	PRES	46.250	30.990	65.780	6.326	0.389	3.250	243.
	TEM1	8.290	8.090	8.420	0.049	-0.416	4.000	243.
	S 1	34.706	34.667	34.732	0.009	-0.397	4.000	243.
	PDIF	5.770	1.721	17.690	2.711	1.151	5.055	242.
Sigmat = 27.100								
	PRES	52.200	36.570	70.890	6.966	0.260	2.400	245.
	TEM1	7.720	7.520	7.840	0.050	-0.309	3.970	245.
	S 1	34.726	34.689	34.749	0.009	-0.292	3.930	245.
	PDIF	6.620	1.533	14.180	2.755	0.512	2.702	240.
Sigmat = 27.200								
	PRES	59.720	41.460	78.390	7.833	0.291	2.405	231.
	TEM1	7.150	7.030	7.280	0.054	0.268	2.507	231.
	S 1	34.749	34.727	34.773	0.010	0.278	2.460	231.
	PDIF	9.510	2.819	24.280	3.629	0.672	3.918	198.
Sigmat = 27.300								
	PRES	69.100	49.990	81.330	5.589	-0.475	2.978	137.
	TEM1	6.580	6.440	6.720	0.069	0.151	2.302	137.
	S 1	34.777	34.752	34.799	0.012	0.163	2.280	137.
	PDIF	17.970	8.342	31.820	5.166	0.376	2.916	33.

table 8.1.17: 54° N to 55° N, 36°26' W to 37°11' W

Surface	Parameter	Mean	Minimum	Maximum	St.Dev.	Skewness	Kurtosis	Datapoints
Sigmat = 26.700								
	PRES	30.040	18.220	44.490	4.796	0.340	3.606	235.
	TEM1	9.880	9.610	10.230	0.109	-0.123	3.112	235.
	S 1	34.651	34.592	34.728	0.024	-0.102	3.114	235.
	PDIF	4.860	0.860	14.140	2.708	1.348	4.675	146.
Sigmat = 26.800								
	PRES	33.860	19.400	48.160	5.237	-0.089	3.168	258.
	TEM1	9.340	9.000	9.660	0.124	-0.598	3.187	258.
	S 1	34.663	34.593	34.732	0.026	-0.571	3.163	258.
	PDIF	4.980	0.720	14.880	2.652	0.976	3.757	258.
Sigmat = 26.900								
	PRES	39.720	20.780	53.010	6.139	-0.482	2.930	259.
	TEM1	8.790	8.390	9.050	0.143	-1.036	3.652	259.
	S 1	34.678	34.600	34.732	0.029	-1.011	3.612	259.
	PDIF	5.970	1.620	17.380	2.622	0.905	4.167	259.
Sigmat = 27.000								
	PRES	45.090	25.460	56.970	6.128	-0.696	3.325	259.
	TEM1	8.260	7.850	8.520	0.135	-1.694	5.247	259.
	S 1	34.700	34.622	34.753	0.026	-1.672	5.197	259.
	PDIF	4.960	1.420	14.160	2.288	1.021	4.330	259.
Sigmat = 27.100								
	PRES	50.140	30.780	62.110	5.891	-0.601	3.438	259.
	TEM1	7.700	7.300	7.870	0.140	-1.849	5.388	259.
	S 1	34.722	34.648	34.754	0.026	-1.833	5.345	259.
	PDIF	5.880	1.260	16.310	2.411	0.988	4.474	259.
Sigmat = 27.200								
	PRES	57.310	38.240	72.960	5.999	-0.193	3.415	259.
	TEM1	7.130	6.670	7.290	0.144	-2.064	6.220	259.
	S 1	34.745	34.665	34.774	0.025	-2.046	6.166	259.
	PDIF	8.450	2.850	20.320	3.258	0.771	3.599	254.
Sigmat = 27.300								
	PRES	66.690	52.220	79.260	5.335	-0.123	2.640	229.
	TEM1	6.520	6.050	6.720	0.162	-1.481	4.405	229.
	S 1	34.767	34.689	34.799	0.027	-1.454	4.340	229.
	PDIF	13.520	5.730	23.960	4.104	0.348	2.338	150.

Table 8.2.1: Statistics of isopycnal surfaces averaged over the total frontal survey, NOA'81.

Area	Surface	Parameter	Mean	Min.	Max.	Variance	Stdev	Skewness	Kurtosis	No of Pos.
-C3-	σ_t = 26.3 kg m^{-3}	T1 [°C]	13.12	11.13	15.47	0.99	0.99	-0.19	1.81	4938
		S1 $*10^3$	34.92	34.42	35.56	0.07	0.26	-0.13	1.84	4938
		P [10^4Pa]	29.67	6.39	53.84	44.88	6.70	-0.12	3.20	4938
		DP	2.30	0.04	29.83	6.98	2.64	4.29	27.76	4830
	σ_t = 26.6 kg m^{-3}	T1	12.00	9.90	14.78	1.29	1.13	-0.08	2.03	5326
		S1	35.02	34.53	35.75	0.08	0.28	0.02	2.13	5326
		P	38.68	11.98	68.14	59.26	7.70	0.07	3.39	5326
		DP	3.94	0.32	25.65	5.91	2.43	1.62	8.06	5225
	σ_t = 26.9 kg m^{-3}	T1	10.88	8.08	13.14	1.42	1.19	-0.51	2.11	5147
		S1	35.14	34.54	35.69	0.07	0.27	0.42	2.07	5147
		P	57.03	23.34	90.96	121.23	11.01	0.17	2.57	5147
		DP	10.94	0.66	45.72	58.67	7.66	1.42	4.69	4001

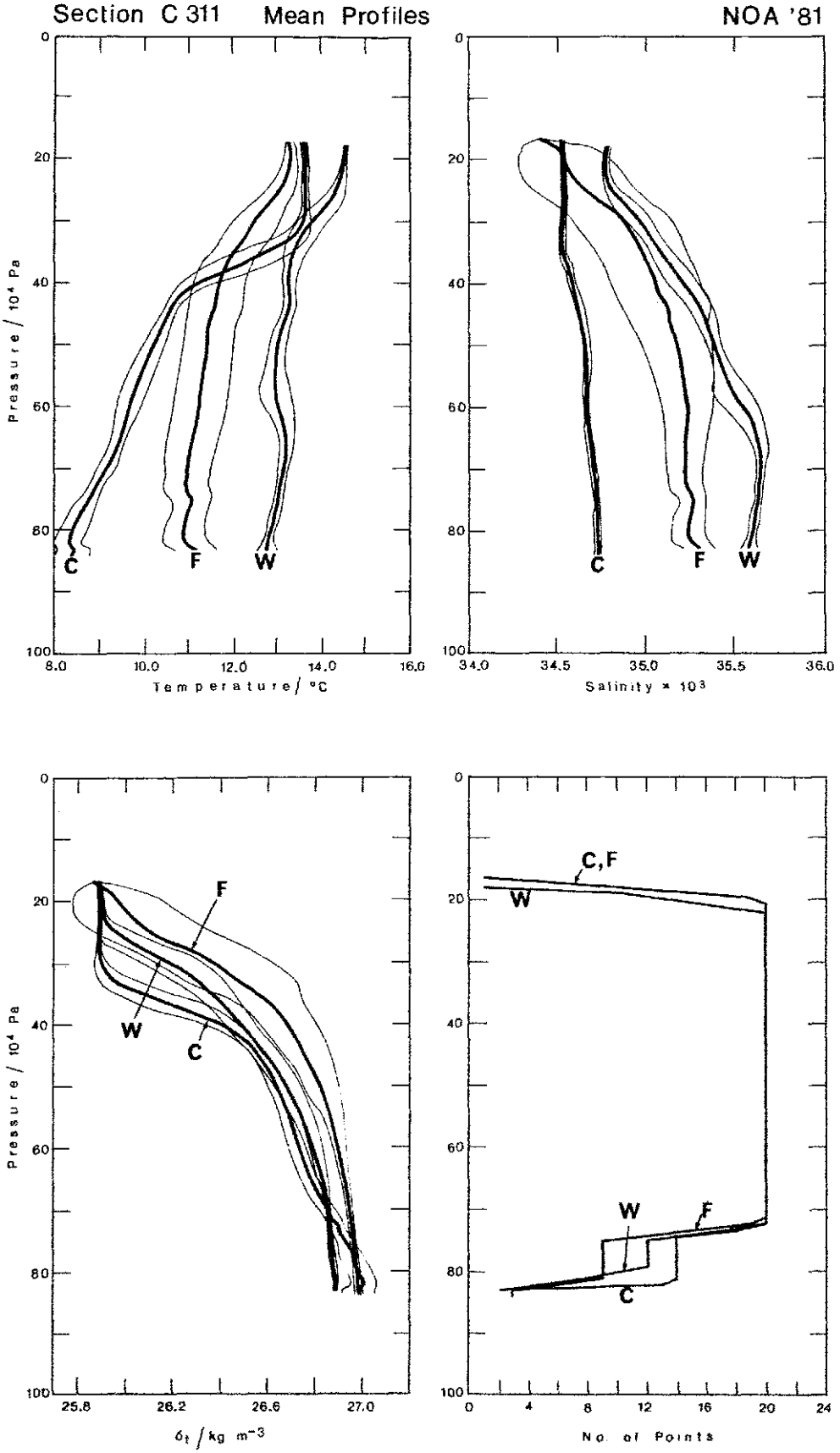

Fig. 8.1.1: Mean and standard deviation profiles for three selected regions; of section C311 averaged on surfaces of constant pressure.

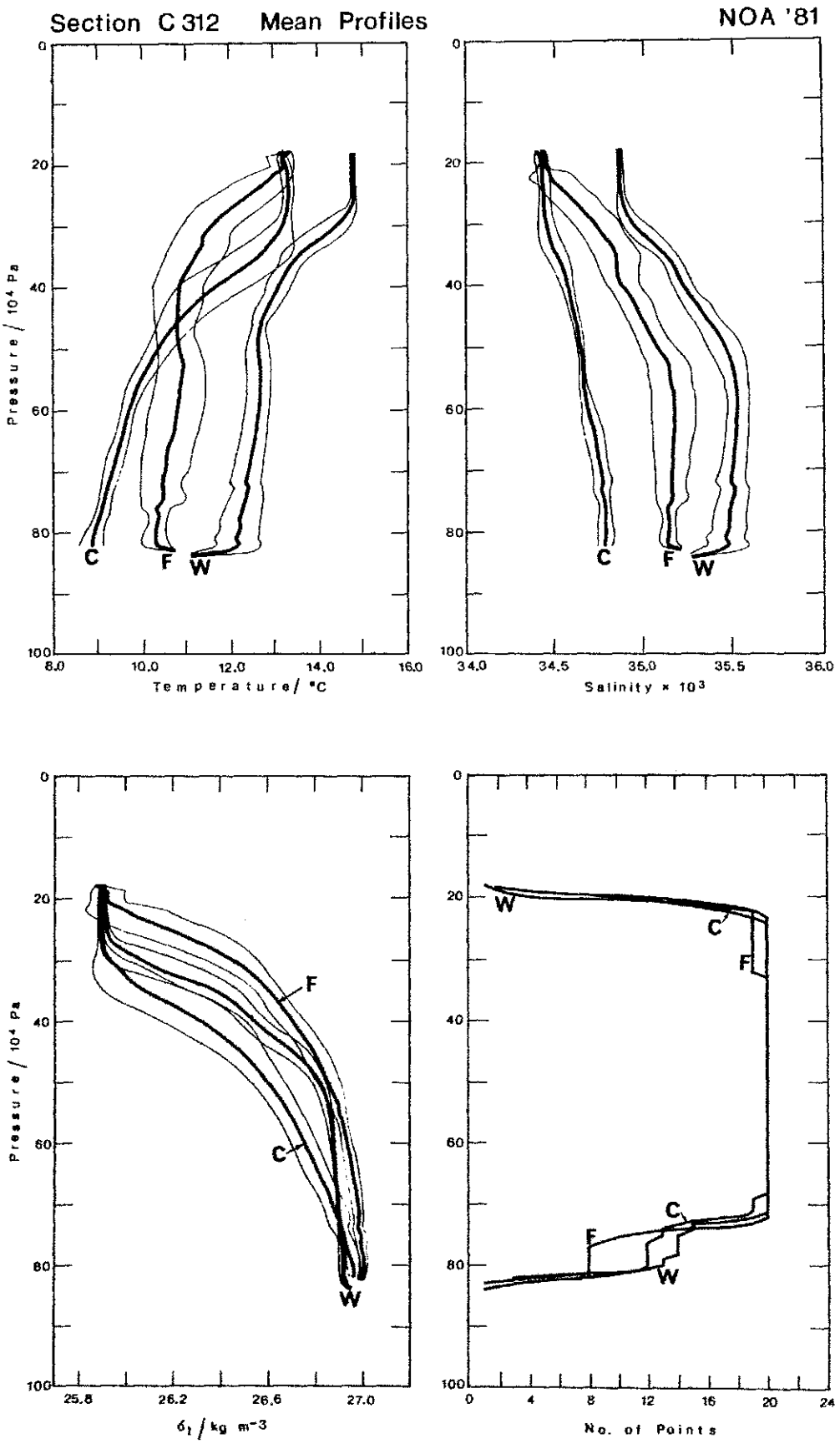

Fig. 8.1.2: Mean and standard deviation profiles for three selected regions of section C312; averaged on surfaces of constant pressure.

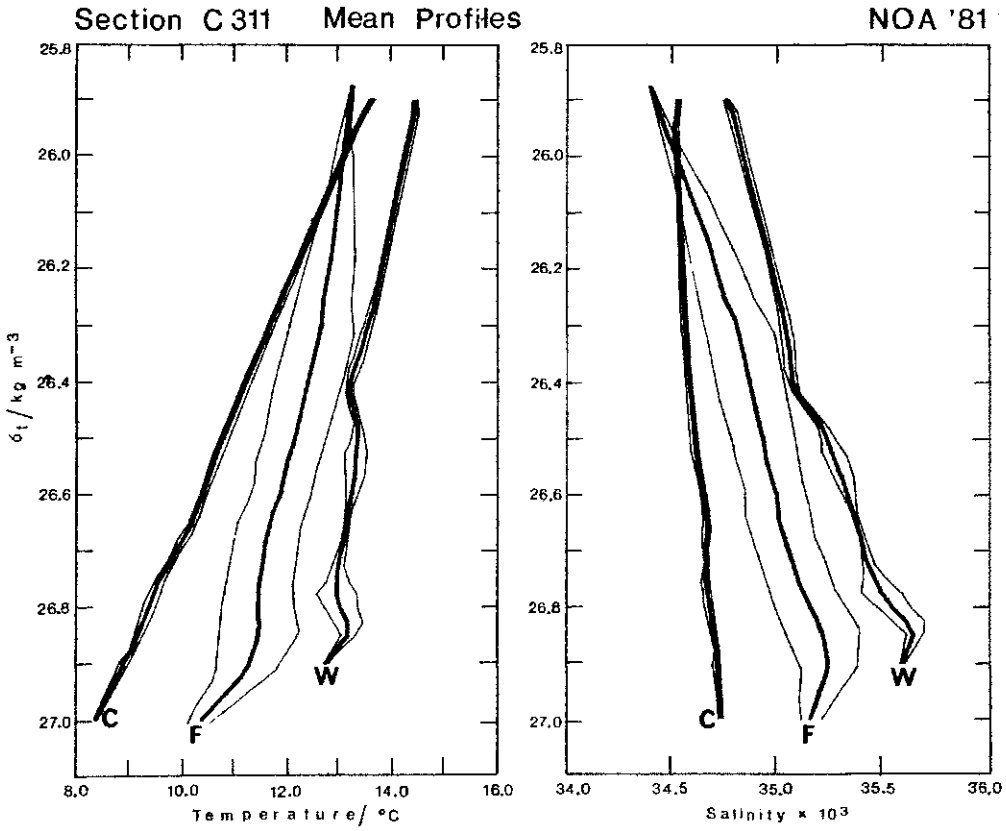

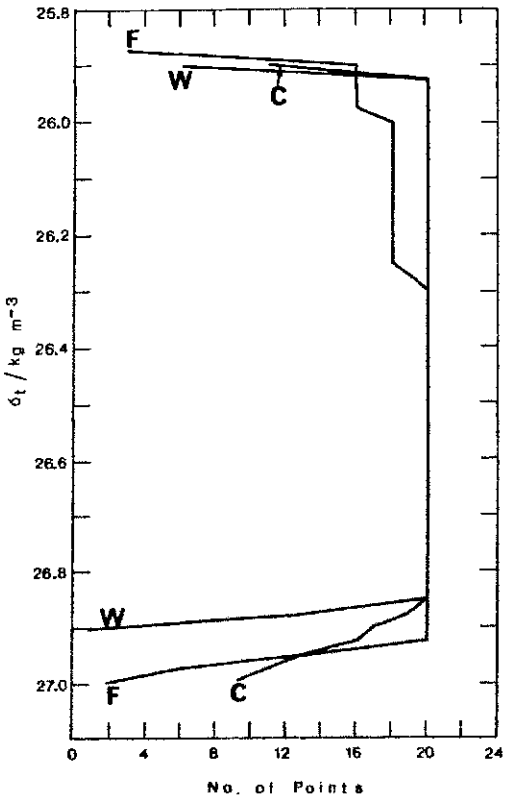

Fig. 8.1.3:

Mean and standard deviation profiles for three selected regions of section C311; averaged on surfaces of constant density and plotted versus σ_t.

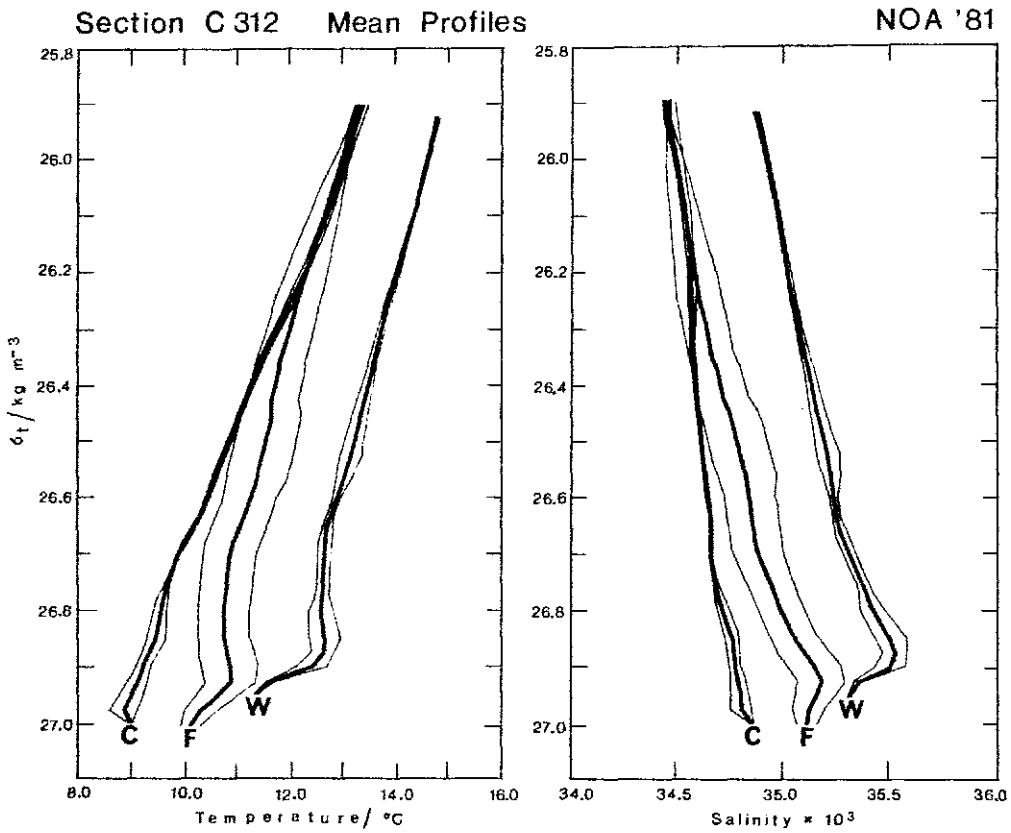

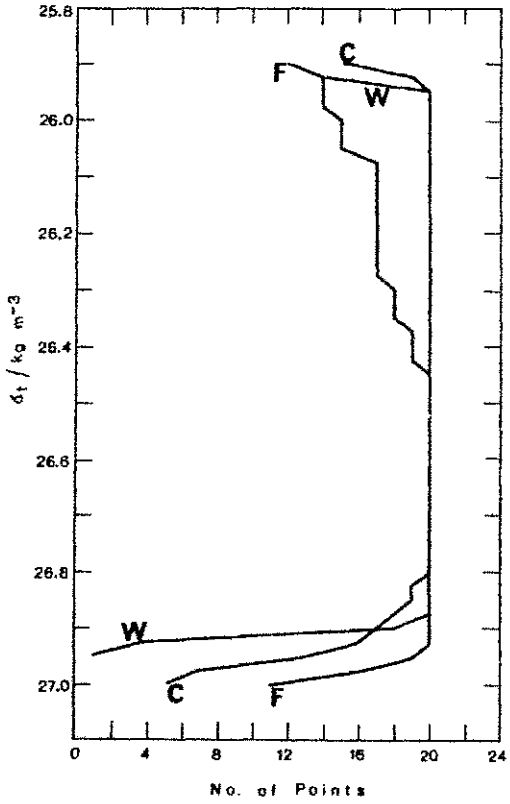

Fig. 8.1.4:

Mean and standard deviation profiles for three selected regions of section C312; averaged on surfaces of constant density and plotted versus σ_t.

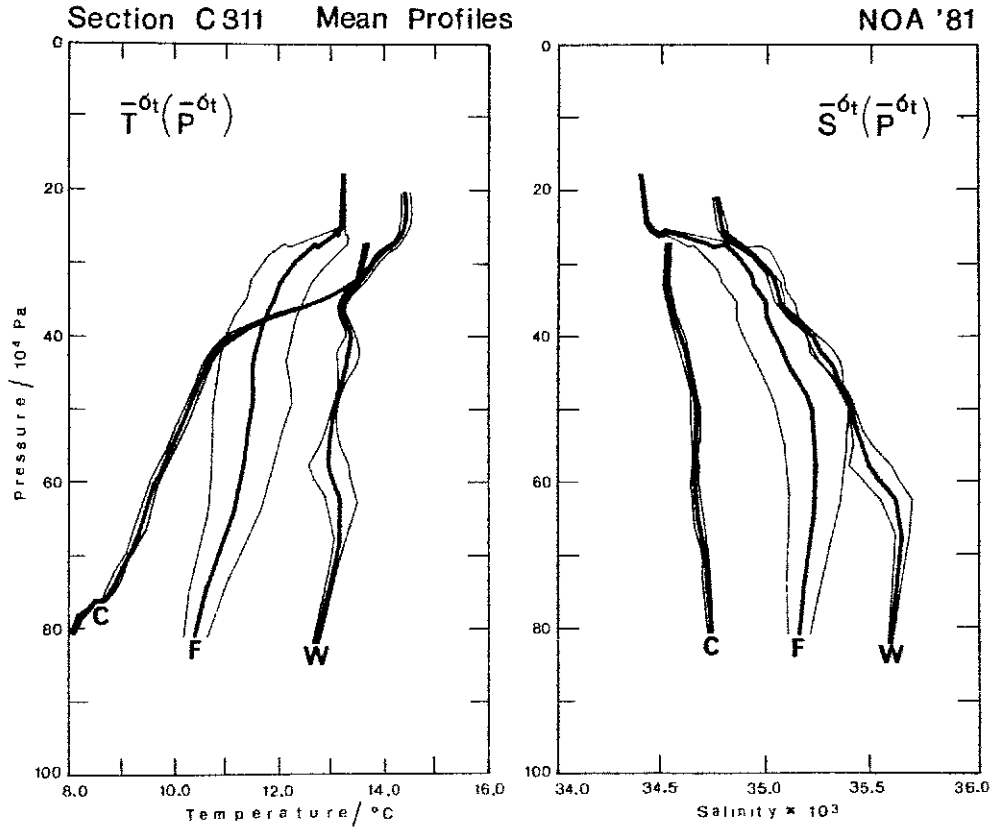

Fig. 8.1.5: Mean and standard deviation profiles for three selected regions of section C311; averaged on surfaces of constant density and plotted versus the mean depth of the density surface in question.

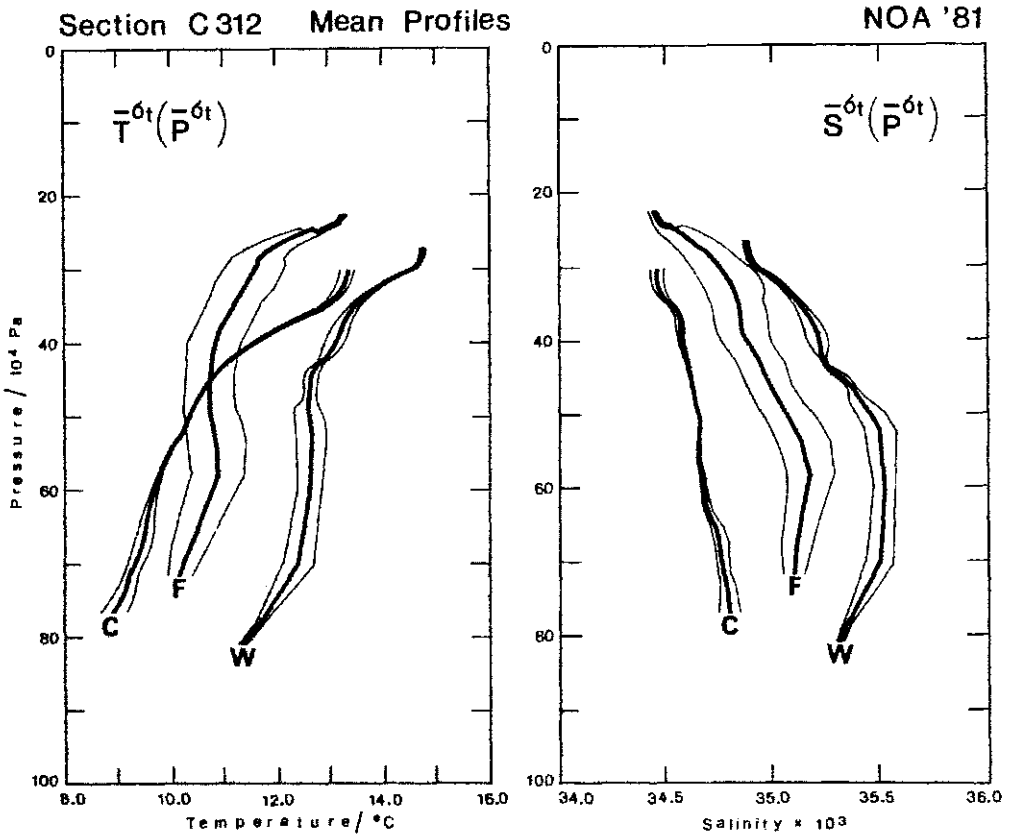

Fig. 8.1.6: Mean and standard deviation profiles for three selected regions of section C312; averaged on surfaces of constant density and plotted versus the mean depth of the density surface in question.

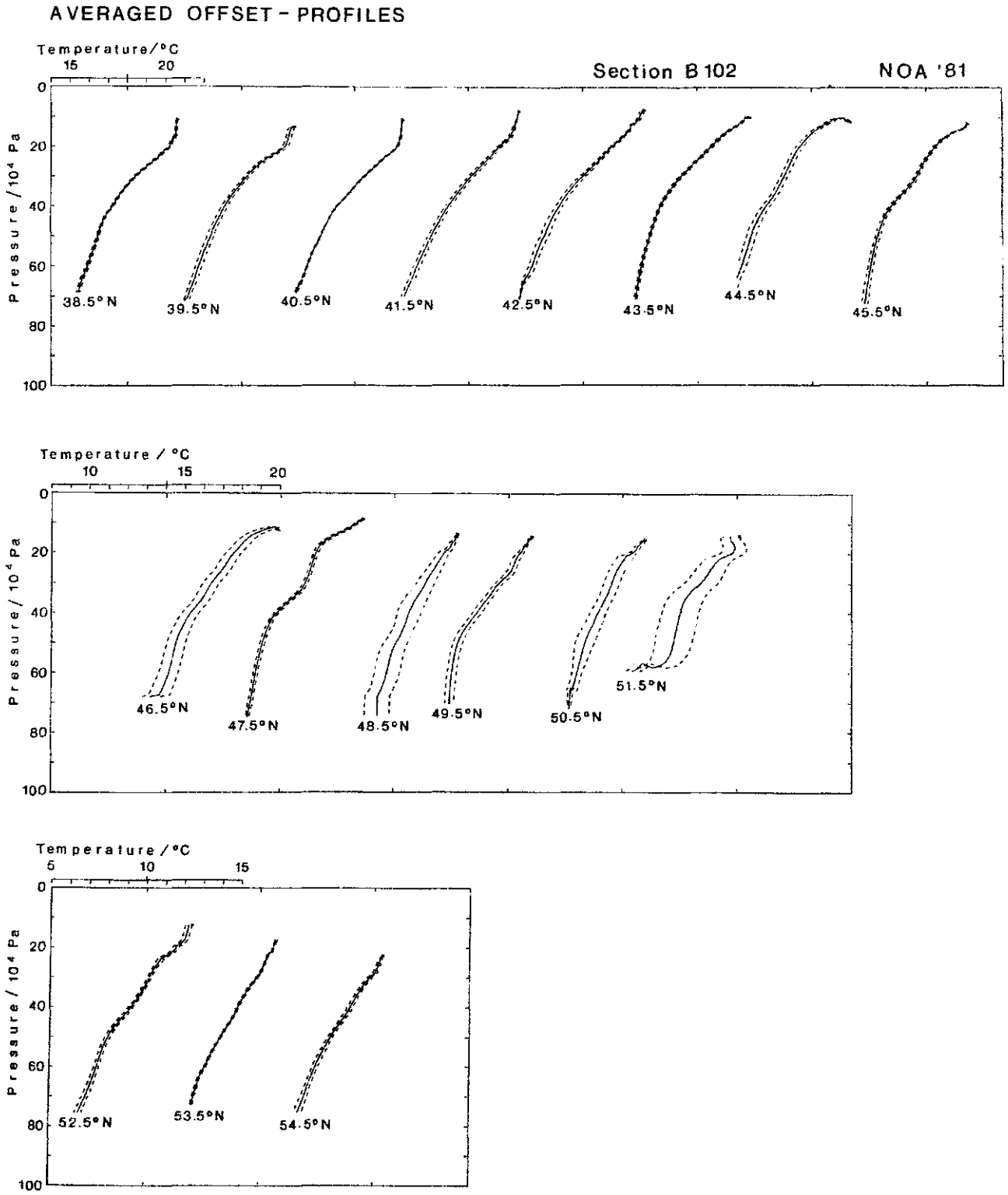

Fig. 8.1.7: Mean and standard deviation profiles of temperature averaged on constant σ_t-surfaces over 1° of latitude along section B102 and plotted versus the mean pressure of the density surfaces.

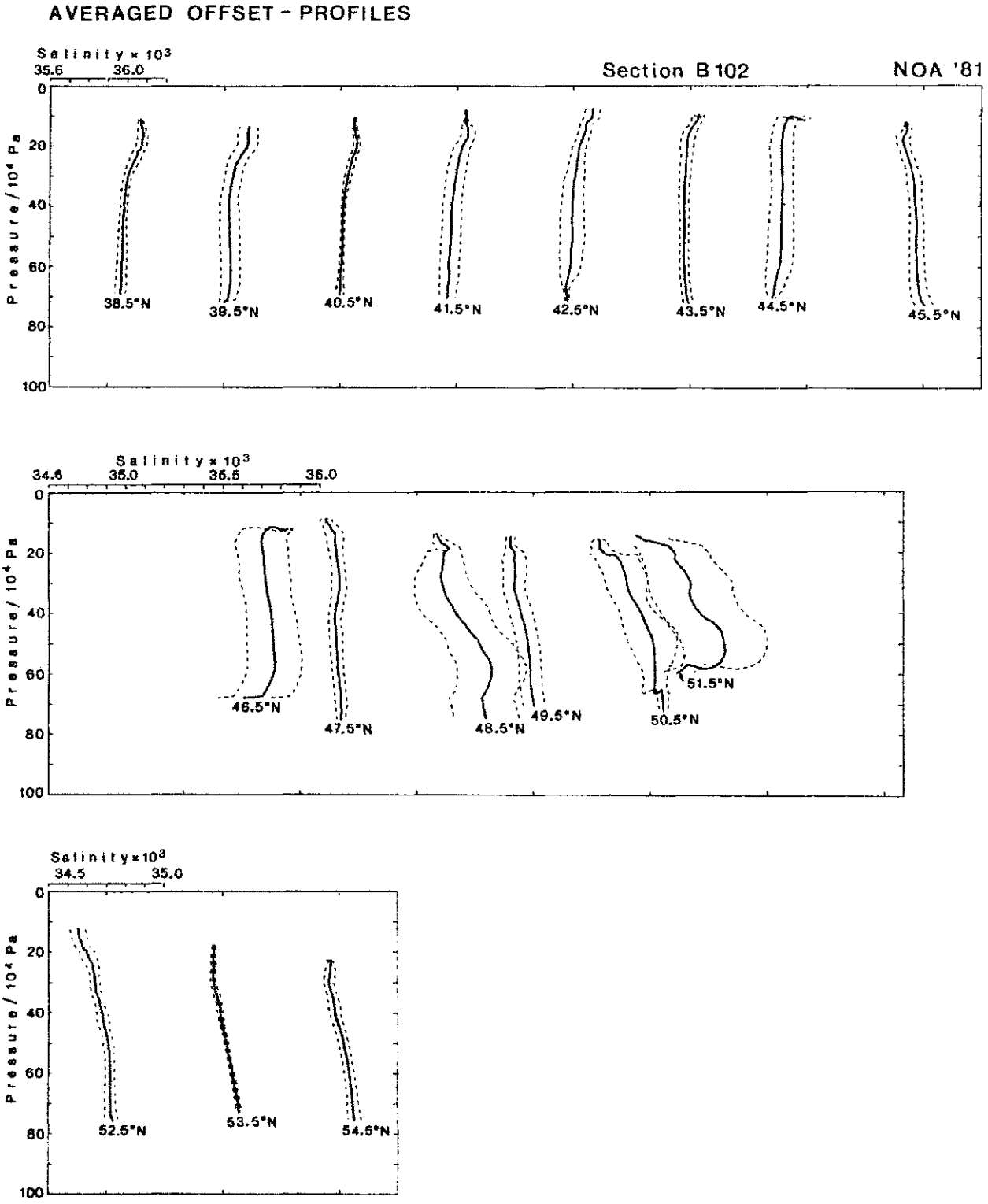

Fig. 8.1.8: Mean and standard deviation profiles of salinity averaged on constant σ_t-surfaces over 1° of latitude along section B102 and plotted versus the mean pressure of the density surfaces.

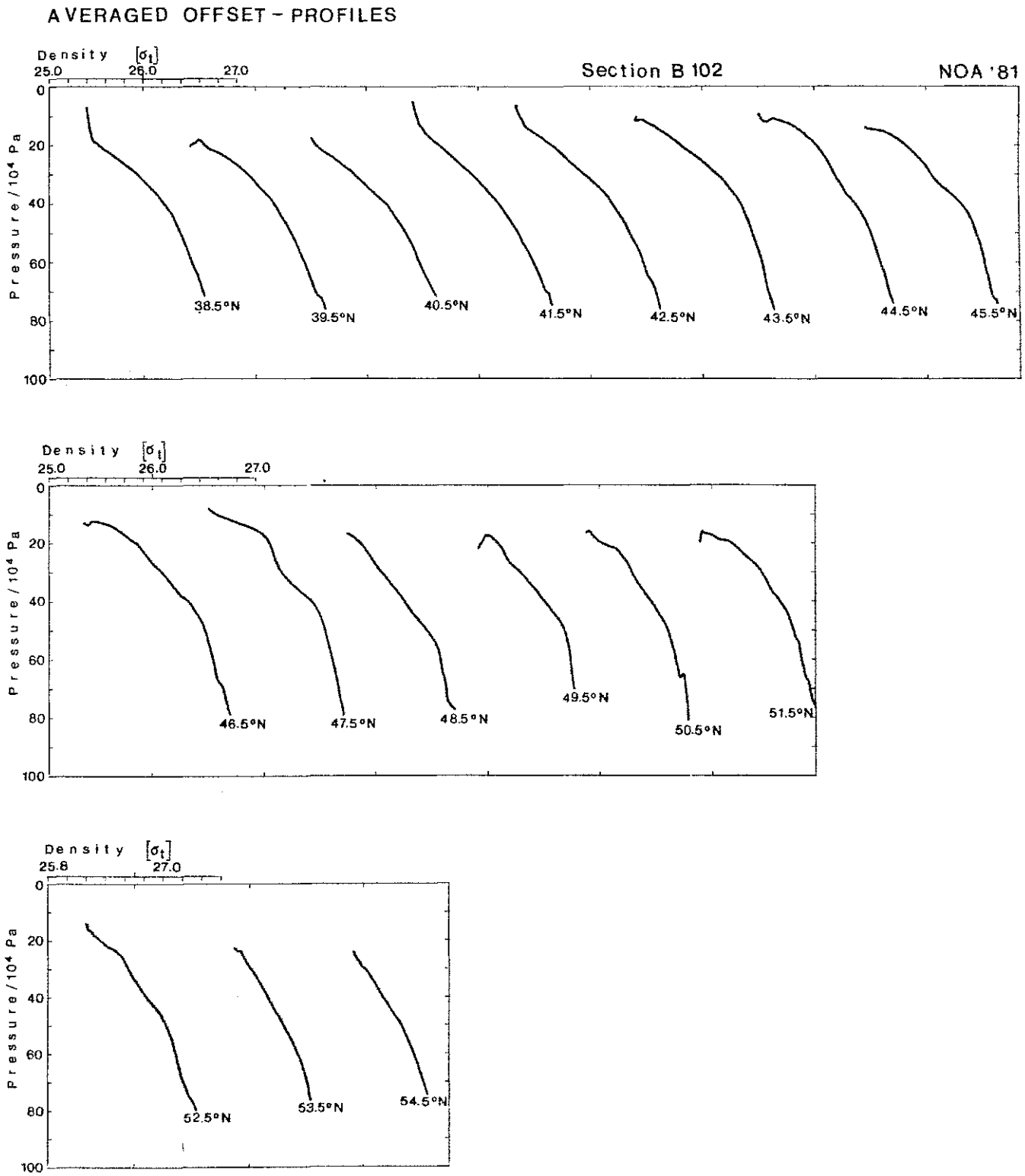

Fig. 8.1.9: Mean profiles of σ_t averaged on constant σ_t-surfaces over 1° of latitude along section B102 and plotted versus the mean pressure on the σ_t-surfaces.

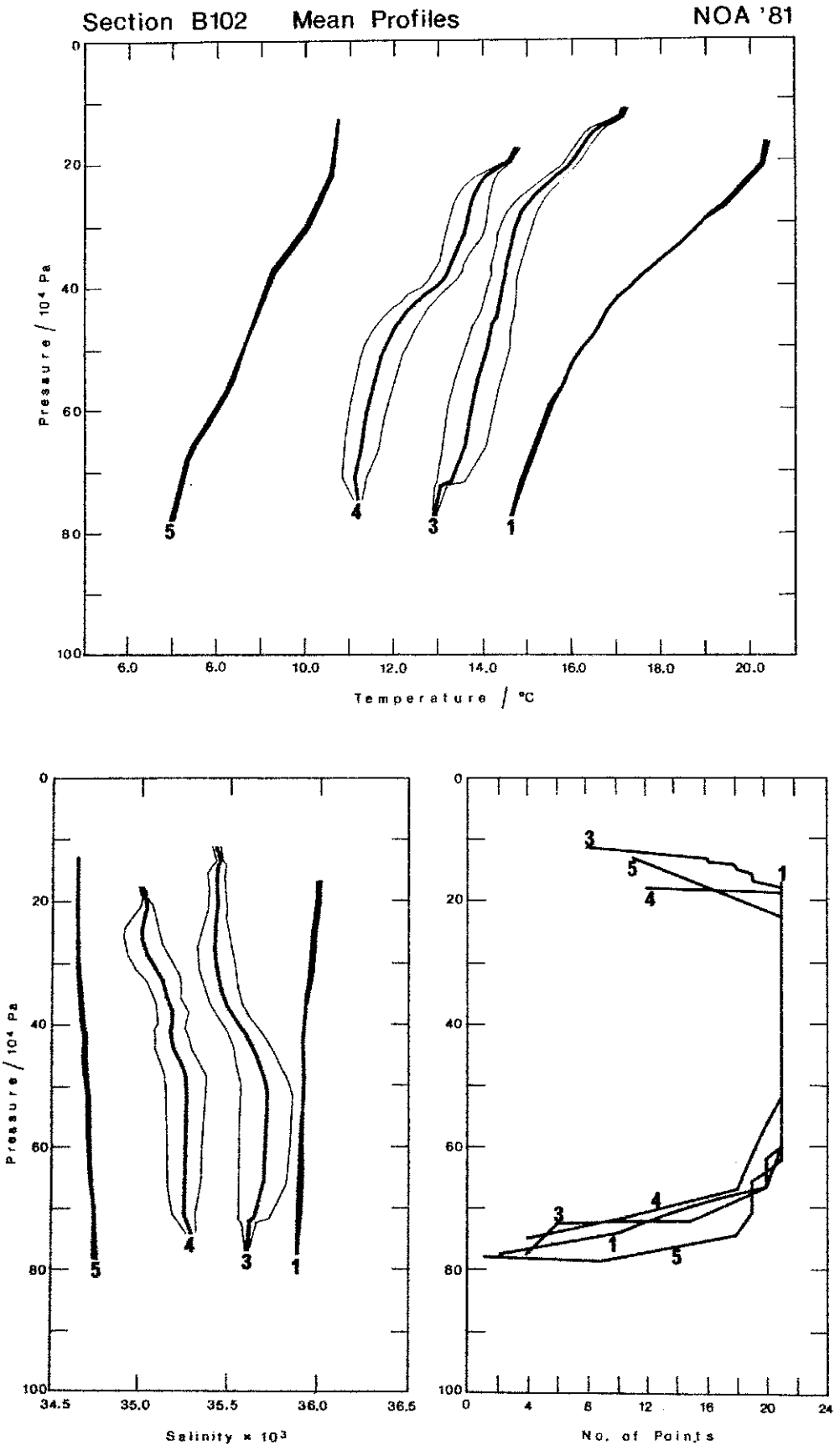

Fig. 8.1.10: Mean and standard deviation profiles of temperature and salinity of selected sets no. 1, 3, 4, 5 on section B102 averaged on constant density surfaces and plotted versus the mean pressure on the σ_t-surfaces.

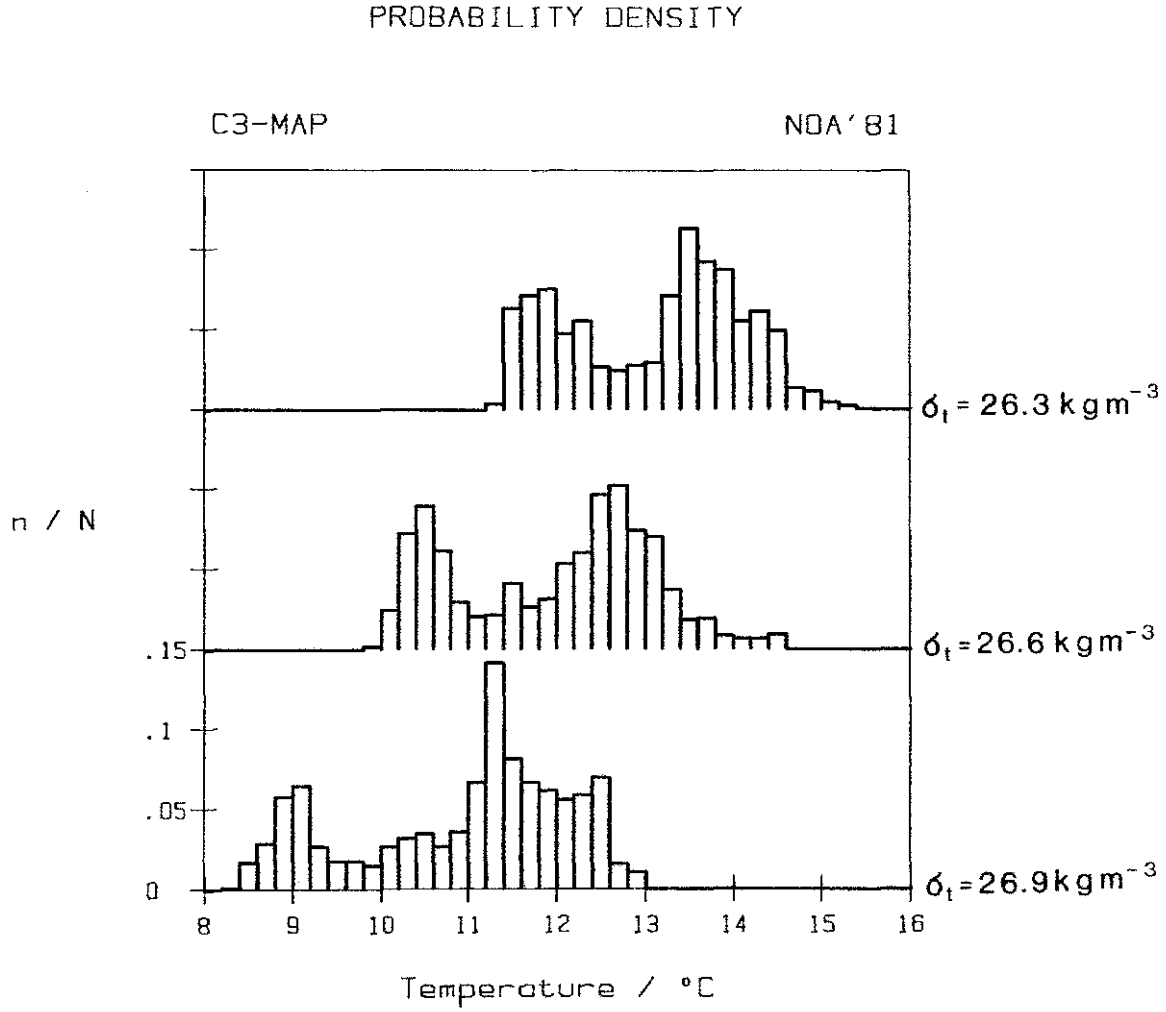

Fig. 8.2.1: Histograms of temperature on three isopycnals from the frontal survey. The number of contributing data points in each class (0.2 K) was normalized by the total number of data points on the surface in question.

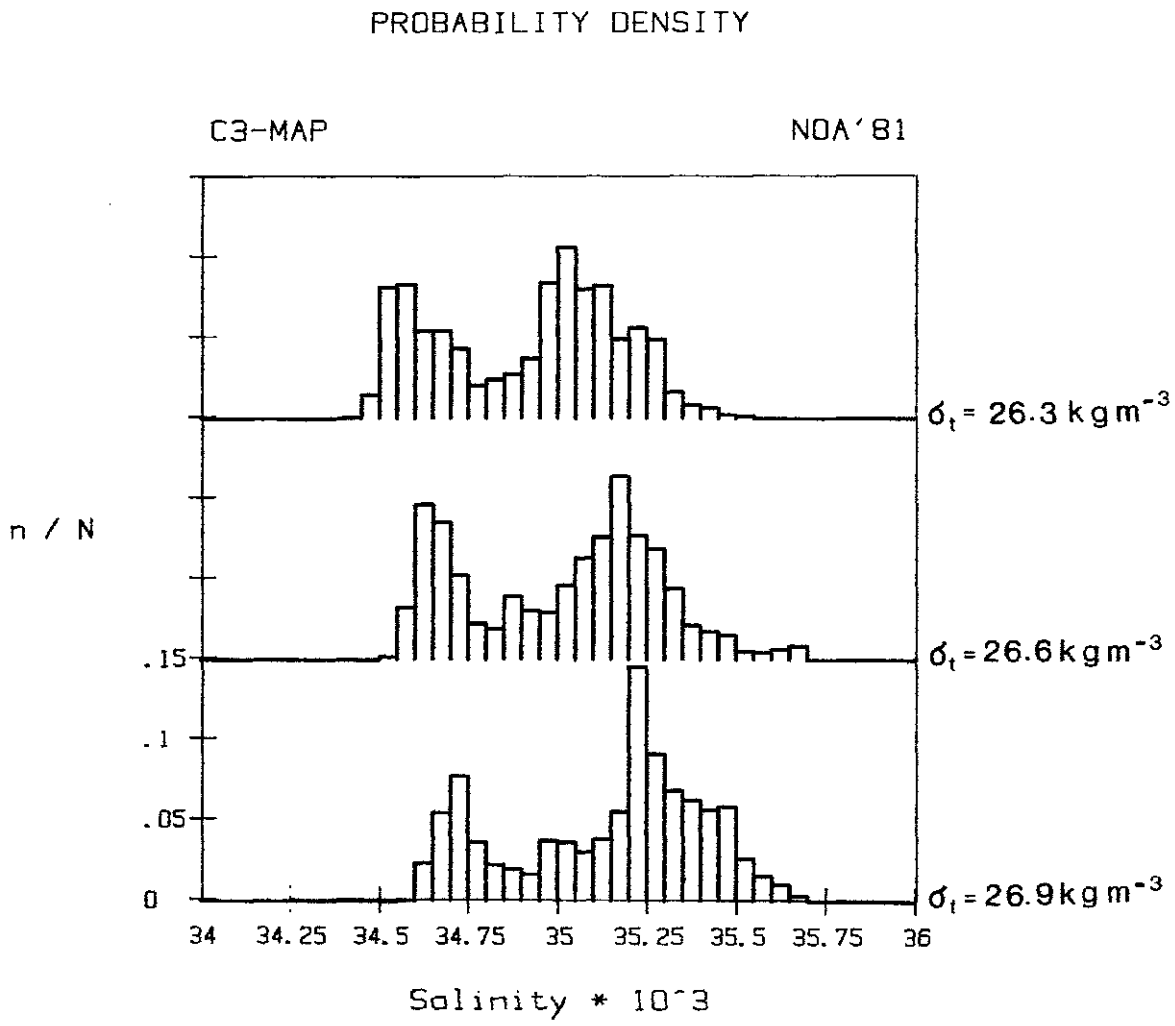

Fig. 8.2.2: Histograms of salinity on three isopycnals from the frontal survey. The number of contributing data points in each class (0.05×10^3) was normalized by the total number of data points on the surface in question.

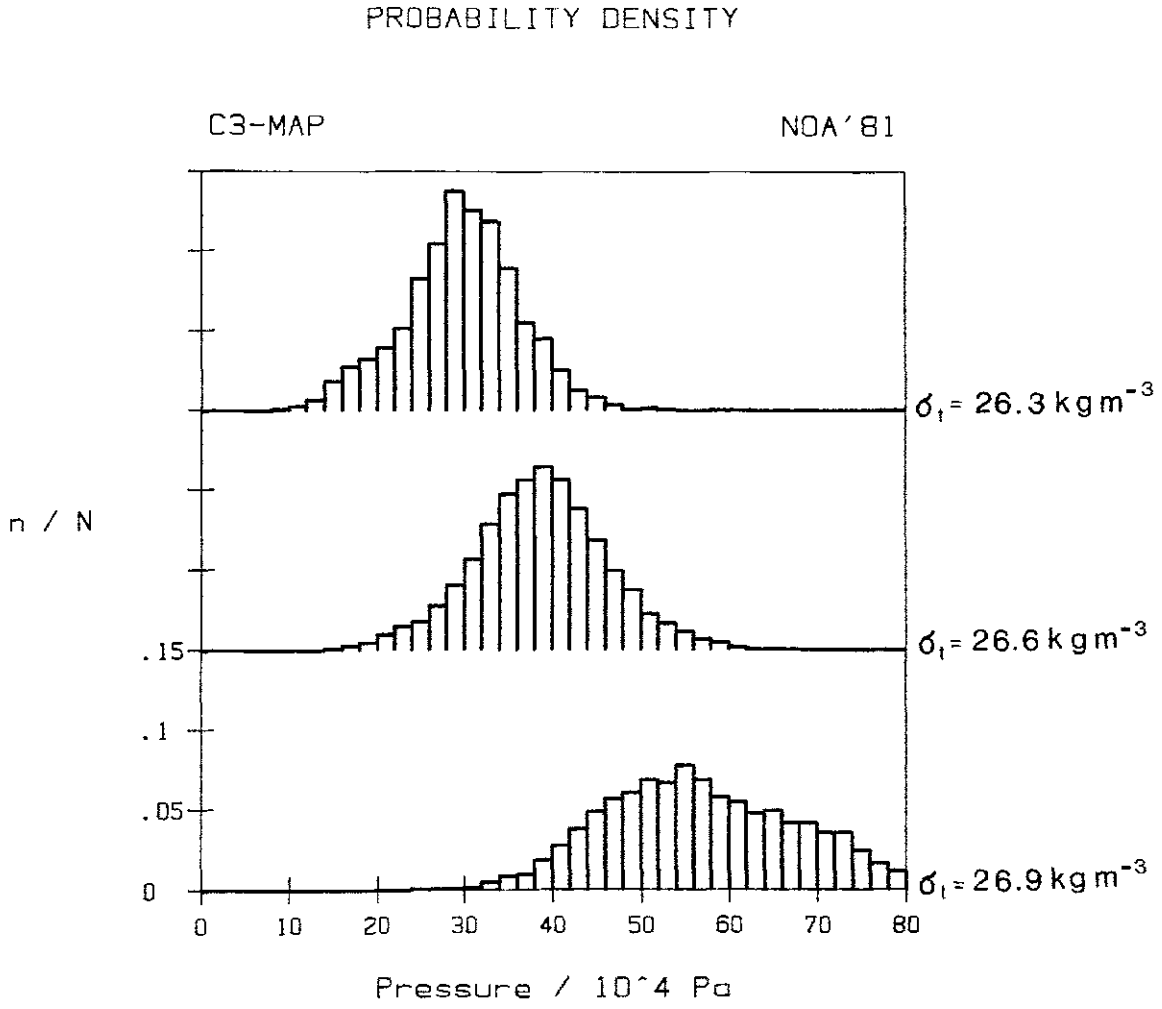

Fig. 8.2.3: Histograms of the depth of three selected isopycnals from the frontal survey. The number of contributing data points in each class (2 x 10 Pa) was normalized by the total number of data points on the surface in question.

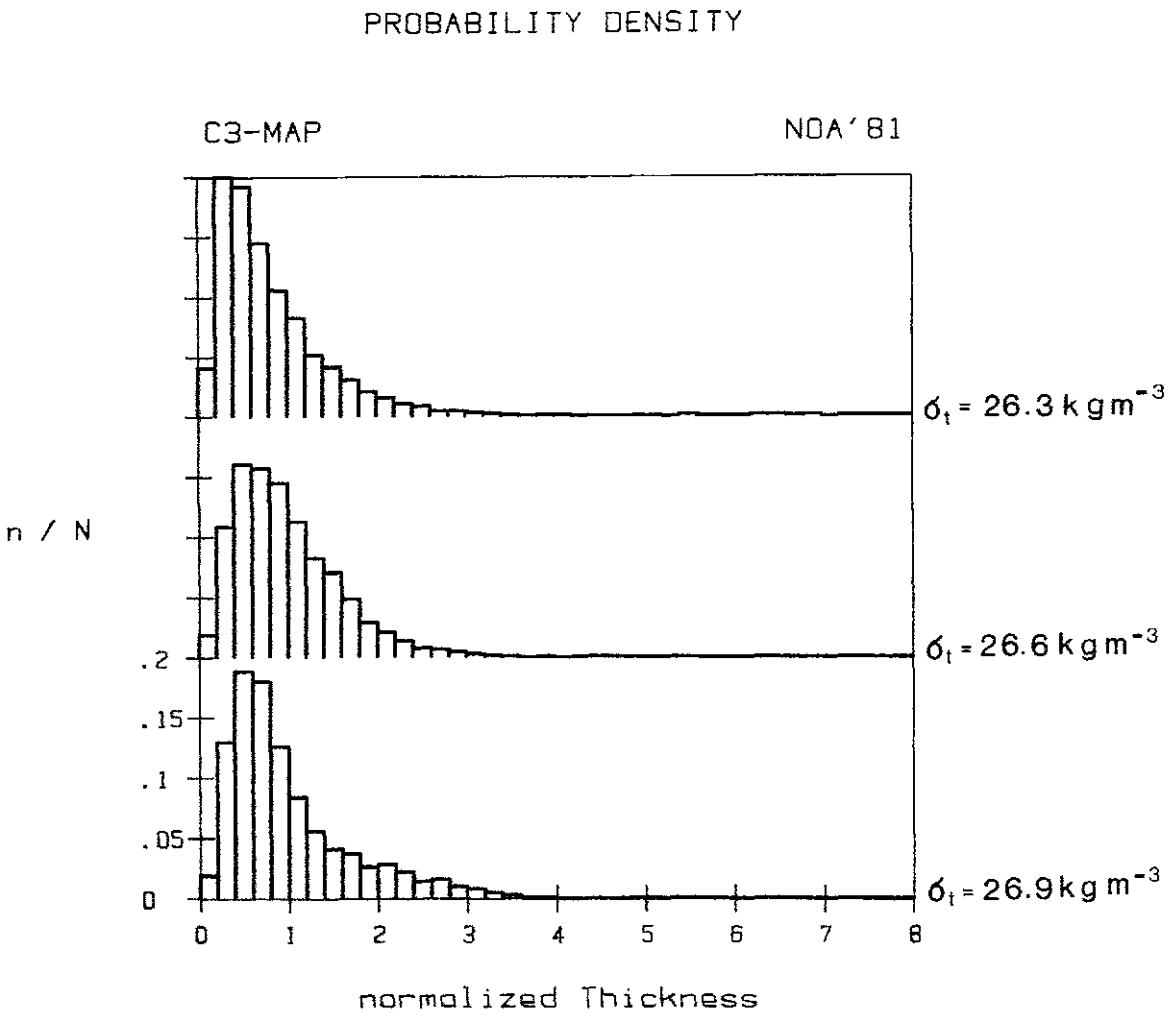

Fig. 8.2.4: Histograms of normalized spacing between isopycnals being 0.1 kg m^{-3} apart and centred around the labelled isopycnal. The spacing was normalized by its ensemble mean. The number of contributing data points in each window (0.2) was normalized by the total number of data points on the surface in question.

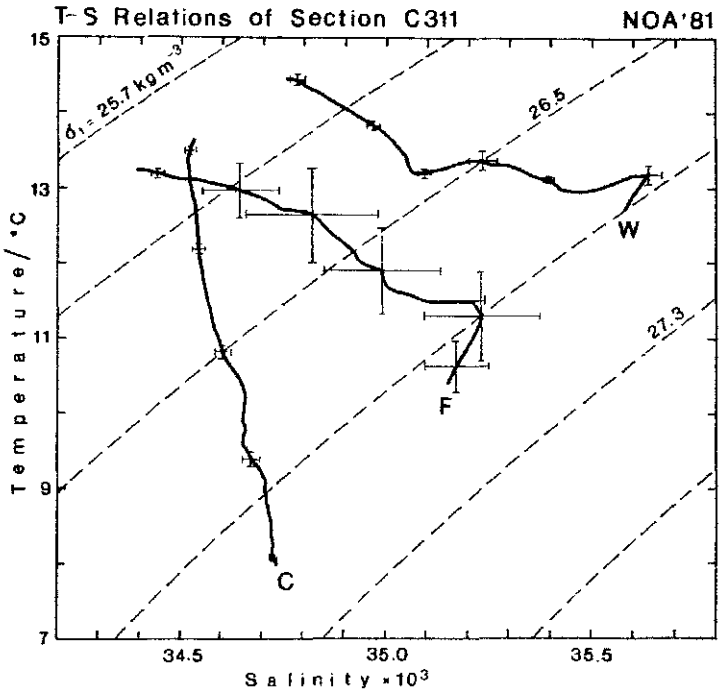

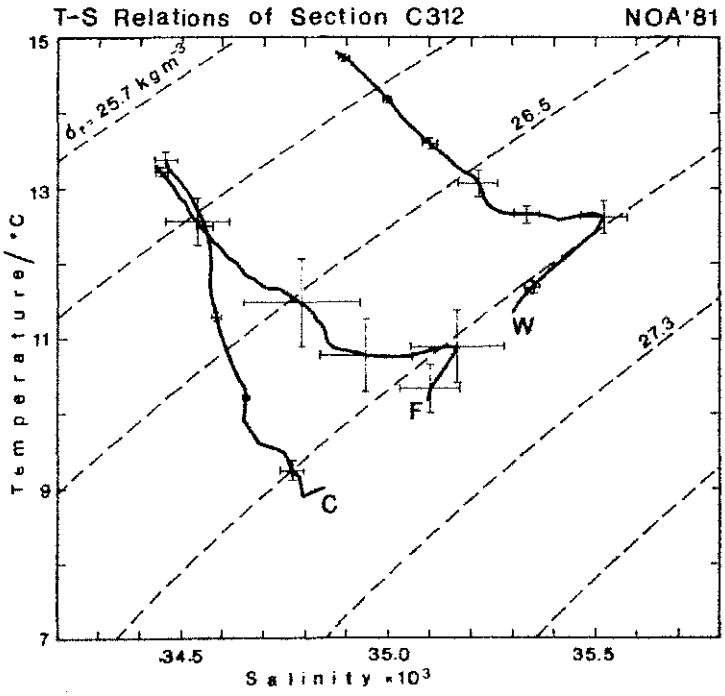

Fig. 8.3.1 und 8.3.2: Mean T-S diagrams for selected regions of the parallel sections C311 and C312. The data were averaged on isopycnals and the standard deviation bars indicate the variability within each interval.

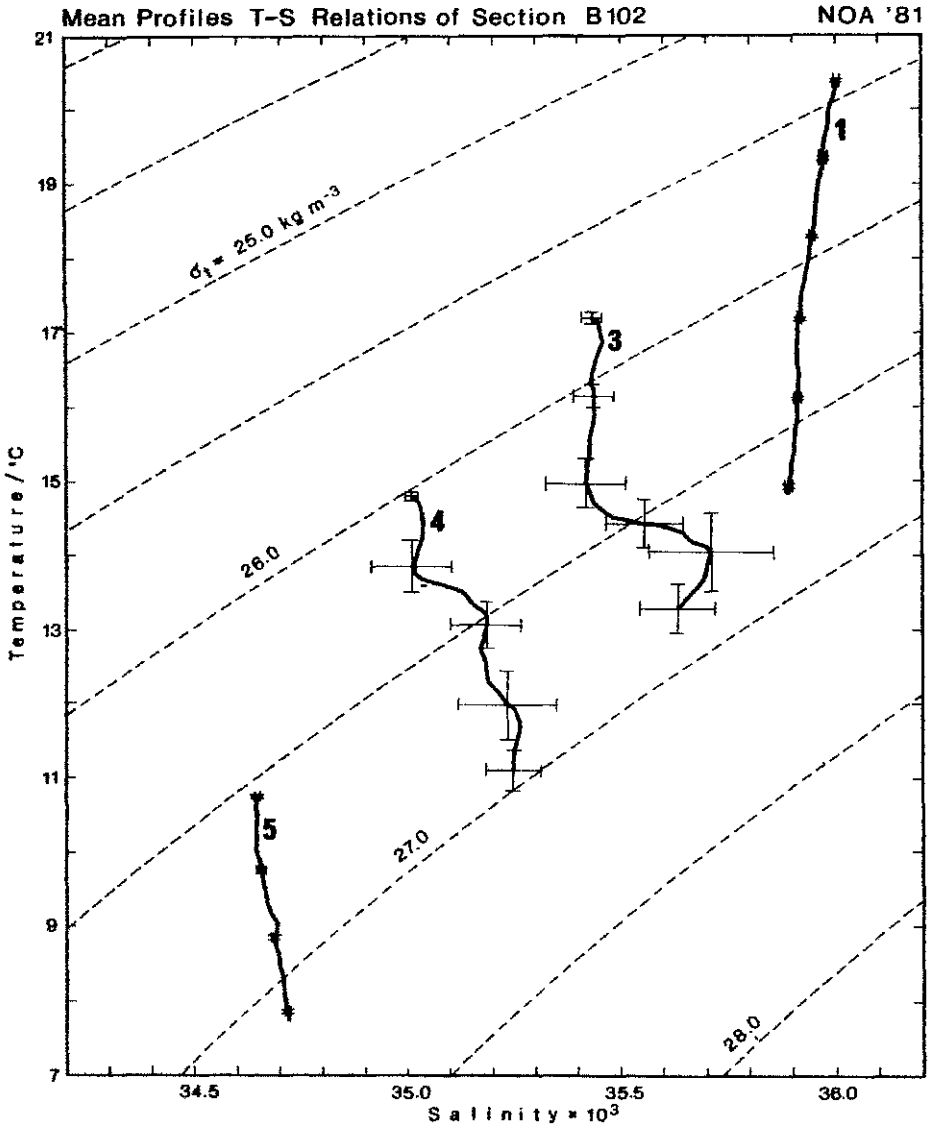

Fig. 8.3.3: Mean T-S diagrams of sets no. 1, 3, 4, 5 of section B102, averaged on isopycnals. The standard deviation bars indicate the variability at certain points in the profile.

9. ISOPYCNIC AND ISOBARIC MAPS FROM THE POLAR FRONT SURVEY

The data presented within this chapter were interpolated onto a regular 10 km x 10 km grid by an objective interpolation procedure as described in section 4.10. The interpolation onto the grid was carried out by using the weighting functions (figure 4.10), which were derived by smoothing the two-dimensional raw autocorrelation function of the variable to be interpolated.

An isopycnic map of temperature on σ_t = 26.6 kg m^{-3} from the seasonal thermocline was already shown in chapter 5.4 together with the error fields (figures 5.4.1 - 5.4.4). For the same isopycnal the depth, i.e. the pressure distribution, is presented in figure 9.1, and the error fields figure 9.2 and 9.4 are calculated in the same way as for temperature. Although the pressure field is contaminated by internal waves, some similarities between the temperature field (internal wave-free) and the pressure field can be seen.

The large-scale trend, with the isopycnals sloping upwards to the north by about 10 m is reflected by the isopycnic depth in the cold tongue, compared with the depth in the warmer part of the meander structure (see also figure 5.3.2). The general north-south trend is distorted by a meander structure of about 200 km wavelength with a region of sharp thermohaline contrast between its troughs. Within the high resolution area between 36° W and 35° W the isolated temperature island (less than 11 °C) is correlated with a depth maximum, which is contradictory to the general trend (cold = shallow).

Spacing between isopycnals 26.55 kg m^{-3} and 26.65 kg m^{-3} is shown in figures 9.5 to 9.8 as the deviation from the mean spacing. This parameter can be understood as one component of the isopycnic potential vorticity (Fischer, Leach and Woods, 1985). This field is thought to be almost internal wave-free, because most of the internal wave energy is concentrated in the lowest wavenumber, which will move the isopycnals up and down together (Leach, Minnett & Woods, 1985). Only the high wavenumber part of the internal wave field will contaminate this signal.

In order to show the structures within the mixed layer, which is not possible by isopycnic analysis, isobaric maps of the salinity and temperature field at 20 m are shown in figures 9.9 and 9.10.

It is possible to create maps for any level within the interval 15 m to 80 m with a vertical separation of 1 m. For the isopycnic maps the interval is σ_t = 25.9 kg m^{-3} to σ_t = 26.9 kg m^{-3} with an increment of 0.025 kg m^{-3}.

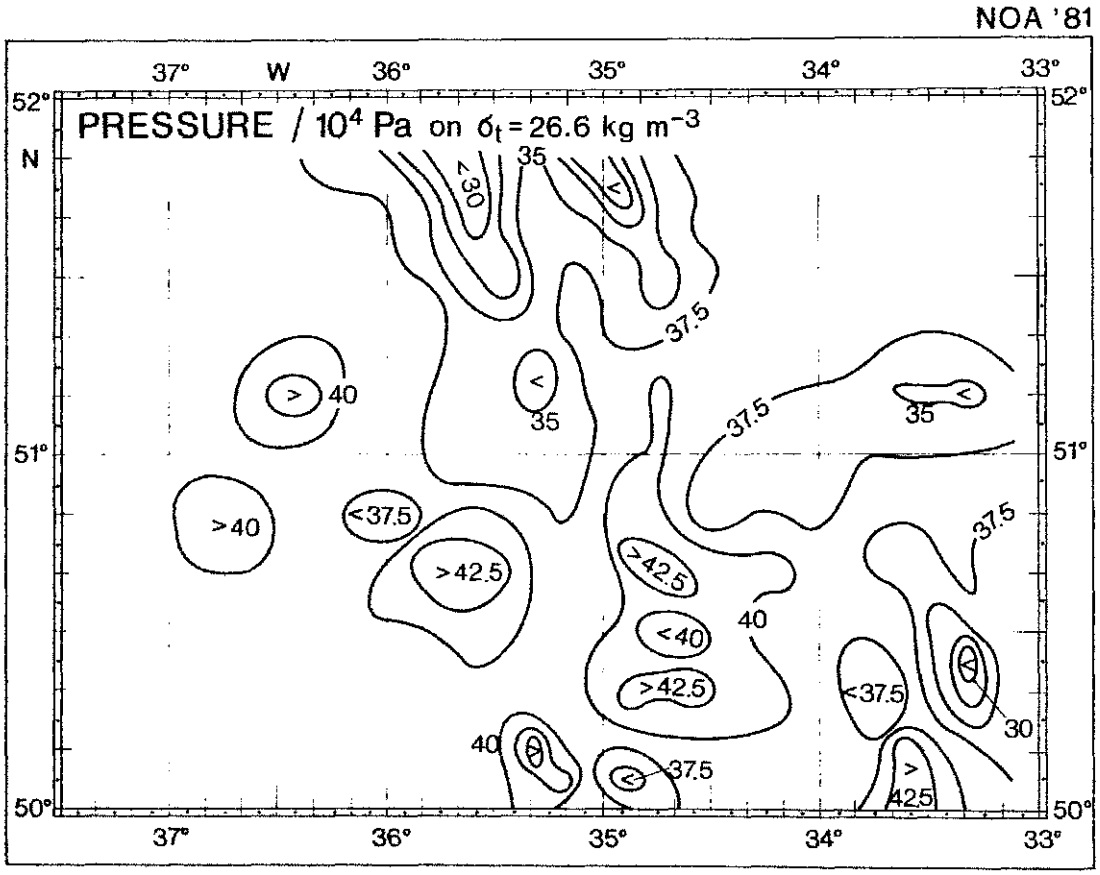

Fig. 9.1: Objectively analysed depth of isopycnal σ_t = 26.6 kg m^{-3} at the Polar Front. Grid dimensions were 10 km x 10 km.

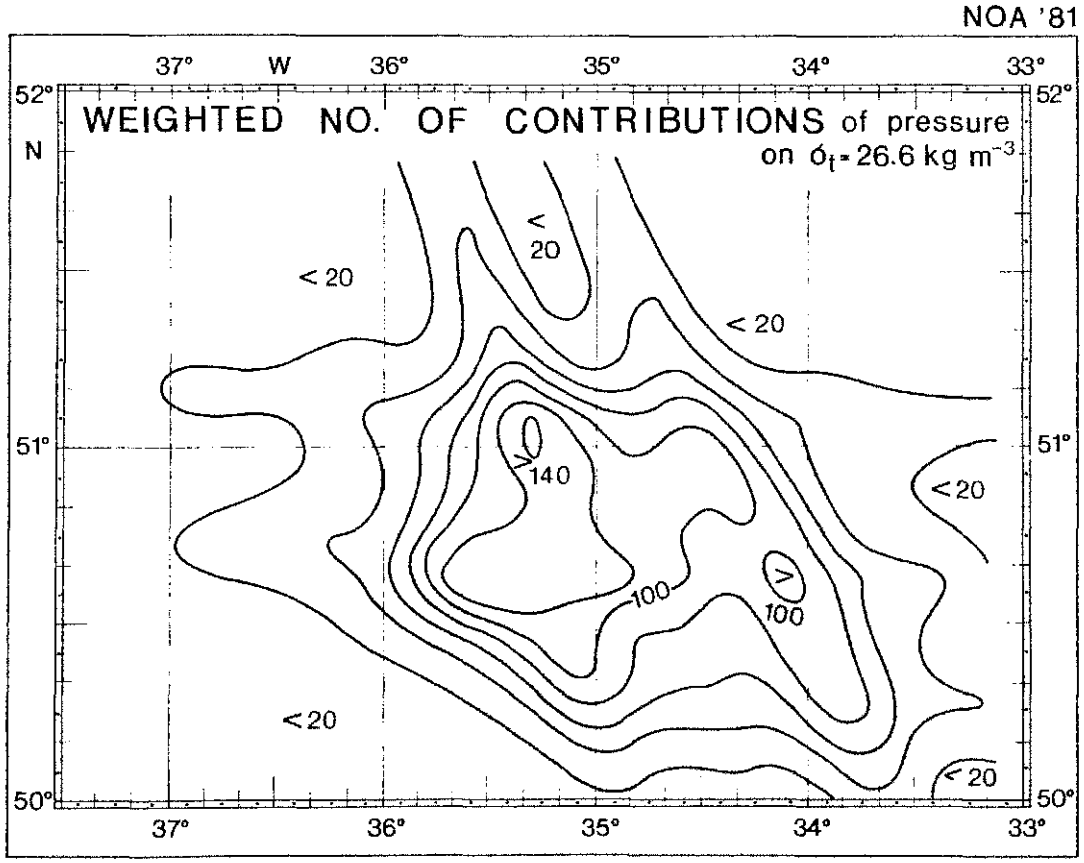

Fig. 9.2: Weighted number of contributions of the depth of σ_t = 26.6 kg m^{-3}. Grid dimensions were 10 km x 10 km.

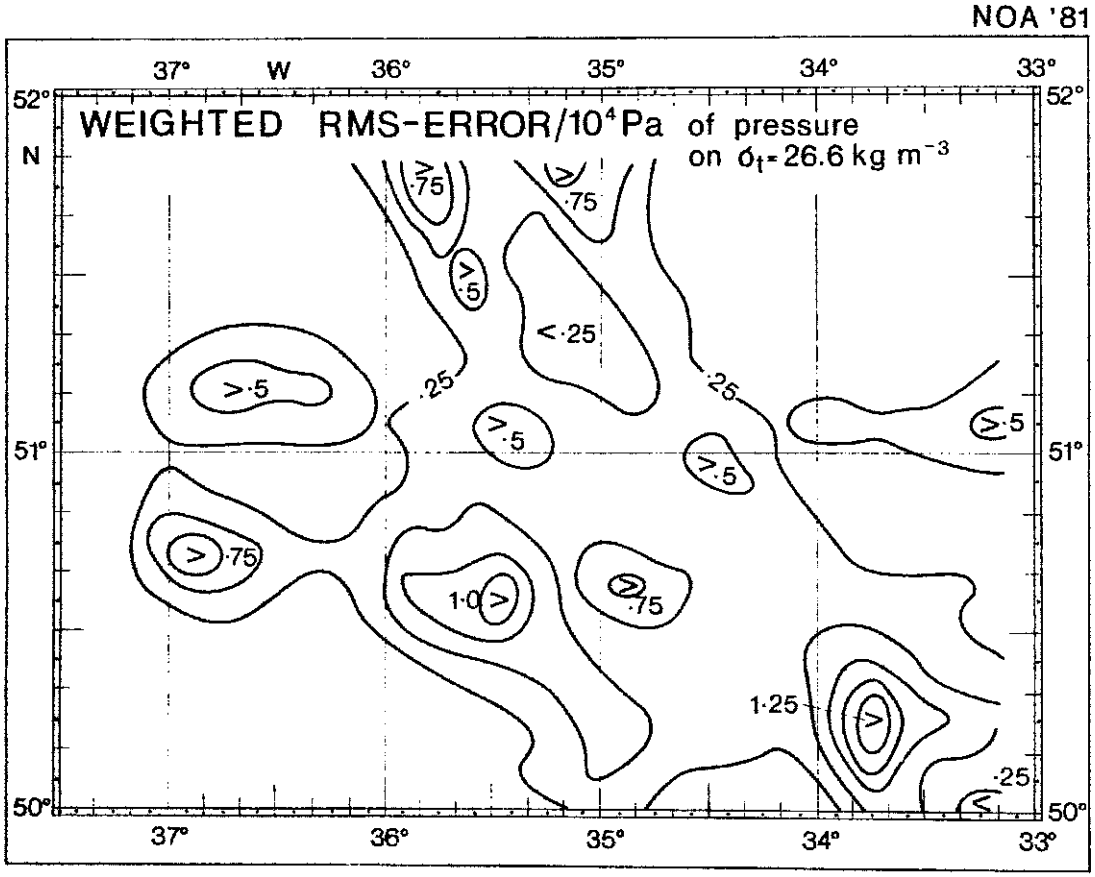

Fig. 9.3: Weighted RMS-error of the depth of σ_t = 26.6 kg m^{-3}. Grid dimensions were 10 km x 10 km.

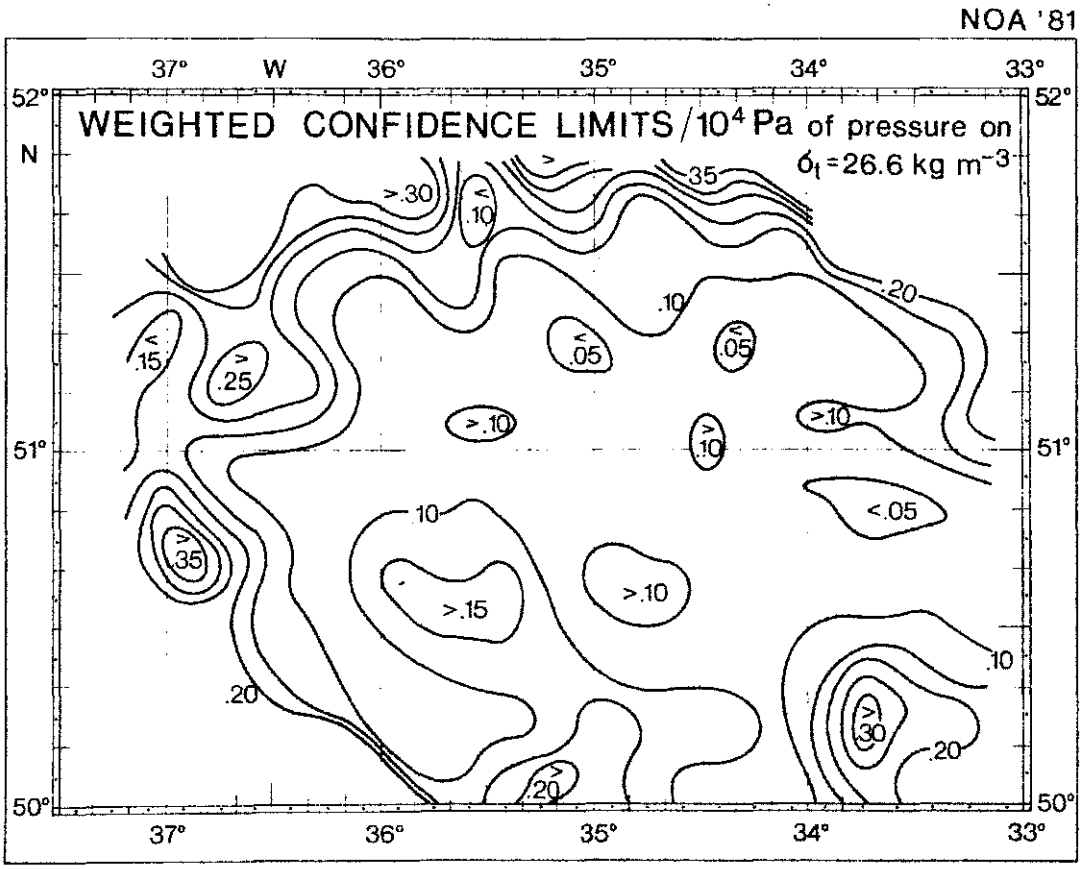

Fig. 9.4: Weighted confidence limits of the depth of σ_t = 26.6 kg m^{-3}. Grid dimensions were 10 km x 10 km.

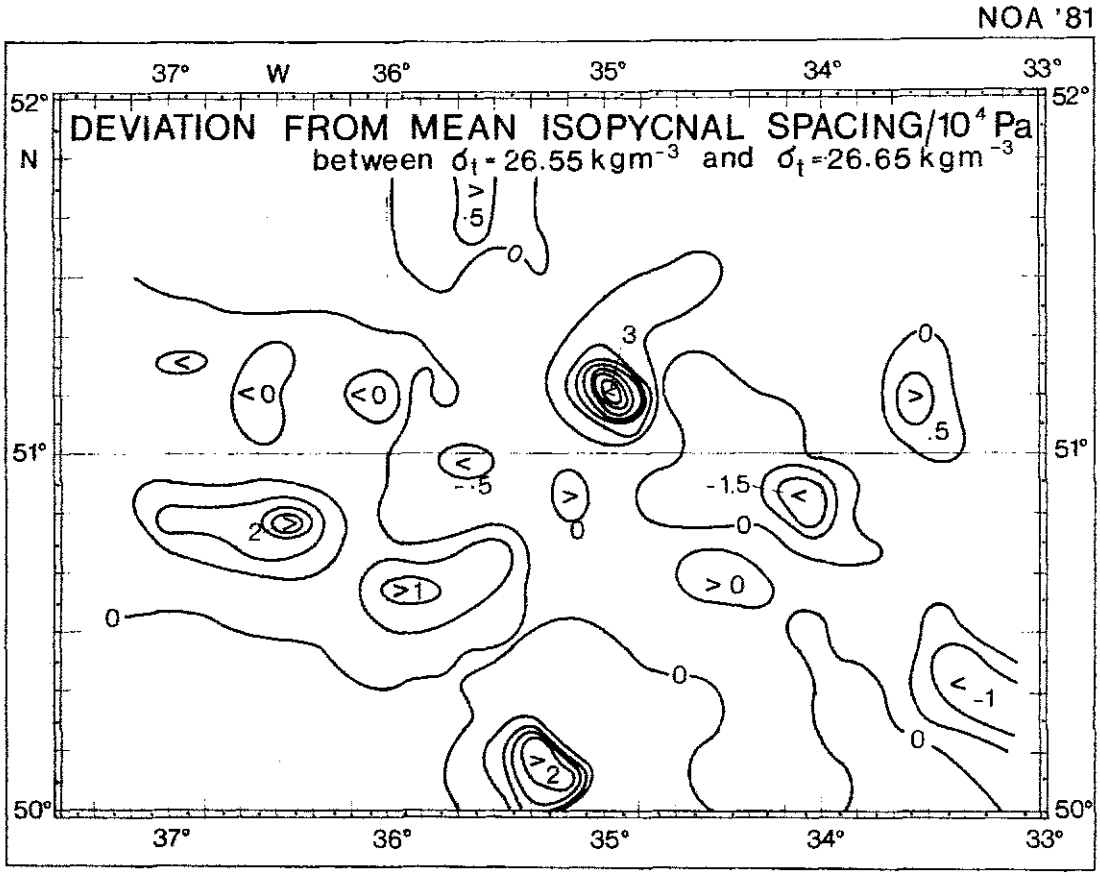

Fig. 9.5: Objectively analysed isopycnic spacing between σ_t = 26.55 kg m^{-3} and σ_t = 26.65 kg m^{-3}. From each data point the ensemble mean of 3.94 x 10 Pa was subtracted. Grid dimensions were 10 km x 10 km.

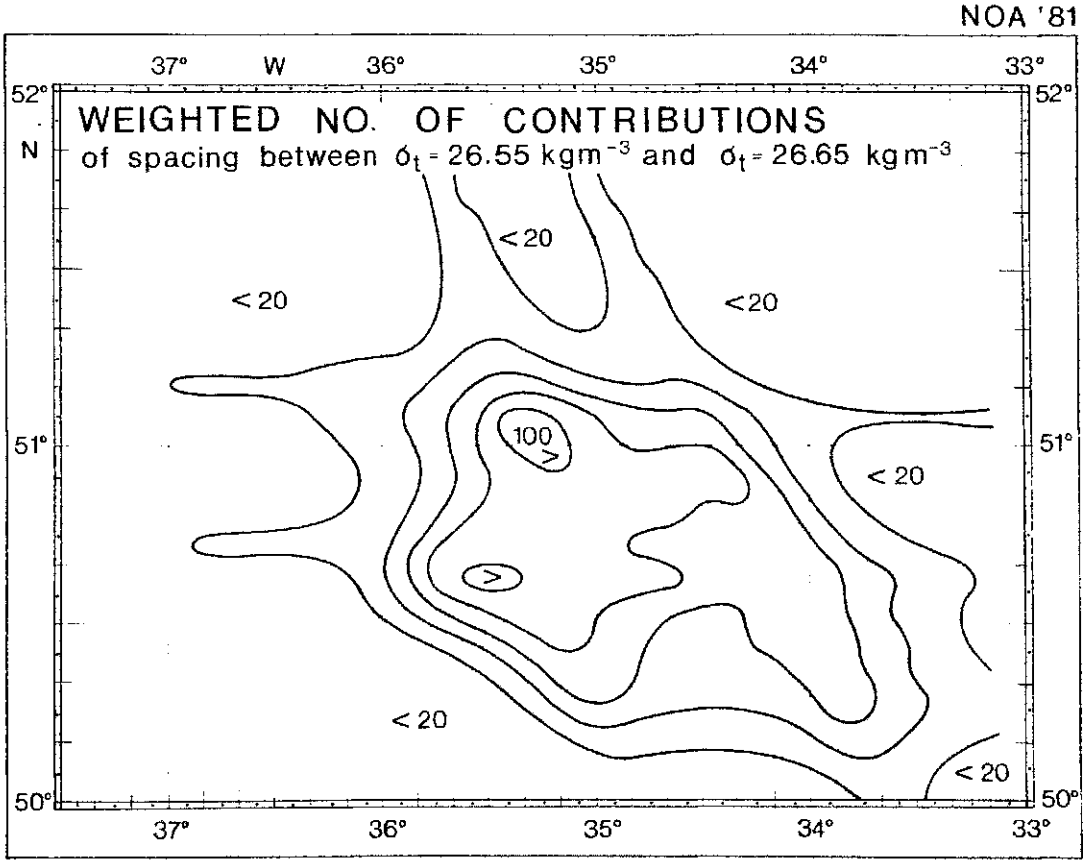

Fig. 9.6: Weighted number of contributions of isopycnic spacing between σ_t = 26.55 kg m^{-3} and σ_t = 26.65 kg m^{-3}. Grid dimensions were 10 km x 10 km.

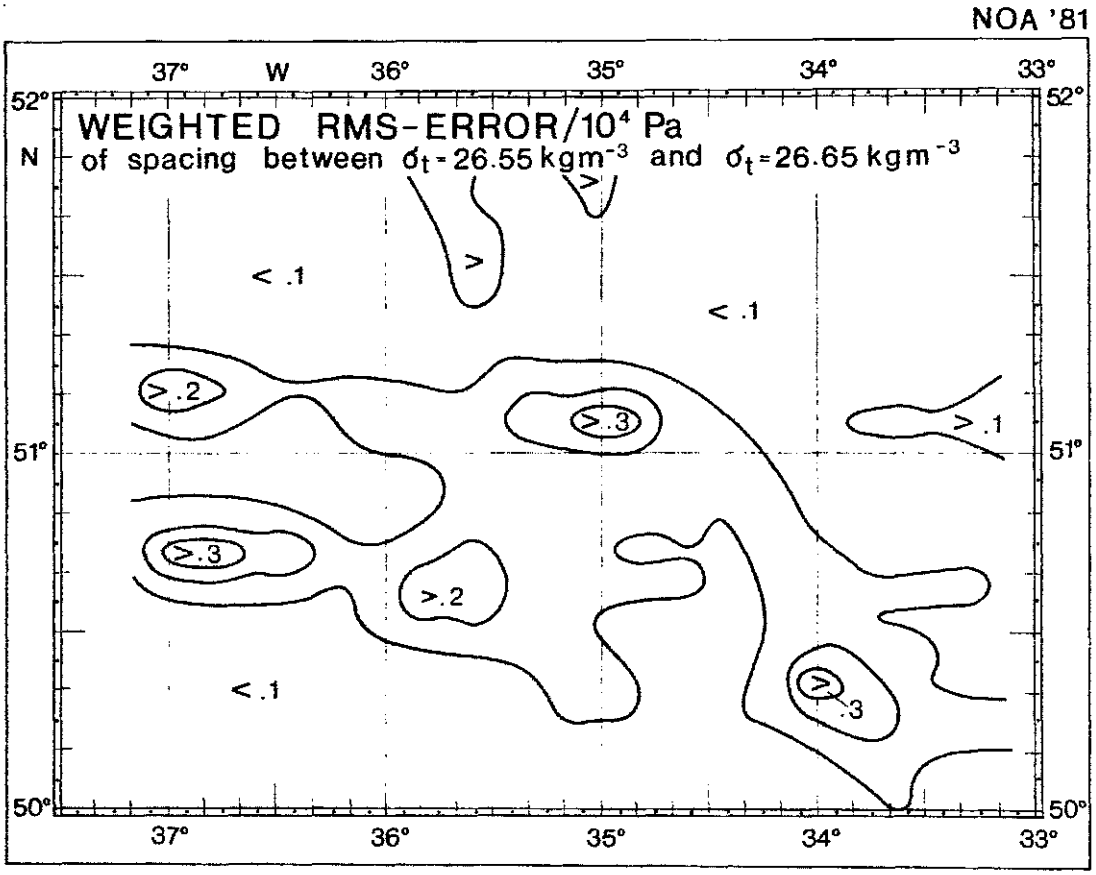

Fig. 9.7: Weighted RMS-error of isopycnic spacing between σ_t = 26.55 km m^{-3} and σ_t = 26.65 kg m^{-3}. Grid dimensions were 10 km x 10 km.

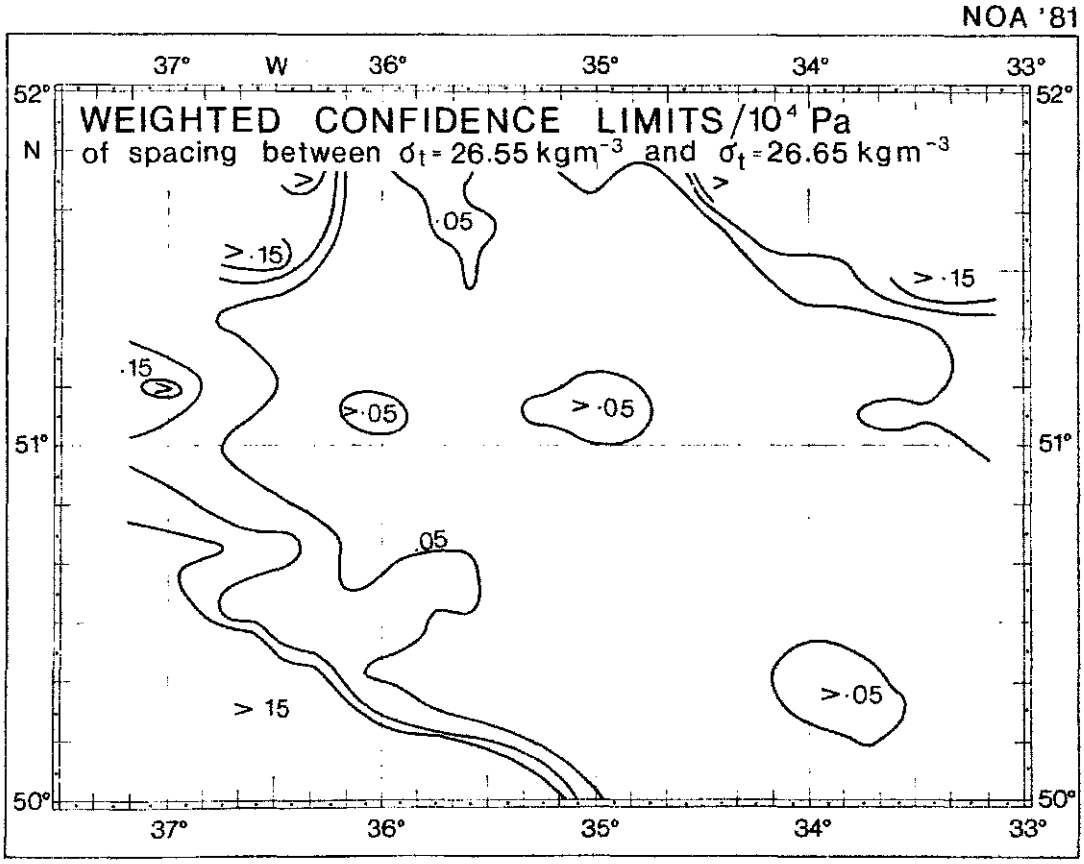

Fig. 9.8: Weighted confidence limits of isopycnic spacing between isopycnals σ_t = 26.55 kg m^{-3} and σ_t = 26.65 kg m^{-3}. Grid dimensions were 10 km x 10 km.

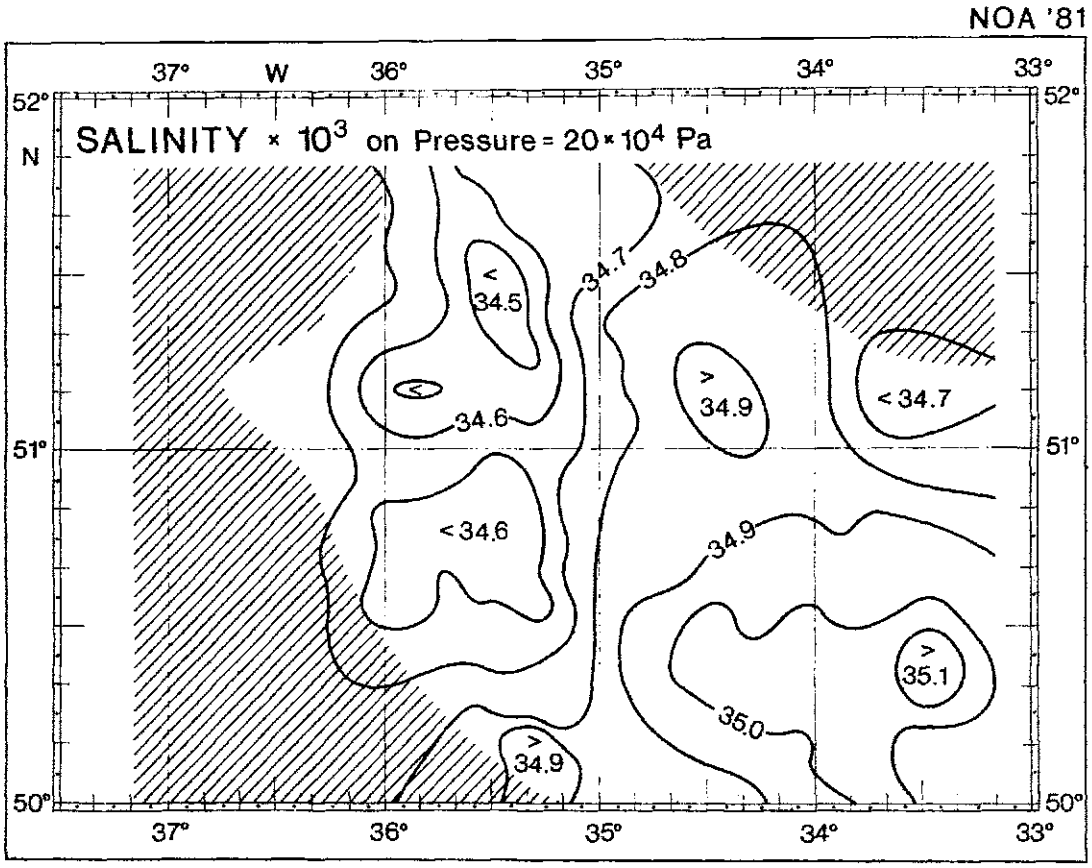

Fig. 9.9: Salinity distribution at 20 m at the Polar Front Survey. In the shaded areas the weighted number of contributions was less than 30. Grid dimensions were 10 km x 10 km.

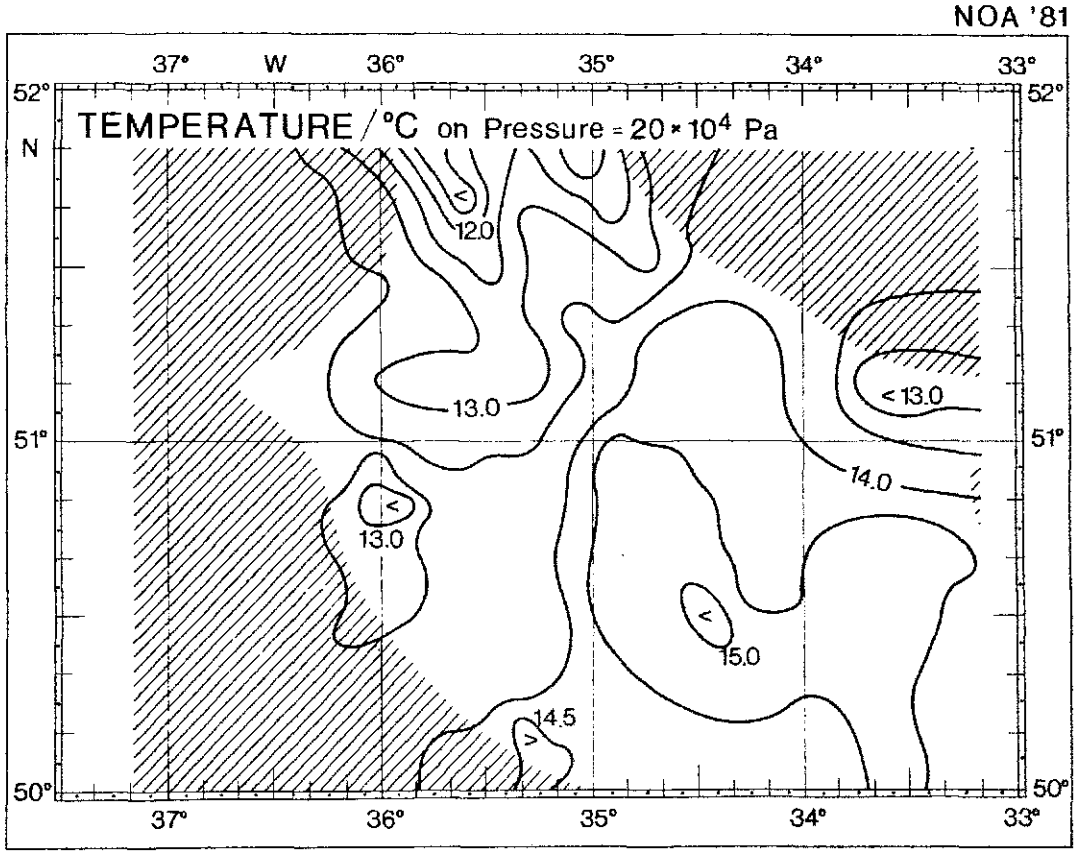

Fig. 9.10: Temperature distribution at 20 m at the Polar Front Survey. In the shaded areas the weighted number of contributions was less than 30. Grid dimensions were 10 km x 10 km.

10. SURFACE CURRENTS

10.1 Data Acquisition

Throughout the Sea Rover legs of the "Poseidon" NOA '81 cruise the flow of water at the sea surface was estimated using the difference of the motion of the ship relative to the sea floor and relative to the water. The absolute motion of the ship was determined using satellite navigation, which gave the absolute position of the ship at irregular intervals ranging between about one and three hours. The motion of the ship relative to the water was obtained by integrating the signal from a two-component electromagnetic log mounted below the ship's well. The integration of the signal from the log was carried out using the ship's HP1000 navigation computer, to which the log was interfaced. The log was calibrated off the Azores on 18 July 1981 using a drifting radar-buoy with a sail centred at the depth of the log. The two components were calibrated separately. The calibration and integration took account of mis-alignment of the head of the log. Further details of the navigation system and the calibration procedure are contained in Leach, 1984.

The position of the ship at times of the satellite fixes and the corresponding relative positions were extracted from the 2-minute protocol printed by the navigation system. These were then typed into the HP9825A desk calculator. The difference in the change of absolute position of the ship between two satellite fixes and change of position relative to the water during the same period was then calculated and divided by the time interval giving the mean surface current for the space and time interval. This was assigned to the mean absolute position of the ship during the interval.

10.2 Derivation of the streamfunction in the synoptic-scale survey area

Within the box 38°W - 30°W and 50°N - 52°N, see figure 11.1, there were 137 satellite fixes between which 136 mean surface current vectors could be calculated. The mean surface velocity is 0.08 m s^{-1} to the eastnortheast (72°) and the rms speed is 0.3 m s^{-1}, while the maximum velocities associated with the core of the jet stream sometimes exceed 1 m s^{-1}, as can be seen in figure 10.2.1.

Visual comparison of the current vectors with the thermohaline structures (figures 10.2.1, 5.4.2) shows that at least in places the current appears

to be flowing quasi-parallel to the isolines of say temperature on density surfaces. This result was sufficient to encourage us to try and obtain a streamfunction which could more easily be compared with the thermohaline structures. After consideration of methods suggested in the literature (see Bretherton et al., 1976, for example) it was decided to try another method as follows. The east (u) and north (v) components of the current were interpolated separately onto a regular grid with 10 km spacing using their auto-correlation functions as weighting functions (figure 10.2.2).

The vorticity field was calculated from the grid point u and v fields (figure 10.2.3), using a central difference scheme. The general feature of this quantity is a banded structure along the axis of the jet, symptomatic of the crossjet shear and with extreme values in the regions of strongest curvature of the flow field. Comparison with the planetary vorticity f shows, that the relative vorticity is of the same order of magnitude, with maximum cyclonic relative vorticity of about 60 % and maximum anticyclonic vorticity of about 70 %. Furthermore the restriction of the estimates of the surface current to one per satellite fix restricts the observable vorticity to about $\pm$ 100 M s^{-1} (when the maximum currents seen of about 1 m s^{-1} are observed with a spacing of some 20 km say). The rms vorticity of the analysed field is 11.6 M s^{-1} or about 10.4 % of f. The ratio of the relative vorticity to the planetary vorticity can be interpreted as a Rossby number ($Ro \approx \frac{\zeta}{f}$) and the large value of this quantity draws attention to the fact, that in regions such as this it is no longer advisable to regard the flow as quasi-geostrophic.

The vorticity field was then integrated using the technique of successive over-relaxation to solve the Poisson equation for the streamfunction. From the u and v fields the gradient, Dirichlet, boundary conditions were available for the integration. The resulting streamfunction shown in figure 10.2.4 bears comparison with the hydrographic structure shown in figure 5.4.2. Both show southward meanders at 35°30'W and 33°0'W and a northward meander at 34°30'W. The general structure of the streamfunction shows a smoother appearance than the temperature field, which may to some extent be due to the analysis technique acting as a filter. It is interesting to note, that the width of the jet between the trough and the ridge is nearly twice that of the thermoclinicity maximum.

By differentiating the streamfunction it is possible to obtain a geostrophic velocity field. This is shown in figure 10.2.5.

Further discussion of the dynamic quantities at the Polar Front is to be found in Fischer, Leach and Woods (1985) and detailed discussion of the analysis of the current data in Leach (1985).

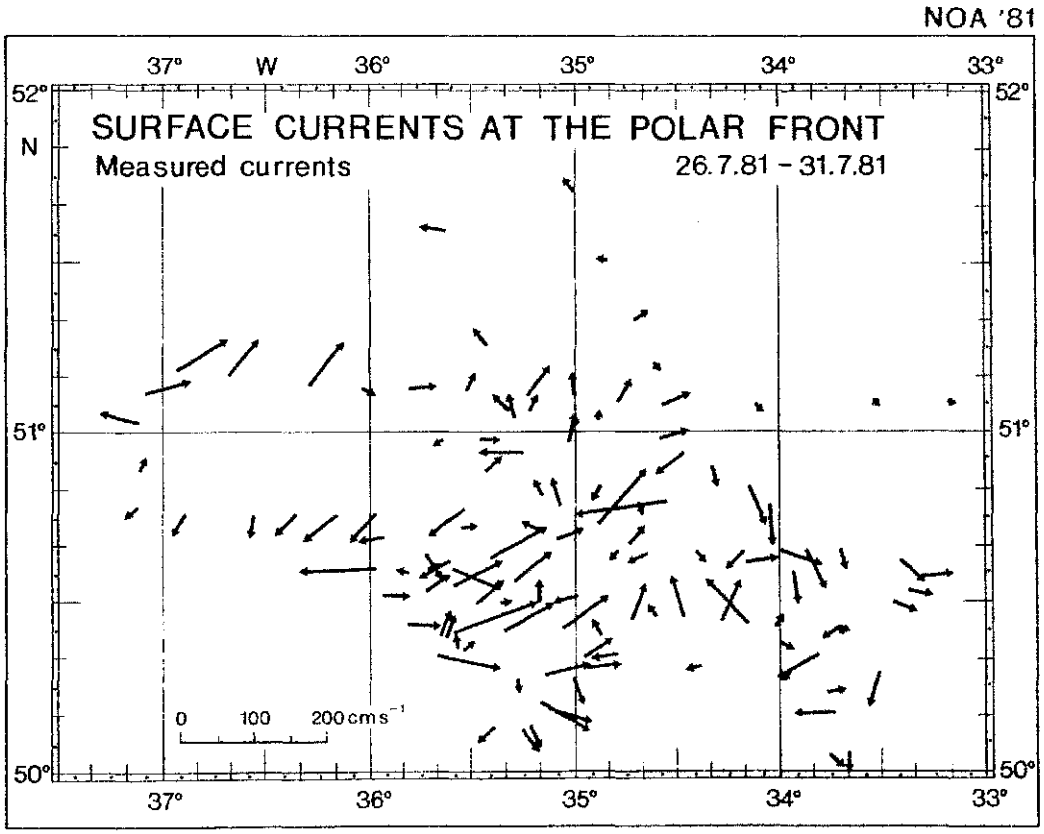

Fig. 10.2.1: Surface currents at the Polar Front as measured by the EM-log and satellite navigation.

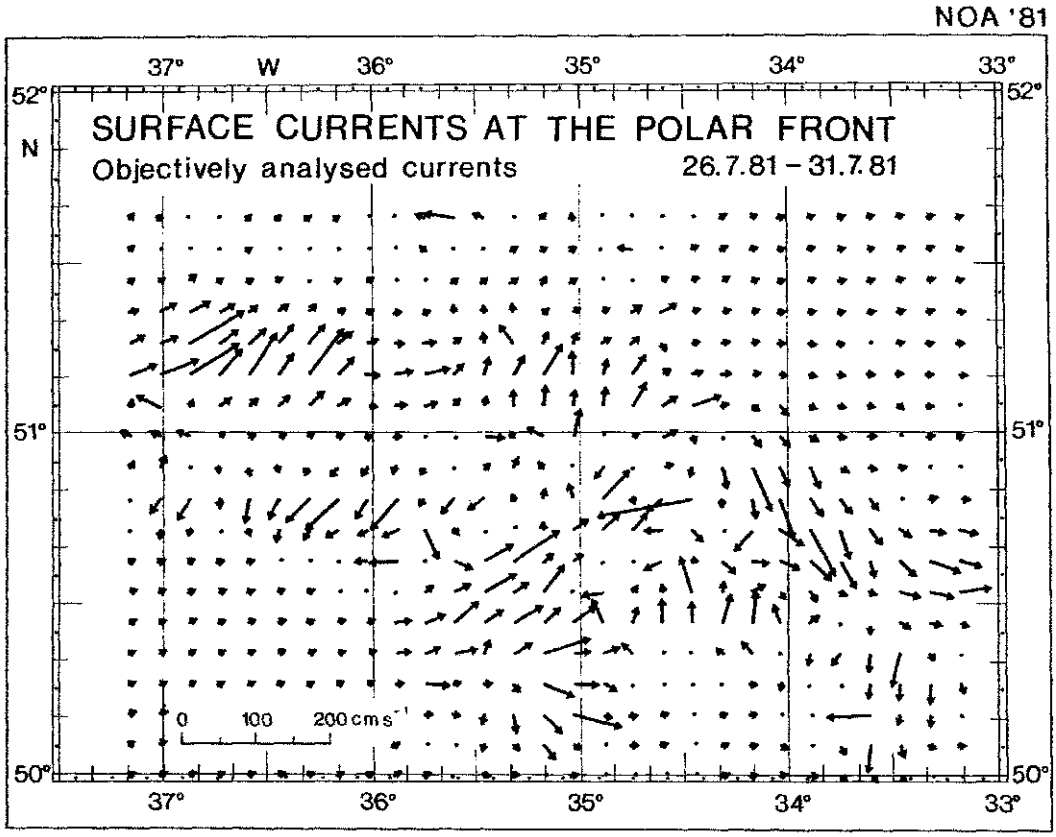

Fig. 10.2.2: Objectively analysed surface currents derived from the raw currents. Grid dimensions were 10 km x 10 km.

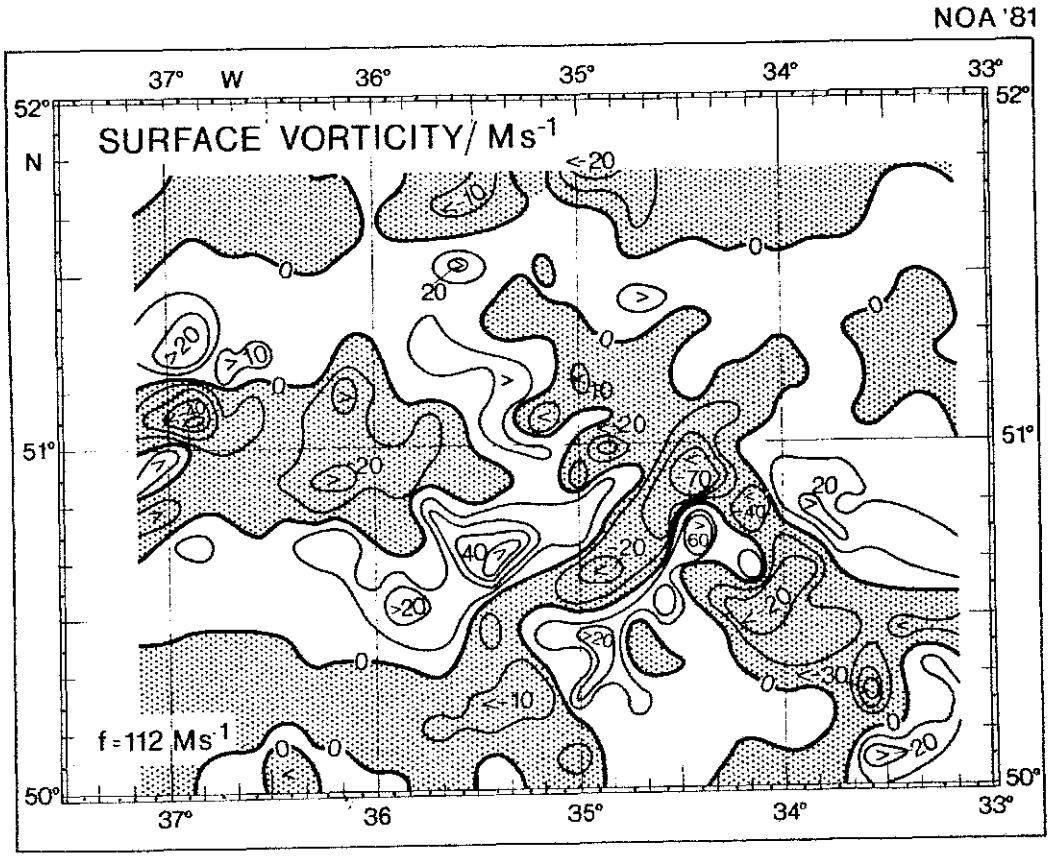

Fig. 10.2.3: Relative vorticity at the surface, derived from objective analysed current field.

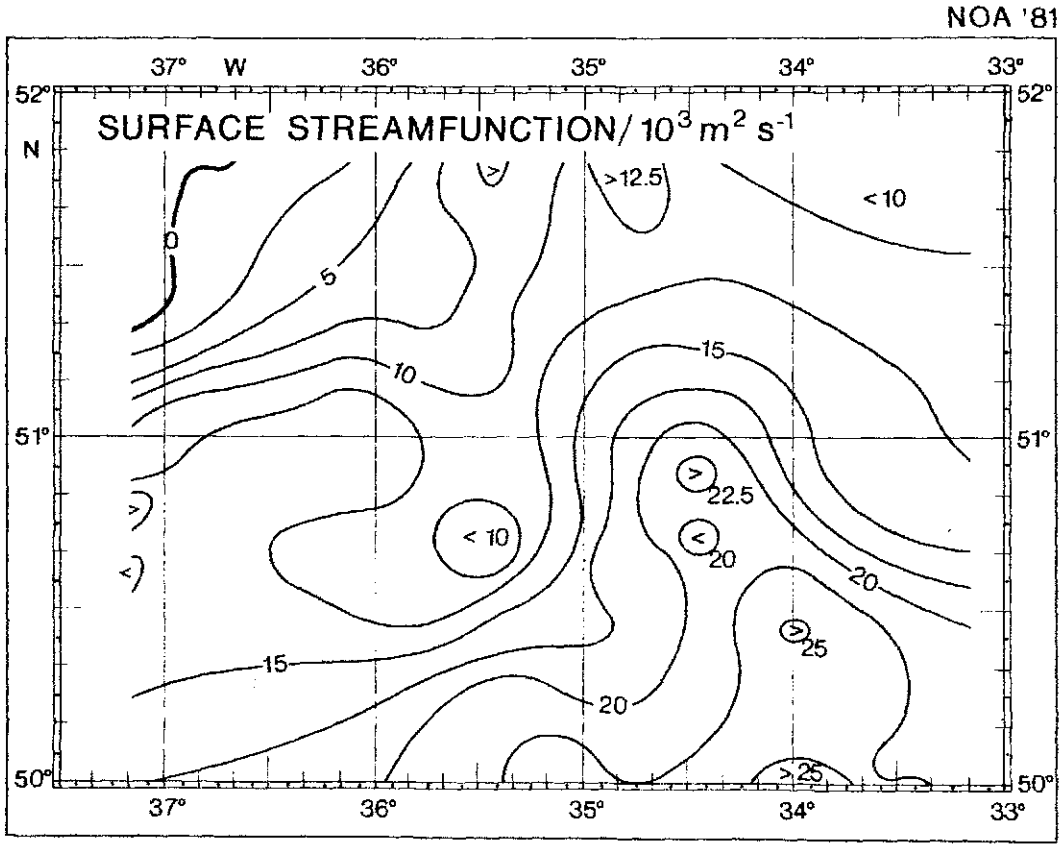

Fig. 10.2.4: Surface streamfunction at the Polar Front derived by integrating the relative vorticity.

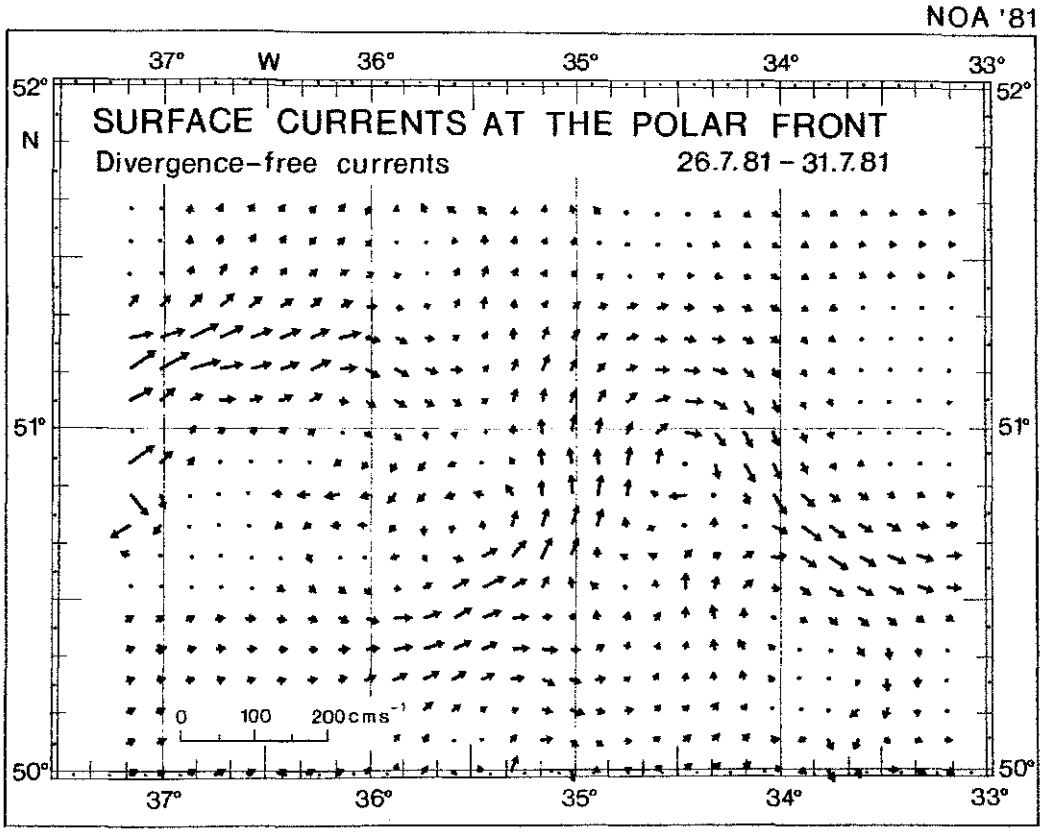

Fig. 10.2.5: Divergence free surface currents at the Polar Front derived by differentiating the surface streamfunction.

11. METEOROLOGICAL DATA

During the NOA'81 expedition two independent automatic systems for measuring meteorological parameters were installed on "Poseidon". The Tefrimet (designed by Fa. Theodor Friedrichs) system recorded dry bulb, wet bulb and sea surface temperatures, wind speed and direction and air pressure with a time interval of one minute.

The new equipment built from a design by Dr. K. Uhlig, Department of Maritime Meteorology, IfM-Kiel, still in the test phase, had the advantage of recording mean values averaged over a predetermined interval. It had two sensors for dry and wet bulb temperatures and one sensor each for wind speed and direction as well as short-wave downward radiation.

Both data sets had large gaps. Therefore the presentation here (fig. 11.1 - 11.3) is the best possible combination of data from both systems.

The wind data are only recorded and displayed relative to the ship's speed and heading.

Figure 11.1 presents the meteorological data during the long section B102. In the first 3 days of the long section FS "Poseidon" steamed through the region of the Azores high pressure area with few clouds, relatively dry air and low winds. Steaming through the anticyclone the ship passed through regions of easterly, southerly and westerly winds. On the 23rd July the ship came into the influence of stronger westerly winds, advecting more humid subpolar air. Passing fronts provided complete cloud cover.

Figure 11.2 presents the meteorology measured on the long legs of the front survey. The first two days the centre of an anticyclone with a central pressure of 1035 hPa was situated 400 km south of the survey region. Due to it the ship operated under cloudless sky, in dry air and southwesterly wind. On the 29th July an occluded front system attached to a cyclone with central pressure of 995 hPa passed over the survey region. The wind increased to 20 ms^{-1} from a southwesterly direction and advected air, which although 2 °C warmer than the local sea surface temperature was highly saturated with water vapour.

During the high resolution part of the front survey the cyclone intensified till the 2nd August to a central pressure of 975 hPa. Its centre was situated 900 miles north of the survey region (figure 11.3).

During the last two days the wind decreased but still advected polar air colder than the sea surface temperature on the cold side of the front. Due to a stationary front the area was covered with stratus clouds.

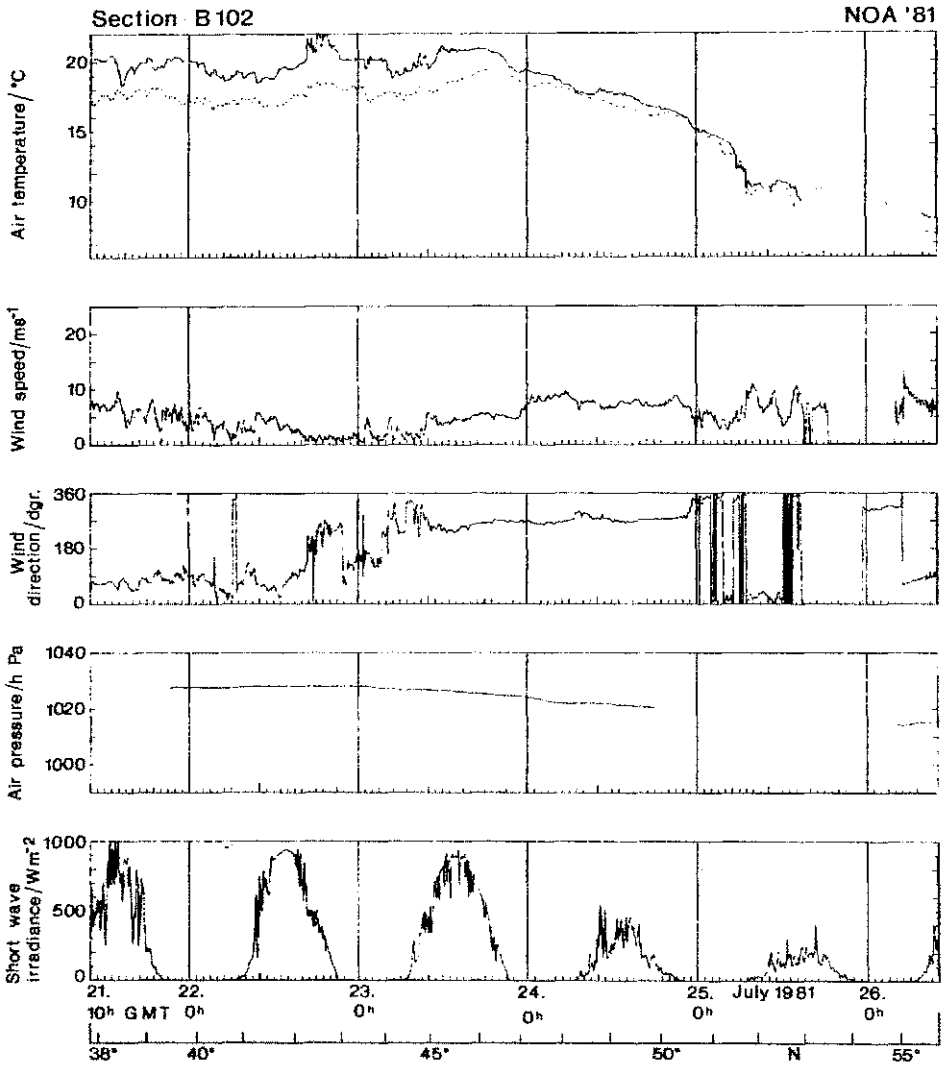

Fig. 11.1: Wet and dry bulb air temperature, wind speed and direction, air pressure and short wave irradiance along the section B102.

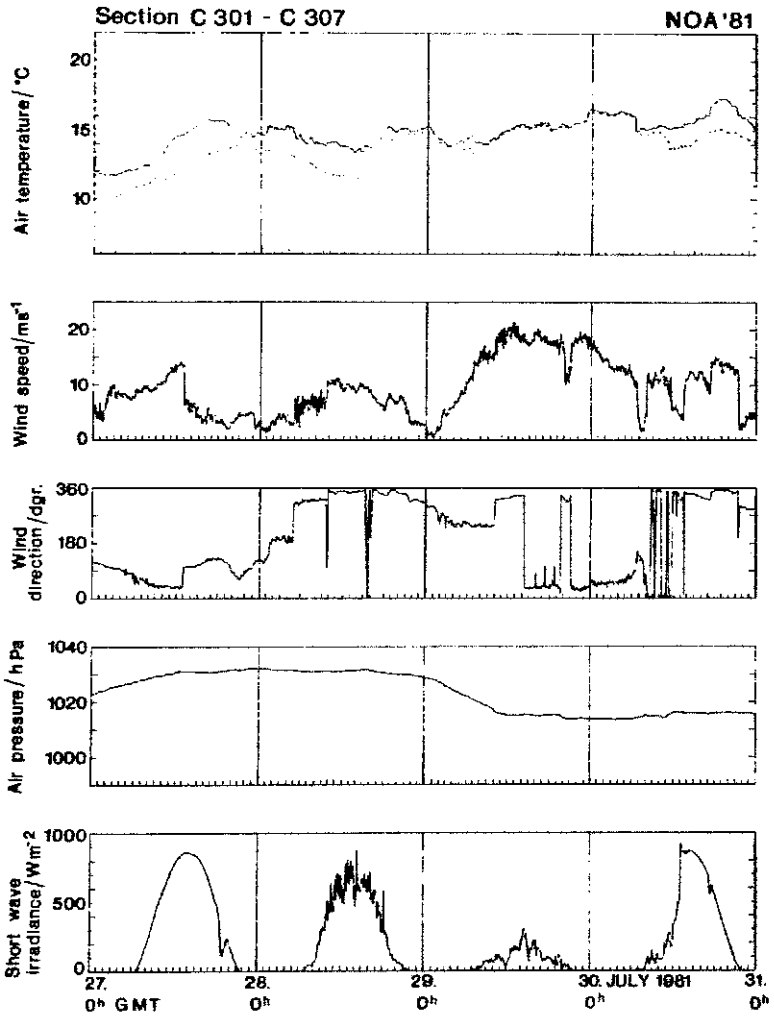

Fig. 11.2: Wet and dry bulb air temperature, wind speed and direction, air pressure and short wave irradiance during the synoptic scale part of the frontal survey.

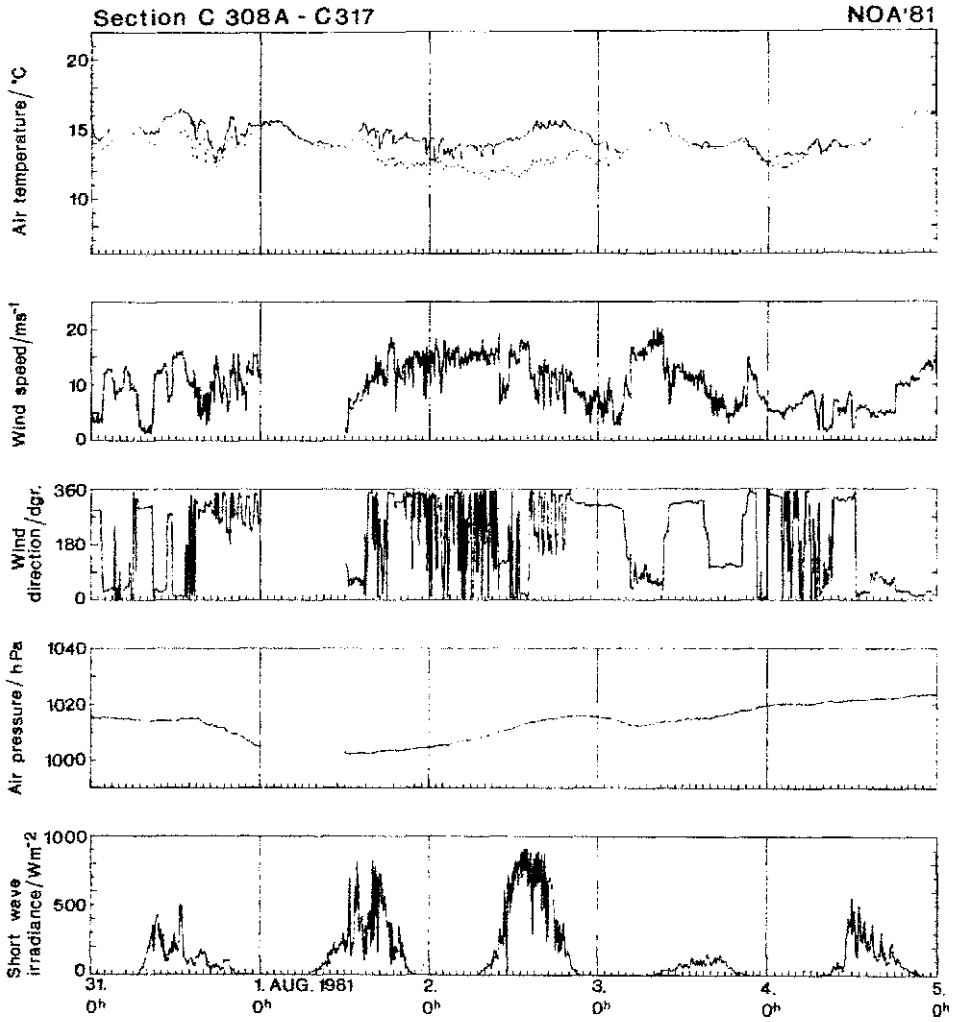

Fig. 11.3: Wet and dry bulb air temperature, wind speed and direction, air pressure and short wave irradiance during the high resolution part of the frontal survey.

12. CONCLUSIONS

The experiment NOA'81 was the first of a series of experiments carried out with our new measurement system, called SEA ROVER.

The SEA ROVER is an integrated system measuring hydrography and currents in the upper boundary layer of the ocean, combined with meteorological measurements, navigation and real-time data processing, from the moving ship, steaming at almost full speed.

We were able to monitor large areas with higher horizontal resolution in shorter time than classical CTD surveys, the cost being the limited depth range and the relatively large technical expense. Real-time data processing allowed a spontaneous adjustment of the survey pattern according to the just measured hydrographic situation. New problems in calibration, time-constant behaviour and temperature dependence of the sensors were caused by high diving speeds of the fish. The applied scheme of recalibration, editing and data reduction succeeded in correcting some of the errors in the measurements. The accuracy was sufficient to resolve the strong signals in the upper boundary layer. In later experiments (NOA'83) the diving speed of the fish was reduced in order to avoid some of the detected error sources.

The NOA'81 experiment provided a data set of hydrography in the upper 80 m, surface currents and meteorology continuously measured over a distance of 12 Mm. The high horizontal resolution over long sections span up a spectral range of 0.4 - 2500 km, the towing speed of 10 knots improved the synopticity of the measurements, and the data rate of 16 cycles per second raise statistical significance. Repeated surveys of the same track on return trips allow to investigate temporal changes.

With the use of isopycnic analysis we were able to discriminate oceanic finestructure from internal waves. For example the presentation of temperature on surfaces of constant σ_t show clearly the extension of different water masses and thus eddies, meanders, tongues and fronts are detectable.

Averaging over a large number of data samples improved the signal to noise ratio and increased the statistical significance. These statistical results can be used for the test of models or the comparison with climatologcial data.

The high horizontal resolution reveals new insights in the large-scale structure of long sections intersecting the streamlines of the subtropical

gyre. Large regions of relatively homogeneous T-S relationship alternate with narrow bands of strong horizontal gradients. The transition zone between the subtropical warm water and the subarctic water extends over 700 km. The transitions themselves are found mainly at four strong fronts not broader than 50 km each. The intermediate regions only show mesoscale variability like the waters near the Azores or north of the Polar Front. The horizontal patterns differ also vertically. While water mass changes in the seasonal thermocline occur nearly steplike, horizontal gradients in the mixed layer are much weaker and often are phase-shifted compared to the structure in the thermocline. Thus the mixed layer masks the pattern of the underlying water, a result which may be important for remote sensing. At the Polar Front between 50° N and 52° N synoptic-scale meanders with wave-lengths of about 200 km have been observed. The structures detected in the hydrographic data show strong similarities with the surface currents on scales larger than 20 km. The lack of horizontal resolution in the navigation data hindered us from comparing hydrogaphy and current measurements on smaller scales. Improvement of the navigation system is therefore necessary for the investigation of structures like the thermoclinicity maximum which was less than 10 km wide.

13. REFERENCES

Baumgartner, A. and E. Reichel, 1975: The World Water Balance. Elsevier, Amsterdam, 179 pp.

Bauer, J. and J.D. Woods, 1984, Isopycnic Atlas of the North Atlantic Ocean. Ber. Inst. f. Meereskunde Kiel, Nr. 132, 173 pp.

Bretherton, F., R.E. Davis and C.B. Fandry (1976): A technique for objective analysis and design of oceanographic experiments applied to MODE-73. Deep-Sea Research, 23, 559-582.

Budyko, M.I., 1974: Climate and Life. International Geophys. Series, Vol. 18, Academic Press, London, 508 pp.

Collins, D.S., R.T. Pollard and S. Pu, 1983: Long Sea Soar CTD sections in the northeast Atlantic Ocean collected during RRS "Discovery" Cruise 116. Institute of Oceanographic Sciences, Report No. 148, 77 pp.

Dessureault, J.G., 1976: "Batfish". A depth controllable towed body for collecting oceanographic data. Ocean Engineering 3, 99-111.

Dettmann, E., 1981: Konzeption, Gestaltung und Anwendung eines ozeanographischen Schleppsystems. Ph.D. Thesis, University of Hannover.

Dietrich, G., 1969: Atlas of the Hydrography of the Northern North Atlantic Ocean. Conseil International pour l'Exploration de la Mer, Service Hydrographique, Charlottenlund Slot - Denmark, 140 pp.

Dietrich, G., K. Kalle, W. Krauss and G. Siedler, 1980: General Oceanography. An Introduction. 2nd edition (translated from German), John-Wiley, New York, 626 pp.

Fischer, J., H. Leach and J.D. Woods, 1985: Synoptic-scale structures in the seasonal thermocline at the North Atlantic Polar Front. (in preparation)

Fischer, J., C. Meinke, P.J. Minnett, V. Rehberg and V. Strass, 1985: A description of the Institut für Meereskunde Schleppfisch-System. Technischer Bericht Nr. 1 der Abt. Regionale Ozeanographie des Instituts für Meereskunde, Kiel, 2. Auflage.

Hardtke, P.G. and J. Meincke, 1984: Kinematical interpretation of infrared surface pattern in the North Atlantic.
Oceanologica Acta 7(3), 373-378.

Horch, A., 1984: Eine Beschreibung der NOVA-Software für Schleppfisch-Experimente.
Technischer Bericht Nr. 5 der Abt. Regionale Ozeanographie des Instituts für Meereskunde, Kiel, 2. Auflage.

Isemer, H.-J. and L. Hasse. 1985: The Bunker climate atlas of the North Atlantic Ocean. Vol.1: Observations, Springer Verlag, Heidelberg, New York, Tokyo. Vol. 2: (in preparation).

Jenkins, G.M. and D.G. Watts, 1968: Spectral Analysis and its applications. Holden-Day, pp. 525.

Krauss, W. and R. Käse, 1984: Mean circulation and eddy kinetic energy in the eastern North Atlantic.
J. Geophys. Res. 89, 3407-3415.

Krauss, W. and J. Meincke, 1982: Drifting buoy trajectories in the North Atlantic Current.
Nature, 296, 737-740.

Kreyszig, E., 1965: Statistische Methoden und ihre Anwendungen.
Vandenhoeck & Ruprecht, Göttingen, p. 422.

Leach, H., 1984: Eine Beschreibung des wissenschaftlichen Navigationssystems des FS "Poseidon".
Technischer Bericht Nr. 2 der Abt. Regionale Ozeanographie des Instituts für Meereskunde, Kiel, 2. Auflage.

Leach, H., 1985: The analysis of currents measured from a moving ship in the region of the North Atlantic Polar Front.
(submitted to Deep-Sea Research).

Leach, H., P.J. Minnett and J.D. Woods, 1985: The GATE Lagrangian Batfish Experiment.
Deep-Sea Res. 32, 575-597.

Meincke., J. and A. Sy, 1983: Large-scale effects of the Mid-Atlantic Ridge on the North Atlantic Current.
ICES Report, C.M./C:8, 10 pp.

Onken, R., R. Bleck and J.D. Woods, 1986: Two-dimensional model of mesoscale frontogenesis. (in preparation).

Robinson, M.K., R.A. Bauer and E.H. Schroeder, 1979): Atlas of North Atlantic - Indian Ocean monthly mean temperatures and mean salinities of the surface layer.
U.S. Naval Oceanographic Office Ref. Pub. 18, Washington D.C.

Woods, J.D., 1985: The physics of thermocline ventilation.
In J.C.J. Nihoul (Editor), Coupled Ocean-Atmosphere Models. Elsevier, Amsterdam.

Woods, J.D., H. Leach and P. Minnett, 1981: The GATE Lagrangian Batfish Experiment.
Ber. Inst. f. Meereskunde Kiel, Nr. 88 and Nr. 89.

Woods, J.D. and P.J. Minnett, 1979: Analysis of mesoscale thermoclinicity with an example from the tropical thermocline during GATE.
Deep-Sea Res. 26A, 85-96.

Sy, A.,1985: An alternative editing technique for oceanographic data.
Deep-Sea Res. (in press).

14. APPENDIX

14.1 Coefficients for sensor calibration

$$y = a_o + a_1 x + a_2 x^2$$

x: raw data value y: calibrated variable

MS38	a_o	a_1	a_2
P	-3.097345×10^{2}	3.653411×10^{-2}	8.021386×10^{-9}
T Sensor 1	-2.441963×10^{1}	2.425639×10^{-3}	2.444443×10^{-10}
T " 2	-2.503945×10^{1}	2.420168×10^{-3}	2.756392×10^{-10}
C " 1	-2.644104×10^{1}	3.399403×10^{-3}	3.781636×10^{-9}
C " 2	-2.702129×10^{1}	3.460328×10^{-3}	2.303073×10^{-9}

MS39	a_o	a_1	a_2
P	-2.8495911×10^{2}	3.7115809×10^{-2}	3.213433×10^{-9}
T Sensor 1	-2.488925×10^{1}	2.439146×10^{-3}	$3.5183501 \times 10^{-12}$
T " 2	-2.4189148×10^{1}	2.4221177×10^{-3}	$-9.9700212 \times 10^{-11}$
C " 1	-2.713648×10^{1}	3.452988×10^{-3}	2.507046×10^{-9}
C " 2	-2.553158×10^{1}	3.249933×10^{-3}	3.663812×10^{-9}

14.2 Coefficients for calibration correction of salinity

$$S_c = a_o + a_1 S$$

S: CTD-salinity S_c = corrected salinity

	a_o	a_1
S Sensor 1	0.4861705987	0.9848659552
S Sensor 2	0.3668513607	0.9860728478

14.3 Coefficients for pressure calibration correction

$$P_c = P + a_o + a_1 Tu$$

P_c: corrected pressure value

P : CTD-pressure

Tu: 4-hour mean of upper turning point temperature

$a_o = 5.79\ 10^4 Pa$

$a_1 = -0.1212\ 10^4 PaK^{-1}$